

**COMPUTATIONAL STUDY OF Pincer Iridium
Catalytic Systems : C-H, N-H, and C-C Bond Activation
and C-C Coupling Reactions**

by

Tian Zhou

A dissertation submitted to the

Graduate School-New Brunswick

Rutgers, The State University of New Jersey

In partial fulfillment of the requirements for the degree of

Doctor of Philosophy

Graduate Program in Chemistry and Chemical Biology

Written under the direction of

Alan S. Goldman

And approved by

New Brunswick, New Jersey

May 2017

ABSTRACT OF THE DISSERTATION

COMPUTATIONAL STUDY OF Pincer Iridium

CATALYTIC SYSTEMS : C-H, N-H, AND C-C BOND ACTIVATION

AND C-C COUPLING REACTIONS

by

Tian Zhou

Dissertation Director:

Alan S. Goldman

Computational chemistry has achieved vast progress in the last decades in the field, which was considered to be only experimental before. DFT (density functional theory) calculations have been proven to be able to be applied to large systems, while maintaining high accuracy. One of the most important achievements of DFT calculations is in exploring the mechanism of bond activation reactions catalyzed by organometallic complexes. In this dissertation, we discuss DFT studies of several catalytic systems explored in the lab of Professor Alan S. Goldman. Headlines in the work are: (1) (R^4 PCP)Ir alkane dehydrogenation catalysts are highly selective and different from (R^4 POCOP)Ir catalysts, predicting different rate-/selectivity-determining steps; (2) The study of the mechanism for double C-H addition/cyclometalation of phenanthrene or biphenyl by (tBu^4 PCP)Ir(I) and (iPr^4 PCP)Ir illustrates that neutral Ir(III) C-H addition products can undergo a very facile second C-H addition, particularly in the case of sterically less-crowded Ir(I) complexes; (3) (iPr^4 PCP)Ir pure solid phase catalyst is highly

effective in producing high yields of α -olefin products, since the activation enthalpy for dehydrogenation is higher than that for isomerization via an allyl pathway; higher temperatures favor the dehydrogenation/isomerization ratio; (4) $(\text{PCP})\text{Ir}(\text{H})_2(\text{N}_2\text{H}_4)$ complex follows a hydrogen transfer mechanism to undergo both dehydrogenation to form N_2 and H_2 , as well as hydrogen transfer followed by N-N bond cleavage to form NH_3 , N_2 , and H_2 ; (5) The key for the catalytic effect of solvent molecule in CO insertion reaction for $\text{RMn}(\text{CO})_5$ is hydrogen bond assisted interaction. The basicity of the solvent determines the strength of the hydrogen bond interaction during the catalytic path and determines the catalytic power of the solvent; and (6) Dehydrogenative coupling of unactivated C-H bonds (intermolecular vinyl-vinyl, intramolecular vinyl-benzyl) is catalyzed by precursors of the $(^{\text{iPr}^4}\text{PCP})\text{Ir}$ fragment. The key step for this mechanism is a $\text{Ir}(\text{III})$ vinyl hydride complex undergoing addition of a styrenyl ortho C-H bond to give an $\text{Ir}(\text{III})$ metalloindene plus H_2

Acknowledgement

My most sincere thanks go to my advisor, Prof. Alan Goldman, for his support, patience, and encouragement throughout my graduate studies. Alan is a great person and a great professor. As a foreign student, I consider myself amazingly fortunate to have a mentor such as Alan, who not only gives me most valuable advice in scientific problems, but also the freedom and encouragement to study, explore and master all kinds of knowledge. I might doubt about the choice of spending such a long time studying abroad away from my family sometime, but I would choose Alan as my mentor every time given that choice.

Besides Alan, Professor Karsten Krogh-Jespersen is the mentor who taught me most if not all computational chemistry materials. Birds of a feather flock together, I do not think it is just coincidence that I get the best and nicest professors as mentors here at Rutgers. They make my time here much quicker than it seems to be, like happy life always flies.

Besides my advisors, I would like to thank the rest of my dissertation committee, Prof. Fuat Celik, Dr. Yury Kissin, and Prof. Kai Hultsch. Their advice and comments guided me through my research towards this dissertation.

I thank the past and present members of Prof. Goldman's Group. Especially, I thank Dr. David Wang and Dr. Jason Hackenberg for their considerable help, when I just entered the group; Dr. Mike Haibach for all his wisdom and helpful discussions; Dr. Michael Blessent, Changjian Guan, Yang Gao, and Bo Li as great collaborators and

great friends. I thank Dr. Katie Field, Dr. Akshai Kumar, and Dr. David Laviska for their support; I benefited a lot from working with them.

Finally, I would like to thank my parents for always supporting me throughout my life.

Dedication

To my family

Table of Contents

ABSTRACT OF THE DISSERTATION	ii
Acknowledgement	iv
Dedication	vi
Table of Contents	vii
Chapter 1: Introduction	1
Chapter 2: Computational Study of C-H Activation by (PCP)Ir and (POCOP)Ir: A Regioselectivity Study	4
Introduction	5
Results and Discussion	7
Conclusions	32
References	36
Computational Details	38
Computational Section References	47
Chapter 3: Computational Study of Double C-H Activation of Biphenyl or Phenanthrene	48
Introduction	49
Results and Discussion	50
Conclusions	75
References	77
Computational Details	80
Computational Section References	94
Chapter 4: Computational Study of Solid-Phase Molecular Pincer-Iridium Catalysts	96
Introduction	97
Results and Discussion	99
Conclusions	134
References	138
Computational Details	141
Computational Section References	147
Chapter 5: Computational Study of N-H Activation by (PCP)IrH₂	148
Introduction	148

Results and Discussion	149
Conclusions	153
References	154
Computational Details	155
Computational Section References	157
Chapter 6: Computational Study of the Solvent Catalysed CO Insertion Reaction for $\text{RMn}(\text{CO})_5$ Complexes	158
Introduction	158
Results and Discussion	159
Conclusions	167
References	168
Computational Details	168
Computational Section References	178
Chapter 7: Computational Study of Catalytic Dehydrogenative C-C Coupling by a Pincer-Ligated Iridium Complex	179
Introduction	180
Results and Discussion	182
Conclusions	204
References	208
Computational Details	209
Computational Section References	222

Chapter 1

Introduction

This dissertation covers computational mechanism studies of C-H, C-C, and N-H activation and CO insertion in organometallic chemistry and catalysis. Themes of the research are arranged in order of introduction, experimental study followed by DFT mechanism explanation.

In the first theme, we have demonstrated that (R^4 PCP)Ir alkane dehydrogenation catalysts are highly selective for the terminal position of *n*-alkanes, whereas (R^4 PCOP)Ir and (R^4 POCOP)Ir catalysts are much less terminal-selective, or are even selective for the formation of internal olefins. DFT calculations reveal that the differences in selectivity between the catalysts investigated are not due to variations in the differences in energy between the pro-terminal and pro-internal TSs *for any given reaction step*. Instead, the different selectivities are attributable to different rate-/selectivity-determining steps for different catalysts. In particular, for (tBu^4 PCP)Ir the rate-/selectivity-determining step is β -H-elimination, whereas for (tBu^4 POCOP)Ir the rate-/selectivity-determining step is loss of the coordinated olefin.

In the second theme, we discuss the mechanism of double C-H addition/cyclometalation of phenanthrene or biphenyl by (tBu^4 PCP)Ir(I) and (iPr^4 PCP)Ir(I) complexes. The rate-determining step with both pincer ligands is calculated to be addition of the sterically hindered ortho C-H bond of biphenyl or the analogue at the C4 position of phenanthrene, affording (tBu^4 PCP)Ir(III) and (iPr^4 PCP)Ir(III) aryl hydride complexes. A second C-H addition, to produce cyclometalated Ir(V) dihydrides, has a

much lower calculated free energy barrier. While C-H addition to iridium is generally associated with Ir(I), this work illustrates that neutral Ir(III) C-H addition products can undergo a very facile second C-H addition, particularly in the case of sterically less-crowded systems. This result may have significant implications for potential C-C coupling catalysts.

In the third theme, we report that pure solid phase (pincer)Ir catalysts are highly effective for the dehydrogenation of *n*-alkanes in the gas phase. (^{*i*}Pr⁴PCP)Ir can produce high yield α -olefin products. As the calculated activation enthalpy for dehydrogenation is higher than that for isomerization via the allyl pathway, higher temperatures favor the dehydrogenation/isomerization ratio and therefore higher α -olefin yields. Thus the high α -olefin yields obtained from the gas-solid systems with (^{*i*}Pr⁴PCP)Ir are in large part simply a result of the conditions that lead to the gas/solid-phase state: use of highly volatile hydrogen acceptors and high temperature, both of which mitigate the hydride isomerization pathway.

In the fourth theme, we demonstrate that the (PCP)Ir(H)₂(N₂H₄) complex follows a hydrogen transfer mechanism to undergo both dehydrogenation to form N₂ and H₂, as well as hydrogen transfer followed by N-N bond cleavage to form NH₃, N₂, and H₂. Small molecule assistance plays a key role in the hydrogen transfer step during the process. Three key steps (α -N-H activation step, β -N-H transfer step, N-N bond cleavage step) are our potential rate determining steps for the ammonia formation. The effect of vacuum in removing dihydrogen from the metal center is supposed to lead to the pure dehydrogenation reaction.

In the fifth theme, we show that the basicity of a catalyst molecule determines the strength of the hydrogen bond interaction during the catalytic path and determines its catalytic power. The key for the catalytic effect of solvent molecule in CO insertion reaction for RMn(CO)_5 is hydrogen bond assisted interaction. Based on whether such an interaction exists, we can predict the solvent catalytic effect for similar metal complex CO insertion reactions as well. The mechanism proposed in this work applies to various catalytic molecules as well as different metal CO insertion systems.

In the sixth and last theme, we explore the dehydrogenative coupling of unactivated C-H bonds (intermolecular vinyl-vinyl, intramolecular vinyl-benzyl) catalyzed by precursors of the $(^i\text{PrPCP})\text{Ir}$ fragment. The reactions proceed via C-H activation to $(^i\text{PrPCP})\text{Ir(I)}$, followed by a second C-H activation by the resulting $(^i\text{PrPCP})\text{Ir(III)}$ product. The C-H additions to Ir(III) occur via TSs that are strongly Ir(V) in character, although the reactions generally do not lead to an Ir(V) product but rather to the formation of a new Ir(III) complex. The Ir(III) vinyl hydride complex undergoes addition of a styrenyl ortho C-H bond to give an Ir(III) metallocene plus H_2 , which is the key step for this mechanism.

Chapter 2: Computational Study of C-H Activation by (PCP)Ir and (POCOP)Ir: A Regioselectivity Study

Parts of this chapter are reproduced with permission from

Michael John Blessent “Development of pincer iridium catalysts for alkane dehydrogenation” Ph. D. Dissertation, Rutgers, The State University of New Jersey,

2016

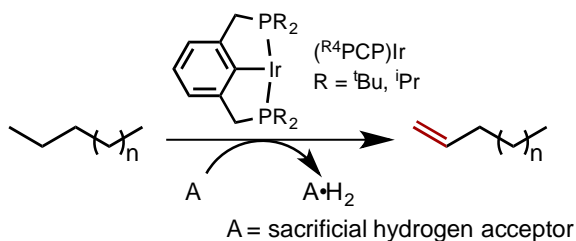
The experimental work described in this chapter was done by Dr. Michael John Blessent from Professor Alan S. Goldman’s group. This work would not have been possible without Michael’s elegant and thorough experiments.

Introduction

Alkanes are both the most abundant and the least synthetically useful class of organic molecules. Olefins by contrast are among the most useful and versatile of organic reagents, and are intermediates in most fuel and commodity chemical processes. The dehydrogenation of alkanes to give olefins is therefore potentially one of the most useful transformations of organic molecules. The nature of alkanes, however, in contrast with other classes of organic molecules, is such that they have no defining functional group; therefore effecting their dehydrogenation (or any other transformation) regioselectively represents a tremendous challenge.¹

α -Olefins² are particularly desirable intermediates or precursors for a number of reactions or products. Accordingly, dehydrogenation of *n*-alkanes with regioselectivity for the terminal position would be particularly useful. Such a reaction, however, involves cleavage of the strongest bond of an *n*-alkane (the primary C-H bond) to give the thermodynamically least stable double-bond isomer. We were therefore very pleased, several years ago, to discover that pincer-iridium complexes (ⁱPr⁴PCP)Ir and (^tBu⁴PCP)Ir in fact catalyzed *n*-alkane dehydrogenation with high selectivity for the terminal position³ (eq 1; the catalyst precursors are dihydrides, tetrahydrides, or olefin complexes, but no significant differences among them in catalytic activity have ever been observed.⁴) It was noteworthy that this selectivity was common to both of these complexes, despite the very large difference in their degree of crowding at the metal center.³ We presumed that this was related to the regioselectivity for the primary position of *n*-alkanes displayed by late transition metal complexes capable of oxidatively adding C-H bonds.⁵ Unfortunately,

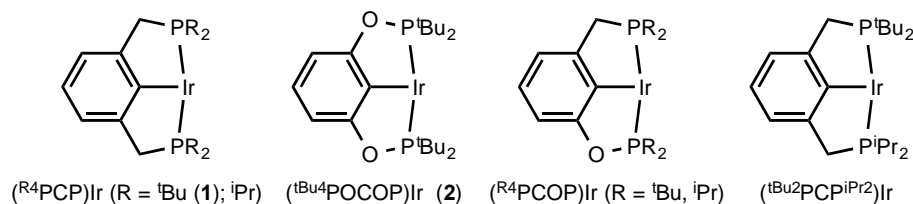
however, subsequent double-bond isomerization precluded the build-up of high concentration of the desirable α -olefin kinetic product.³



(1)

Since these initial reports we have exploited these dehydrogenation catalysts for a number of reactions,⁴ including incorporating dehydrogenation, in tandem with olefin metathesis, into a cycle for catalytic alkane metathesis (AM).⁶⁻⁸ Dehydrogenation at the terminal position would be expected to lead to C_{2n-2} *n*-alkane plus ethane in such a cycle. Accordingly, when (^tBu⁴PCP)Ir (**1**) was used as dehydrogenation co-catalyst we found that metathesis of *n*-hexane gave *n*-decane as the major product.^{6,7} The selectivity was much lower than the kinetic regioselectivity found for dehydrogenation but this could be attributed to olefin isomerization occurring prior to metathesis. In marked contrast, when the dehydrogenation co-catalyst was the bis-phosphinite complex (^tBu⁴POCOP)Ir (**2**; Scheme 1), *n*-decane was found to be the *least* abundant of the heavy products potentially resulting from metathesis of *n*-hexane. A priori, this could be attributed to more rapid olefin isomerization in the case of **2**. Control experiments, however, indicated that **2** was no more effective as an olefin isomerization catalyst than **1**.⁹

Scheme 1. Bis-phosphinite and hybrid phosphine-phosphinite pincer catalysts used in this work.



In view of the importance of selectivity in the AM reaction, and dehydrogenation-based reactions in general, we decided to conduct an in-depth comparative study of the regioselectivity of dehydrogenation (independent of AM) by the two seemingly similar catalysts, **1** and **2**, as well as derivatives thereof; our goal was to obtain insight into the fundamental factors determining dehydrogenation regioselectivity. Herein we report the results of such a study, including an entirely unanticipated explanation for the large variations in regioselectivity found among these catalysts.

Result and Discussion

Direct determination of regioselectivity. The regioselectivity of *n*-octane dehydrogenation by **1** was investigated using 1-hexene as hydrogen acceptor. An α -olefin was chosen as acceptor so that it could be assumed that the transfer of hydrogen from *n*-octane to **1** would be followed by hydrogenation of the acceptor, rather than back-reaction of **1-H2** with octene, as long as α -olefin is present in excess over the octene product. (The back-reaction/hydrogenation of octenes at early reaction times would misleadingly influence the apparent regioselectivity for the production of free octene.)

In qualitative agreement with previously reported results,³ it is clear from the data shown in Figure 1 that the selectivity for dehydrogenation at the terminal position of *n*-octane is quite high. The ratio of internal alkenes to 1-alkene product increases over time due to isomerization, but using the modeling program COPASI¹⁰ the results can be fit to a

relative kinetic selectivity for the terminal position (the initial rate of formation of 1-alkene over the rate of formation of total alkene) of >96%.

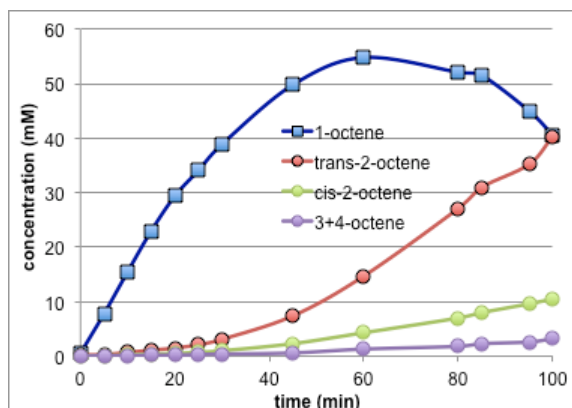


Figure 1. *n*-octane/1-hexene transfer dehydrogenation catalyzed by **1** (2.5 mM) at 125 °C.

Steric crowding at the metal center is probably the most obvious explanation, a priori, for the regioselective dehydrogenation of the terminal position. We therefore synthesized and investigated the selectivity of the much less crowded species (^tBu₂PCPⁱPr₂)Ir. The terminal regioselectivity of this catalyst was determined to be 95% (Figure 2a), equal within experimental error to that obtained from **1** (Figure 1). Even in the case of the very uncrowded complex (ⁱPr₄PCP)Ir, terminal regioselectivity was found to be quite high at 91% (Figure 2b). Thus all (^R₄PCP)Ir catalysts studied are found to be highly regioselective for *n*-alkane dehydrogenation at the terminal position, and regioselectivity is apparently insensitive to the degree of steric crowding.

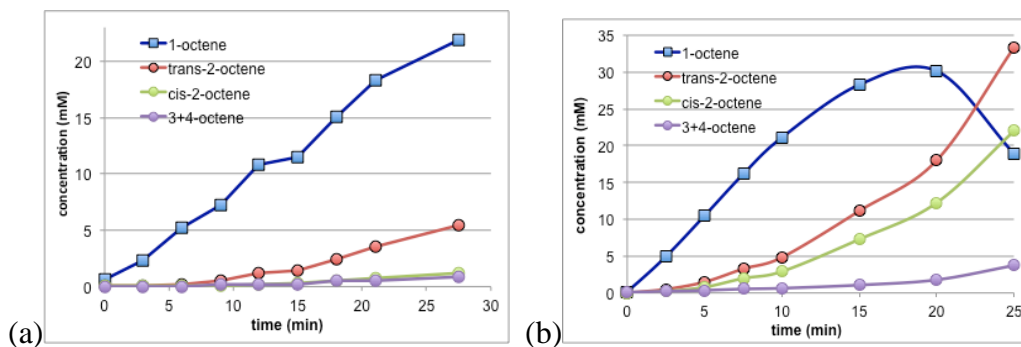


Figure 2. *n*-octane/1-hexene transfer dehydrogenation catalyzed at 125 °C by (a) $(^t\text{Bu}_2\text{PCP}^i\text{Pr}_2)\text{Ir}$ (2.5 mM) and (b) $(^i\text{Pr}_4\text{PCP})\text{Ir}$ (2.5 mM).

In striking contrast to the insensitivity of regioselectivity toward the nature of the phosphinoalkyl groups, substituting an oxygen atom for even one of the two methylene linkers has a dramatic effect on selectivity. *n*-Octane/1-hexene transfer dehydrogenation catalyzed by the hybrid phosphine-phosphinite pincer catalyst $(^t\text{Bu}_4\text{PCOP})\text{Ir}$ affords only ca. 50% selectivity for 1-octene (the remainder being mostly *trans*-2- and *cis*-2-octene). Surprisingly, the less hindered $(^i\text{Pr}_4\text{PCOP})\text{Ir}$ analogue, while significantly less terminal-selective than the $(^R\text{PCP})\text{Ir}$ catalysts, is actually more selective (ca. 80%) for the terminal position than is $(^t\text{Bu}_4\text{PCOP})\text{Ir}$.

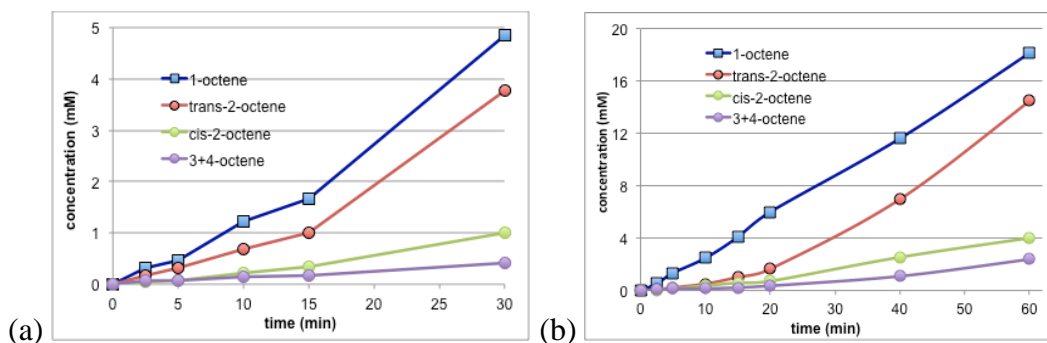


Figure 3. *n*-octane/1-hexene transfer dehydrogenation catalyzed at 125 °C by (a) (${}^t\text{Bu}^4\text{PCOP}$)Ir and (b) catalyzed by (${}^i\text{Pr}^4\text{PCOP}$)Ir (2.5 mM).

Attempts to conduct the analogous experiment using (${}^t\text{Bu}^4\text{POCOP}$)Ir (**2**) were initially much less successful. Although **2** has been reported to be a very good catalyst for cyclooctane/*t*-butylethylene (COA/TBE) transfer dehydrogenation, it was found to be a very poor catalyst for the *n*-octane/1-hexene couple. As seen in Figure 3, for example, using catalyst **1** at 125 °C, 39 mM 1-octene of a total of 44 mM octenes had formed after 30 min. In contrast, with catalyst **2**, no significant formation of 1-octene (< 1 mM) was observed even at 150 °C after 135 min, while the formation of total octenes was only 1.5 mM. During this time, the 1-hexene acceptor had been isomerized such that only 24 mM of the hexene remaining (of a total of 220 mM) was 1-hexene. Thus, double-bond isomerization is fast relative to (the very slow) *n*-alkane/1-alkene transfer dehydrogenation by **2**, and such an experiment cannot reliably give us the regioselectivity of *n*-alkane dehydrogenation by **2**.

We considered that the extremely low level of catalytic activity of **2** was

attributable to strong binding of the 1-hexene acceptor. Accordingly, we used a more sterically hindered acceptor, *trans*-5-decene; the resulting catalytic dehydrogenation of *n*-octane was indeed much faster, although still slow relative to the above experiments with **1**-catalyzed *n*-octane/1-hexene transfer dehydrogenation. After 70 min a total of 32 mM octenes had formed. Even at the earliest reaction time and lowest conversion, 1-octene was not the major product (Figure 4), and the percentage of total octenes represented by 1-octene did not show any systematic variation during this interval. These results thus indicated that (^tBu⁴POCOP)Ir, like (^tBu⁴PCOP)Ir (**2**) but in marked contrast with (^tBu⁴PCP)Ir (**1**), does not regioselectively dehydrogenate the terminal position of *n*-alkanes. Instead, it appears to show some selectivity for dehydrogenation at the C2-C3 position of *n*-octane, while somewhat disfavoring the C3-C4 and C4-5 positions.

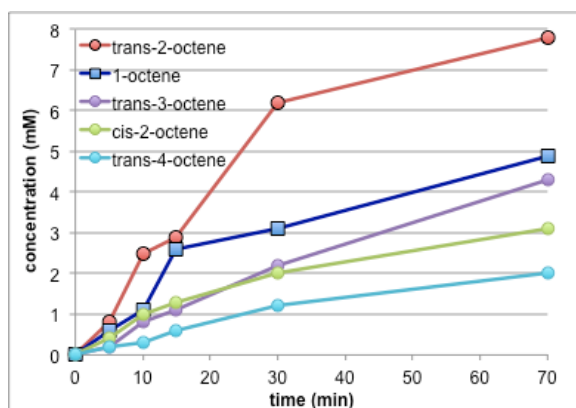


Figure 4. *n*-octane/5-decene transfer dehydrogenation catalyzed by (^tBu⁴POCOP)Ir (1 mM) at 125 °C.

Indirect determination of regioselectivity. The regioselective formation of α -olefin by **1** as well as by $(^t\text{Bu}_2\text{PCP}^{\text{iPr}_2})\text{Ir}$ and $(^{\text{iPr}_4}\text{PCP})\text{Ir}$ was proven by the above experiments, but we wished to further test the possibility that the apparent lack of selectivity by $(^t\text{Bu}_4\text{PCOP})\text{Ir}$, $(^{\text{iPr}_4}\text{PCOP})\text{Ir}$, and especially by **2**, was not due to isomerization of the thermodynamically less stable α -olefin subsequent to its production. In this connection, we conducted two types of experiments, (i) competition between *n*-alkanes and cycloalkanes and (ii) determination of regioselectivity for the reverse reaction, transfer-hydrogenation.

Competition experiments between *n*-alkane and cyclooctane. In order to conduct an intermolecular version of the intramolecular regioselectivity experiments described above we designed a competition experiment between *n*-alkanes and cycloalkane. To most closely model the internal positions of *n*-alkanes we chose a large cycloalkane, cyclododecane (CDA), which is considered to have minimal ring strain¹¹ (Scheme 2).

Dehydrogenation catalyst **1** showed ca. 25:1 selectivity for the initial dehydrogenation of *n*-pentane (to give predominantly 1-pentene at early reaction times) vs. CDA (Figure 5a). The analogous experiments were also conducted with bis-phosphine pincer catalysts $(^t\text{Bu}_2\text{PCP}^{\text{iPr}_2})\text{Ir}$ and $(^{\text{iPr}_4}\text{PCP})\text{Ir}$; these catalysts also exhibited high selectivity for the dehydrogenation of *n*-pentane (also to give predominantly 1-pentene) vs. CDA, ca. 15:1 and 11:1, respectively (Figures 5b and 5c).

Scheme 2

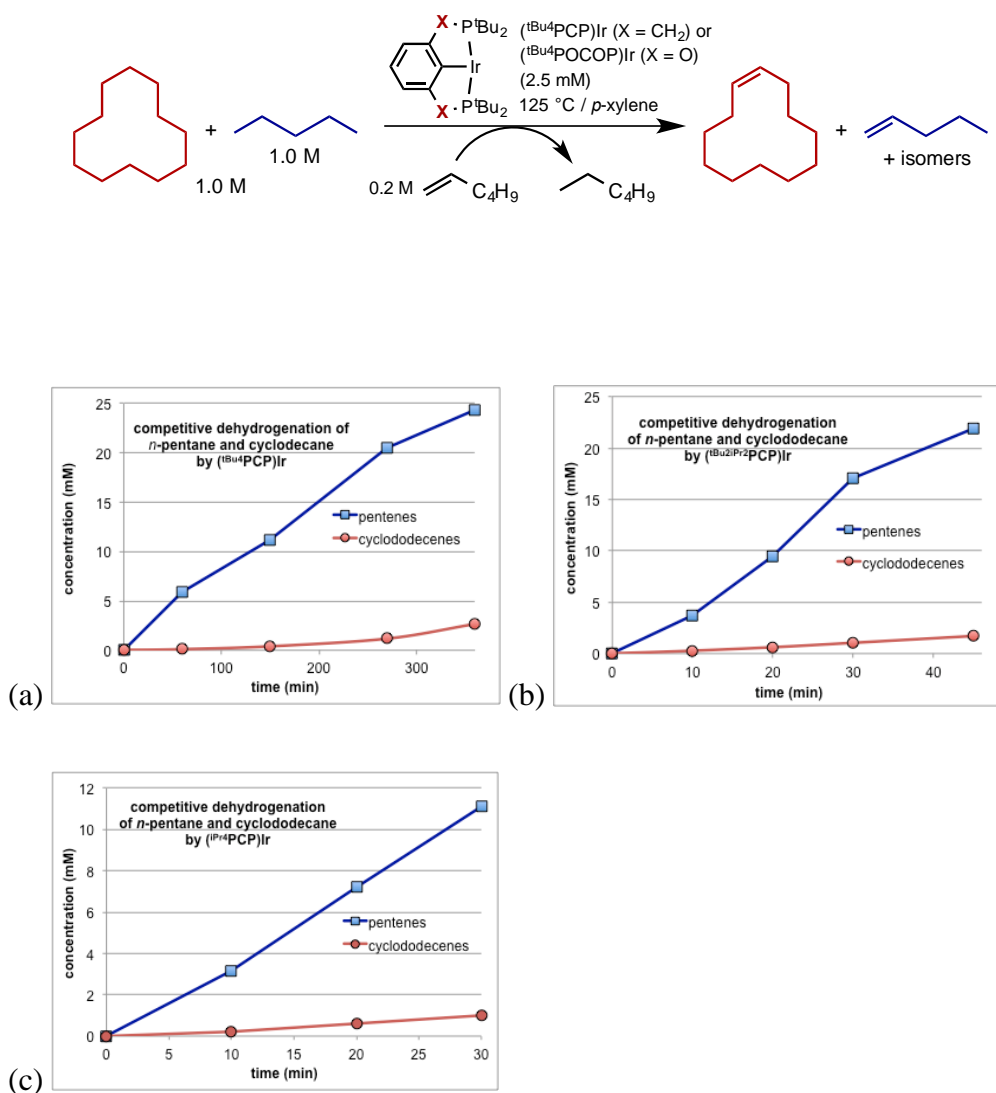


Figure 5. Competition experiments: transfer dehydrogenation of *n*-pentane vs. cyclododecane, 125 °C, catalyzed by (a) (tBu⁴PCP)Ir; (b) (tBu₂iPr₂PCP)Ir and (c) (iPr⁴PCP)Ir.

In very marked contrast, **2** showed slight selectivity for dehydrogenation of cyclododecane (Figure 6a). Thus, the inter-molecular competition experiments are in excellent agreement with the conclusions drawn from the direct determination of

regioselectivity, namely, that the (R^4 PCP)Ir catalysts, but not catalyst **2**, are highly selective for dehydrogenation of the *n*-alkane terminal position vs. internal positions.

Even the hybrid phosphine-phosphinite pincer catalyst (tBu^4 PCOP)Ir exhibited slight selectivity for dehydrogenation of cyclododecane (Figure 6b), indicating that the effect of the O-for-CH₂ linker substitution is a threshold effect, rather than a continuum.

Interestingly, the less bulky (iPr^4 PCOP)Ir catalyst showed slightly greater selectivity for *n*-pentane (Figure 6c) vs. cyclododecane than did (tBu^4 PCOP)Ir. Presumably this is related to its somewhat higher terminal selectivity as compared with (tBu^4 PCOP)Ir in the case of *n*-octane dehydrogenation (Figure 3); likewise, it highlights the point that the selectivity for the terminal alkane position is not predominantly attributable to steric crowding at the iridium center.

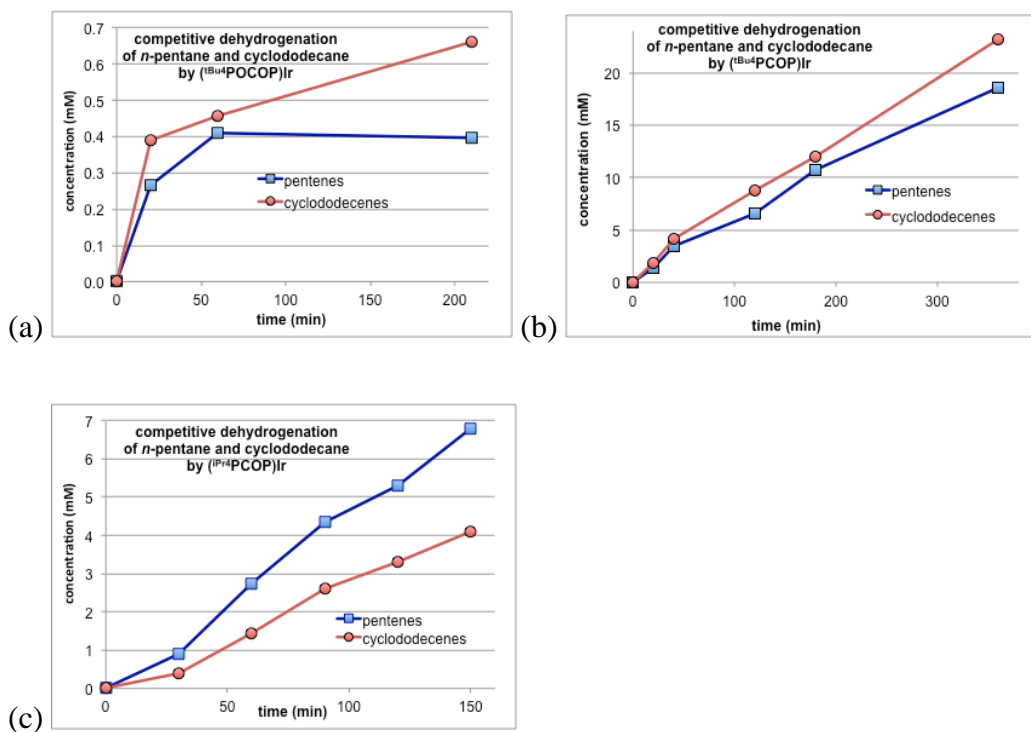


Figure 6. Competition experiments: transfer dehydrogenation of *n*-pentane vs. cyclododecane, 125 °C, catalyzed by (a) (^tBu⁴POCOP)Ir; (b) (^tBu⁴PCOP)Ir and (c) (ⁱPr⁴PCOP)Ir.

Determination of regioselectivity for transfer-hydrogenation. As discussed above, direct determination of regioselectivity for dehydrogenation is complicated by the possibility of rapid isomerization of the olefin product. The same transition state can be investigated in the reverse direction, however, by studying an *inter-molecular* competition between hydrogenation of internal and terminal olefins, thereby avoiding the isomerization problem. As illustrated in Figure 7, the parameter of interest is X, the difference in free energies of activation for dehydrogenation at an internal position ($\Delta G_{\text{int-d}}^{\ddagger}$) vs. dehydrogenation at the terminal position ($\Delta G_{\text{term-d}}^{\ddagger}$). This value is equal to the difference in the corresponding value of ΔG^{\ddagger} for hydrogenation of internal vs. terminal olefins by (pincer)IrH₂, minus the thermodynamic difference between the internal and terminal olefins ($\Delta G^{\circ} = \text{ca. } 2.0 \text{ kcal/mol}$).¹²

$$X = \Delta G_{\text{int-d}}^{\ddagger} - \Delta G_{\text{term-d}}^{\ddagger} = \Delta G_{\text{int-h}}^{\ddagger} - \Delta G_{\text{term-h}}^{\ddagger} - 2.0 \text{ kcal/mol} \quad (2)$$

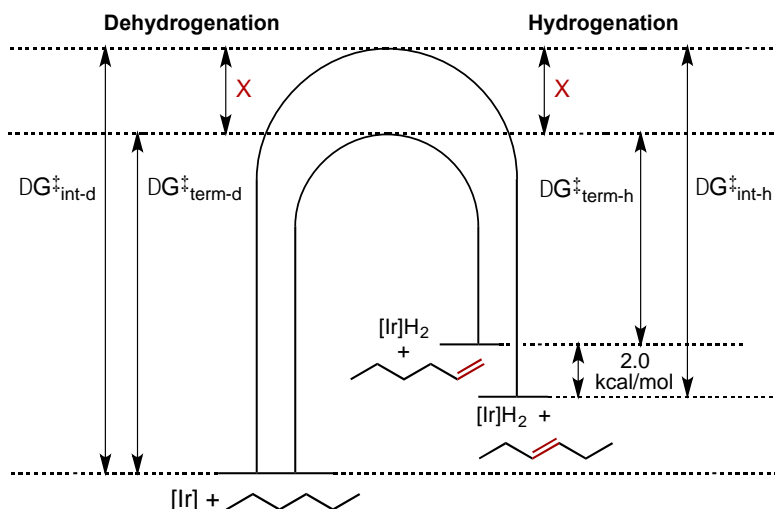


Figure 7. Schematic energy profile illustrating relationships indicated in eq 2.

For these studies we chose to conduct a competition between 1-octene and *trans*-5-decene. By choosing an internal olefin in which the double bond is far removed from the terminus, we minimized the possibility of isomerization to the 1-alkene followed by hydrogenation. The hydrogenation was conducted as a transfer hydrogenation so as to mimic the conditions of the reverse reaction (*n*-alkane transfer dehydrogenation). Cyclooctane (COA) was chosen as the hydrogen donor, since its dehydrogenation is thermodynamically more favorable than that of typical alkanes, thus minimizing the possibility of any back reaction with the resulting alkene product. Since we expected that 1-alkene would be more rapidly hydrogenated than internal (based in part on the reverse rates for dehydrogenation and the more favorable thermodynamics of the *n*-alkane/1-alkene couple in the hydrogenation direction) the experiments were conducted with a ratio of internal to terminal olefin much greater than 1.

A COA stock solution of 1-octene (30 mM) and *trans*-5-decene (600 mM) was prepared, to which was added the (pincer)Ir catalyst to give a concentration of 5 mM,

followed by heating at 100 °C. Catalyst **1** showed very high selectivity for hydrogenation of 1-octene (Figure 8). In spite of the 20:1 excess of *trans*-5-decene:1-octene the ratio of *n*-octane to *n*-decane formed in the reaction after 30 min was ca. 24, indicating a selectivity of ca. $24 \times 20 = 480$, corresponding to $(\Delta G_{\text{int-h}}^{\ddagger} - \Delta G_{\text{term-h}}^{\ddagger}) = \Delta G_{\text{int-h/term-h}}^{\ddagger} = 4.6$ kcal/mol. (We assume that $\Delta S^{\ddagger} \sim 0$ and thus $\Delta G^{\ddagger} \sim \Delta H^{\ddagger}$ which is thus approximately independent of temperature). The analogous experiment with catalyst **2** gave a *n*-octane:*n*-decane ratio of 0.9 ± 0.1 , corresponding to a selectivity of ca. $0.9 \times 20 = 18$ and $\Delta G_{\text{int-h/term-h}}^{\ddagger} = 2.1$ kcal/mol.

Based on these values and equation 2 we calculate that the respective values for $(\Delta G_{\text{int-d}}^{\ddagger} - G_{\text{term-d}}^{\ddagger})$ i.e. the difference in barrier for terminal vs. internal *de*hydrogenation, are 2.6 kcal/mol and 0.1 kcal/mol for catalysts **1** and **2**, respectively. These values correspond to predicted terminal/internal selectivity values for *n*-alkane *de*hydrogenation of 22 : 1 and 1.1 : 1, respectively. We find these results to be in excellent (even if not precisely quantitative) agreement with the results of the direct *de*hydrogenation experiments, confirming the very high terminal *de*hydrogenation selectivity of catalyst **1** and very low selectivity of **2**.

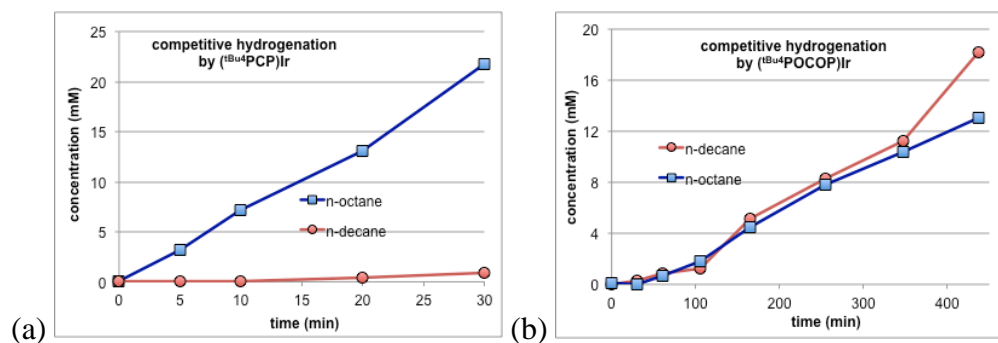
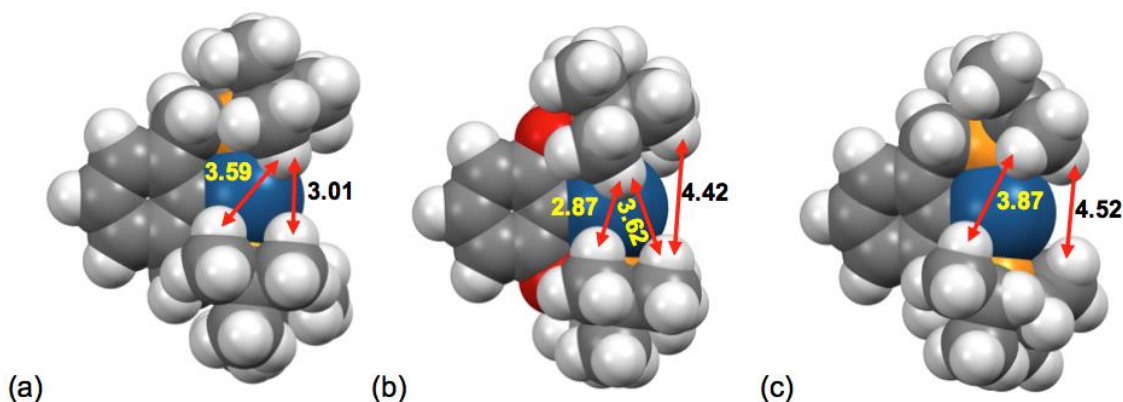


Figure 8. Competition experiments: transfer hydrogenation (100 °C; COA as hydrogen

donor) of 1-octene vs. *trans*-5-decene (1:20) by (a) **1-H₂**; (b) **2-H₂**.

Computational elucidation of the origin of differences in regioselectivity between (pincer)Ir complexes. The above results empirically establish that there is a major difference in the true kinetic regioselectivity between (POCOP)Ir or (PCOP)Ir vs. (PCP)Ir complexes. A priori, the most obvious factor that would favor terminal regioselectivity would be greater steric crowding. Owing to the smaller size of an O atom linker as compared with CH₂, and the greater C-E-P (E = O or CH₂) angle imposed by the O atom linker (114° vs. 108°), the dialkylphosphino groups are “held back” in fragment **2** (C-Ir-P angles are 81.8° and 84.9° in **2** and **1**, respectively) and therefore the degree of crowding at the metal center of **2** is indeed apparently less than in **1**.⁹ Close distances between H atoms of opposing dialkylphosphino groups are shown in Scheme 3.



Scheme 3. Shortest distances between H atoms of the two dialkylphosphino groups in DFT-calculated structures of (a) (^tBu₄PCP)Ir, (b) (^tBu₄POCOP)Ir and (c) (ⁱPr₄PCP)Ir.

Taken out of context, these metrics of **1** and **2** could seem to support a sterics-based explanation for the difference in selectivity between these two catalysts. However, the fact that (ⁱPr₄PCP)Ir shows terminal dehydrogenation selectivity very comparable to that

of **1**, although it is clearly much less crowded (Scheme 3c) than **2**, seems entirely inconsistent with a purely sterics-based explanation. Considering all the pincer complexes studied it is clear that the O linker dramatically disfavors terminal/internal regioselectivity, but not via a simple modulation of crowding at the metal center.

If differential steric effects can apparently be ruled out as the major source of the differences in regioselectivity, then the experimental results would seem to support an explanation based on electronic effects. We assume however, that differences in the electronic demands of the presumed reaction steps for terminal dehydrogenation vs. internal dehydrogenation would be relatively small; accordingly, it was quite difficult to understand how the subtle differences in the electronic properties engendered by the O vs. CH₂ linkers could account for the striking differences observed in regioselectivity. As will be seen below, however, the problem was resolved through an extensive application of DFT calculations. We focus on ^tBu₄PCP catalyst **1** and ^tBu₄POCOP catalyst **2**. As would be expected, and consistent with experimental results, the relative energies of the PCOP species are intermediate between those of the PCP and POCOP analogues.

We have previously proposed that the catalytic transfer-dehydrogenation cycle proceeds as shown in Figure 9;¹³ all the calculations described herein are consistent with that proposal. While the 14e (pincer)Ir fragment is certainly not the resting state during the catalytic cycle (indeed, we have never succeeded in observing this species in spite of many attempts to do so), it serves as a convenient zero energy point for the stated thermodynamic parameters, particularly since the nature of the resting state should have no effect on the regioselectivity.

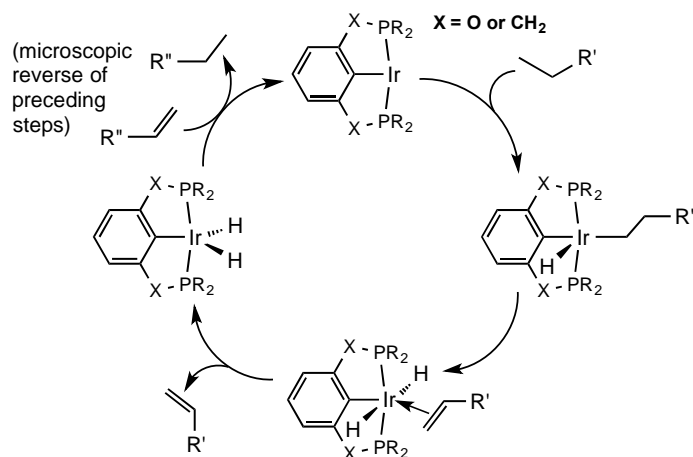


Figure 9. Catalytic cycle for (pincer)Ir-catalyzed transfer dehydrogenation (from reference 13b).

DFT calculations of the reaction of (^tBu⁴PCP)Ir with *n*-hexane indicate that the rate- and selectivity-determining step is β -H elimination by (^tBu⁴PCP)Ir(hexyl)(H) (Figure 10). The β -H elimination transition state (**TS- β -H-elim**) leading to (^tBu⁴PCP)Ir(H)₂(2-hexene) is 5.2 kcal/mol higher in free energy than the lowest TS leading to (^tBu⁴PCP)Ir(H)₂(1-hexene); this value of $\Delta G(\text{TS}_{\beta\text{-H-elim-int}}) - \Delta G(\text{TS}_{\beta\text{-H-elim-term}})$ accounts for (or over-accounts for) the observed regioselectivity.

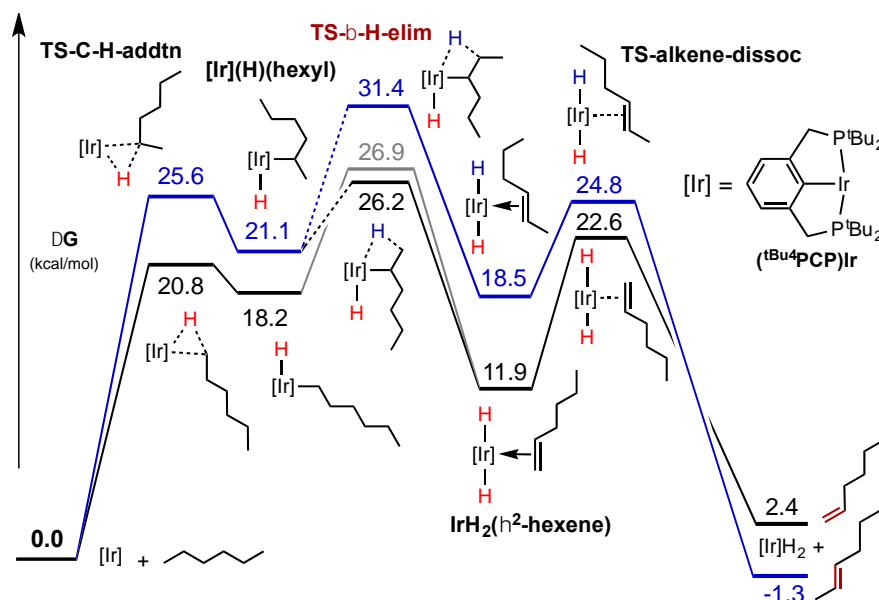


Figure 10. Free-energy diagram for the reaction of $(t\text{Bu}^4\text{PCP})\text{Ir}$ with n -hexane. $[\text{Ir}] =$

$(t\text{Bu}^4\text{PCP})\text{Ir}$. (Lowest-energy isomers of each intermediate or TS are shown.)

C-H addition at the primary position is significantly favored over addition at C2, both kinetically ($\Delta G^\ddagger = 20.8$ kcal/mol and 25.6 kcal/mol, respectively) and thermodynamically ($\Delta G^\circ = 18.2$ kcal/mol and 21.1 kcal/mol, respectively). Surprisingly, however, the lowest-energy TS leading to the 1-hexene complex is a 2,1- β -H-elimination, i.e. elimination at C1 from the secondary (2-hexyl) hydride (although the difference is small at 26.2 kcal/mol vs. 26.9 kcal/mol). *Thus, neither the kinetic nor thermodynamic favorability of C-H addition at the primary position of alkanes is calculated to influence regioselectivity.* Similarly, the most favorable TS leading to the 2-hexene complex is elimination at C2 from the 3-hexyl hydride (31.4 kcal/mol vs. 32.0 kcal/mol for elimination at C3 from the 2-hexyl hydride).

Chemical intuition would suggest that the nature of the linker (O vs. CH₂) could not drastically affect and even change the direction of the difference in energy between TS_{β-H-elim-int} and TS_{β-H-elim-term} ($\Delta G_{\text{TS}_{\beta\text{-H-elim-int/term}}}$). Indeed, the value of $\Delta G_{\text{TS}_{\beta\text{-H-elim-int/term}}}$ for (^tBu⁴POCOP)Ir (5.1 kcal/mol; Figure 11) is found to be essentially identical to that for (^tBu⁴PCP)Ir (5.2 kcal/mol); thus the formation of the 1-alkene dihydride complex is calculated to be strongly favored with either pincer ligand.

The origin of the difference in regioselectivity is revealed by the calculations, however, when the step following β-H-elimination is considered. Whereas β-H-elimination is rate- and selectivity-determining in the case of (^tBu⁴PCP)Ir, *in the case of (^tBu⁴POCOP)Ir the rate- and selectivity-determining step is calculated to be the subsequent step, loss of olefin.* The large difference in the energies of pro-terminal and pro-internal β-H-elimination TSs is thus not relevant for (^tBu⁴POCOP)Ir. Instead, the relevant parameter is the very small difference in free energy of the TS for loss of 1-hexene compared with the TS for loss of 2-hexene (23.0 and 23.3 kcal/mol, respectively), consistent with the very low level of regioselectivity for formation of 1-alkene vs. 2-alkene.

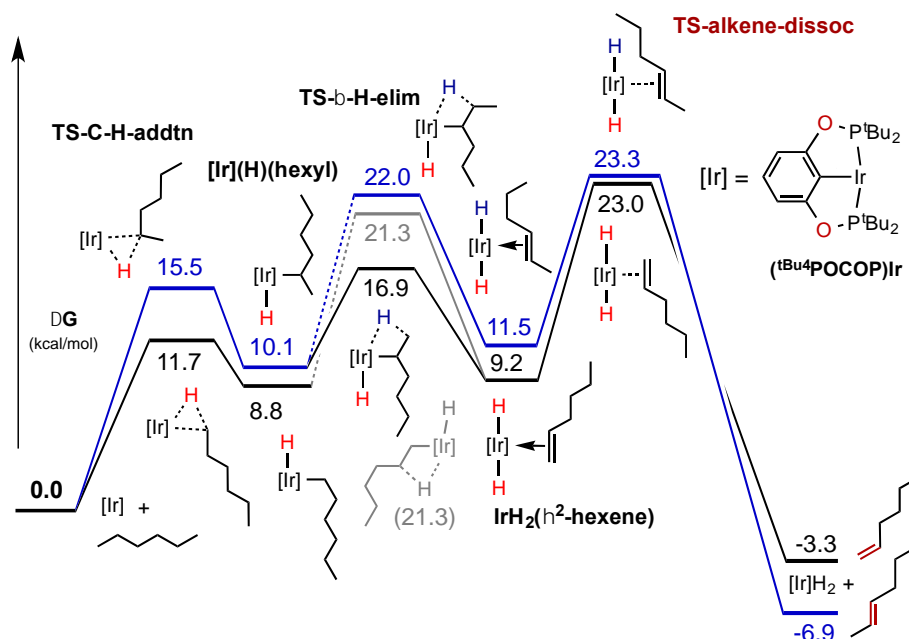


Figure 11. Free-energy diagram for the reaction of $(t\text{Bu}^4\text{POCOP})\text{Ir}$ with n -hexane. $[\text{Ir}] = (t\text{Bu}^4\text{POCOP})\text{Ir}$. (Lowest-energy isomers of each intermediate or TS are shown.)

The fact that such a remarkable difference in selectivity is correctly predicted by the results of the DFT calculations gives us a very high level of confidence in the validity of this explanation. However, it clearly raises the question: What is the underlying origin of the high energy of the TS for olefin dissociation from $(t\text{Bu}^4\text{POCOP})\text{IrH}_2(\text{alkene})$ as compared with the $t\text{Bu}^4\text{PCP}$ analogue?

Origin of the high barriers to loss of olefin from $(\text{pincer})\text{IrH}_2(\text{olefin})$. Generally, barriers to ligand loss are assumed to be closely associated with the thermodynamics of the corresponding metal-ligand bonds. As seen in Figs. 10 and 11, however, the thermodynamics of alkene loss from complexes of $(t\text{Bu}^4\text{POCOP})\text{Ir}$ and $(t\text{Bu}^4\text{PCP})\text{Ir}$ are

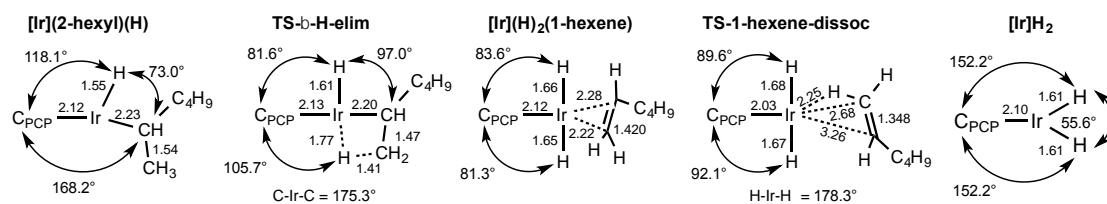
both highly exergonic, and actually more favorable for $(^{\text{tBu}}\text{POCOP})\text{Ir}(\text{1-hexene})$ ($\Delta G = -12.5$ kcal/mol) than for dissociation from $(^{\text{tBu}}\text{PCP})\text{Ir}(\text{1-hexene})$ (-9.5 kcal/mol).

The Ir-alkene Bond Dissociation Enthalpy (BDE) calculated for *trans*- $(^{\text{tBu}}\text{PCP})\text{IrH}_2(\text{1-hexene})$ is 7.8 kcal/mol while that for *trans*- $(^{\text{tBu}}\text{POCOP})\text{IrH}_2(\text{1-hexene})$ is 5.6 kcal/mol. The kinetic enthalpic barriers (ΔH^\ddagger) to olefin loss, however, are significantly greater. The calculated value of ΔH^\ddagger is 12.9 kcal/mol for the $^{\text{tBu}}\text{PCP}$ complex. Most importantly, the value calculated for $(^{\text{tBu}}\text{POCOP})\text{IrH}_2(\text{1-hexene})$ is 4.0 kcal/mol greater, at 16.9 kcal/mol, although as noted above the Ir-olefin BDE is 2.2 kcal/mol less than that of the $^{\text{tBu}}\text{PCP}$ analogue.

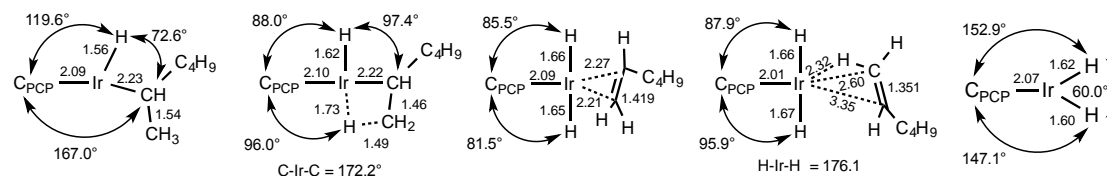
The origin of these high kinetic barriers to olefin loss can be traced to the geometry of the product. As predicted and explained in pioneering work by Eisenstein¹⁴ the geometry of *trans*- L_2IrXH_2 complexes (which are formally analogous to $(^{\text{R}4}\text{PCP})\text{IrH}_2$ and derivatives) is severely distorted from square pyramidal; a geometry in which the hydride ligands are mutually *trans* would be particularly unfavorable. Completely in accord with that work, we calculate that H-Ir-H angles in **1-H2** and **2-H2** are severely acute, 55.6° and 60.0°, respectively. The coordination geometry of the olefin-dissociation TS resembles that typically expected of a TS for ligand loss, i.e. a geometry similar to that of the bound complex, but with a greatly weakened interaction between the metal and the departing ligand (key metric parameters are shown in Scheme 4.) Indeed, for both complexes, there is little indication of any olefin π -bonding in the TS, the major Ir-olefin bonding being a fairly long σ -C-H bonding interaction. Most importantly, the hydride ligands are situated almost rigorously *trans* (H-Ir-H = ca. 177°) in the olefin dissociation TS, in marked contrast with the very acute H-Ir-H angle in the product. Thus, the TS for

olefin dissociation requires loss of most of the metal-olefin interaction, but realizes none of the benefit of the subsequent relaxation to give the low energy complex with an acute H-Ir-H angle.

Scheme 4. Key metric parameters for *trans*-(pincer)IrH₂(1-hexene), TS for loss of 1-hexene, and product of 1-hexene loss. (a) pincer = ^tBu⁴PCP (b) pincer = ^tBu⁴POCOP



(a) (^tBu⁴PCP)Ir



(b) (^tBu⁴POCOP)Ir

Since the character of **TS-alkene-dissoc** closely resembles that of *trans*-(pincer)IrH₂ plus free olefin, it is of significantly higher energy than that of the actual products, geometrically unconstrained (pincer)IrH₂ plus free olefin. Just as significantly, to the extent this characterization of the **TS-alkene-dissoc** is valid, and in the limit where the Ir-alkene interaction is energetically negligible, if this is the TS for the rate-determining step then the catalyst would necessarily favor formation of the more stable, internal, olefin;

hence this model provides a very direct rationale for the lack of terminal regioselectivity by such catalysts.

Calculations of the other pincer-Ir catalysts investigated in this work predict generally smaller differences between the energies of **TS-C-H-addition**, **TS-β-H-elim** and **TS-alkene-dissoc**. In the case of (ⁱPr⁴PCP)Ir, **TS-β-H-elim** is slightly higher in energy than **TS-alkene-dissociation** for both 1- and 2-hexene formation and the difference in energies of the respective **TS-β-H-elim** isomers is large enough (2.2 kcal/mol) to account for the observed selectivity. However, the TS for secondary C-H addition is actually higher in energy than the TS for β-H-elimination that leads to 2-hexene; thus either one of these TS's may be responsible for the observed regioselectivity. We have not calculated the energetics for the catalysis by (^tBu²PCPⁱPr²)Ir, but assuming that they are somewhere intermediate between the (^tBu⁴PCP)Ir and (ⁱPr⁴PCP)Ir, then olefin dissociation is not rate-determining for any of the three (PCP)Ir complexes.

As would be expected, for the PCOP catalysts, the calculated energies are intermediate between those of the PCP and POCOP catalysts. The small differences in calculated energies of the key TSs makes any calculation-based predictions of their regioselectivity extremely questionable. Nevertheless, the trends unambiguously predict relatively lower energies of **TS-β-H-elim** vs. **TS-alkene-dissociation** as CH₂ linkers are replaced with O atoms. This yields a fairly simple explanation for the highly unexpected effect of the nature of the linkers; we therefore believe this justifies a high level of confidence in this explanation of the differential regioselectivity.

Origin of the different rate-determining steps for reactions of PCP and POCOP

(and PCOP) complexes. The DFT calculations offer an explanation for the different regioselectivity of the different catalysts based upon different rate-determining steps. In this section we address the origin of these differences in the rate-determining steps.

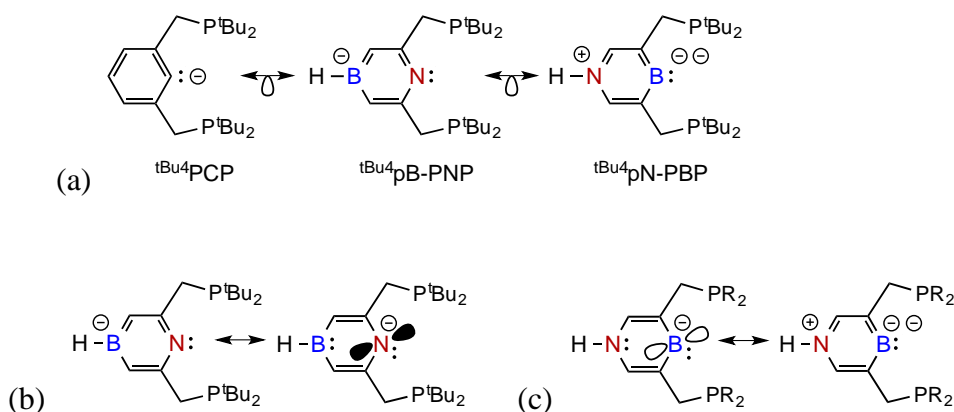
An O linker, bound to the carbon ortho to the metal center, is expected to act as a σ -withdrawing and π -donating group. As a result, the ipso carbon atom bound to Ir is expected to be less σ -donating and more π -electron-rich. The greater σ -donating ability of the Ir-bound carbon of the PCP aryl groups should engender a stronger trans influence. This, in turn, would be expected to favor **TS-alkene-dissoc** relative to **TS- β -H-elim**, as the Ir-bound pincer aryl carbon in **TS-alkene-dissoc** is trans to a very weakly bound (departing) olefin, as opposed to the strong-trans-influence alkyl group at that position in the case of **TS- β -H-elim** (Scheme 4).

In **TS- β -H-elim** there is what may be considered a partially vacant coordination site cis to the pincer ipso carbon. In **TS-alkene-dissoc**, in contrast, the analogous site is occupied by a hydride ligand, which can effectively act as a strong π -donor with respect to ligands situated cis to it.¹⁵ Increased π -electron density at the Ir-bound carbon, due to π -donation by the O linkers in PCOP and POCOP complexes, should therefore favor **TS- β -H-elim** relative to **TS-alkene-dissoc**.

The above reasoning suggests that both the σ -withdrawing and π -donating effects of the O linkers would lower the energy of **TS- β -H-elim** relative to **TS-alkene-dissoc**, in accord with the calculated energies as well as the experimentally observed regioselectivity. We wished to further test this hypothesis that the effects of the linker are electronic and are exerted via the Ir-bound carbon, and therefore sought to design model

compounds in which the nature of the Ir-bound atom was varied without any linker variation. We therefore explored (computationally) the effect of varying atoms within the aromatic ring of the pincer ligand, by conducting calculations on complexes of 1,4-azaborinine-based pincers (Scheme 5), which are isoelectronic with PCP.

Scheme 5. Azaborinine-based pincer complexes with their isoelectronic relationship to PCP indicated (a), and resonance forms (b and c) indicating the respective σ - and π -donating/withdrawing properties of their respective central coordinating atoms.



It would be expected that the coordinating N atom of $(t\text{Bu}^4\text{pB-PNP})\text{Ir}$ would be much less σ -donating than the PCP carbon but much more π -donating; in this sense it would exaggerate the electronic properties of POCOP. This effect is highlighted by the non-aromatic resonance form shown in Scheme 5b.

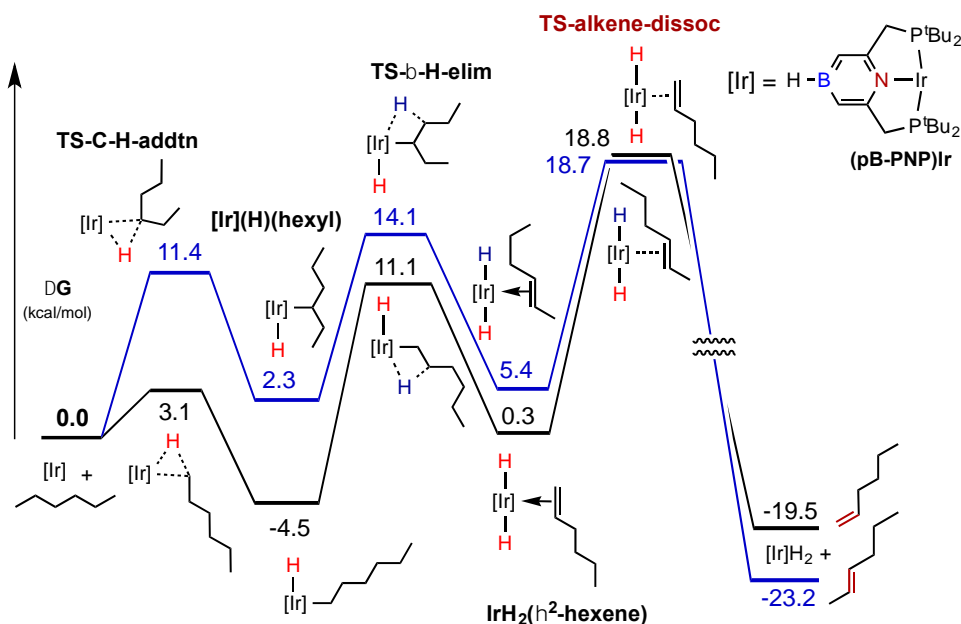


Figure 12. Free-energy diagram for the reaction of $(^{\text{tBu}}_4\text{pB-PNP})\text{Ir}$ with n -hexane. $[\text{Ir}] = (^{\text{tBu}}_4\text{pB-PNP})\text{Ir}$. (Lowest-energy isomers of each intermediate or TS are shown.)

The calculated energy profile shown in Figure 12 is consistent with our hypothesis that greater π -donation and decreased σ -donation by the central coordinating pincer group favors **TS- β -H-elim** relative to **TS-alkene-dissoc** (cf. Figure 10). The alkene dissociation TSs in this case are of higher energy than **TS- β -H-elim** by 7.7 kcal/mol and 4.6 kcal/mol, differences which are significantly greater than those found for $(^{\text{tBu}}_4\text{POCOP})\text{Ir}$. (For example, in the conformationally simplest case, 1,2- β -H-elimination vs. dissociation of the 1-hexene, the difference is 1.7 kcal/mol for the $^{\text{tBu}}_4\text{POCOP}$ complex vs. 7.7 kcal/mol for $(^{\text{tBu}}_4\text{pB-PNP})\text{Ir}$.)

At the other extreme, the B atom of $(^{\text{tBu}}_4\text{pN-PBP})\text{Ir}$ should be a very strong σ -donor but much less π -donating (or more π -withdrawing) than the PCP carbon (as indicated by the non-aromatic resonance form shown in Scheme 5b). Calculations of the catalytic

cycle show a striking reversal in the relative energies of **TS- β -H-elim** relative to **TS-alkene-dissoc**, with the former TSs ca. 15 kcal/mol higher in free energy than the latter, as compared with a ca. 6 kcal/mol difference – in the opposite direction – for (^tBu⁴pN-PBP)Ir.

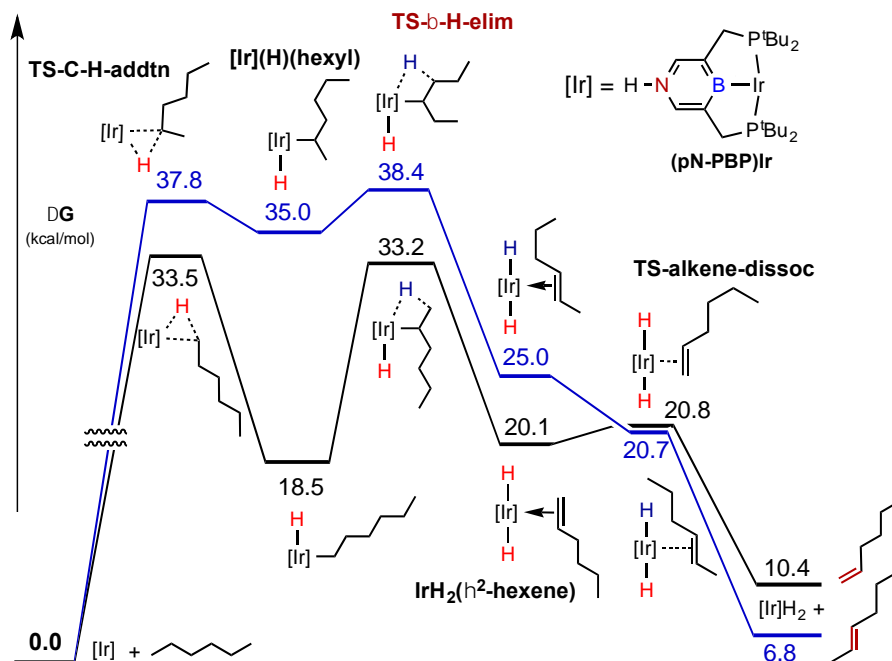


Figure 13. Free-energy diagram for the reaction of (^tBu⁴pN-PBP)Ir with *n*-hexane. [Ir] = (^tBu⁴pN-PBP)Ir. (Lowest-energy isomers of each intermediate or TS are shown.)

We have also examined the more subtle effects of varying substituents on the *para*-carbon of (^tBu⁴PCP)Ir derivatives. Table 1 shows the resulting difference between the calculated free energies of **TS- β -H-elim** (both 1,2- β -H-elimination and 2,1- β -H-elimination) and **TS-1-hexene-dissoc**. Consistent with our hypothesis, π -donating and σ -withdrawing Me₂N and MeO substituents lower the free energy of **TS- β -H-elimination** relative to **TS-1-hexene-dissoc**. The *p*-NO₂ group exerts an effect in the opposite

direction that is much smaller; this may be due to σ - and π -effects acting in opposite directions. As expected, the effects of varying the atoms in the ring are much greater than either varying para-substituents or the linkers/ortho-substituents. In particular, the effect appears to be mostly due to the nature of the coordinating atom; thus the cationic ($^{\text{tBu}}\text{PCNP}$)Ir was calculated to have an energy profile not very different from that of the neutral ($^{\text{tBu}}\text{pB-PNP}$)Ir analogue.

Table 1. $G[\text{TS-}\beta\text{-H-elim}] - G[\text{TS-1-hexene-dissoc}]$. Free energies (kcal/mol) of the TSs for β -H-elimination (1,2- and 2,1-elimination) relative to the TS for dissociation of 1-hexene from (pincer)IrH₂(1-hexene)

Pincer	(1,2)	(2,1)
$^{\text{tBu}}\text{PCP}$	4.4	3.6
MeO- $^{\text{tBu}}\text{PCP}$	1.9	0.6
Me ₂ N- $^{\text{tBu}}\text{PCP}$	1.9	1.2
NO ₂ - $^{\text{tBu}}\text{PCP}$	4.6	3.8
$^{\text{tBu}}\text{POCOP}$	-1.6	-6.1
$^{\text{tBu}}\text{PCOP}$	0.4	-2.6
$^{\text{tBu}}\text{pB-PNP}$	-7.7	-9.3
$^{\text{tBu}}\text{pN-PBP}$	12.4	16.3

The sign of the value of $G[\text{TS-}\beta\text{-H-elim}] - G[\text{TS-1-hexene-dissoc}]$ indicates whether β -H-elimination or olefin dissociation is calculated to be rate-determining in the case of each alkane dehydrogenation catalyst studied. Catalysts with positive values (and thus rate-determining β -H-elimination steps) are predicted to show greater selectivity for dehydrogenation of the terminal position in *n*-alkane than those with negative values. Note, however, that the magnitude of these values does not predict the degree of such selectivity, which is dependent on the difference in energy between **TS- β -H-elim** for 1-alkene formation vs. **TS- β -H-elim** internal alkene formation.

Conclusions

We have demonstrated in this work that (R^4PCP)Ir alkane dehydrogenation catalysts are highly selective for the terminal position of *n*-alkanes, whereas (R^4PCOP)Ir and (R^4POCOP)Ir catalysts (i.e. analogous complexes with one or two O-atom linkers) are much less terminal-selective, or are even selective for the formation of internal olefins. The difference is a genuine kinetic effect, and not due to isomerization of free olefin (although such isomerization does lead, eventually, to predominantly internal olefin with all of the catalysts studied).

DFT calculations reveal that the differences in selectivity between the catalysts investigated are not due to variations in the differences in energy between the pro-terminal and pro-internal TSs *for any given reaction step*; for example, such differences are nearly identical for the two parent complexes studied in this work, (tBu^4PCP)Ir and (tBu^4POCOP)Ir. Instead the different selectivities are attributable to different rate-

/selectivity-determining steps for different catalysts. In particular, for (^tBu⁴PCP)Ir the rate-/selectivity-determining step is β -H-elimination, whereas for (^tBu⁴POCOP)Ir the rate-/selectivity-determining step is loss of the coordinated olefin.

The selectivity exhibited by (^tBu⁴PCP)Ir and other (^R4PCP)Ir complexes derives from a pro-terminal β -H-elimination TS that is of lower energy than the corresponding pro-internal β -H-elimination TS. There are two isomeric pro-terminal TSs leading to 1-alkene complex, β -H-elimination from the 1-alkyl (1,2-elimination) or, from the 2-alkyl (2,1-elimination), products of *n*-alkane C-H addition. Surprisingly, although the initial C-H addition at the primary position to give (pincer)Ir(1-hexyl)(H) is both kinetically and thermodynamically more favorable, the TS for β -H-elimination from (pincer)Ir(2-hexyl)(H) is the TS that is of lower energy in all cases studied. Independently of that point, for all catalysts investigated, both of the β -H-elimination TSs leading to 1-alkene complex are lower than any β -H-elimination TS leading to internal alkene complex. Thus, the 1-alkene dihydride complexes are formed more rapidly than the 2-alkene dihydrides, in all cases studied, including those catalysts that are *not* selective for the formation of free terminal olefin.

In the TS for olefin dissociation, the departing olefin moiety has the character of a fully-formed olefin, while the remaining fragment has a geometry very similar to that found in the fully bound olefin complex trans-(pincer)IrH₂(alkene). In the limiting case where (a) this (simplified) characterization is valid, and (b) the olefin-metal interaction is negligibly weak in this TS, the difference in energy between the pro-terminal and pro-internal olefin-dissociation TSs will be equal to the difference between the terminal and internal olefins, and will thus favor formation of internal olefin.

The Ir-alkene bond in the trans-(pincer)IrH₂(alkene) intermediate is thermodynamically very weak. For example, the bond dissociation enthalpies for (tBu⁴PCP)IrH₂(1-hexene) and (tBu⁴POCOP)IrH₂(1-hexene) are calculated as only 5.1 kcal/mol and 5.6 kcal/mol, respectively, while ΔG° for dissociation is actually calculated to be quite negative (-9.5 kcal/mol and -12.5 kcal/mol, respectively). On that basis, it might be expected that the barrier to olefin loss would be small, and the TS for alkene dissociation from (pincer)IrH₂(alkene) would be much lower in energy than the preceding β -H-elimination TS (which is also the TS for the back reaction, i.e. olefin insertion). However, despite the thermodynamically weak binding, the kinetic barrier to olefin loss is surprisingly high. Importantly, it is higher in the case of the POCOP vs. the PCP catalysts; e.g., $\Delta G^\ddagger = 10.7$ kcal/mol for loss of 1-hexene from (tBu⁴PCP)IrH₂(1-hexene) and 13.8 kcal/mol for (tBu⁴POCOP)IrH₂(1-hexene) (the corresponding values of ΔH^\ddagger are 12.9 kcal/mol and 16.9 kcal/mol).

The experimental results indicate that the differences in selectivity between catalysts is very significant, and is *not* based primarily on steric factors. The calculations indicate that the origin of the low selectivity in the POCOP and PCOP complexes is an outcome of the high kinetic barrier to alkene loss; as a result, formation of the corresponding 1-alkene complexes is reversible and the major alkene eventually liberated is internal. These experimentally and computationally based conclusions are integrated in terms of an electronics-based explanation for an olefin-loss TS that is higher than the TS for β -H-elimination in the case of POCOP and PCOP, but not PCP complexes. Specifically, the O-atom linkers engender an Ir-bound carbon atom that is more π -electron rich and less σ -

donating relative to the Ir-bound carbon of (PCP)Ir; both factors favor an olefin-dissociation rate-determining step.

The barrier to ligand dissociation from transition metal complexes is typically thought to be determined by the corresponding metal-ligand bond strengths. This is found not to be the case in the present systems, and it is shown to have a dramatic and unexpected effect, leading to major differences in regioselectivity among very closely related alkane dehydrogenation catalysts.

References

- (1) (a) Burk, M. J.; Crabtree, R. H.; McGrath, D. V. *J. Chem. Soc., Chem. Commun.* **1985**, 1829-1830. (b) Felkin, H.; Fillebeen-Khan, T.; Holmes-Smith, R.; Lin, Y. *Tetrahedron Lett.* **1985**, 26, 1999-2000. (c) Burk, M. J.; Crabtree, R. H. *J. Am. Chem. Soc.* **1987**, 109, 8025-8032.
- (2) Lutz, E. F. *J. Chem. Educ.* **1986**, 63, 202-203.
- (3) Liu, F.; Pak, E. B.; Singh, B.; Jensen, C. M.; Goldman, A. S. *J. Am. Chem. Soc.* **1999**, 121, 4086-4087.
- (4) Choi, J.; MacArthur, A. H. R.; Brookhart, M.; Goldman, A. S. *Chem. Rev.* **2011**, 111, 1761-1779.
- (5) Some lead references to organometallic C-H addition, with particular emphasis on selectivity: (a) Bennett, J. L.; Vaid, T. P.; Wolczanski, P. T. *Inorg. Chim. Acta.* **1998**, 270(1-2), 414-423 (b) Wick, D. D.; Jones, W. D. *Organometallics* **1999**, 18, 495-505. (c) Asbury, J. B.; Hang, K.; Yeston, J. S.; Cordaro, J. G.; Bergman, R. G.; Lian, T. *J. Am. Chem. Soc.* **2000**, 122, 12870 -12871. (d) Vetter, A. J.; Flaschenriem, C.; Jones, W. D. *J. Am. Chem. Soc.* **2005**, 127, 12315-12322. (e) Balcells, D.; Clot, E.; Eisenstein, O. *Chem. Rev.* **2010**, 110, 749-823.
- (6) Goldman, A. S.; Roy, A. H.; Huang, Z.; Ahuja, R.; Schinski, W.; Brookhart, M. *Science* **2006**, 312, 257-261.
- (7) Haibach, M. C.; Kundu, S.; Brookhart, M.; Goldman, A. S. *Acc. Chem. Res.* **2012**, 45, 947-958.
- (8) Ahuja, R.; Kundu, S.; Goldman, A. S.; Brookhart, M.; Vicente, B. C.; Scott, S. L. *Chem. Commun.* **2008**, 253-255.
- (9) Biswas, S.; Huang, Z.; Choliy, Y.; Wang, D. Y.; Brookhart, M.; Krogh-Jespersen, K.; Goldman, A. S. *J. Am. Chem. Soc.* **2012**, 134, 13276-13295.
- (10) Hoops, S.; Sahle, S.; Gauges, R.; Lee, C.; Pahle, J.; Simus, N.; Singhal, M.; Xu, L.; Mendes, P.; Kummer, U. *Bioinformatics* **2006**, 22, 3067-3074.
- (11) Harnisch, R.; Lauterbach, G.; Pritzkow, W. *Journal für Praktische Chemie/Chemiker-Zeitung* **1995**, 337, 60-62.
- (12) Afeefy, H. Y.; Liebman, J. F.; Stein, S.E. "Neutral Thermochemical Data" in NIST Chemistry WebBook, NIST Standard Reference Database Number 69, Eds. P.J. Linstrom and W.G. Mallard, National Institute of Standards and Technology, Gaithersburg MD, 20899, <http://webbook.nist.gov>, (retrieved January 3, 2015)
- (13) (a) Krogh-Jespersen, K.; Czerw, M.; Kannelberger, M.; Goldman, A. S. *J. Chem. Inf. Comput. Sci.* **2001**, 41, 56-63. (b) Renkema, K. B.; Kissin, Y. V.; Goldman, A. S. *J. Am. Chem. Soc.* **2003**, 125, 7770-7771.
- (14) (a) Jean, Y.; Eisenstein, O. *Polyhedron* **1988**, 7, 405-407. (b) Rachidi, I. E. I.; Eisenstein, O.; Jean, Y. *New J. Chem.* **1990**, 14, 671-677.

- (15) Abu-Hasanayn, F.; Goldman, A. S.; Krogh-Jespersen, K. *Inorg. Chem.* **1994**, 33, 5122-5130.

Computational Details

All electronic structure calculations employed the DFT method¹ and the PBE² exchange-correlation functional. A relativistic, small-core ECP and corresponding basis set were used for the Ir atom (LANL2TZ model);^{3,4} all-electron 6-311G(d) basis sets were applied to all P, N, C and B atoms; 311G basis sets were applied to all H atoms and, in addition, a set of diffuse p-type functions (exponent = 0.75) were placed on all hexane H atoms involved in C-H activation.⁵⁻⁸ Reactant, transition state and product geometries were fully optimized, and the stationary points were characterized further by normal mode analysis. Expanded integration grid sizes (pruned (99,590) atomic grids invoked using the integral=ultrafine keyword) were applied to increase numerical accuracy and stability in both geometry optimizations and normal mode analyses.⁹ The (unscaled) vibrational frequencies formed the basis for the calculation of vibrational zero-point energy (ZPE) corrections; standard thermodynamic corrections (based on the harmonic oscillator/rigid rotor approximations and ideal gas behavior) were made to convert from purely electronic (reaction or activation) energies to (standard) enthalpies (H) and Gibbs free energies (G; P = 1 atm).¹⁰ H, entropy (S), and G were evaluated at two temperatures, T = 25 °C (= 298 K) and T = 125 °C (= 398 K). All energy values quoted in the principal text refer to T = 25 °C. In Supporting Information, we tabulate enthalpies, entropies, and free energies at T = 298 K (P = 1 atm) as well as free energies at T = 398 K (P = 1 atm). The latter T (125 °C = 398 K) approximates the temperature used in the experimental work. All calculations were executed using the GAUSSIAN 09 series of computer programs.¹¹

Table S1. Potential energies, enthalpies, entropies and free energies using PBE functionals for hexane dehydrogenation by (^tBu⁴PCP)Ir.^a

Species	ΔE	ΔH	$\Delta G(298\text{ K})$	ΔS	$\Delta G(398\text{ K})$
[Ir](1-hexene)	-20.5	-18.3	-2.4	-53.3	3.0
[Ir] + <i>n</i> -hexane	0.0	0.0	0.0	0.0	0.0
[Ir]- σ -C1-H	-3.1	-2.2	9.9	-40.5	13.9
[Ir]- σ -C2-H	0.1	1.3	13.1	-39.6	17.1
[Ir]- σ -C3-H	0.1	1.2	13.2	-40.3	17.2
TS-C-H-addtn-C1(-C2)	8.3	7.2	20.8	-45.6	25.3
TS-C-H-addtn-C2(-C1)	12.8	11.3	25.8	-48.8	30.7
TS-C-H-addtn-C2(-C3)	12.2	10.9	25.6	-49.4	30.6
TS-C-H-addtn-C3(-C2)	13.8	12.5	27.6	-50.8	32.7
[Ir](H)(C1) (C1-C2)	4.7	4.1	18.2	-47.4	22.9
[Ir](H)(C2) (C2-C1)	8.8	8.0	22.2	-47.7	27.0
[Ir](H)(C2) (C2-C3)	7.7	6.8	21.1	-47.9	25.9
[Ir](H)(C3) (C3-C2)	9.3	8.9	24.1	-51.0	29.2
TS- β -H-elim-C1-C2	12.5	9.4	26.9	-58.7	32.8
TS- β -H-elim-C2-C1	12.1	9.3	26.2	-56.8	31.9
TS- β -H-elim-C2-C3-E	17.7	14.5	32.0	-58.9	37.9
TS- β -H-elim-C3-C2-E	16.2	13.4	31.4	-60.3	37.4
[Ir]H ₂ (1-hexene)	-3.5	-5.4	11.9	-58.0	17.7
[Ir]H ₂ (2-hexene-E)	2.3	0.5	18.5	-60.6	24.6
TS-dis-1-hexene	11.1	7.5	22.6	-50.6	27.6
TS-dis-2-hexene	14.0	10.5	24.8	-47.9	29.6
[Ir]H ₂ + 1-hexene	6.9	2.4	2.4	-0.1	2.4
[Ir]H ₂ + 2-hexene-E	3.4	-1.2	-1.3	0.2	-1.3

^a Units are kcal/mol for ΔE , ΔH , and ΔG ; units are cal/(deg·mol) for ΔS . The standard state for each species participating in the reaction is P = 1 atm; T = 298.15 K.

Table S2. Potential energies, enthalpies, entropies and free energies using PBE functionals for hexane dehydrogenation by (^tBu⁴POCOP)Ir.^a

Species	ΔE	ΔH	$\Delta G(298\text{ K})$	ΔS	$\Delta G(398\text{ K})$
[Ir](1-hexene)	-29.0	-27.5	-13.3	-47.5	-8.6
[Ir] + <i>n</i> -hexane	0.0	0.0	0.0	0.0	0.0
[Ir]- σ -C1-H	-6.7	-6.3	5.4	-39.1	9.3
[Ir]- σ -C2-H	-5.0	-4.5	6.5	-36.8	10.1
[Ir]- σ -C3-H	-4.2	-3.8	6.9	-35.7	10.4
TS-C-H-addtn-C1(-C2)	0.9	-0.7	11.7	-41.6	15.9
TS-C-H-addtn-C2(-C1)	3.6	1.7	15.5	-46.3	20.2
TS-C-H-addtn-C2(-C3)	4.2	2.5	16.1	-45.8	20.7
TS-C-H-addtn-C3(-C2)	5.0	3.2	17.1	-46.9	21.8
[Ir](H)(C1) (C1-C2)	-3.0	-4.2	8.8	-43.5	13.1
[Ir](H)(C2) (C2-C1)	-1.9	-2.9	10.8	-46.3	15.5
[Ir](H)(C2) (C2-C3)	-2.2	-3.2	10.1	-44.7	14.6
[Ir](H)(C3) (C3-C2)	-0.9	-1.9	11.9	-46.4	16.6
TS- β -H-elim-C1-C2	8.7	5.3	21.3	-53.7	26.7
TS- β -H-elim-C2-C1	4.2	1.0	16.9	-53.4	22.2
TS- β -H-elim-C2-C3-E	9.1	5.7	22.0	-54.8	27.5
TS- β -H-elim-C3-C2-E	10.4	7.1	23.9	-56.1	29.5
[Ir]H ₂ (1-hexene)	-5.4	-7.5	9.2	-55.9	14.8
[Ir]H ₂ (2-hexene-E)	-2.9	-5.1	11.5	-55.9	17.1
TS-dis-1-hexene	13.3	9.4	23.0	-45.5	27.5
TS-dis-2-hexene	13.6	9.6	23.3	-45.8	27.9
[Ir]H ₂ + 1-hexene	2.8	-1.9	-3.3	4.4	-3.7
[Ir]H ₂ + 2-hexene-E	-0.6	-5.5	-6.9	4.7	-7.4

^a Units are kcal/mol for ΔE , ΔH , and ΔG ; units are cal/(deg·mol) for ΔS . The standard state for each species participating in the reaction is P = 1 atm; T = 298.15 K.

Table S3. Potential energies, enthalpies, entropies and free energies using PBE functionals for hexane dehydrogenation by (^tBu⁴PCOP)Ir.^a

Species	ΔE	ΔH	$\Delta G(298\text{ K})$	ΔS	$\Delta G(398\text{ K})$
[Ir](1-hexene)	-24.0	-21.9	-6.3	-52.2	-1.1
[Ir] + <i>n</i> -hexane	0.0	0.0	0.0	0.0	0.0
[Ir]- σ -C1-H	-4.3	-3.5	9.0	-41.7	13.1
[Ir]- σ -C2-H	-1.8	-1.1	9.6	-35.8	13.2
[Ir]- σ -C3-H	-2.0	-1.3	9.8	-37.3	13.6
TS-C-H-addtn-C1(-C2)	4.9	3.7	17.2	-45.1	21.7
TS-C-H-addtn-C2(-C1)	7.9	6.5	21.2	-49.2	26.1
TS-C-H-addtn-C2(-C3)	8.0	6.6	21.3	-49.3	26.2
TS-C-H-addtn-C3(-C2)	9.3	8.0	23.2	-51.0	28.3
[Ir](H)(C1) (C1-C2)	1.3	0.7	14.6	-46.7	19.3
[Ir](H)(C2) (C2-C1)	3.4	2.7	17.0	-48.3	21.9
[Ir](H)(C2) (C2-C3)	2.3	1.7	16.4	-49.3	21.3
[Ir](H)(C3) (C3-C2)	4.3	3.7	18.5	-49.6	23.5
TS- β -H-elim-C1-C2	11.0	8.0	25.2	-57.7	31.0
TS- β -H-elim-C2-C1	8.2	5.5	22.3	-56.4	27.9
TS- β -H-elim-C2-C3-E	13.0	9.9	26.9	-57.3	32.7
TS- β -H-elim-C3-C2-E	14.0	11.3	28.7	-58.3	34.5
[Ir]H ₂ (1-hexene)	-4.2	-6.1	11.5	-58.9	17.4
[Ir]H ₂ (2-hexene-E)	-0.2	-2.2	15.7	-59.9	21.7
TS-dis-1-hexene	13.6	10.0	24.8	-49.7	29.8
TS-dis-2-hexene	13.7	10.2	24.7	-48.8	29.6
[Ir]H ₂ + 1-hexene	4.9	0.5	0.3	0.7	0.2
[Ir]H ₂ + 2-hexene-E	1.5	-3.1	-3.4	1.0	-3.5

^a Units are kcal/mol for ΔE , ΔH , and ΔG ; units are cal/(deg·mol) for ΔS . The standard state for each species participating in the reaction is P = 1 atm; T = 298.15 K.

Table S4. Potential energies, enthalpies, entropies and free energies using PBE functionals for hexane dehydrogenation by (ⁱPr₄PCP)Ir.^a

Species	ΔE	ΔH	$\Delta G(298\text{ K})$	ΔS	$\Delta G(398\text{ K})$
[Ir](1-hexene)	-31.1	-29.9	-15.7	-51.0	-9.6
[Ir] + <i>n</i> -hexane	0.0	0.0	0.0	0.0	0.0
[Ir]- σ -C1-H	-8.4	-7.8	4.7	-42.1	9.0
[Ir]- σ -C2-H	-6.9	-6.2	5.9	-40.8	10.0
[Ir]- σ -C3-H	-6.3	-5.5	7.2	-42.5	11.4
TS-C-H-addtn-C1(-C2)	1.2	-0.4	13.7	-47.3	18.5
TS-C-H-addtn-C2(-C1)	3.7	1.8	16.6	-49.8	21.6
TS-C-H-addtn-C2(-C3)	3.9	2.1	17.0	-50.1	22.0
TS-C-H-addtn-C3(-C2)	4.5	2.7	17.9	-51.1	23.0
[Ir](H)(C1) (C1-C2)	-2.1	-3.1	11.7	-49.7	16.7
[Ir](H)(C2) (C2-C1)	-2.1	-3.3	11.6	-49.7	16.5
[Ir](H)(C2) (C2-C3)	-1.0	-2.2	12.4	-49.2	17.3
[Ir](H)(C3) (C3-C2)	-0.6	-1.9	12.9	-49.5	17.8
TS- β -H-elim-C1-C2	0.9	-2.7	14.0	-56.0	19.6
TS- β -H-elim-C2-C1	-0.6	-4.2	13.0	-57.6	18.8
TS- β -H-elim-C2-C3-E	2.6	-1.2	16.2	-58.3	22.0
TS- β -H-elim-C3-C2-E	3.0	-0.7	16.9	-59.0	22.8
[Ir]H ₂ (1-hexene)	-14.7	-17.3	0.1	-58.2	5.9
[Ir]H ₂ (2-hexene-E)	-11.9	-14.6	3.1	-59.3	9.0
TS-dis-1-hexene	2.9	-1.4	13.7	-50.6	18.7
TS-dis-2-hexene	4.4	0.1	14.5	-48.2	19.3
[Ir]H ₂ + 1-hexene	3.1	-1.6	-0.9	-2.4	-0.6
[Ir]H ₂ + 2-hexene-E	-0.4	-5.1	-4.5	-2.1	-4.3

^a Units are kcal/mol for ΔE , ΔH , and ΔG ; units are cal/(deg·mol) for ΔS . The standard state for each species participating in the reaction is P = 1 atm; T = 298.15 K.

Table S5. Potential energies, enthalpies, entropies and free energies using PBE functionals for hexane dehydrogenation by (ⁱPr⁴POCOP)Ir.^a

Species	ΔE	ΔH	$\Delta G(298\text{ K})$	ΔS	$\Delta G(398\text{ K})$
[Ir](1-hexene)	-36.8	-35.5	-20.5	-50.2	-15.5
[Ir] + <i>n</i> -hexane	0.0	0.0	0.0	0.0	0.0
[Ir]- σ -C1-H	-12.5	-12.1	0.2	-41.1	4.3
[Ir]- σ -C2-H	-10.9	-10.5	1.2	-39.1	5.1
[Ir]- σ -C3-H	-10.2	-9.7	2.7	-41.5	6.9
TS-C-H-addtn-C1(-C2)	-6.1	-7.7	5.5	-44.5	10.0
TS-C-H-addtn-C2(-C1)	-4.3	-6.3	8.0	-48.0	12.8
TS-C-H-addtn-C2(-C3)	-3.8	-5.7	8.5	-47.6	13.2
TS-C-H-addtn-C3(-C2)	-3.5	-5.4	9.7	-50.6	14.8
[Ir](H)(C1) (C1-C2)	-9.2	-10.2	3.6	-46.2	8.2
[Ir](H)(C2) (C2-C1)	-10.9	-12.2	2.1	-48.1	6.9
[Ir](H)(C2) (C2-C3)	-11.2	-12.3	1.6	-46.9	6.3
[Ir](H)(C3) (C3-C2)	-10.6	-11.8	3.1	-49.8	8.0
TS- β -H-elim-C1-C2	-8.1	-11.9	5.1	-56.8	10.8
TS- β -H-elim-C2-C1	-8.2	-12.0	4.4	-55.3	10.0
TS- β -H-elim-C2-C3-E	-7.0	-11.0	6.5	-58.6	12.4
TS- β -H-elim-C3-C2-E	-5.2	-9.0	8.8	-59.7	14.8
[Ir]H ₂ (1-hexene)	-18.2	-20.9	-3.9	-57.0	1.8
[Ir]H ₂ (2-hexene-E)	-17.3	-20.1	-2.5	-59.0	3.4
TS-dis-1-hexene	2.3	-2.1	12.1	-47.6	16.9
TS-dis-2-hexene	1.7	-2.7	11.9	-48.8	16.7
[Ir]H ₂ + 1-hexene	-2.1	-6.7	-6.3	-1.3	-6.2
[Ir]H ₂ + 2-hexene-E	-5.6	-10.3	-10.0	-1.0	-9.9

^a Units are kcal/mol for ΔE , ΔH , and ΔG ; units are cal/(deg·mol) for ΔS . The standard state for each species participating in the reaction is P = 1 atm; T = 298.15 K.

Table S6. Potential energies, enthalpies, entropies and free energies using PBE functionals for hexane dehydrogenation by $(iPr_4PCOP)Ir$.^a

Species	ΔE	ΔH	$\Delta G(298\text{ K})$	ΔS	$\Delta G(398\text{ K})$
$[Ir](1\text{-hexene})$	-31.0	-29.7	-15.7	-47.0	-11.0
$[Ir] + n\text{-hexane}$	0.0	0.0	0.0	0.0	0.0
$[Ir]-\sigma\text{-C1-H}$	-5.4	-5.1	6.1	-37.6	9.9
$[Ir]-\sigma\text{-C2-H}$	-3.6	-3.1	8.2	-38.0	12.0
$[Ir]-\sigma\text{-C3-H}$	-3.3	-2.9	8.2	-37.4	12.0
TS-C-H-addtn-C1(-C2)	0.3	-1.7	10.9	-42.1	15.1
TS-C-H-addtn-C2(-C1)	4.5	2.5	16.1	-45.6	20.6
TS-C-H-addtn-C2(-C3)	3.2	1.1	14.8	-45.8	19.4
TS-C-H-addtn-C3(-C2)	5.7	3.7	17.1	-45.0	21.6
$[Ir](H)(C1)(C1-C2)$	-1.5	-2.9	9.6	-42.1	13.8
$[Ir](H)(C2)(C2-C1)$	-0.7	-1.9	11.4	-44.8	15.9
$[Ir](H)(C2)(C2-C3)$	0.9	-1.0	14.5	-52.3	19.8
$[Ir](H)(C3)(C3-C2)$	0.2	-1.0	12.6	-45.5	17.1
TS- β -H-elim-C1-C2	2.5	-1.0	15.3	-54.5	20.7
TS- β -H-elim-C2-C1	0.0	-3.5	12.1	-52.3	17.3
TS- β -H-elim-C2-C3-E	4.5	0.9	17.6	-56.1	23.2
TS- β -H-elim-C3-C2-E	3.6	0.0	16.4	-55.0	21.9
$[Ir]H_2(1\text{-hexene})$	-9.6	-12.0	4.1	-53.9	9.5
$[Ir]H_2(2\text{-hexene-E})$	-8.4	-11.0	5.7	-56.0	11.3
TS-dis-1-hexene	5.4	1.2	15.9	-49.2	20.8
TS-dis-2-hexene	6.4	2.1	16.6	-48.7	21.5
$[Ir]H_2 + 1\text{-hexene}$	7.5	3.1	2.7	1.2	2.6
$[Ir]H_2 + 2\text{-hexene-E}$	4.1	-0.5	-1.0	1.5	-1.1

^a Units are kcal/mol for ΔE , ΔH , and ΔG ; units are cal/(deg·mol) for ΔS . The standard state for each species participating in the reaction is $P = 1\text{ atm}$; $T = 298.15\text{ K}$.

Table S7. Potential energies, enthalpies, entropies and free energies using PBE functionals for hexane dehydrogenation by (^tBu⁴pB-PNP)Ir.^a

Species	ΔE	ΔH	$\Delta G(298\text{ K})$	ΔS	$\Delta G(398\text{ K})$
[Ir](1-hexene)	-40.5	-38.2	-22.3	-53.6	-16.9
[Ir] + <i>n</i> -hexane	0.0	0.0	0.0	0.0	0.0
[Ir]- σ -C1-H	-11.1	-10.7	2.1	-42.8	6.3
[Ir]- σ -C2-H	-5.3	-4.2	9.2	-45.0	13.7
[Ir]- σ -C3-H	-5.3	-4.3	9.3	-45.3	13.8
TS-C-H-addtn-C1(-C2)	-8.2	-7.6	3.1	-35.9	6.7
TS-C-H-addtn-C2(-C1)	-3.3	-4.3	10.4	-49.1	15.3
TS-C-H-addtn-C2(-C3)	-4.7	-5.6	9.3	-50.0	14.3
TS-C-H-addtn-C3(-C2)	-2.0	-3.0	11.4	-48.1	16.2
[Ir](H)(C1) (C1-C2)	-18.6	-18.7	-4.5	-47.4	0.2
[Ir](H)(C2) (C2-C1)	-12.7	-12.8	1.6	-48.2	6.4
[Ir](H)(C2) (C2-C3)	-14.2	-14.6	-0.3	-47.8	4.5
[Ir](H)(C3) (C3-C2)	-11.9	-12.3	2.3	-48.7	7.1
TS- β -H-elim-C1-C2	-3.5	-6.3	11.1	-58.3	16.9
TS- β -H-elim-C2-C1	-4.9	-7.4	9.5	-56.6	15.2
TS- β -H-elim-C2-C3-E	0.9	-1.9	15.8	-59.2	21.7
TS- β -H-elim-C3-C2-E	-0.9	-3.6	14.1	-59.4	20.1
[Ir]H ₂ (1-hexene)	-16.0	-17.4	0.3	-59.1	6.2
[Ir]H ₂ (2-hexene-E)	-11.2	-12.7	5.4	-60.6	11.4
TS-dis-1-hexene	7.0	3.5	18.8	-51.4	23.9
TS-dis-2-hexene	16.1	12.7	27.9	-51.2	33.1
[Ir]H ₂ + 1-hexene	-16.1	-19.7	-19.5	-0.7	-19.5
[Ir]H ₂ + 2-hexene-E	-19.5	-23.3	-23.2	-0.4	-23.1

^a Units are kcal/mol for ΔE , ΔH , and ΔG ; units are cal/(deg·mol) for ΔS . The standard state for each species participating in the reaction is P = 1 atm; T = 298.15 K.

Table S8. Potential energies, enthalpies, entropies and free energies using PBE functionals for hexane dehydrogenation by $^{(t\text{Bu})_4\text{pN-PBP}}\text{Ir}$.^a

Species	ΔE	ΔH	$\Delta G(298 \text{ K})$	ΔS	$\Delta G(398 \text{ K})$
[Ir](1-hexene)	-5.8	-3.9	12.0	-53.1	17.3
[Ir] + <i>n</i> -hexane	0.0	0.0	0.0	0.0	0.0
[Ir]- σ -C1-H	-0.6	0.6	9.7	-30.4	12.8
[Ir]- σ -C2-H	0.1	1.4	8.7	-24.5	11.2
[Ir]- σ -C3-H	0.0	1.3	7.3	-20.1	9.3
TS-C-H-addtn-C1(-C2)	20.3	18.9	33.5	-48.9	38.4
TS-C-H-addtn-C2(-C1)	26.0	24.4	39.9	-51.9	45.1
TS-C-H-addtn-C2(-C3)	24.9	23.2	37.8	-48.9	42.7
TS-C-H-addtn-C3(-C2)	26.4	24.7	40.5	-53.0	45.8
[Ir](H)(C1) (C1-C2)	4.1	4.0	18.5	-48.6	23.4
[Ir](H)(C2) (C2-C1)	22.9	21.9	37.2	-51.1	42.3
[Ir](H)(C2) (C2-C3)	21.4	20.5	35.0	-48.7	39.9
[Ir](H)(C3) (C3-C2)	21.6	20.4	37.8	-58.6	43.7
TS- β -H-elim-C1-C2	18.5	15.2	33.2	-60.4	39.3
TS- β -H-elim-C2-C1	21.2	19.1	37.1	-60.6	43.2
TS- β -H-elim-C2-C3-E	23.6	20.2	38.4	-61.1	44.5
TS- β -H-elim-C3-C2-E	22.6	19.5	38.2	-62.6	44.4
[Ir]H ₂ (1-hexene)	3.9	1.9	20.1	-61.3	26.3
[Ir]H ₂ (2-hexene-E)	8.6	6.5	25.0	-62.2	31.2
TS-dis-1-hexene	9.5	6.1	20.8	-49.6	25.8
TS-dis-2-hexene	10.7	7.5	23.8	-54.8	29.3
[Ir]H ₂ + 1-hexene	23.7	18.8	19.4	-2.0	19.6
[Ir]H ₂ + 2-hexene-E	20.3	15.2	15.7	-1.7	15.9

^a Units are kcal/mol for ΔE , ΔH , and ΔG ; units are cal/(deg·mol) for ΔS . The standard state for each species participating in the reaction is P = 1 atm; T = 298.15 K.

Computational Section References

1. Koch, W.; Holthausen, M. C. *A Chemist's Guide to Density Functional Theory*; Wiley: New York, 2001.
2. Perdew, J. P.; Burke, K.; Ernzerhof, M. *Phys. Rev. Lett.* **1996**, 77, 3865–3868.
3. Hay, P.J.; Wadt, W.R. *J. Chem. Phys.* **1985**, 82, 299–310.
4. Roy, L. E.; Hay, P. J.; Martin, R. L. *J. Chem. Theory Comput.* **2008**, 4, 1029-1031.
5. Ditchfield, R.; Hehre, W. J.; Pople, J. A. *J. Chem. Phys.* **1971**, 54, 724-728.
6. Hariharan, P. C.; Pople, J. A. *Mol. Phys.* **1974**, 27, 209-214.
7. Raghavachari, K.; Binkley, J. S.; Seeger, R.; Pople, J. A. *J. Chem. Phys.* **1980**, 72, 650-654.
8. McLean, A. D; Chandler, G. S. *J. Chem. Phys.* **1980**, 72, 5639-5648.
9. Frisch, Å; Frisch, M. J.; Clemente, F. R.; Trucks, G. W. *Gaussian 09 User's Reference*, Gaussian, Inc., Wallingford CT, 2009, pp 167.
10. McQuarrie, D. A. *Statistical Thermodynamics*; Harper and Row: New York, 1973.
11. Gaussian 09, Revision D.01, Frisch, M. J.; Trucks, G. W.; Schlegel, H. B.; Scuseria, G. E.; Robb, M. A.; Cheeseman, J. R.; Scalmani, G.; Barone, V.; Mennucci, B.; Petersson, G. A.; Nakatsuji, H.; Caricato, M.; Li, X.; Hratchian, H. P.; Izmaylov, A. F.; Bloino, J.; Zheng, G.; Sonnenberg, J. L.; Hada, M.; Ehara, M.; Toyota, K.; Fukuda, R.; Hasegawa, J.; Ishida, M.; Nakajima, T.; Honda, Y.; Kitao, O.; Nakai, H.; Vreven, T.; Montgomery, J. A., Jr.; Peralta, J. E.; Ogliaro, F.; Bearpark, M.; Heyd, J. J.; Brothers, E.; Kudin, K. N.; Staroverov, V. N.; Kobayashi, R.; Normand, J.; Raghavachari, K.; Rendell, A.; Burant, J. C.; Iyengar, S. S.; Tomasi, J.; Cossi, M.; Rega, N.; Millam, J. M.; Klene, M.; Knox, J. E.; Cross, J. B.; Bakken, V.; Adamo, C.; Jaramillo, J.; Gomperts, R.; Stratmann, R. E.; Yazyev, O.; Austin, A. J.; Cammi, R.; Pomelli, C.; Ochterski, J. W.; Martin, R. L.; Morokuma, K.; Zakrzewski, V. G.; Voth, G. A.; Salvador, P.; Dannenberg, J. J.; Dapprich, S.; Daniels, A. D.; Farkas, Ö.; Foresman, J. B.; Ortiz, J. V.; Cioslowski, J.; Fox, D. J. Gaussian, Inc., Wallingford CT, 2009.

Chapter 3: Computational Study of Double C-H Activation of Biphenyl or Phenanthrene

Majority of this chapter is reproduced with permission from

Single and Double C-H Activation of Biphenyl or Phenanthrene. An Example of C-H Addition to Ir(III) more Facile than Addition to Ir(I)

David A. Laviska, Tian Zhou, Akshai Kumar, Thomas J. Emge,

Karsten Krogh-Jespersen and Alan S. Goldman

Organometallics, **2016**, 35 (11), pp 1613–1623

Copyright © 2016 American Chemical Society

Introduction

Complexes of Ir(I) have played a key role in the development of C-H bond activation chemistry, dating back to the original reports of oxidative addition of alkanes by Bergman¹ and dehydrogenation of alkanes by Crabtree.² More recently, iridium complexes of R^4PCP ($R^4PCP = \kappa^3-C_6H_3-2,6-(CH_2PR_2)_2$) and related pincer ligands have emerged as the most effective class of complexes for the catalytic dehydrogenation of alkanes.^{3,4} This chemistry, as well as a wide range of other reactions including oxidative addition of C-O and C-F bonds,^{5,6} stoichiometric and catalytic cleavage of C-O bonds,^{7,8} catalytic dimerization of acetylenes,⁹ and even olefin isomerization,¹⁰ proceeds via C-H bond oxidative addition by a 14-electron (pincer)Ir(I) fragment.¹¹

The unusual ability of Ir(I) complexes to undergo addition of non-polar bonds has been partly attributed to the central metal atom being particularly electron-rich.¹² In addition, both three-coordinate Ir(I) complexes and the CpIr(I)L fragments originally reported to add alkane C-H bonds¹ feature an electronic configuration with a low-energy empty orbital of sigma symmetry and a high-energy filled orbital of pi-symmetry which, as was explained by Hoffmann, allows a kinetically very facile C-H addition.¹³

Although complexes $(R^4PCP)Ir(alkyl)H$ have never been observed for simple alkyls, the addition of aryl C-H bonds affords adducts that are isolable; however, these five-coordinate d^6 complexes tend to rapidly and reversibly undergo C-H bond elimination.^{14,15} In this contribution, we report unexpected results emerging from a systematic study¹⁵ of C-H bond additions of bicyclic and polycyclic arenes to $(PCP)Ir(I)$. In reactions with phenanthrene or biphenyl, the resulting Ir(III) C-H addition product undergoes an unanticipated second C-H activation. Although far less common than C-H

activation by Ir(I), a substantial number of reports of C-H activation by Ir(III) have been published¹⁶⁻²¹ These examples have generally proven to be less amenable to mechanistic characterization than simple C-H oxidative additions by Ir(I). In this work we also report that the barrier to C-H addition to Ir(III) is calculated to be remarkably low, consistent with the experimental observations.

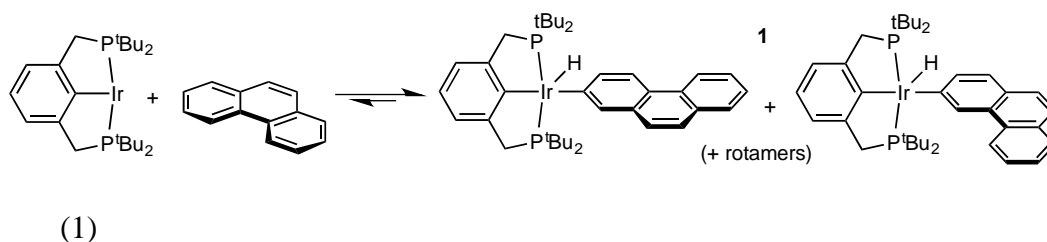
Result and Discussion

Experimental Results. In a J-Young NMR tube at room temperature, 0.010 mmol of (^tBu⁴PCP)IrH₂ (^R4PCP = κ^3 -C₆H₃-2,6-(CH₂PR₂)₂) was dissolved in 0.5 mL of mesitylene-d₁₂ and 2.0 equiv norbornene (NBE; stock solution in *p*-xylene) was added; this is known to yield (^tBu⁴PCP)Ir(NBE),²² a labile complex that gives a broad singlet in the ³¹P NMR spectrum at δ 62.9 ppm.

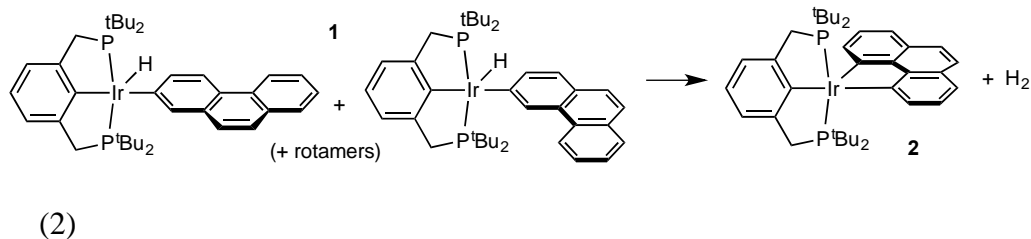
Phenanthrene (1.1 eq; 0.011 mmol) was added to the resulting solution; after shaking for ca. one minute, the solution turned from dark red-orange to bright orange. The ³¹P NMR spectrum of the resulting mixture showed one major peak (95%) at δ 68.3 ppm, in addition to a minor peak at δ 43.1 ppm. A broad hydride (Ir-H) resonance was observed at δ -45.4 ppm, very close to the chemical shift seen for the (^tBu⁴PCP)Ir(aryl)(H) (aryl = phenyl, naphthyl, anthracenyl) complexes,^{14,23} and clearly indicative of the presence of a five-coordinate d⁶ metal complex. As the temperature of the NMR sample was lowered below 10 °C, the hydride (Ir-H) signal at ca. δ -45.4 ppm begins to separate into two distinct resonances. The remainder of the spectrum transformed from an assemblage of fairly broad peaks at room temperature to significantly sharper resonances that are indicative of a non-symmetric environment: ^tBu⁴PCP t-butyl and methylene linker protons were each resolved as multiple inequivalent sets, and signals attributable to η^1 -

phenanthrenyl ligands appear. At -40 °C, the far-upfield signal in the ^1H NMR spectrum resolved into two overlapping triplets at δ -45.39 ppm and δ -45.48 ppm ($J_{\text{HP}} = 13$ Hz). In the ^{31}P NMR spectrum, the resonance at δ 68.3 ppm is partially resolved into two peaks.

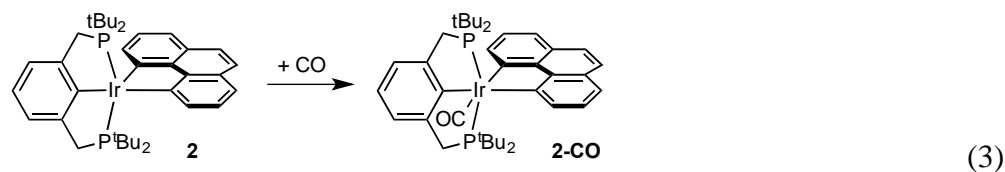
We attribute the major peak(s) in the NMR spectra at δ 68.3 ppm (^{31}P) and δ -45.4 ppm (^1H) to the formation of two closely related C-H activation products; at room temperature, C-H elimination is sufficiently rapid to give substantial broadening of the signals. These results compare with those observed for the complex ($^t\text{Bu}^4\text{PCP}$)IrPhH in benzene solution: at -40 °C, a ^{31}P NMR signal is found at δ 67.7 ppm and a hydride signal at δ -45.55 ppm ($J_{\text{HP}} = 13.5$ Hz), while warming to room temperature results in a symmetrical ligand spectrum and broadening, and then loss of the hydride signal (at ca. 25 °C). Qualitatively, the spectroscopic observations more closely resemble those obtained from the reaction of ($^t\text{Bu}^4\text{PCP}$)Ir with toluene.²⁴ Toluene has two C-H bonds (para and meta to the methyl group) that can easily undergo addition/elimination; the meta isomer generates two possible rotamers with respect to the Ir-tolyl bond, while the ortho C-H bond is too sterically hindered to allow addition. At room temperature, a single very broad hydride ^1H NMR signal and a single ^{31}P NMR signal are observed, while at lower temperatures NMR signals attributable to the three possible isomer/rotamers of toluene addition are resolved. Like toluene, phenanthrene has two sterically unhindered inequivalent aryl C-H bonds. Therefore, we attribute the above observations to the formation of two of the four possible rotamers of 2- and 3-phenanthrenyl iridium hydride complexes (in accord with DFT calculations discussed below) (eq 1), which we collectively refer to as **1**.



Within 24 hours at room temperature the initially minor signal observed at δ 43.1 ppm in the ^{31}P NMR spectrum grew to become the major signal (80%); no corresponding hydride resonance in the ^1H NMR spectrum was observed. After 48 hours, the ^{31}P NMR spectrum showed exclusively this peak at δ 43.1 ppm (with an integral indicating quantitative conversion). This chemical shift is characteristic of a cyclometalated 5-coordinate complex *without* a hydride ligand.²⁵ Broad resonances attributable to the *t*-butyl and methylene groups in the ^1H NMR spectrum indicated a fluxional geometry at room temperature. Both square pyramidal and trigonal bipyramidal geometries should yield sharp, well-defined NMR signals. In the former case, the *t*-butyl and methylene protons would be subjected to very different local magnetic fields due to different placements relative to aromatic rings, leading to two sets of peaks in each case. In the latter case, a single, sharp NMR signal would be seen for the 36 *t*-butyl hydrogens and another for the 4 methylene hydrogens. Since neither of these descriptions match the observed NMR data, we propose the structure shown in eq 2 for complex **2** with the assumption of some degree of fluxional behavior for the bidentate phenanthren-4,5-diyl ligand.



Given that the proposed formulation of **2** is a 16-electron species, we added an atmosphere of CO in an attempt to obtain the corresponding 18-electron adduct. Although CO addition to 16-electron, five-coordinate iridium complexes generally occurs immediately upon mixing,^{14,25} for the conversion of **2** to **2-CO** the diagnostic color change (deep red-orange to bright yellow) observed upon CO addition required several hours to go to completion. Nevertheless, addition of CO was eventually complete, yielding product **2-CO** (eq 3). The NMR spectroscopic properties of **2-CO** are unremarkable for a six-coordinate (PCP)Ir(III) complex, except that the difference between the t-Bu group resonances is very large; the values are δ 1.05 ppm and δ 0.18 ppm ($\Delta\delta$ = 0.87 ppm), indicating a very unsymmetrical environment with respect to aromatic rings. A similar, less pronounced effect is seen for the methylene resonances at δ 3.84 ppm and δ 3.18 ppm ($\Delta\delta$ = 0.66 ppm).



Both complexes **2** and **2-CO** were successfully crystallized by slow evaporation from a mixture of pentane and benzene (4:1 by volume) and their structures were

determined by X-ray crystallography (Figure 1) to be in accord with those proposed on the basis of the NMR studies.

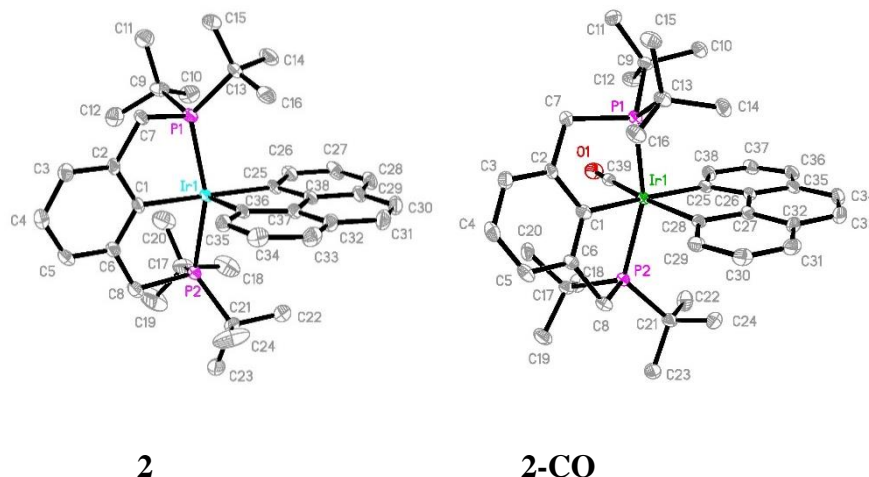


Figure 1. Molecular structures of compounds **2** and **2-CO**. Selected bond lengths (Å) and angles (deg): **2**: Ir(1)-C(1) 2.099(5), Ir(1)-C(25) 2.126(5), Ir(1)-C(36) 2.015(5), Ir(1)-P(1) 2.3379(14), Ir(1)-P(2) 2.3243(14), C(36)-Ir(1)-C(1) 92.25(19), C(36)-Ir(1)-C(25) 82.0(2), C(1)-Ir(1)-C(25) 174.08(19), C(1)-Ir(1)-P(1) 81.66(15), C(1)-Ir(1)-P(2) 82.14(15), P(2)-Ir(1)-P(1) 160.61(5). **2-CO**: Ir(1)-C(39) 1.887(3), Ir(1)-C(1) 2.107(3), Ir(1)-C(28) 2.116(3), Ir(1)-C(25) 2.127(3), Ir(1)-P(1) 2.4008(9), Ir(1)-P(2) 2.3790(8), C(39)-Ir(1)-C(1), 99.76(13), C(1)-Ir(1)-C(28) 92.56(12), C(39)-Ir(1)-C(25) 88.30(13), C(28)-Ir(1)-C(25) 79.46(12), C(1)-Ir(1)-P(1) 79.19(9), C(1)-Ir(1)-P(2) 77.20(9), P(2)-Ir(1)-P(1) 156.31(3).

The X-ray structure of **2** reveals that the coordination geometry is almost ideally square pyramidal. In particular, in the plane bisecting the P-Ir-P axis the relevant angles are $C(PCP)-Ir-C(phen) = 92^\circ$, $C(phen)-Ir-C(phen) = 82^\circ$, and $C(PCP)-Ir-C(phen) = 174^\circ$. The observation of a single (broad) peak at δ 1.23 ppm in the 1H NMR spectrum of **2**, attributable to the t-butyl groups which are inequivalent in the crystal structure, indicates fluxional behavior in solution.

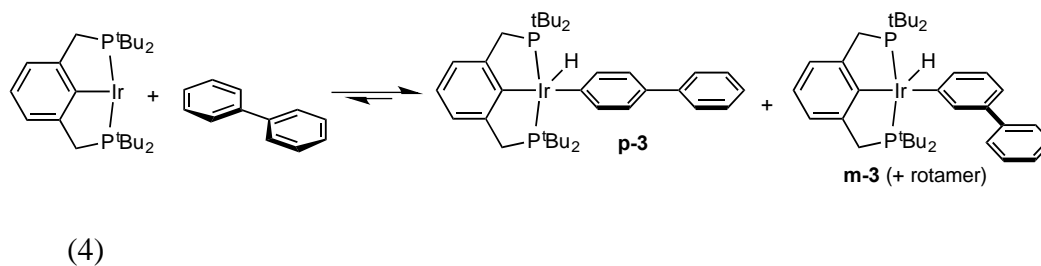
The structure of **2-CO** offers an explanation for the large magnetic inequivalence of the t-Bu groups observed in the NMR experiments (δ 1.05 ppm and δ 0.18 ppm): one t-Bu group on each phosphorus lies essentially over or under the phenanthrene ring system, which should result in an upfield shift in the ^1H NMR resonances, while the remaining two t-Bu groups are located well outside the phenanthrene ring. For the t-butyl groups positioned toward the center of the phenanthrene ring, the distances between methyl groups and the carbon atoms of the central phenanthrene ring (C26 and C27; Figure 1) are as short as 2.5 Å, well below the sum of the van der Waals radii for aryl and methyl groups, and indicating significant and directed H- π interactions.^{26,27}

Biphenyl was found to react with $(^t\text{Bu}^4\text{PCP})\text{IrH}_2$ and NBE; the reaction proceeded for the most part analogously to the reactions with phenanthrene. Complete disappearance of the $(^t\text{Bu}^4\text{PCP})\text{IrH}_2$ signal in the ^{31}P NMR spectrum was accompanied by the appearance of a major signal at δ 68.1 ppm (95%) and a minor signal at δ 42.5 ppm (5%) within 30 min of mixing. The ^1H NMR spectrum at room temperature shows broad signals characteristic of a coordinated $^t\text{Bu}^4\text{PCP}$ ligand. A broad hydride (Ir-H) resonance is observed at δ -45.6 ppm, indicative of a five-coordinate d^6 metal complex and particularly $(^t\text{Bu}^4\text{PCP})\text{Ir}(\text{aryl})(\text{H})$.

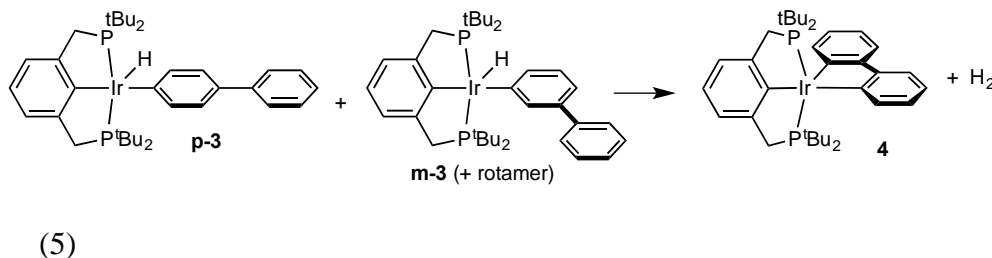
At -20 °C, the far-upfield signal in the ^1H NMR spectrum resolves into three overlapping triplets at δ -45.52 ppm, δ -45.58 ppm, and δ -45.65 ppm ($J_{\text{HP}} = 13.3$ Hz). In the ^{31}P NMR spectrum, the major resonance is partially resolved into three signals at δ 67.7 ppm, δ 67.5 ppm, and δ 67.4 ppm, approximately in a 1:1:1 ratio corresponding to the three hydride signals. The minor ^{31}P NMR signal at δ 42.5 ppm remains sharp at low

temperatures; the remainder of the ^1H NMR is broad and poorly resolved, consistent with the presence of three closely related species.

The major species formed, with highly upfield ^1H NMR resonances, are presumably the products of biphenyl C-H bond addition and, specifically, addition of the para- and meta-C-H bonds (eq 4).

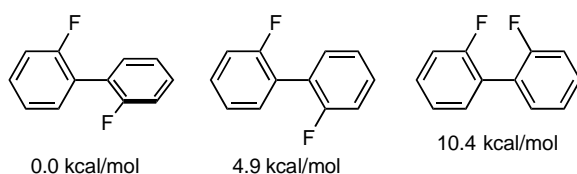


After 24 h at ambient temperature, the resonance at δ 42.5 ppm in the ^{31}P NMR spectrum had grown to represent 65% of the product in solution. Additional NBE acceptor (2 equiv) was added, and after an additional 24 h at ambient temperature, the ^{31}P NMR spectrum showed only a single resonance at δ 42.5 ppm and complete disappearance of any hydride resonances. The NMR data are consistent with cyclometalation to afford product **4** (eq 5), which has been previously identified (and crystallographically characterized) as the product of biphenylene C-C bond addition to $(^t\text{BuPCP})\text{Ir}$.²⁵



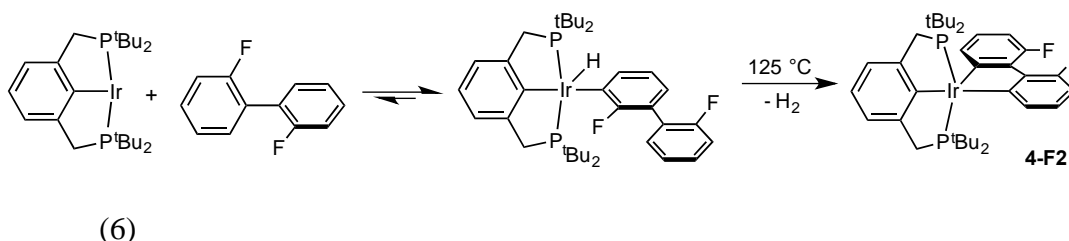
Thus, reactions of (^tBu⁴PCP)Ir, NBE, and either biphenyl or phenanthrene result in rapid C-H activation at the least hindered carbons of the arenes, but the final product results from activation of two hindered C-H bonds (ortho to the inter-ring C-C bond) to yield cyclometalated, five-coordinate Ir(III) complexes.

Note that, in contrast to the planar geometry observed for phenanthrene, the arene rings of free biphenyl are not co-planar in the lowest energy conformation. We calculate (PBE/6-311G(d,p)) that the planar biphenyl conformation (D_{2h} symmetry), which serves as the transition state between equivalent rotational conformers, is only about 3.5 kcal/mol higher in free energy than the minimum structure in which the two rings are canted ca. 40° from co-planarity (C₂ symmetry). We wished to explore a comparable case in which a planar arene conformation (as observed in complexes **4** and **4-CO**) was significantly *higher* in energy and surmised that the species 2,2'-difluorobiphenyl might satisfy this requirement. The minimum energy 2,2'-difluorobiphenyl conformer (C₂ symmetry; twist angle ~ 45°) is 4.9 kcal/mol below the planar conformer in which the two fluorine atoms are *anti* (C_{2h} symmetry; TS). However, the planar conformation required for the double C-H activation and cyclometalation processes requires the F atoms to be mutually *syn* (C_{2v} symmetry; TS) and is computed to be 10.4 kcal/mol higher in energy than the twisted minimum energy conformer.^{28,29}



The reaction of (^tBu⁴PCP)IrH₂ and NBE with 2,2'-difluorobiphenyl at ambient temperature yielded products resulting exclusively from *ortho* C-H activation, in accord

with the known stability of *ortho*-F substituted metal aryl complexes.^{30,31} Consistent with that stability, the sharper peaks in the ¹H NMR spectrum indicated a lower rate of exchange than observed for the unsubstituted biphenyl iridium hydride, **2**. Unlike in the case of the parent biphenyl, even after two hours there was no spectral evidence for cyclometalation. The solution was heated at 75 °C for 24 h at which point the NMR spectrum revealed ca. 5% conversion to a cyclometalated product **4-F2**, indicating a much greater barrier to double C-H activation for 2,2'-difluorobiphenyl than unsubstituted biphenyl. After heating at 125 °C for 24 h, however, NMR analysis showed 75% conversion to **4-F2**, and full conversion to the cyclometalated product was finally observed after an additional 24 h at 125 °C (eq 6).



A single-crystal X-ray structure of complex **4-F2** was obtained (Figure 2). Undoubtedly due to steric repulsion between the F atoms, the biphenyldiyl aromatic rings of complex **4-F2** are significantly distorted from co-planarity; this is most clearly illustrated by the value of the C(29)-C(30)-C(31)-C(32) torsional angle (with C(29) and C(32) bonded to F atoms) which is 19.4°. The distance between the two F atoms is 2.46 Å, well below twice the van der Waals radius for F (1.47 Å).³²

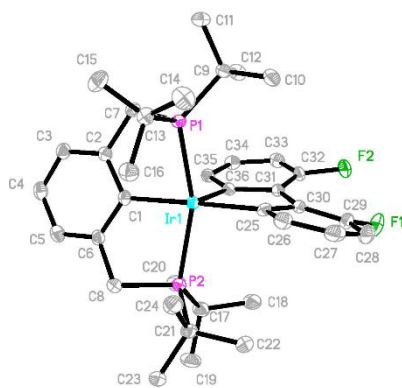
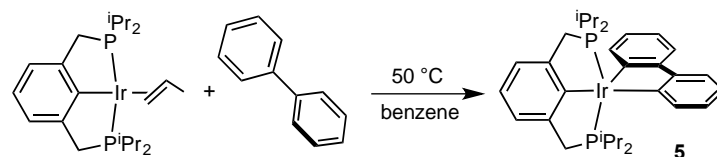


Figure 2. Molecular structure of compound **4-F2**. Selected bond lengths (Å) and angles (deg): Ir(1)-C(36) 1.995(3), Ir(1)-C(25) 2.092(3), Ir(1)-C(1) 2.111(3), Ir(1)-P(1) 2.3062(8), Ir(1)-P(2) 2.3685(8), C(36)-Ir(1)-C(25) 80.23(12), C(36)-Ir(1)-C(1) 98.23(11), C(25)-Ir(1)-C(1) 177.93(11), C(1)-Ir(1)-P(1) 81.20(8), C(1)-Ir(1)-P(2) 81.24(8), P(1)-Ir(1)-P(2) 160.87(3)

The reactivity of biphenyl with ($i\text{Pr}^4\text{PCP}$)Ir, a pincer-ligated fragment less hindered than ($t\text{Bu}^4\text{PCP}$)Ir, was also investigated. Formation of the analogous double C-H addition product was observed, but without the appearance of an observable single-addition intermediate.

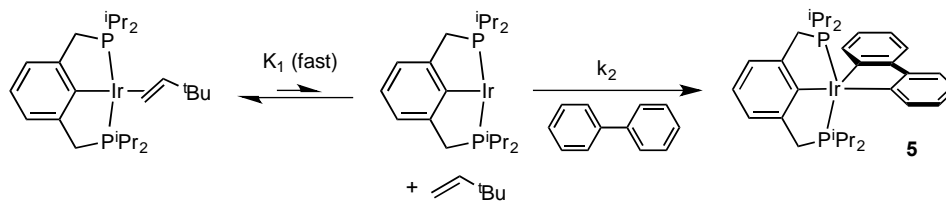


(7)

($i\text{Pr}^4\text{PCP}$)Ir(propene) (50 mM) reacted over ca. 25 hours in p -xylene- d_{10} with biphenyl (50 mM) to give the previously characterized²⁵ cyclometalated complex **5** (eq 7). The reaction with biphenyl in higher concentration (260 mM) proceeded significantly more rapidly (10 mM after 30 min and 50 mM after 12 h), but at an even higher biphenyl concentration (520 mM) the rate of reaction was unchanged. These observations indicate

that the rate limiting step of eq 7 at the higher biphenyl concentrations is loss of propene, and thus the reaction of “(ⁱPr⁴PCP)Ir” to afford the double C-H addition product is in fact much more rapid than the observed rate of formation of **5**.

To obtain a more meaningful lower limit for the reaction rate of the fragment (ⁱPr⁴PCP)Ir with biphenyl, we added H₂ to a solution of (ⁱPr⁴PCP)Ir(propene) (50 mM) in C₆D₆, which resulted in the formation of (ⁱPr⁴PCP)IrH₄. To this solution was added t-butylethylene (TBE, 200 mM). Hydrogenation of 2 mol TBE per mol (ⁱPr⁴PCP)IrH₄ gave a solution of a product presumed to be (ⁱPr⁴PCP)Ir(TBE) which is much more labile than (ⁱPr⁴PCP)Ir(propene), with 50 mM unreacted TBE remaining. Biphenyl (260 mM) was added to this solution at ambient temperature, and within 10 min ¹H NMR spectroscopy revealed the formation of **5** with 85% conversion and the remaining 15% of (ⁱPr⁴PCP)Ir(TBE) unreacted; within 20 min, 100% conversion to **5** was observed. When the reaction kinetics were monitored by NMR spectroscopy at 10 °C, the reaction proceeded to completion with an approximate pseudo-first order rate constant of ca. $5.5 \times 10^{-4} \text{ s}^{-1}$. A kinetic simulation (COPASI³³) assuming a pre-equilibrium loss of TBE from (ⁱPr⁴PCP)Ir(TBE) with equilibrium constant K₁, followed by a second-order reaction of (ⁱPr⁴PCP)Ir with biphenyl with rate constant k₂ (eq 8), gave an excellent fit to the data with K₁•k₂ = $1.34 \times 10^{-4} \text{ s}^{-1}$ (Figure 3). This value corresponds to a standard free energy difference between the TBE complex and the rate-determining transition state (with a composition of (ⁱPr⁴PCP)Ir plus biphenyl) of ΔG = 21.6 kcal/mol.



(8)

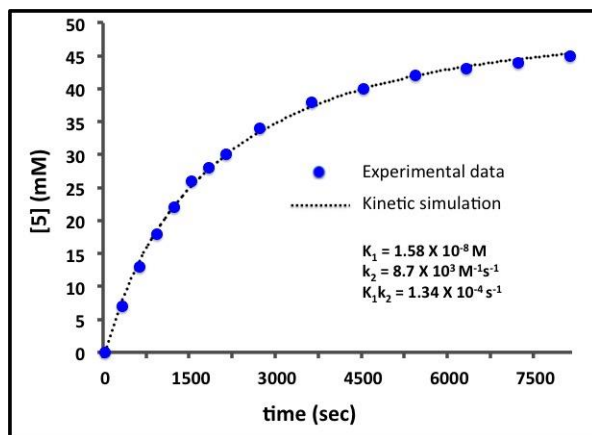


Figure 3. Formation of cyclometalated complex **5** in the reaction of $(i\text{Pr}^4\text{PCP})\text{Ir}(\text{TBE})$ with biphenyl (260 mM) at 10 °C.

Computational results and discussion. The results from DFT electronic structure calculations on the reactions of $(t\text{Bu}^4\text{PCP})\text{Ir}$ (and model pincer complexes) with phenanthrene or biphenyl are fully consistent with and facilitate explaining the experimental observations. We applied the PBE³⁴ functionals and valence basis sets of triple-zeta plus polarization quality (PBE/LANL2TZ+f+spdf/6-311G(d,p)); the pincer ligand retained its bulky $t\text{Bu}$ groups. Enthalpies (H°) and Gibbs free energies (G° ; $T = 298.15 \text{ K}$, $P = 1 \text{ atm}$) were obtained from the electronic energies (E) using standard statistical mechanical expressions. Complete computational details are provided in the Computational Details.

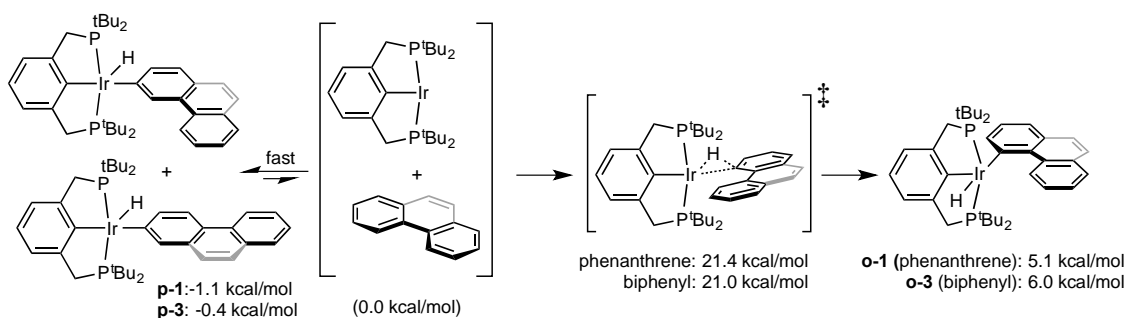
Consistent with the rapid formation of two C-H addition isomers from each of the reactions of (^tBu₄PCP)Ir with phenanthrene and biphenyl, the four C-H bond cleavage transition states (TS's) for eqs 1 and 4 are calculated to be very similar and quite low in free energy, ranging from 10.9 kcal/mol to 11.3 kcal/mol relative to free (^tBu₄PCP)Ir and hydrocarbon. These TS's are only slightly higher (ca. 2-3 kcal/mol) in free energy than the sigma-C-H bond complexes that precede them on the energy surface; the sigma bond complexes are calculated to have enthalpies ca. 4.5 kcal/mol below the free species. The *meta*- and *para*-C-H addition products are calculated to have free energies in the range of -0.1 to -1.1 kcal/mol relative to free (^tBu₄PCP)Ir plus free biphenyl or phenanthrene. The actual free energies for adduct or product formation are undoubtedly lower (more favorable) than the calculated values. The PBE electron density functional is purely local and therefore tends to overstate steric repulsions, since it does not include medium- or long-range correlation energy (and hence omits dispersion interactions).³⁵ Also, in a condensed phase the translational and rotational motions become partially restricted, and the use of (computed) gas phase entropies for bimolecular solution phase reactions thus leads to an overestimation of the unfavorable entropic contribution to the free energy of complex formation.³⁶

For addition of the C-H bonds ortho to the inter-ring C-C bond, the free energy of the TS's are significantly higher than those for addition at the *m*- and *p*-positions: 21.4 kcal/mol and 21.0 kcal/mol relative to (^tBu₄PCP)Ir and hydrocarbon for phenanthrene and biphenyl, respectively, or 22.5 kcal/mol and 21.4 kcal/mol relative to the corresponding *para*-C-H addition products (Scheme 1). However, while these ortho-C-H transition states are significantly higher in free energy than the less hindered C-H addition TS's,

they are not so high as to prohibit the additions from occurring at ambient temperature.

The calculated overall barriers (energies of the TS minus energies of the *para* C-H addition resting states) correspond to rate constants of $1.3 \times 10^{-4} \text{ s}^{-1}$ ($t_{1/2} \sim 5,200 \text{ s}$) and $8.7 \times 10^{-4} \text{ s}^{-1}$ ($t_{1/2} \sim 800 \text{ s}$), respectively, at 22 °C.

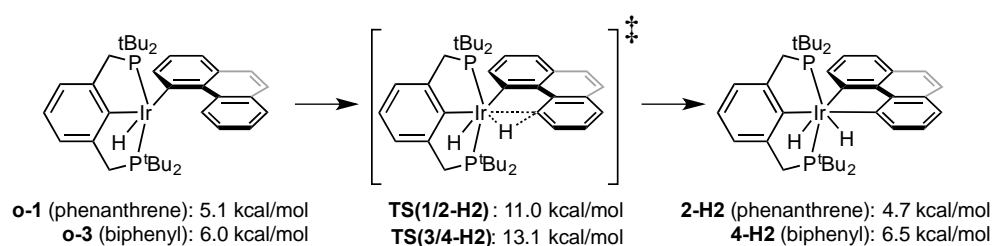
Scheme 1. Conversion of *meta*- and *para*-C-H addition products to *ortho*-C-H addition products, with free energies shown (relative to free species).



The products of *ortho*-C-H addition (**o-1** and **o-3**) are calculated to be 6.2 kcal/mol and 6.4 kcal/mol above the *para*-C-H adducts; thus, the calculations indicate that the *ortho*-C-H addition products would never be present in an observable equilibrium concentration.

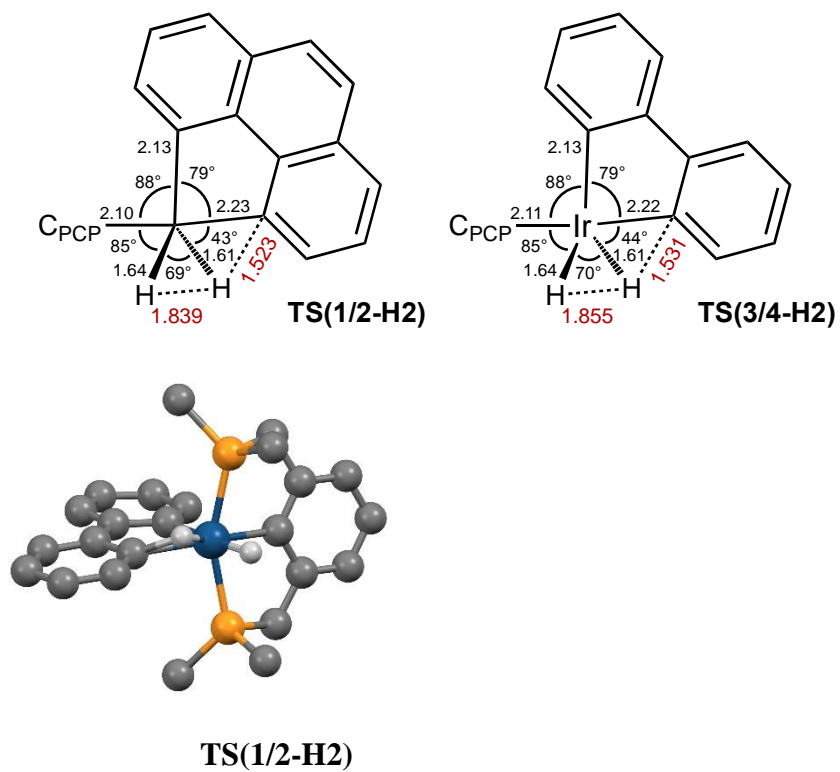
The barrier to the second C-H addition to (^tBu⁴PCP)Ir (eq 9), i.e. the cyclometalation of phenanthrene or biphenyl, is calculated to be remarkably low: $\Delta G^\ddagger = 5.9 \text{ kcal/mol}$ for phenanthrene and $\Delta G^\ddagger = 7.1 \text{ kcal/mol}$ for biphenyl ($\Delta H^\ddagger = 6.1 \text{ kcal/mol}$ and 7.3 kcal/mol , respectively). The transition states (Scheme 2) are structurally quite similar to the products (Scheme 3) with the new Ir-H bonds fully formed (1.61 Å) and the developing Ir-C bond only slightly longer than in the product (ca. 2.23 Å in TS vs 2.14 Å

in product); the C-H distances of ca. 1.53 Å are typical for a C-H bond cleavage TS. The biphenyl group, the iridium atom, and the *ipso*-carbon atom of the ^tBu₄PCP ligand are approximately coplanar, but the H atom undergoing C-H addition is clearly outside that plane (0.68 Å outside the mean plane of the biphenyl carbon atoms). Hence, this TS is perhaps most easily viewed as a hydride migrating to the biphenyl-diyl group, i.e., in terms of the reverse reaction, C-H elimination.

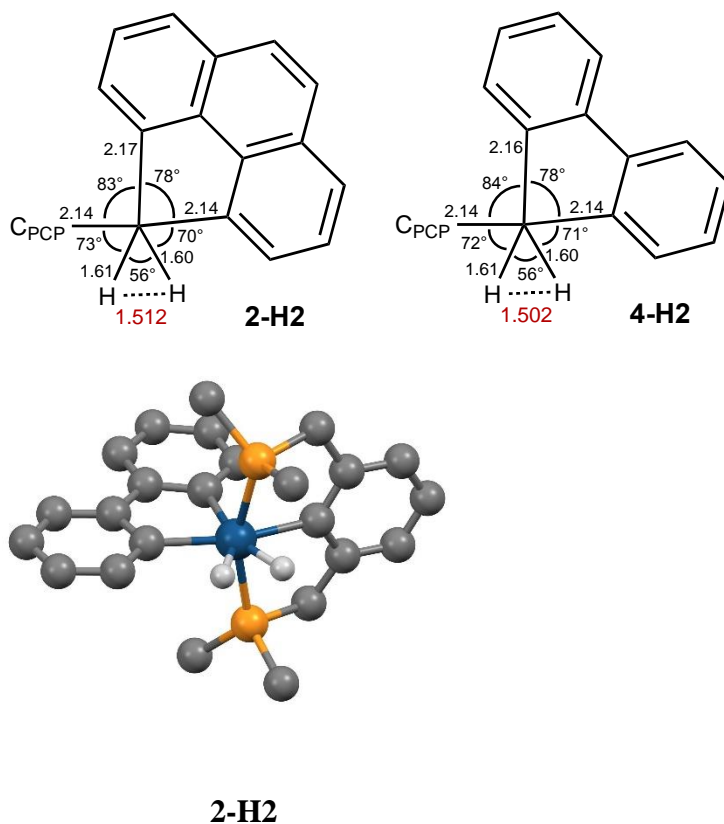


(9)

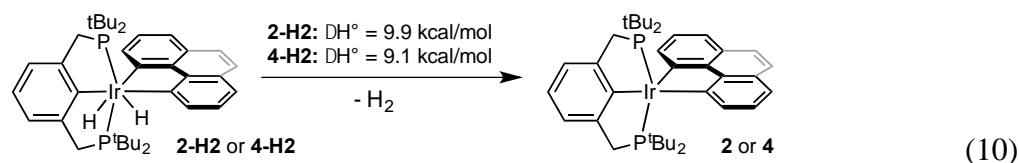
Scheme 2. Calculated bond lengths and angles for atoms in the coordination sphere of TS(1/2-H2) and TS(3/4-H2), and graphic illustration of TS(1/2-H2) (methyl groups and H atoms not bound to Ir omitted for clarity).



Scheme 3. Calculated bond lengths and angles for atoms in the coordination sphere of **2-H₂** and **4-H₂**, and graphic illustration of **2-H₂** (methyl groups, and H atoms not bound to Ir omitted for clarity).



The calculated (thermodynamic) free energies and enthalpies of the addition reaction of eq 9 are close to zero ($\Delta G^\circ_{\text{phen}} = -0.4$ kcal/mol; $\Delta H^\circ_{\text{phen}} = 0.6$ kcal/mol; $\Delta G^\circ_{\text{biph}} = 0.5$ kcal/mol; $\Delta H^\circ_{\text{biph}} = 1.3$ kcal/mol). The calculated distances between the hydrides in products **2-H2** and **4-H2** are ca. 1.51 Å. Accordingly, there is no significant dihydrogen character in either species, and the Ir atom in these products of the second C-H addition may be viewed as being fully oxidized, i.e. Ir(V). The Ir center, the PCP ipso-carbon atom, the hydrides, and the coordinated aryl carbons are all located within 0.001 Å of their mean planes.

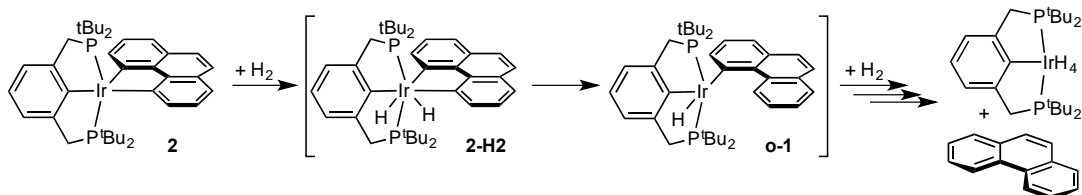


We are unable to locate a conventional transition state for subsequent loss of H_2 from the Ir(V) dihydride intermediates, **2-H2** and **4-H2** (eq 10). If we assume that $\Delta H_{10}^\ddagger \sim \Delta H_{10}^\circ$ (i.e. the back reaction, addition of H_2 to **2** or **4**, has no enthalpic barrier) and, further, assume that $\Delta S_{10}^\ddagger = 0$ for H_2 loss, then the free energy barriers for H_2 loss (“**TS-10**”) are ca. 3 kcal/mol above the TS's of eq 9 for the formation of the dihydrides (**TS(1/2-H2)** and **TS(3/4-H2)**); loss of H_2 (eq 10) would then be the rate-determining step for the overall formation of **2** and **4**. However, if $\Delta S_{10}^\ddagger \geq \text{ca. } 10 \text{ eu}$ (and hence $T\Delta S^\ddagger \geq \text{ca. } 3 \text{ kcal/mol}$ at $T \geq 300 \text{ K}$), which seems plausible for a dissociative process, then loss of H_2 would proceed more rapidly than the back reaction and consequently cyclometalation (eq 9) would be the rate-determining step. In any case, given the error margin of the calculations, the calculated barriers for the formation of **2-H2** and **4-H2** are equal or approximately equal to the overall barriers for the formation of **2** and **4**; and, as noted above, the computed values of these barriers are consistent with the experimental timescale of formation of these species.

Further experimental evidence in support of the calculated Ir(V) pathway is obtained from the reaction of **2** with H_2 . A rapid reaction is observed upon addition of H_2 to a solution of **2** affording $(\text{PCP})\text{IrH}_4$ (Scheme 4). Presumably this reaction proceeds initially via the reverse of the reaction steps that lead to **2** (cyclometalation to give the Ir(V) intermediate **2-H2**, followed by loss of H_2). The fact that the overall reaction of Scheme 4 proceeds rapidly is of course consistent with the calculated low energy of the C-H

addition/elimination (Ir(III)/Ir(V)) transition state **TS(1/2-H2)**, which connects **2-H2** and **o-1**, calculated to be only 6.3 kcal/mol above **2-H2** in free energy.

Scheme 4. Reaction of **2** with H₂



It should be noted that the formation of **2** and **4**, as presented in eqs 2 and 5, are both uphill reactions in which H₂ is the co-product ($\Delta G^\circ = 6.2$ kcal/mol and 7.1 kcal/mol, respectively). However, since the reactants **1** and **3** were formed via the displacement of NBE from (PCP)Ir(NBE), *free* NBE is present and may undergo hydrogenation. Since NBE hydrogenation is exothermic by 33 kcal/mol,³⁷ the overall reaction is thus significantly exergonic. The observed rates of eqs 2 and 5 can therefore only be regarded as lower limits, since it is quite plausible that H₂ is dissociated from **2-H2** or **4-H2**, reversibly, preceding the H₂ addition to NBE. Nevertheless, the fact that reactions 2 and 5 proceed at room temperature on the timescale of hours, combined with the fact that the equilibrium concentration of **o-1** and **o-3** are too small to be observed, does provide experimental evidence that cyclometalation of **o-1** or **o-3** to give Ir(V), eq 9, has a low kinetic barrier; this is certainly consistent with the (non-rate-determining) calculated values of $\Delta G_9^\ddagger = 5.9$ kcal/mol (phenanthrene) and 7.1 kcal/mol (biphenyl). An overall free energy diagram for the reaction of (tBu⁴PCP)Ir with phenanthrene is shown in Figure 4.

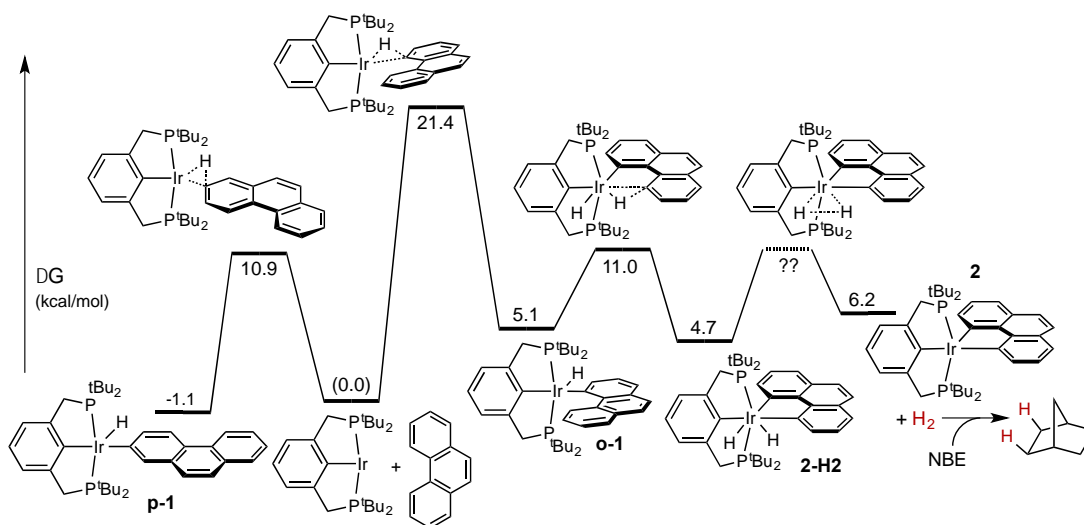
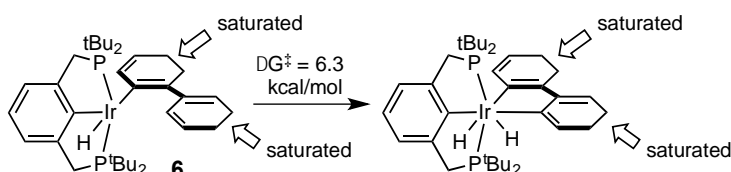


Figure 4. DFT-calculated free energy diagram for the formation of complex **2**.

We have considered the possibility that the very low barrier to C-H addition to Ir(III) to give Ir(V) intermediates **2-H2** or **4-H2** was attributable, at least in part, to conjugation between the arene ring systems. In particular, the formation of the metallocyclopentadiene core seemed, a priori, as though it might strongly favor cyclometalation; however, several calculations on model species indicated this was not the case. For example, the cyclometalation of complex **6**, a double C-H addition product of tetrahydrobiphenyl, would not lead to any such conjugation. The barrier calculated for the cyclometalation step of Scheme 5 is 6.3 kcal/mol, which is no greater (in fact, it is slightly less) than the corresponding reaction for biphenyl, $\Delta G_9^\ddagger = 7.1$ kcal/mol; likewise, the thermodynamics of Scheme 5 and eq 9 (biphenyl), $\Delta G^\circ = 0.5$ kcal/mol, are exactly equal (somewhat coincidentally). We conclude that formation of the Ir-H and Ir-C(sp²) bonds serves as the only major driving force in the cyclometalation reaction.

Scheme 5. Calculated cyclometalation of tetrahydrobiphenyl affording a metallacycle product which lacks a metallocyclopentadiene core.



Steric factors also seem to play an only minor role in the kinetics and thermodynamics of the cyclometalation step. When the calculations are conducted with phosphinomethyl ($R = \text{PMe}_2$ in $(^R\text{PCP})\text{Ir}$) groups instead of the very bulky phosphino-*t*-butyl ($R = \text{P}^t\text{Bu}_2$) groups, the initial C-H addition of phenanthrene is thermodynamically and kinetically more favorable, but the thermodynamic difference between the PMe_2 analogues of **o-1** and **p-1** is calculated as 5.9 kcal/mol, essentially equal to the value of 6.2 kcal/mol calculated for the P^tBu_2 complexes. The kinetic barrier to the cyclometalation step is essentially unchanged at $\Delta G^\ddagger = 5.1$ kcal/mol for the PMe_2 analogue vs. $\Delta G^\ddagger = 5.9$ kcal/mol for the P^tBu_2 species, while $\Delta G^\circ = -2.1$ kcal/mol vs. -0.4 kcal/mol, respectively. The pronounced difference in steric crowding is, however, illustrated in the following step, loss of H_2 from $(^R\text{PCP})\text{Ir}(\text{phen})\text{H}_2$, for which $\Delta G^\circ = 8.8$ kcal/mol with $R = \text{PMe}_2$ in contrast to 1.5 kcal/mol when $R = \text{P}^t\text{Bu}_2$. Similar results are obtained for the reaction of biphenyl (for the cyclometalation step, $\Delta G^\ddagger = 6.3$ kcal/mol and 7.1 kcal/mol calculated for PMe_2 and P^tBu_2 groups, respectively).

Steric factors are also calculated to play a role in the kinetics of formation of the C-H addition product **o-1**. The calculated TS for the ortho C-H addition of phenanthrene to $(^{\text{Me}4}\text{PCP})\text{Ir}$ to give **o-1-Me** is 15.4 kcal/mol above **p-1-Me** and, in the case of biphenyl,

12.3 kcal/mol above **m-3-Me**. These values, which represent the rate-determining barriers for the conversion of the lowest energy (meta or para) mono-C-H addition product to the cyclometalated species, are 7-9 kcal/mol less than the above noted values of 22.5 kcal/mol and 21.4 kcal/mol for the reaction of (^tBu⁴PCP)Ir with phenanthrene and biphenyl, respectively.

The conclusion of a significant steric contribution to the barrier for formation of the ortho C-H addition product is in agreement with experimental observations in the reaction of biphenyl with (ⁱPr⁴PCP)Ir(TBE). The calculated barrier (Figure 5) for the conversion of the lowest energy mono-C-H addition product (**m-3-iPr**) to give **o-3-iPr** is $\Delta G^\ddagger = 16.8$ kcal/mol. (ⁱPr⁴PCP)Ir(TBE) is calculated to be substantially lower in energy than **m-3-iPr**; accordingly, in the reaction of (ⁱPr⁴PCP)Ir(TBE) with biphenyl, neither products of biphenyl single C-H-addition nor any other intermediates are observed. The calculated overall barrier of the reaction is 22.4 kcal/mol, in excellent agreement with the value inferred from the kinetics of eq 8, $\Delta G_8^\ddagger = 21.6$ kcal/mol at 10 °C. The subsequent cyclometalation, a C-H addition to the Ir(III) complex **o-3-iPr**, has a computed barrier of 10.3 kcal/mol.

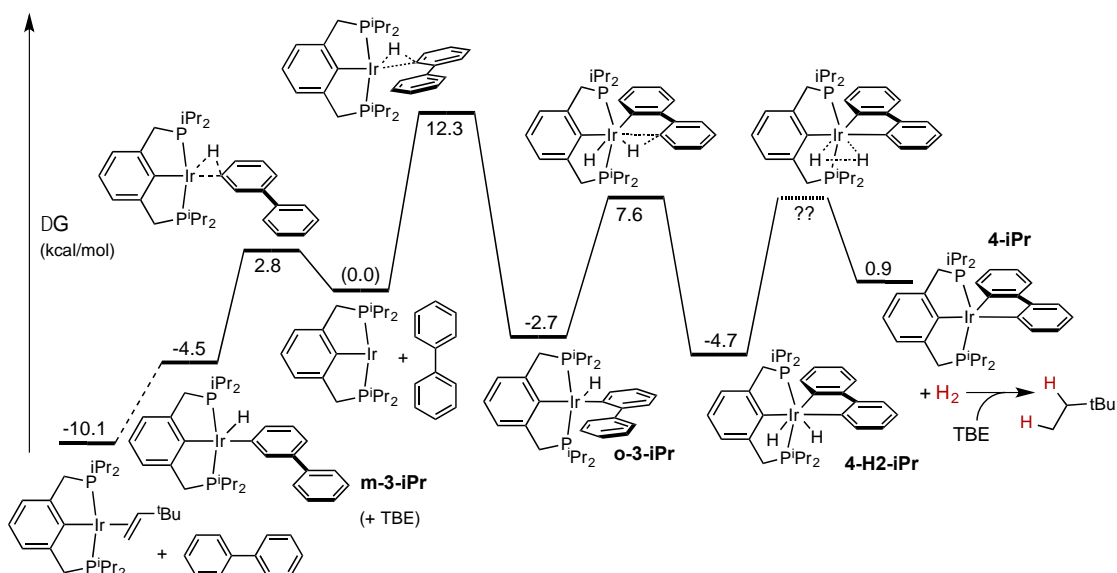
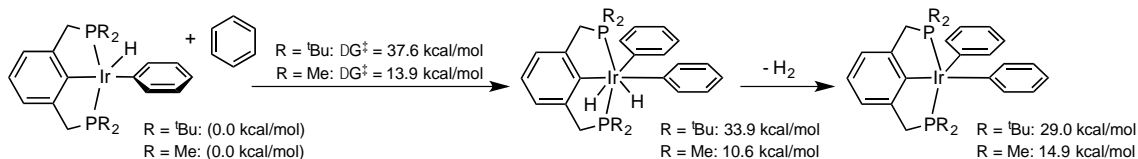


Figure 5. DFT-calculated free energy diagram for the formation of complex **4-iPr**.

We have also computationally explored the possibility of double *intermolecular* C-H addition; such reactions could be of great interest in the context of catalytic C-C coupling. As noted above ($^{t\text{Bu}}\text{PCP}$)Ir is well established to undergo C-H addition of benzene to yield ($^{t\text{Bu}}\text{PCP}$)IrPhH. Addition of a second benzene molecule (Scheme 6) to give ($^{t\text{Bu}}\text{PCP}$)Ir(Ph)₂(H)₂ has a calculated barrier of $\Delta G^\ddagger = 37.6$ kcal/mol. This substantial barrier is clearly mostly attributable to the highly unfavorable *thermodynamics* for the second C-H addition reaction, $\Delta G^\circ = 33.9$ kcal/mol; the reverse reaction, Ir(V)/Ir(III) C-H elimination, is thus kinetically very facile: $\Delta G^\ddagger = 3.7$ kcal/mol.

Scheme 6. Calculated addition of a second benzene molecule to (^RPCP)IrPhH. The calculations are gas-phase but assume a molarity of benzene equal to that of neat liquid and take into account the availability of 6 C-H bonds per molecule.



In contrast with the cyclometalations of species **o-3**, steric factors play a large role in the intermolecular case, where a second molecule of benzene is introduced to the coordination sphere. Accordingly, benzene C-H addition to the much less crowded complex (^{Me4}PCP)IrPhH affording (^{Me4}PCP)Ir(Ph)₂(H)₂ has a calculated barrier of only $\Delta G^\ddagger = 13.9$ kcal/mol (cf. $\Delta G^\ddagger = 37.6$ kcal/mol with (^{tBu4}PCP)Ir) (Figure 6). Notably, this free energy barrier is almost entirely due to a large calculated entropic component ($\Delta S^\ddagger = -38$ eu; $-T\Delta S^\ddagger = 11.3$ kcal/mol); the enthalpic barrier is extremely small, $\Delta H^\ddagger = 2.6$ kcal/mol.

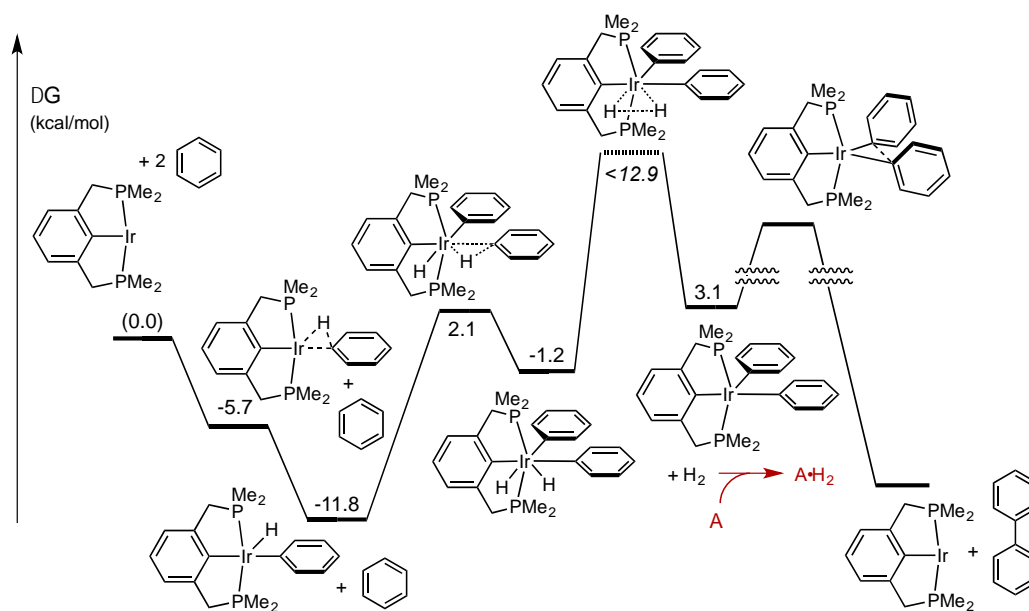


Figure 6. DFT-calculated free energy diagram for dehydrocoupling of benzene by $(^{\text{Me}4}\text{PCP})\text{Ir}$, coupled with hydrogenation of a sacrificial acceptor. The calculations are gas-phase but assume a molarity of benzene equal to that of neat liquid and take into account the availability of 6 C-H bonds per molecule.

Thermodynamically, the second C-H addition to $(^{\text{Me}4}\text{PCP})\text{Ir}$ is endergonic but only by 10.6 kcal/mol ($\Delta H^\circ = -0.1$ kcal/mol; $\Delta S^\circ = -36$ eu, so $-T\Delta S^\circ = 10.7$ kcal/mol). Subsequent loss of H_2 , to give $(^{\text{Me}4}\text{PCP})\text{Ir}(\text{Ph})_2$, is endergonic by 4.3 kcal/mol (with $\Delta H^\circ = 14.1$ kcal/mol), and the overall reaction ($(^{\text{Me}4}\text{PCP})\text{IrPhH} + \text{PhH} \rightarrow (^{\text{Me}4}\text{PCP})\text{Ir}(\text{Ph})_2 + \text{H}_2$) is hence endergonic by only 14.9 kcal/mol. The rate-determining step for formation of the $(^{\text{Me}4}\text{PCP})\text{Ir}(\text{Ph})_2$ species would presumably be loss of H_2 ; although the TS for H_2 loss was not located, its free energy may be estimated (in the manner noted above, assuming that $\Delta S^\ddagger \geq 10$ eu) very approximately as 7 kcal/mol (or less) above the product, or ca. 22 kcal/mol (or less) above $(^{\text{Me}4}\text{PCP})\text{IrPhH}$.

Thus, in spite of the very high barrier calculated for the addition reaction of two benzene moieties to (^tBu⁴PCP)Ir, these computed results suggest that in the absence of severe steric crowding, a double intermolecular C-H addition would be quite feasible. If the H₂ co-product is consumed by an acceptor, the overall reaction for formation of (^{Me}⁴PCP)Ir(Ph)₂ would be exergonic (alternatively, H₂ could be purged from solution. Subsequent reductive elimination of biphenyl from (^{Me}⁴PCP)Ir(Ph)₂ is calculated to have a barrier $\Delta G^\ddagger = 20.0$ kcal/mol. Thus, a catalytic cycle for dehydrogenative C-C coupling may be envisioned, proceeding through an Ir(V) intermediate; if coupled with efficient removal of H₂, the formation of the bi(phenyl)iridium complex would be the rate-determining segment of the cycle, with a low kinetic barrier attributable to a rate-determining loss of H₂ from the Ir(V) intermediate.

Conclusions

The double C-H addition/cyclometalation of phenanthrene or biphenyl by (^tBu⁴PCP)Ir(I) and (ⁱPr⁴PCP)Ir(I) complexes has been found to occur under mild conditions. The reaction pathways have been calculated in detail, and the computational results are found to be in full agreement with all experimental observations. The rate-determining step with both pincer ligands is calculated to be addition of the sterically hindered ortho C-H bond of biphenyl or the analogue at the C4 position of phenanthrene, affording (^tBu⁴PCP)Ir(III) and (ⁱPr⁴PCP)Ir(III) aryl hydride complexes. A second C-H addition, to produce cyclometalated Ir(V) dihydrides, has a much lower calculated free energy barrier, ca. 6 kcal/mol for (^tBu⁴PCP)Ir and 10.3 kcal/mol for (ⁱPr⁴PCP)Ir with biphenyl. While C-H addition to iridium is generally associated with Ir(I), this work illustrates that neutral Ir(III) C-H addition products can undergo a very facile second C-H addition, particularly

in the case of sterically less-crowded systems. This result may have significant implications for potential C-C coupling catalysts.

We also note the relationship with a recent report¹⁷ in which C-H elimination from a PNP-pincer Ir(III) alkyl hydride was found to be very slow, precluding an Ir(I)/Ir(III) catalytic olefin hydrogenation cycle. Catalytic olefin hydrogenation did proceed, however, via addition of H₂ to the Ir(III) alkyl hydride and subsequent C-H elimination from the resulting Ir(V) complex. We suggest that the kinetics of Ir(III)/Ir(V) interconversions are typically quite facile, and the thermodynamics may be more typically favorable for catalysis (i.e. nearly thermoneutral) than is widely appreciated.

References

- (1) (a) Janowicz, A. H.; Bergman, R. G. *J. Am. Chem. Soc.* **1982**, *104*, 352-354. (b) Arndtsen, B. A.; Bergman, R. G.; Mobley, T. A.; Peterson, T. H. *Acc. Chem. Res.* **1995**, *28*, 154-162.
- (2) (a) Crabtree, R. H.; Mihelcic, J. M.; Quirk, J. M. *J. Am. Chem. Soc.* **1979**, *101*, 7738-7739. (b) Crabtree, R. H.; Mellea, M. F.; Mihelcic, J. M.; Quirk, J. M. *J. Am. Chem. Soc.* **1982**, *104*, 107-113. (c) Burk, M. J.; Crabtree, R. H.; Parnell, C. P.; Uriarte, R. J. *Organometallics* **1984**, *3*, 816-817.
- (3) Choi, J.; MacArthur, A. H. R.; Brookhart, M.; Goldman, A. S. *Chem. Rev.* **2011**, *111*, 1761-1779.
- (4) Kumar, A.; Goldman, A. S. In *Top. Organomet. Chem.*; van Koten, G., Gossage, R. A., Eds.; Springer International Publishing: 2016; Vol. 54, p 307-334.
- (5) Choi, J.; Choliy, Y.; Zhang, X.; Emge, T. J.; Krogh-Jespersen, K.; Goldman, A. S. *J. Am. Chem. Soc.* **2009**, *131*, 15627-15629.
- (6) Choi, J.; Wang, D. Y.; Kundu, S.; Choliy, Y.; Emge, T. J.; Krogh-Jespersen, K.; Goldman, A. S. *Science* **2011**, *332*, 1545-1548.
- (7) Kundu, S.; Choi, J.; Wang, D. Y.; Choliy, Y.; Emge, T. J.; Krogh-Jespersen, K.; Goldman, A. S. *J. Am. Chem. Soc.* **2013**, *135*, 5127-5143.
- (8) Haibach, M. C.; Lease, N.; Goldman, A. S. *Angew. Chem., Intl. Ed.* **2014**, *53*, 10160-10163.
- (9) Ghosh, R.; Zhang, X.; Achord, P.; Emge, T. J.; Krogh-Jespersen, K.; Goldman, A. S. *J. Am. Chem. Soc.* **2007**, *129*, 853-866.
- (10) Biswas, S.; Huang, Z.; Choliy, Y.; Wang, D. Y.; Brookhart, M.; Krogh-Jespersen, K.; Goldman, A. S. *J. Am. Chem. Soc.* **2012**, *134*, 13276-13295.
- (11) Renkema, K. B.; Kissin, Y. V.; Goldman, A. S. *J. Am. Chem. Soc.* **2003**, *125*, 7770-7771.
- (12) (a) Collman, J. P. *Acc. Chem. Res.* **1968**, *1*, 136-140. (b) Vaska, L.; Werneke, M. F. *Ann. N. Y. Acad. Sci.* **1971**, *172*, 546-562. (c) Cotton, F. A.; Wilkinson, G.; Murillo, C. A.; Bochmann, M. *Advanced Inorganic Chemistry*, 6th ed.; John Wiley & Sons: New York, 1999, p. 1177. (d) Hartwig, J. F. *Organotransition Metal Chemistry*; University Science Books: Sausalito, CA, 2010, p. 263 (e) Crabtree, R. H. *The Organometallic Chemistry of the Transition Metals*; 5th ed.; John Wiley & Sons, Inc.: Hoboken, NJ, 2014, p. 165.
- (13) Saillard, J.; Hoffmann, R. *J. Am. Chem. Soc.* **1984**, *106*, 2006-2026.
- (14) Kanzelberger, M.; Singh, B.; Czerw, M.; Krogh-Jespersen, K.; Goldman, A. S. *J. Am. Chem. Soc.* **2000**, *122*, 11017-11018.
- (15) Laviska, D. A.; Wang, D. Y.; Krogh-Jespersen, K.; Goldman, A. S. Abstracts of Papers, 243rd ACS National Meeting & Exposition, San Diego, CA, United States, March 25-29, 2012, INOR-1223.
- (16) For some relevant examples of Ir(V) complexes and discussions of factors stabilizing them, see: (a) Klei, S. R.; Tilley, T. D.; Bergman, R. G. *J. Am. Chem. Soc.* **2000**, *122*, 1816-1817. (b) Kawamura, K.; Hartwig, J. F. *J. Am. Chem. Soc.* **2001**, *123*, 8422-8423.

- (c) Mohammad, H. A. Y.; Grimm, J. C.; Eichele, K.; Mack, H.-G.; Speiser, B.; Novak, F.; Quintanilla, M. G.; Kaska, W. C.; Mayer, H. A. *Organometallics* **2002**, *21*, 5775-5784. (d) Krogh-Jespersen, K.; Czerw, M.; Summa, N.; Renkema, K. B.; Achord, P. D.; Goldman, A. S. *J. Am. Chem. Soc.* **2002**, *124*, 11404-11416. (e) Webster, C. E.; Hall, M. B. *Coord. Chem. Rev.* **2003**, *238-239*, 315-331. (f) Lam, W. H.; Lam, K. C.; Lin, Z.; Shimada, S.; Perutz, R. N.; Marder, T. B. *Dalton Trans.* **2004**, 1556-1562. (g) Bernskoetter, W. H.; Lobkovsky, E.; Chirik, P. J. *Organometallics* **2005**, *24*, 4367-4373.
- (17) Cheng, C.; Kim, B. G.; Guironnet, D.; Brookhart, M.; Guan, C.; Wang, D. Y.; Krogh-Jespersen, K.; Goldman, A. S. *J. Am. Chem. Soc.* **2014**, *136*, 6672-6683.
- (18) Klei, S. R.; Tilley, T. D.; Bergman, R. G. *J. Am. Chem. Soc.* **2000**, *122*, 1816-1817.
- (19) Krogh-Jespersen, K.; Czerw, M.; Kanzelberger, M.; Goldman, A. S. *J. Chem. Inf. Comput. Sci.* **2001**, *41*, 56-63.
- (20) Brandt, P.; Hedberg, C.; Andersson, P. G. *Chem. - Eur. J.* **2003**, *9*, 339-347.
- (21) Bernskoetter, W. H.; Lobkovsky, E.; Chirik, P. J. *Organometallics* **2005**, *24*, 4367-4373.
- (22) Ghosh, R.; Kanzelberger, M.; Emge, T. J.; Hall, G. S.; Goldman, A. S. *Organometallics* **2006**, *25*, 5668-5671.
- (23) Laviska, D. A. Ph.D. Dissertation, Rutgers University, 2013
- (24) Kanzelberger, M. T. Ph.D. Dissertation, Rutgers University, 2004
- (25) Laviska, D. A.; Guan, C.; Emge, T. J.; Wilklow-Marnell, M.; Brennessel, W. W.; Jones, W. D.; Krogh-Jespersen, K.; Goldman, A. S. *Dalton Trans.* **2014**, *43*, 16354-16365.
- (26) Pauling, L. *The Nature of the Chemical Bond*; 3rd ed.; Cornell University Press: Ithaca, NY, 1960.
- (27) (a) Desiraju, G.; Steiner, T. *The Weak Hydrogen Bond: Applications to Structural Chemistry and Biology*; Oxford Univ Press, 1999. (b) Perutz, M. F. *Philos. Trans. R. Soc. London, Ser. A* **1993**, *345*, 105-12. (c) Tsuzuki, S.; Honda, K.; Uchamaru, T.; Mikami, M.; Tanabe, K. *J. Am. Chem. Soc.* **2000**, *122*, 3746-3753.
- (28) Grein, F. *J. Phys. Chem. A* **2002**, *106*, 3823-3827.
- (29) Sadlej-Sosnowska, N. *J. Phys. Chem. A* **2003**, *107*, 8671-8676.
- (30) Clot, E.; Megret, C.; Eisenstein, O.; Perutz, R. N. *J. Am. Chem. Soc.* **2009**, *131*, 7817-7827.
- (31) Evans, M. E.; Burke, C. L.; Yaibuathes, S.; Clot, E.; Eisenstein, O.; Jones, W. D. *J. Am. Chem. Soc.* **2009**, *131*, 13464-13473.
- (32) Bondi, A. *J. Phys. Chem.* **1964**, *68*, 441-51.
- (33) Hoops, S.; Sahle, S.; Gauges, R.; Lee, C.; Pahle, J.; Simus, N.; Singhal, M.; Xu, L.; Mendes, P.; Kummer, U. *Bioinformatics* **2006**, *22*, 3067-3074.
- (34) Perdew, J. P.; Burke, K.; Ernzerhof, M. *Phys Rev. Lett.* **1996**, *77*, 3865-3868.
- (35) Zhao, Y.; Truhlar, D. G. *Chem. Phys. Lett.* **2011**, *502*, 1-13.

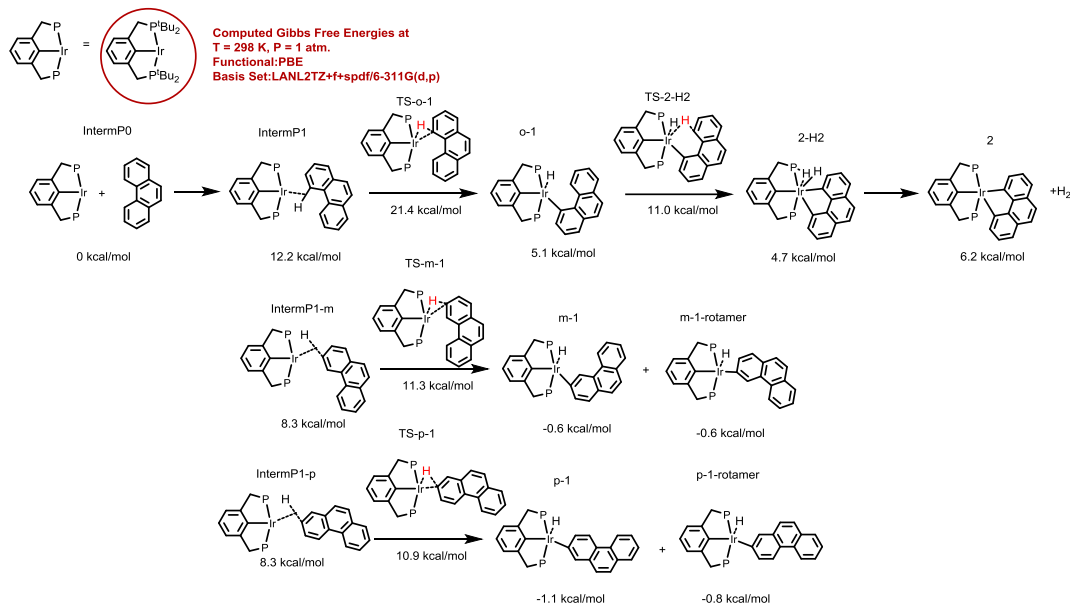
- (36) Mammen, M.; Shakhnovich, E. I.; Deutch, J. M.; Whitesides, G. M. *J. Org. Chem.* **1998**, *63*, 3821-3830.
- (37) Afeefy, H. Y.; Liebman, J. F.; Stein, S.E. "Neutral Thermochemical Data" in NIST Chemistry WebBook, NIST Standard Reference Database Number 69, Eds. P.J. Linstrom and W.G. Mallard, National Institute of Standards and Technology, Gaithersburg MD, 20899, <http://webbook.nist.gov>, (retrieved January 3, 2015)

Computational Details

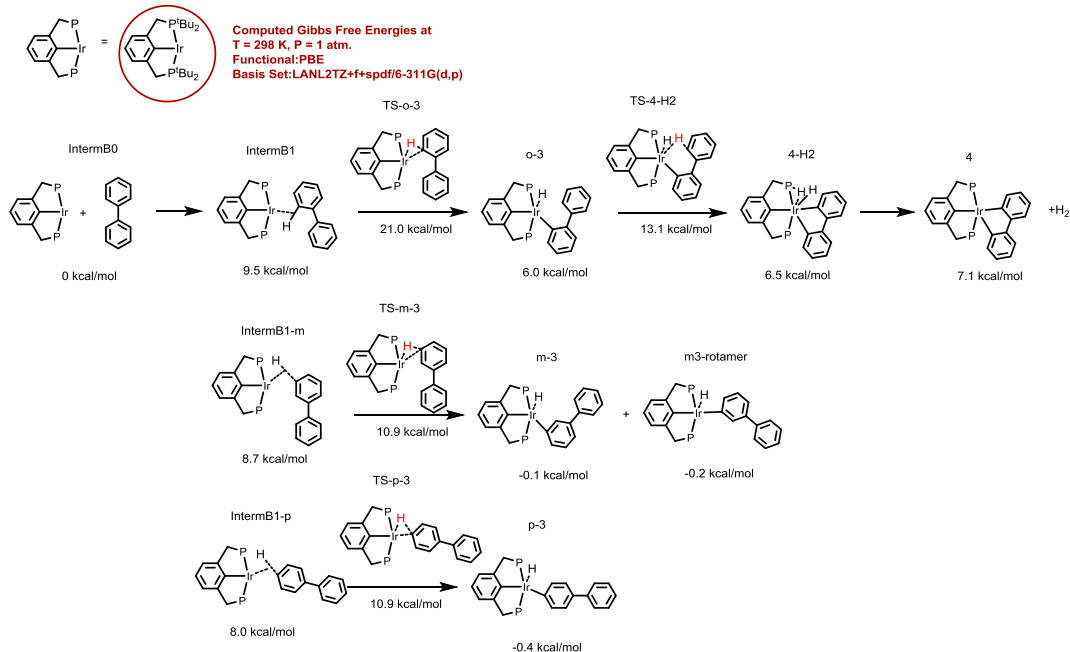
We made use of DFT methodology¹ implemented in the Gaussian 09 program.² All calculations employed the PBE exchange-correlation functional.³ For the Ir atom, we applied the Hay-Wadt relativistic effective (small) core potential (ECP)⁴ and the LANL2TZ basis set^{4,5} augmented by an f-type polarization function⁶ and a full complement of diffuse (s,p,d,f) functions;⁷ other atoms (P,C and H) were assigned 6-311G(d,p) basis sets.⁸⁻¹¹ We abbreviate the chosen functional, ECP, basis set combination as PBE/LANL2TZ+f+spdf/6-311G(d,p). In most calculations, the (^{R4}PCP)Ir (^{R4}PCP = κ^3 -2,6-(R₂PCH₂)₂C₆H₃) species was modeled with R = ^tBu, the phosphine substituents actually used in the experiments; selected calculations used R = ⁱPr or Me for truncated model system comparisons. Reactant, transition state, and product geometries were fully optimized, and stationary points located on the potential energy surfaces were characterized further by normal mode analysis. Expanded integration grid sizes (pruned (99,590) atomic grids, invoked using the integral=ultrafine keyword) were applied to increase numerical accuracy and stability in both geometry optimizations and normal mode analysis.¹² The (unscaled) vibrational frequencies formed the basis for the calculation of vibrational zero-point energy (ZPE) corrections; standard thermodynamic corrections (based on the harmonic oscillator/rigid rotor approximations and ideal gas behavior) were made to convert from purely electronic (reaction or activation) energies (E) to (standard) enthalpies (H°) and Gibbs free energies (G°; P = 1 atm).¹³ H, entropy (S°), and G were evaluated at room temperature, T = 25 °C (= 298 K), the approximate reaction temperature for the experimental work.

Figure S1. Reaction mechanism with computed free energies for C-H activation of phenanthrene, biphenyl and benzene by $(^t\text{Bu}_4\text{PCP})\text{Ir}$ [PBE/LANL2TZ+f+spdf/6-311G(d,p)].

Phenanthrene + $(^t\text{Bu}_4\text{PCP})\text{Ir}$



Biphenyl + $(^t\text{Bu}_4\text{PCP})\text{Ir}$



Benzene + (tBu⁴PCP)Ir

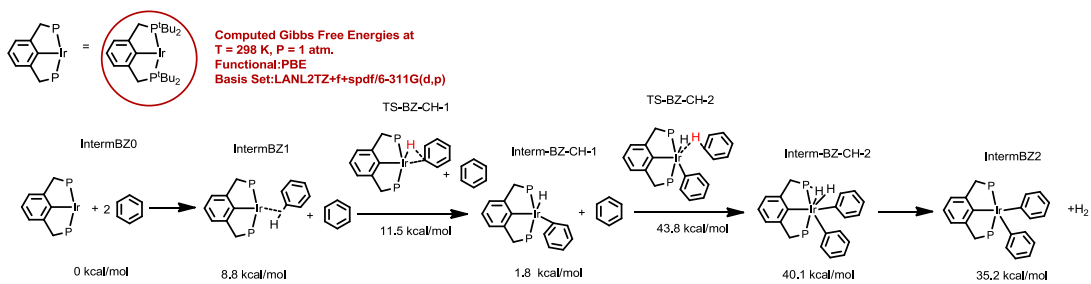


Table S1. Potential energies, enthalpies, entropies and free energies for C-H activation of phenanthrene, biphenyl and benzene by (^tBu⁴PCP)Ir [PBE/LANL2TZ+f+spdf/6-311G(d,p)].^a

Phenanthrene + (^tBu⁴PCP)Ir	Structure Label	E	H	G	S
^t Bu ⁴ PCPIr + H ₂ phen	IntermP0	0.0	0.0	0.0	0
sigma-C-H coordinated complex	IntermP1	-2.5	-1.3	12.2	-45
sigma-C-H coordinated complex-m	IntermP1-m	-5.8	-4.7	8.3	-43
sigma-C-H coordinated complex-p	IntermP1-p	-5.6	-4.5	8.3	-43
TS-ortho-C-H activation	TS-o-1	7.4	5.8	21.47	-52
ortho-PCPIrHphenanthryl	o-1	- 12.5	- 12.9	5.1	-60
TS-ring-closing second CH activation	TS-2-H2	-4.3	-6.8	11.0	-60
PCPH ₂ _concerted ring	2-H2	- 10.7	- 12.3	4.7	-57
PCP_concerted ring + H ₂	2+H2	2.1	-2.4	6.2	-29
TS-meta-C-H activation	TS-m-1	-2.7	-3.6	11.3	-50
meta-PCPIrHphenanthryl	m-1	- 14.3	- 14.5	-0.6	-47
meta-PCPIrHphenanthryl_rotamer	m-1-rotamer	- 14.4	- 14.6	-0.6	-47
TS-para-C-H activation	TS-p-1	-2.8	-3.7	10.9	-49
para-PCPIrHphenanthryl	p-1	- 14.5	- 14.8	-1.1	-46
para-PCPIrHphenanthryl_rotamer	p-1-rotamer	- 14.4	- 14.7	-0.7	-47
Biphenyl + (^tBu⁴PCP)Ir	Structure Label	E	H	G	S
^t Bu ⁴ PCPIr + H ₂ Biphen	IntermB0	0.0	0.0	0.0	0
sigma-C-H coordinated complex	IntermB1	-4.6	-3.6	9.5	-44
sigma-C-H coordinated complex-m	IntermB1-m	-5.6	-4.4	8.7	-44
sigma-C-H coordinated complex-p	IntermB1-p	-5.5	-4.5	8.0	-42
TS-ortho-C-H activation	TS-o-3	6.9	5.7	21.0	-51
ortho-PCPIrHBiphenyl	o-3	- 11.9	- 12.2	6.0	-61
TS-ring-closing second CH activation	TS-4-H2	-2.2	-4.8	13.1	-60

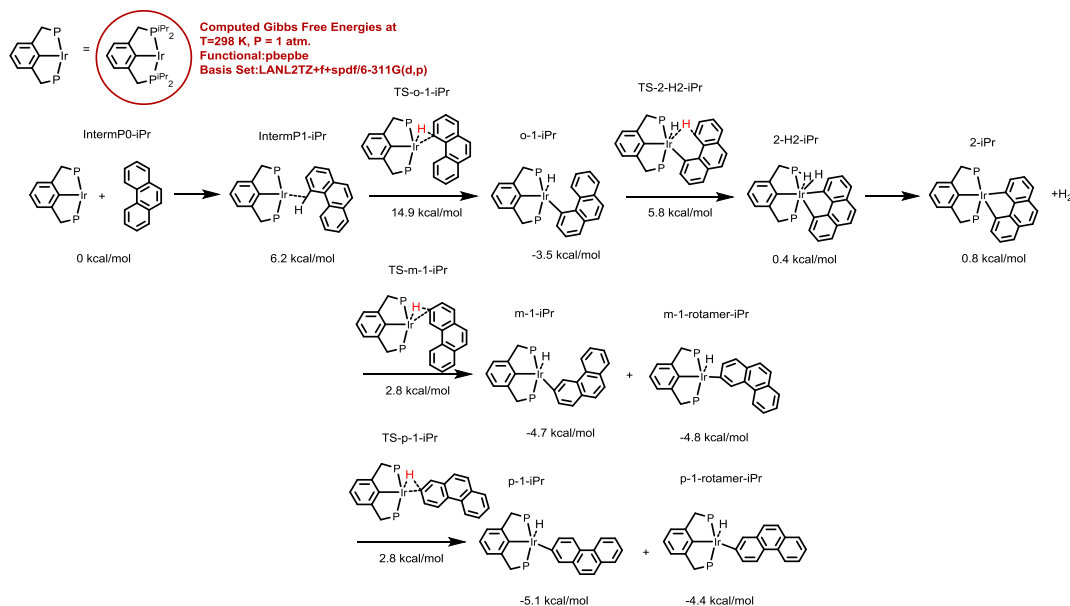
PCPH2_concerted ring	4-H2	-9.2	- 10.9	6.5	-58
PCP_concerted ring + H2	4+H2	2.8	-1.8	7.1	-30
TS-meta-C-H activation	TS-m-3	-2.8	-3.7	10.9	-49
meta-PCPIrHBiphenyl	m-3	- 13.7	- 14.1	-0.1	-47
meta-PCPIrHBiphenyl_rotamer	m-3-rotamer	- 13.8	- 14.1	-0.2	-47
TS-para-C-H activation	TS-p-3	-2.9	-3.8	10.9	-49
para-PCPIrHBiphenyl	p-3	- 13.9	- 14.2	-0.4	-46
Benzene + (tBu⁴PCP)Ir	Structure Label	E	H	G	S
tBu ⁴ PCPIr + H2benzene	IntermBZ0	0.0	0.0	0.0	0
sigma-C-H coordinated complex	IntermBZ1	-5.4	-4.2	8.8	-43
TS-C-H activation first benzene	TS-BZ-CH-1	-2.3	-3.3	11.5	-50
Interm-C-H activation first_benzene	Interm-BZ-CH-1	- 11.4	- 11.7	1.8	-45
TS-C-H activation second_benzene	TS-BZ-CH-2	15.3	14.3	43.8	-99
Interm-C-H activation _second_benzene	Interm-BZ-CH-2	10.5	10.7	40.1	-99
PCPIr(phenyl) ₂	IntermBZ2+H2	17.8	15.0	35.2	-68

^aUnits are kcal/mol for ΔE , ΔH , and ΔG ; units are cal/(deg·mol) for ΔS . The standard state

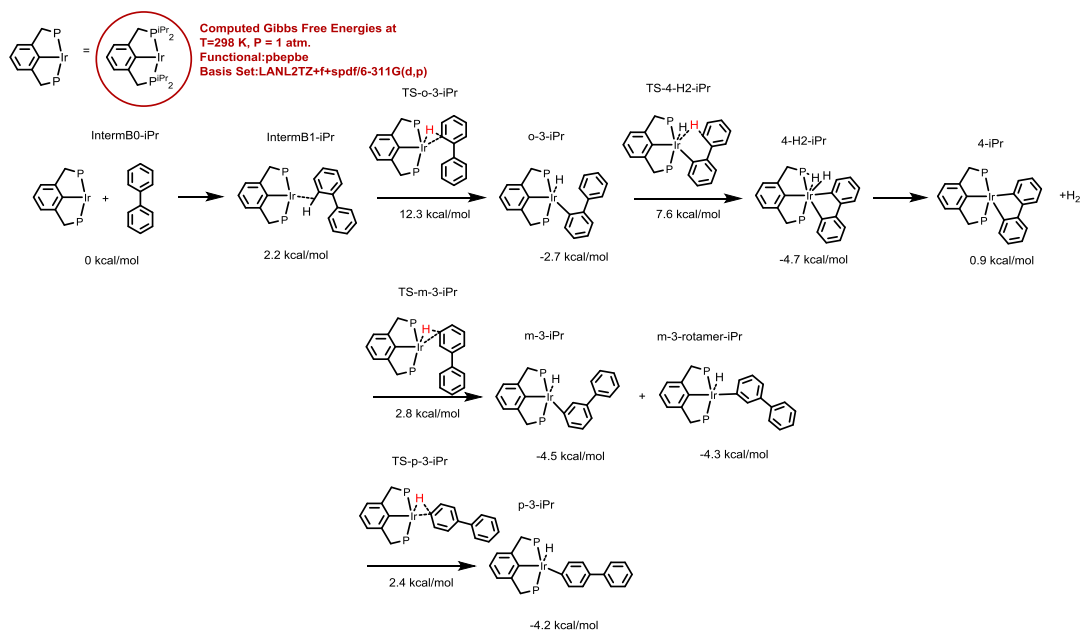
for concentrations is $P = 1$ atm for each species participating in the reaction; $T = 298.15$ K.

Figure S2. Reaction mechanisms with computed free energies for C-H activation of phenanthrene, biphenyl and benzene by (*i*Pr⁴PCP)Ir [PBE/LANL2TZ+f+spdf/6-311G(d,p)].

Phenanthrene + (*i*Pr⁴PCP)Ir



Biphenyl + (*i*Pr⁴PCP)Ir



Benzene + (*i*Pr⁴PCP)Ir

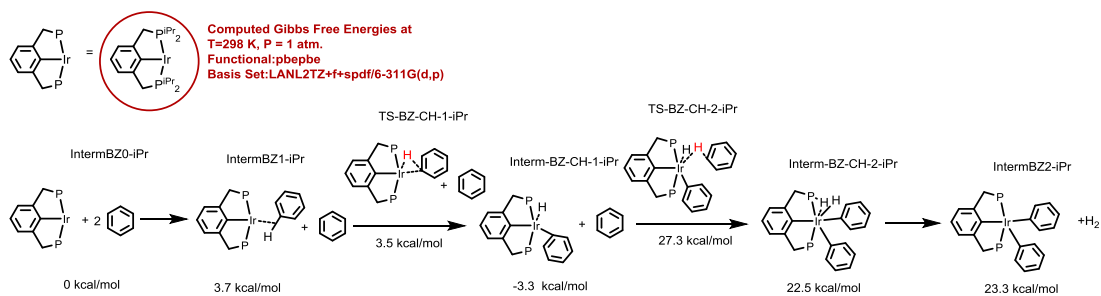


Table S2. Potential energies, enthalpies, entropies and free energies for C-H activation of phenanthrene, biphenyl and benzene by (ⁱPr⁴PCP)Ir [PBE/LANL2TZ+f+spdf/6-311G(d,p)].^a

Phenanthrene + (ⁱ Pr ⁴ PCP)Ir	Structure Label	E	H	G	S
tBu ⁴ PCPIr + H ₂ phen	IntermP0-iPr	0.0	0.0	0.0	0
sigma-C-H coordinated complex	IntermP1-iPr	-9.0	-8.3	6.2	-49
sigma-C-H coordinated complex-m	IntermP1-m-iPr	-11.7	-11.5	2.5	-47
sigma-C-H coordinated complex-p	IntermP1-p-iPr	-11.7	-11.4	3.1	-49
TS-ortho-C-H activation	TS-o-1-iPr	0.3	-1.4	14.9	-55
ortho-PCPIrHphenanthryl	o-1-iPr	-21.0	-21.9	-3.5	-62
TS-ring-closing second CH activation	TS-2-H2-iPr	-9.9	-12.8	5.8	-62
PCPH ₂ _concerted ring	2-H2-iPr	-16.2	-18.4	0.4	-63
PCP_concerted ring + H ₂	2+H2-iPr	-2.9	-7.8	0.8	-29
TS-meta-C-H activation	TS-m-1-iPr	-11.0	-12.5	2.8	-51
meta-PCPIrHphenanthryl	m-1-iPr	-17.8	-18.5	-4.7	-46
meta-PCPIrHphenanthryl_rotamer	m-1-rotamer-iPr	-18.0	-18.7	-4.8	-47
TS-para-C-H activation	TS-p-1-iPr	-11.1	-12.6	2.8	-52
para-PCPIrHphenanthryl	p-1-iPr	-18.1	-18.9	-5.1	-46
para-PCPIrHphenanthryl_rotamer	p-1-rotamer-iPr	-18.0	-18.7	-4.4	-48
Biphenyl + (tBu ⁴ PCP)Ir	Structure Label	E	H	G	S
tBu ⁴ PCPIr + H ₂ Biphen	IntermB0-iPr	0.0	0.0	0.0	0

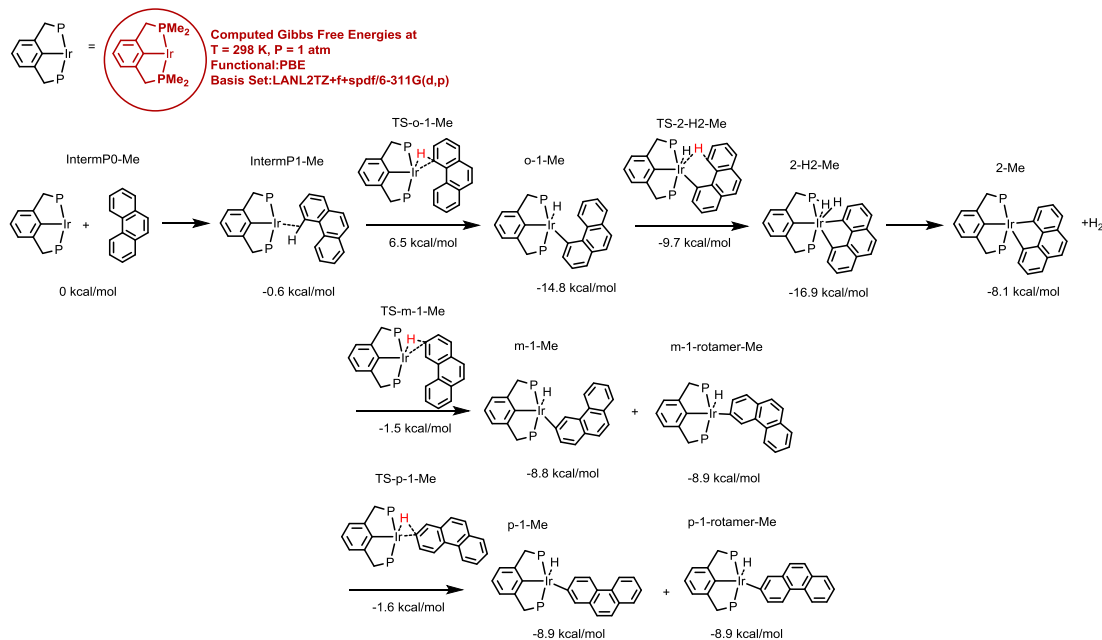
sigma-C-H coordinated complex	IntermB1-iPr	-12.3	-12.1	2.2	-48
sigma-C-H coordinated complex-m	IntermB1-m-iPr	-11.1	-11.0	3.4	-48
sigma-C-H coordinated complex-p	IntermB1-p-iPr	-11.4	-11.3	3.0	-48
TS-ortho-C-H activation	TS-o-3-iPr	-3.5	-4.7	12.3	-57
ortho-PCPIrHBiphenyl	o-3-iPr	-20.6	-21.4	-2.7	-63
TS-ring-closing second CH activation	TS-4-H2-iPr	-8.3	-11.3	7.6	-63
PCPH2_concerted ring	4-H2-iPr	-21.0	-23.3	-4.7	-62
PCP_concerted ring + H2	4+H2-iPr	-2.6	-7.6	0.9	-29
TS-meta-C-H activation	TS-m-3-iPr	-10.9	-12.4	2.8	-51
meta-PCPIrHBiphenyl	m-3-iPr	-17.4	-18.2	-4.5	-46
meta-PCPIrHBiphenyl_rotamer	m-3-rotamer-iPr	-17.5	-18.3	-4.3	-47
TS-para-C-H activation	TS-p-3-iPr	-11.0	-12.6	2.4	-50
para-PCPIrHBiphenyl	p-3-iPr	-17.6	-18.4	-4.2	-48
Benzene + (tBu⁴PCP)Ir	Structure Label	E	H	G	S
tBu ⁴ PCPIr + H2benzene	IntermBZ0-iPr	0.0	0.0	0.0	0
sigma-C-H coordinated complex	IntermBZ1-iPr	-10.7	-10.6	3.7	-48
TS-C-H activation first benzene	TS-BZ-CH-1-iPr	-10.4	-11.9	3.5	-52
Interm-C-H activation first_benzene	Interm-BZ-CH-1-iPr	-16.7	-17.5	-3.3	-48

TS-C-H activation second_benzene	TS-BZ-CH-2-iPr	-0.4	-2.1	27.3	-99
Interm-C-H activation _second_benzene	Interm-BZ-CH-2- iPr	-6.1	-6.8	22.5	-98
PCPIr(phenyl) ₂	IntermBZ2-iPr +H ₂	7.1	3.6	23.3	-66

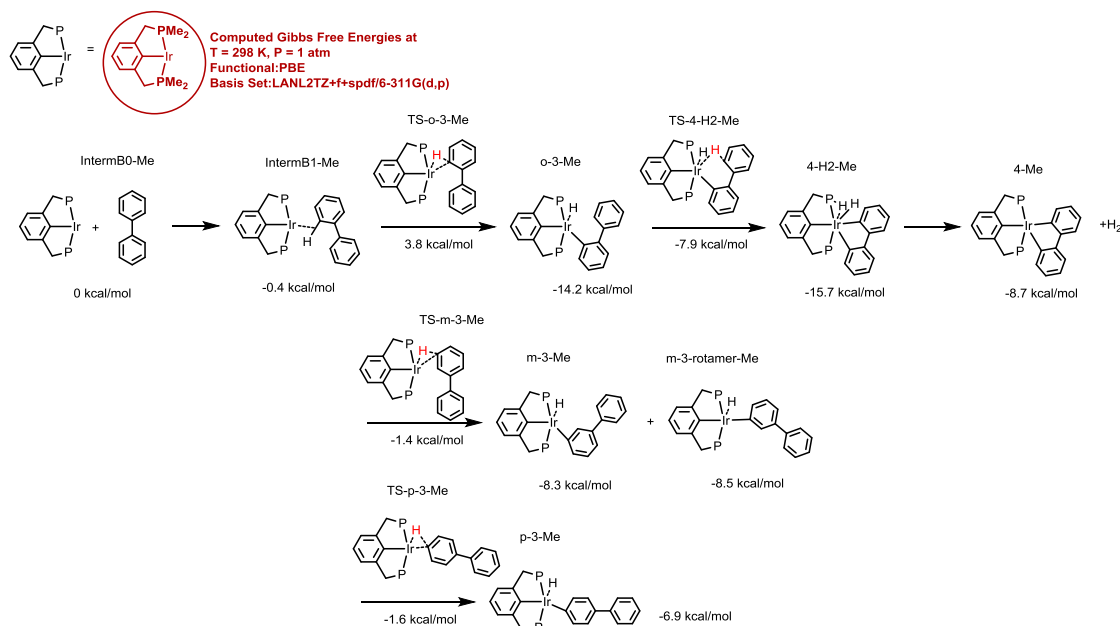
^aUnits are kcal/mol for ΔE , ΔH , and ΔG ; units are cal/(deg·mol) for ΔS . The standard state for concentrations is $P = 1$ atm for each species participating in the reaction; $T = 298.15$ K.

Figure S3. Reaction mechanisms with computed free energies for C-H activation of phenanthrene, biphenyl and benzene by $(\text{Me}^4\text{PCP})\text{Ir}$ [PBE/LANL2TZ+f+spdf/6-311G(d,p)]

Phenanthrene + $(\text{Me}^4\text{PCP})\text{Ir}$



Biphenyl + $(\text{Me}^4\text{PCP})\text{Ir}$



Benzene + (Me⁴PCP)Ir

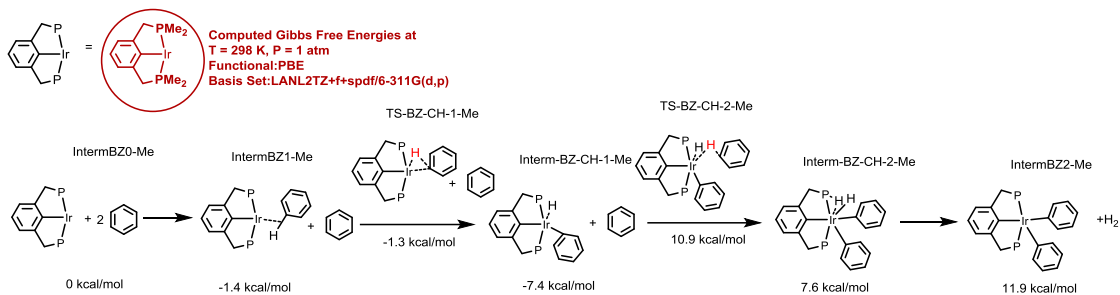


Table S3. Potential energies, enthalpies, entropies and free energies for C-H activation of phenanthrene, biphenyl and benzene by (^{Me4}PCP)Ir [PBE/LANL2TZ+f+spdf/6-311G(d,p)]. ^a

Phenanthrene + (^{Me4}PCP)Ir	Structure Label	E	H	G	S
^{Me4} PCPIr + H ₂ phen	IntermP0	0.0	0.0	0.0	0.0
sigma-C-H coordinated complex	IntermP1-Me	-12.6	-12.4	-0.6	-39.3
TS-ortho-C-H activation	TS-o-1-Me	-4.2	-6.6	6.5	-43.8
ortho-PCPIrHphenanthryl	o-1-Me	-28.0	-29.8	-14.8	-50.2
TS-ring-closing second CH activation	TS-2-H2-Me	-21.4	-25.2	-9.7	-51.9
PCPH ₂ _concerted ring	2-H2-Me	-29.0	-32.1	-16.9	-51.0
PCP_concerted ring + H ₂	2+H2-Me	-7.3	-12.7	-8.1	-15.5
TS-meta-C-H activation	TS-m-1-Me	-12.4	-14.2	-1.5	-42.5
meta-PCPIrHphenanthryl	m-1-Me	-18.4	-19.6	-8.8	-36.2
TS-para-C-H activation	TS-p-1-Me	-12.5	-14.4	-1.6	-42.9
para-PCPIrHphenanthryl	p-1-Me	-18.5	-19.7	-8.9	-36.3
Biphenyl + (^{Me4}PCP)Ir	Structure Label	E	H	G	S
^{Me4} PCPIr + H ₂ Biphen	IntermB0	0.0	0.0	0.0	0.0
sigma-C-H coordinated complex	IntermB1-Me	-12.0	-12.1	-0.4	-39.3
TS-ortho-C-H activation	TS-o-3-Me	-8.0	-9.9	3.8	-45.9
ortho-PCPIrHBiphenyl	o-3-Me	-27.7	-29.4	-14.2	-50.8
TS-ring-closing second CH activation	TS-4-H2-Me	-19.6	-23.6	-7.9	-52.6
PCPH ₂ _concerted ring	4-H2-Me	-27.8	-30.9	-15.7	-51.2
PCP_concerted ring + H ₂	4+H2-Me	-7.8	-13.5	-8.7	-16.1
TS-meta-C-H activation	TS-m-3-Me	-12.3	-14.2	-1.4	-42.7
meta-PCPIrHBiphenyl	m-3-Me	-17.7	-18.9	-8.3	-35.6
meta-PCPIrHBiphenyl_rotamer	m-3-rotamer-Me	-17.8	-19.0	-8.5	-35.3

TS-para-C-H activation	TS-p-3-Me	-12.5	-14.3	-1.6	-42.9
para-PCPIrHBiphenyl	p-3-Me	-18.0	-19.8	-6.9	-43.0
Benzene + (^{Me4}PCP)Ir	Structure Label	E	H	G	S
^{Me4} PCPIr + H ₂ benzene	IntermBZ0-Me	0.0	0.0	0.0	0.0
sigma-C-H coordinated complex	IntermBZ1-Me	-12.7	-13.0	-1.4	-38.8
TS-C-H activation first benzene	TS-BZ-CH-1-Me	-11.8	-13.7	-1.3	-41.5
Interm-C-H activation first_benzene	Interm-BZ-CH-1-Me	-17.3	-18.5	-7.4	-37.0
TS-C-H activation second_benzene	TS-BZ-CH-2-Me	-13.2	-15.9	10.9	-90.1
Interm-C-H activation second_benzene	Interm-BZ-CH-2-Me	-16.9	-18.6	7.6	-87.8
PCPIr(phenyl) ₂	IntermBZ2-Me +H ₂	-0.2	-4.5	11.9	-54.9

^aUnits are kcal/mol for ΔE, ΔH, and ΔG; units are cal/(deg·mol) for ΔS. The standard state for concentrations is P = 1 atm for each species participating in the reaction; T = 298.15 K.

Computational Section References

1. Koch, W.; Holthausen, M. C. *A Chemist's Guide to Density Functional Theory*; Wiley: New York, 2001.
2. Gaussian 09, Revision D.01, Frisch, M. J.; Trucks, G. W.; Schlegel, H. B.; Scuseria, G. E.; Robb, M. A.; Cheeseman, J. R.; Scalmani, G.; Barone, V.; Mennucci, B.; Petersson, G. A.; Nakatsuji, H.; Caricato, M.; Li, X.; Hratchian, H. P.; Izmaylov, A. F.; Bloino, J.; Zheng, G.; Sonnenberg, J. L.; Hada, M.; Ehara, M.; Toyota, K.; Fukuda, R.; Hasegawa, J.; Ishida, M.; Nakajima, T.; Honda, Y.; Kitao, O.; Nakai, H.; Vreven, T.; Montgomery, J. A., Jr.; Peralta, J. E.; Ogliaro, F.; Bearpark, M.; Heyd, J. J.; Brothers, E.; Kudin, K. N.; Staroverov, V. N.; Kobayashi, R.; Normand, J.; Raghavachari, K.; Rendell, A.; Burant, J. C.; Iyengar, S. S.; Tomasi, J.; Cossi, M.; Rega, N.; Millam, J. M.; Klene, M.; Knox, J. E.; Cross, J. B.; Bakken, V.; Adamo, C.; Jaramillo, J.; Gomperts, R.; Stratmann, R. E.; Yazyev, O.; Austin, A. J.; Cammi, R.; Pomelli, C.; Ochterski, J. W.; Martin, R. L.; Morokuma, K.; Zakrzewski, V. G.; Voth, G. A.; Salvador, P.; Dannenberg, J. J.; Dapprich, S.; Daniels, A. D.; Farkas, Ö.; Foresman, J. B.; Ortiz, J. V.; Cioslowski, J.; Fox, D. J. Gaussian, Inc., Wallingford CT, 2009.
3. Perdew, J. P.; Burke, K.; Ernzerhof, M. Generalized Gradient Approximation Made Simple. *Phys. Rev. Lett.* **1996**, 77, 3865–3868.
4. Hay, P.J.; Wadt, W.R. Ab-initio Effective Core Potentials for Molecular Calculations – Potentials for K to Au Including the Outermost Core Orbitals. *J. Chem. Phys.* **1985**, 82, 299–310.
5. Roy, L. E.; Hay, P. J.; Martin, R. L. Revised Basis Sets for the LANL Effective Core Potentials. *J. Chem. Theory Comput.* **2008**, 4, 1029-1031.

6. Ehlers, A. W.; Böhme, M.; Dapprich, S.; Gobbi, A.; Höllwarth, A.; Jonas, V.; Köhler, K. F.; Stegmann, R.; Veldkamp, A.; Frenking, G. A set of f-polarization functions for pseudo-potential basis sets of the transition metals Sc-Cu, Y-Ag and La-Au. *Chem. Phys. Lett.* **1993**, *208*, 111–114.
7. Figgen, D.; Peterson, K. A.; Dolg, M.; Stoll, H. Energy-consistent pseudopotentials and correlation consistent basis sets for the 5d elements Hf-Pt, *J. Chem. Phys.* **2009**, *130*, 164108.
8. Ditchfield, R.; Hehre, W. J.; Pople, J. A. Self-Consistent Molecular Orbital Methods. IX. An Extended Gaussian-Type Basis for Molecular Orbital Studies of Organic Molecules. *J. Chem. Phys.* **1971**, *54*, 724-728.
9. Hariharan, P. C.; Pople, J. A. Accuracy of AH_n Equilibrium Geometries by Single Determinant Molecular Orbital Theory. *Mol. Phys.* **1974**, *27*, 209-214.
10. Krishnan, R.; Binkley, J. S.; Seeger, R.; Pople, J. A. Self-Consistent Molecular Orbital Methods. XX. A Basis Set for Correlated Wavefunctions. *J. Chem. Phys.* **1980**, *72*, 650-654.
11. McLean, A. D.; Chandler, G. S. Contracted Gaussian-Basis Sets for Molecular Calculations. I. Second Row Atoms, $Z=11-18$. *J. Chem. Phys.* **1980**, *72*, 5639-5648.
12. Frisch, Æ; Frisch, M. J.; Clemente, F. R.; Trucks, G. W. *Gaussian 09 User's Reference*, Gaussian, Inc., Wallingford CT, 2009, pp 167.
13. McQuarrie, D. A. *Statistical Thermodynamics*; Harper and Row: New York, 1973.

Chapter 4: Computational Study of Solid-Phase Molecular Pincer-Iridium Catalysts

Majority of this chapter is reproduced with permission from

Dehydrogenation of *n*-Alkanes by Solid-Phase Molecular Pincer-Iridium Catalysts. High Yields of α -Olefin Product

Akshai Kumar, Tian Zhou, Thomas J. Emge, Oleg Mironov, Robert J. Saxton

Karsten Krogh-Jespersen and Alan S. Goldman

J. Am. Chem. Soc., **2015**, *137* (31), pp 9894–9911

Copyright © 2015 American Chemical Society

Introduction

Olefins are key intermediates in many, perhaps even most, processes in the fuel and commodity chemical industries, and are also of great importance in the synthesis of fine chemicals. The development of catalysts for the regioselective dehydrogenation of alkanes and alkyl groups to afford olefins is therefore a goal of great interest to a broad range of chemists.

The most significant progress toward the goal of practical regioselective alkane dehydrogenation catalysts has been realized with pincer-ligated iridium complexes, beginning with the report by Kaska and Jensen¹ of alkane dehydrogenation by (^{*t*}Bu⁴PCP)IrH_n (**1-H_n**; ^{*R*}4PCP = κ^3 -C₆H₃-2,6-(CH₂PR₂)₂; n = 2 or 4). Our group subsequently reported the synthesis and generally greater catalytic activity of the less crowded ^{*i*}Pr⁴PCP analogue (**2**)² and soon discovered that both complexes showed kinetic selectivity for dehydrogenation of *n*-alkanes at the terminal position to give the highly desirable corresponding α -olefins.³ Catalysts **1** and **2** were also found to be effective for the acceptorless dehydrogenation of alkanes.^{2,4} Work with these complexes has been followed by reports of numerous catalytically active variants with the (PCP)Ir motif,⁵⁻⁹ including other bis-phosphines,¹⁰⁻¹⁴ bis-phosphinites (POCOP),¹⁵⁻¹⁸ hybrid phosphine–phosphinites (PCOP),^{19,20} arsines (AsOCOAs),²¹ hybrid phosphine-thiophosphinites (PSCOP)²² and hybrid amine-phosphinites (NCOP)²³. In addition to simple alkane dehydrogenation, these complexes have been employed for numerous other catalytic transformations of hydrocarbons, including alkane metathesis,^{6,8,9,20,24-26} alkyl group metathesis,²⁷ dehydroaromatization,^{19,28,29} alkane–alkene coupling reactions,³⁰⁻³² borylation of alkanes²³ and the dehydrogenation of several non-alkane substrates.^{22,33,34} Several pincer motifs more recently explored, such as (CCC)Ir,³⁵⁻³⁸ (PCP)Ru³⁹⁻⁴¹,

(PCP)Os⁴², and (NCN)Ir^{43,44} have been found to show promise for alkane dehydrogenation but as of yet none have proven to be competitive with the well investigated PCP-type iridium-based systems.²⁶

In early alkane dehydrogenation studies⁴⁵ 3,3-dimethyl-1-butene (TBE) was found by Crabtree to be a singularly effective hydrogen acceptor. In addition to being resistant to double-bond isomerization, the bulky TBE is only weakly coordinating; in contrast, ethylene was found to completely inhibit catalytic activity.⁴⁵ TBE has thus become the most commonly used acceptor for alkane transfer dehydrogenation.^{8,9} We have found that norbornene (NBE) is also very effective, presumably for similar reasons.^{3,6} However, on a large scale, the use of smaller olefins, such as ethylene or propene, would be much more practical. Ethylene, in particular, is efficiently dehydrogenated with heterogeneous catalysts, which could allow for recycling of ethane (without necessarily requiring the costly separation of ethylene and ethane).⁴⁶ We have earlier reported the use of propene as acceptor for dehydroaromatization reactions.¹⁹ Very recently Brookhart and co-workers have demonstrated the role of ethylene as both an acceptor and a dienophile in the synthesis of piperylene,⁴⁷ toluene⁴⁷ and *p*-xylene.⁴⁸

The dehydrogenation of lighter alkanes, e.g. butane and pentane,^{47,49} is of particular interest. Such alkanes are generally undesirable as transportation fuel components, while the corresponding olefins and dienes have many chemical applications and could potentially be dimerized (or cross-dimerized) to give alkanes of molecular weight more suitable for fuel.³²

Given these considerations we were led to study the transfer-dehydrogenation of lighter alkanes using gaseous olefins. At high temperatures, mixtures of these

hydrocarbons are entirely in the gas phase, while the catalyst is (at least primarily) in the solid phase.⁵⁰ Much to our surprise the turnover rates resulting from such dual-phase systems were found to be remarkably high. Although heterogeneous solid-gas systems for alkane dehydrogenation are very well known,⁴⁶ to our knowledge these are the first examples of purely *molecular* solid-phase catalysts for alkane dehydrogenation. Characteristic of their behavior in solution, and in contrast with non-molecular solid-phase dehydrogenation catalysts, these systems are selective for the formation of α -olefins. Most remarkably, the maximum yields of α -olefin from these heterogeneous systems are found to be much *greater* than have been previously obtained from homogeneous solution phase systems (the highest previously reported yield being 97 mM 1-octene³ from the transfer dehydrogenation of *n*-octane with 0.5 M 1-decene catalyzed by **1-H_n**).

Result and Discussion

A crystalline precursor of (*i*Pr⁴PCP)Ir. As initial results (see below) indicated the particular effectiveness of (*i*Pr⁴PCP)Ir for our purposes, we explored several synthetic routes to viable precursors of this catalyst. We successfully obtained crystalline (*i*Pr⁴PCP)Ir(C₂H₄) (**2-C₂H₄**), which was characterized by X-ray diffraction (Figure 1). This is the first report of a crystal structure of a direct precursor of the (*i*Pr⁴PCP)Ir catalyst.

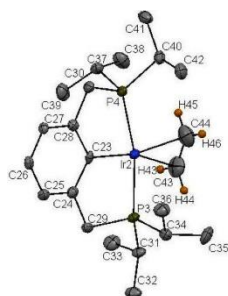


Figure 1. ORTEP diagram of ($i\text{Pr}^4\text{PCP}$)Ir(C₂H₄) with ellipsoids drawn at the 50% probability level. For the sake of clarity only H atoms on the ethylene ligand are shown.

Transfer dehydrogenation by various pincer-iridium complexes: gas-solid phase.

In a typical experimental set-up (Figure 2) 100 μL of a stock *n*-pentane solution of catalyst (1 mM) was added to a custom-made thick-walled long-neck 1.5-mL ampoule inside an argon-filled glove box. The ampoule was then connected to a Kontes adapter via Tygon tubing and degassed on a high-vacuum line. Propene (1.0 atm) was then introduced to the system. The contents of the vials were frozen in liquid nitrogen, and the vials were flame sealed. (The total gas volume before sealing was 3 mL; thus, after condensation, sealing, and warming, the pressure of propene is approximately 2 atm. The vials were then placed in a pre-heated aluminum block inside an oven maintained at 240 °C [*note: extreme caution must be exercised during this process, including the use of appropriate safety shields*] and subjected to interval free heating for a stipulated time. The oven was then cooled to room temperature, the ampoules were removed, the contents were frozen in liquid nitrogen, the ampoules were broken open, and the contents were analyzed by GC.

The vapor pressure of *n*-pentane at 200 °C and 240 °C is calculated to be 32 atm and 52 atm, respectively.^{51,52} 100 μL *n*-pentane in a 1.5 mL vial, upon converting fully to the gas phase, will generate pressures of approximately 22 atm and 24 atm at 200 °C and 240 °C, respectively. Thus, all hydrocarbons are expected to be in the gas phase under these conditions.

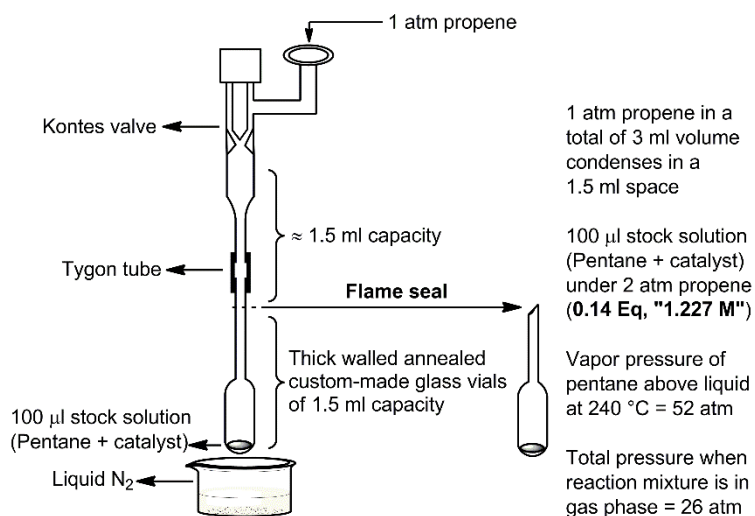
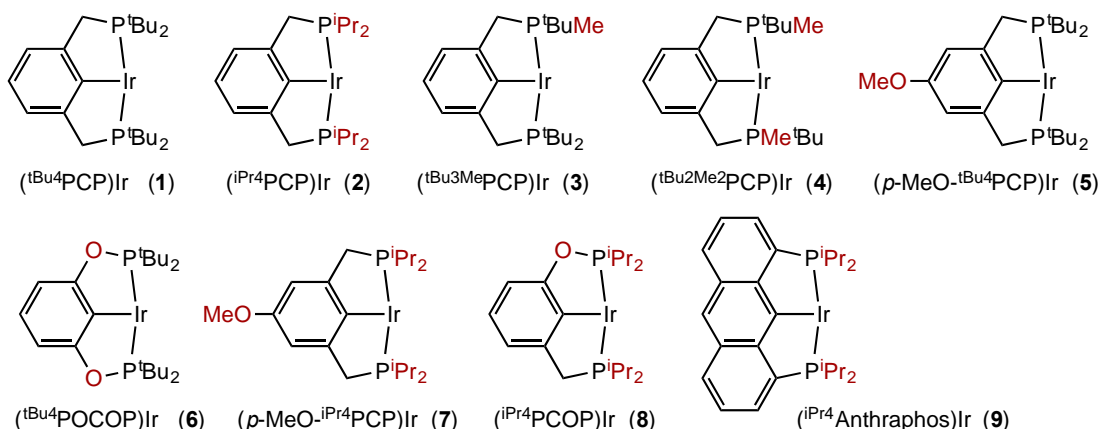


Figure 2. Experimental setup for transfer dehydrogenation of *n*-pentane catalyzed by pincer-iridium complexes using ethylene or propene as acceptor (values given for 2 atm acceptor at 240 °C).

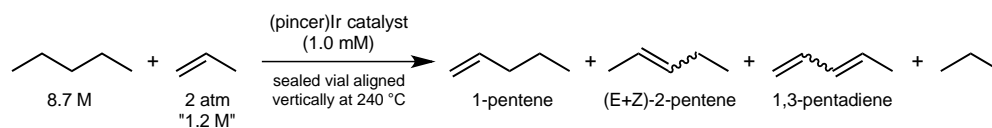
n-Pentane/propene transfer dehydrogenation was initially investigated with nine different pincer-Ir complexes (Table 1 and Scheme 1). We have previously reported that the relatively uncrowded mixed methyl/*t*-butyl substituted complexes (*t*Bu³MePCP)IrH_n (**3**) and (*t*Bu²Me²PCP)IrH_n (**4**) are catalytically more active than **1** for the transfer dehydrogenation of *n*-octane using either TBE or NBE as acceptor.⁶ (Note that under transfer-dehydrogenation conditions, olefin, dihydride and tetrahydride complexes are equivalent as precursors of the catalytically active (pincer)Ir fragments.) Likewise, complexes (*p*-OMe-*i*Pr⁴PCP)IrH₄ (**7-H₄**) and (*i*Pr⁴PCP)IrH₄ (**2-H₄**) were reported to be more active than **1** for transfer dehydrogenation of *n*-alkanes using TBE.^{3,5,49}

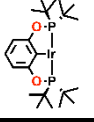
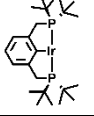
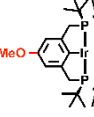
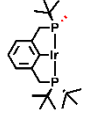
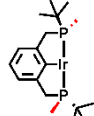
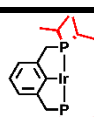
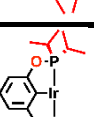
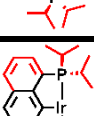
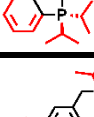
Scheme 1. Pincer-Ir catalysts investigated in this study



Transfer dehydrogenation of gas phase *n*-pentane using propene (2 atm) was successfully catalyzed under these conditions by the relatively crowded complexes $(^t\text{Bu}_4\text{PCP})\text{IrH}_n$ (**1**), the *p*-methoxy derivative $(p\text{-OMe-}^t\text{Bu}_4\text{PCP})\text{IrH}_n$ (**5**) and the bisphosphinite complex $(^t\text{Bu}_4\text{POCOP})\text{IrH}_n$ (**6**). These catalysts all gave relatively low TO numbers, less than 30 TO after 180 min at 240 °C (entries 1-3, Table 1). The apparent initial rates with catalysts **1** and **5** were moderately high, but were not maintained over the course of the reaction (e.g. catalyst **1** gave 20 TO after 10 min, but the same TON was found after 40 min). Catalyst **3**, in which one of the ^tBu groups of **1** is substituted by a methyl group, showed slightly greater catalytic activity (entry 4, Table 1; 59 TO after 40 min). To our knowledge these are the first examples of presumed molecular catalysts effecting heterogeneous (gas-solid phase) dehydrogenation of alkane.

Table 1. Dehydrogenation of *n*-pentane “[8.7 M]”^a by various pincer-Ir catalysts, under 2 atm propene “[1.2 M]”^a at 240 °C^b



Entry	Catalyst / 1 mM	Time / min	Total Olefins ^c / mM	1-Pentene / mM (% total monoenes)	% Propene conversion (by GC)	Dienes / mM
1	 6	10	0	0	ND	0
		180	8	4 (50%)	ND	–
2	 1	10	20	15 (75%)	ND	–
		40	20	17 (85%)	ND	–
3	 5	10	23	18 (75%)	ND	1
		180	25	20 (77%)	ND	1
4	 3	10	0	0	ND	0
		40	59	50 (85%)	ND	0
5	 4	10	340	105 (33%)	30	21
		180	950	200 (24%)	98	150
6	 2	10	630	140 (24%)	63	40
		180	1050	230 (24%)	90	110
7	 8	10	96	53 (56%)	10	2
		180	630	170 (29%)	52	40
8	 9	10	110	79 (72%)	ND	2
		180	160	100 (64%)	ND	4
9	 7	10	170	120 (70%)	ND	3
		180	310	180 (61%)	ND	10

^a Concentrations given represent concentrations obtained after the indicated time of heating, followed by cooling of the reaction vessel to 25 °C so that all species are condensed or dissolved into liquid solution phase.

^b Reaction vessels (glass ampoules) were oriented vertically.

^c Most runs were repeated; results given are the average of two or more runs. Reproducibility averaged $\pm 3\%$.

In contrast with the moderate activity noted above, much higher rates and TONs were obtained with the use of catalyst **4**, in which methyl groups replace two of the *t*Bu groups of **1** (entry 5, Table 1). After 10 min, 340 TO had been obtained, corresponding to consumption of ca. 30% of the propene in the vessel, while after 180 min, the TON was 950, corresponding to hydrogenation of >90% of the propene. Dehydrogenation catalyzed by (*i*Pr⁴PCP)Ir(C₂H₄) (**2**) proceeded even more rapidly (entry 6, Table 1); 630 TO were obtained after 10 min and >1000 TO after 180 min. These rates and turnover numbers are unprecedented even for solution phase alkane dehydrogenation systems.

The very high catalytic efficiency of (*t*Bu₂Me²PCP)IrH₄ (**4**) compared to (*t*Bu₃MePCP)IrH₄ (**3**) contrasts with our earlier observations on *n*-octane transfer dehydrogenation with TBE or NBE as acceptors.⁶ Studies on **3** and **4** for *n*-octane transfer dehydrogenation using TBE or NBE indicated that **3** was the more effective of the two catalysts (although both **3** and **4** provided higher activity than **1**). However, as **4** showed a tendency to form dinuclear clusters, it was unclear whether this was responsible for its lesser activity. Given the presumably much greater binding ability of propene vs. the bulkier TBE or NBE, the formation of dimers or oligomers should be much less significant in the presence of propene; the much greater reactivity of **4** vs. **3** when using propene thus lends support to this explanation for the lesser activity of **4** obtained when NBE or TBE is used as acceptor.

The activity levels of hybrid phosphine-phosphinite catalyst (*i*Pr⁴PCOP)Ir(C₂H₄) (**8**) (entry 6, Table 1), and (*i*Pr⁴Anthrphos)Ir(C₂H₄) (**9**) (entry 7, Table 1) were high, but less than those of either **4** or **2**. The *p*-methoxy derivative of **2**, (*p*-OMe*i*Pr⁴PCP)Ir(C₂H₄) (**6**) appeared to give a good initial rate (170 TO after 10 min) but much lower conversion

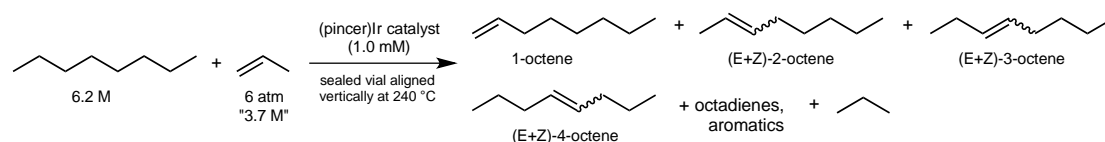
than **2** after 180 min. We suspect this is due to intermolecular reactions involving the methoxy groups, leading to catalytically inactive species.^{53,54}

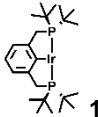
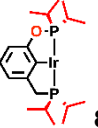
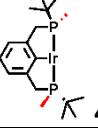
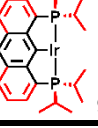
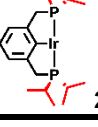
The great differences in catalytic activity among these various catalysts, and particularly the disparity between the more crowded (three or more *t*-Bu groups) and less crowded complexes was not expected. Previous studies in our lab and others have indicated that less crowded complexes did indeed tend to be more active, but the difference was much less dramatic. These studies generally utilized NBE and TBE as hydrogen acceptors and, of course, were in the liquid phase. For example, the difference between the activity of ^{*t*Bu}4PCP and ^{*i*Pr}4PCP catalysts was found to be a factor of ca. 3-fold.⁶ The present results therefore raised the question as to whether the large differences between the catalysts, most notably the ^{*t*Bu}4PCP and ^{*i*Pr}4PCP derivatives, were a result of the different acceptors used in this study, or a result of the unusual conditions, particularly the solid vs. solution phase.

Accordingly, we conducted *solution-phase* experiments (using *n*-octane as dehydrogenation substrate) under similar conditions, including the nature of the acceptor and the unusually high temperature (240 °C). Results are shown in Table 2. A very pronounced difference in activity is observed between the (^{*t*Bu}4PCP)Ir and (^{*i*Pr}4PCP)Ir precursors: a factor of ca. 11 in the initial data point, a value which is of the same magnitude as the factor of ca. 30 observed in the gas-solid-phase experiments. Further, we find that in the case of catalyst **1** and propene as acceptor, in both solid and liquid phases the rate decreases dramatically after an initial period of catalysis with a relatively slow rate. We are not able to fully explain this behavior of catalyst **1**, but our observations all seem applicable to both solution and solid phase. Indeed, the fact that we

observe, in both solution and solid phase, both the dramatic difference between catalysts **1** and **2** and the particular temporal profile of catalyst **1**, strongly indicates that the catalysts are operating as discrete molecular species even in the solid phase.

Table 2. Dehydrogenation of *n*-octane [6.2 M]^a by various pincer-Ir catalysts, under 6 atm propene “[3.7 M]”^a at 240 °C^b



Entry	Catalyst / 1 mM	Time / min	Total Olefins ^c / mM	1-Octene / mM (% total monoenes)	% Propene conversion (by GC)	Dienes / mM
1		10	170	56 (34%)	4	7
		40	190	43 (23%)	4	8
2		10	290	75 (28%)	4	15
		40	600	140 (25)	10	61
3		10	180	73 (31%)	2	8
		40	1100	140 (16%)	15	260
4		10	1250	250 (24%)	15	230
		40	1310	270 (24%)	20	190
5		10	1930	160 (13%)	44	670
		40	2430	130 (10%)	65	1130

^a Concentrations given represent concentrations obtained after the indicated time of heating, followed by cooling of the reaction vessel to 25 °C so that all species are condensed or dissolved into liquid solution phase.

^b Reaction vessels (glass ampoules) were oriented vertically.

^c Most runs were repeated; results given are the average of two or more runs. Reproducibility averaged $\pm 2\%$.

In an effort to determine the physical distribution of catalyst during the gas-solid phase experiments, after several runs the GC oven temperature was lowered from 240 °C to 60 °C and slowly opened in the range of a camcorder (see SI for images of one such experiment with ($i\text{Pr}^4\text{PCP}$)Ir(C₂H₄) (**2**)). At this point the top portion of the vial was cool relative to the base, which was still hot as it was enclosed in the aluminum block. The resulting images clearly show bright red droplets formed along the topmost portions of the vial as pentane condenses on the catalyst that had deposited on the glass. This observation could be explained by vigorous splashing, when the pentane solution is heated to 240 °C (followed by rapid solvent evaporation) or alternatively, by sublimation of the catalyst at this temperature. To distinguish between these possibilities, an ampoule containing solid catalyst was heated under the same conditions as the catalytic runs, including the presence of 2 atm propene but in the absence of pentane or other liquid. Under such conditions, no significant migration of the iridium complex within the ampoule was observed. Thus, rather than sublimation of catalyst, it seems likely that when a pentane solution of catalyst is heated at 240 °C, the solution splashes and coats the glass surface before the solvent is fully evaporated.

If it is assumed that the catalyst coats the glass surface, then, by having vials aligned horizontally rather than vertically, the catalyst would have a greater surface area and should function more efficiently. When the ampoules were positioned horizontally (using catalysts **2**, **8** and **9** which proved most effective in the experiments, cf. Table 1) even higher rates were achieved as shown in Table 3. Remarkably, in the case of catalyst **2**, the reaction had effectively proceeded to completion ($\geq 97\%$ consumption of propene, > 1000 TO) after 10 min.

Table 3. Dehydrogenation of *n*-pentane “8.7 M”^a under 2 atm propene “1.2 M”^a at 240 °C with selected catalysts and ampoules positioned horizontally^b

8.7 M + 2 atm "1.2 M" $\xrightarrow[\text{sealed vial aligned horizontally at 240 } ^\circ\text{C}]{\text{(pincer)Ir catalyst (1.0 mM)}}$ 1-pentene + (E+Z)-2-pentene + 1,3-pentadiene + n-pentane

Entry	Catalyst / 1 mM	Time / min	Total Olefins ^c / mM	1-Pentene / mM (% total monoenes)	% Propene conversion (by GC)	Dienes / mM
1	 8	10	220	120 (54%)	21	3
		180	920	170 (20%)	74	82
2	 9	10	520	240 (50%)	48	32
		180	680	190 (31%)	67	64
3	 2	10	1090	200 (20%)	97	110
		180	1200	190 (17%)	97	114

^a Concentrations given represent concentrations obtained after the indicated time of heating, followed by cooling of the reaction vessel to 25 °C so that all species are condensed or dissolved into liquid solution phase.

^b Reaction vessels (glass ampoules) were oriented horizontally.

^c Most runs were repeated; results given are the average of two or more runs. Reproducibility averaged $\pm 1\%$.

n-Butane was also investigated as a dehydrogenation substrate. Into an ampoule containing the same quantity of catalyst **2** that was used in the experiments of Tables 1-3, a 1:1 butane/propene gas mixture was condensed (see Fig. 2) such that upon sealing and warming to room temperature the pressures of butane and propene each reached 3 atm. High rates and turnover numbers were observed (Table 4). In view of the much higher volatility of butane (b.p. = -1 °C) than pentane (b.p. = 36 °C), these results may be interpreted as arguing against the possibility of a condensed amorphous catalyst/alkane phase as opposed to a “true” solid-gas interaction. (It is well beyond the scope of this

work, however, to address in detail the question of the “phase” of any hydrocarbon adsorbed to the solid.)

Table 4. Dehydrogenation of *n*-butane (3 atm) “[6.1 M]”^a with propene (3 atm) “[6.1 M]”^a at 240 °C catalyzed by 2. ^b

3 atm "6.1 M" + 3 atm "6.1 M" $\xrightarrow[\text{sealed vial aligned horizontally at 240 } ^\circ\text{C}]{\text{(pincer)Ir catalyst (1.0 mM)}}$ 1-butene + (E+Z)-2-butene + butadiene +

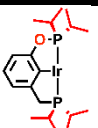
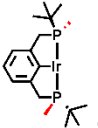
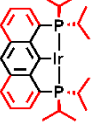
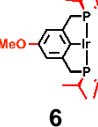
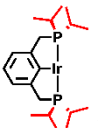
Catalyst / 1 mM	Time / min	Total Olefin ^c / TON	Butadiene / TON	1-Butene / TON	1-Butene Fraction / %
	10	335	40	185	65
	40	590	40	370	65
	180	680	65	280	45

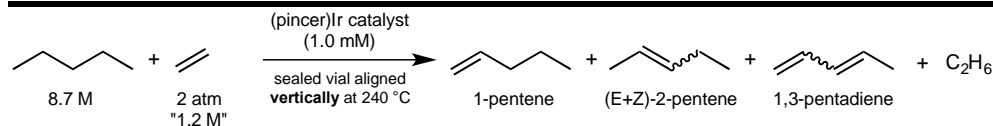
^a Concentrations given represent concentrations obtained after the indicated time of heating, followed by cooling of the reaction vessel to -15 °C so that all species are condensed or dissolved into liquid solution phase.

^b Reaction vessels (glass ampoules) were oriented horizontally.

Ethylene would be even more attractive as a hydrogen acceptor than propene (in addition to the abundance of ethylene derived from shale gas in North America, ethane could be more easily recycled via separation from the alkane substrate and conventional dehydrogenation methods⁴⁶). In this context, experiments with ethylene gave highly encouraging results (Table 5), although rates were roughly a factor of ten slower than when propene was used as acceptor.

Table 5. Dehydrogenation of *n*-pentane “[8.7 M]”^a with ethylene (2 atm, “1.2 M”)^a at 240 °C^b by various pincer-Ir catalysts

Entry	Catalyst / 1 mM	Time / min	Total Olefins ^c / mM	1-Pentene / mM (% total monoenes)	% Ethylene conversion (by GC)	Dienes / mM
1		10	17	12 (71%)	ND	0
		40	45	34 (76%)	ND	0
2		10	98	70 (71%)	ND	1
		180	254	135 (55%)	ND	7
3		10	41	36 (88%)	ND	0
		180	150	120 (78%)	ND	1
4		10	41	36 (88%)	ND	0
		180	156	120 (78%)	ND	1
5		10	72	60 (88%)	4	2
		40	320	250 (79%)	ND	5
		100	660	430 (65%)	ND	28
		180	720	420 (61%)	44	41



^a Concentrations given represent concentrations obtained after the indicated time of heating, followed by cooling of the reaction vessel to 25 °C so that all species are condensed or dissolved into liquid solution phase.

^b Reaction vessels (glass ampoules) were oriented vertically.

^c Most runs were repeated; results given are the average of two or more runs. Reproducibility averaged $\pm 2\%$.

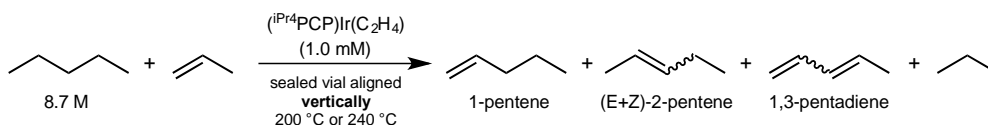
Selectivity for production of α -olefins. Regioselective functionalization of the terminal position of *n*-alkanes (or *n*-alkyl groups) has long been one of the major goals of research in catalytic hydrocarbon conversion. Ever since the earliest examples of organometallic C-H bond activation revealed selectivity for oxidative addition at 1° vs. 2°

positions⁵⁵ – and thus a remarkable preference for cleaving stronger C-H bonds – this selectivity has been viewed as perhaps the most important potential advantage of “homogeneous” vs. “heterogeneous” catalysts for the functionalization of alkanes or alkyl groups. Thus, we were quite surprised to observe that the heterogeneous systems described above appeared to show *greater* selectivity for the formation of α -olefins than the homogeneous (solution-phase) systems based on the same catalysts. For example, **2**-catalyzed pentane-ethylene transfer dehydrogenation yielded 430 mM α -olefin (upon condensation to the liquid phase; entry 5, Table 5) and formation of 660 mM total olefin. This is an unprecedented yield of α -olefin from *n*-alkane dehydrogenation; as noted above, to our knowledge the highest yield of α -olefin previously reported from *any* catalytic alkane dehydrogenation system was 97 mM (out of a total conversion to olefin of 143 mM).⁵⁶

The high selectivity, in even a qualitative sense, for α -olefin formation resulting from a heterogeneous system is certainly noteworthy; for example, after 10 min at 240 °C, 88% selectivity with total conversion to 72 mM (upon condensation) is obtained (entry 5, Table 5). This observed regioselectivity certainly supports the argument that the catalyst, although not in solution, is still operating as a discrete molecular species. But even more remarkable is the appearance of even *greater* selectivity for α -olefin formation from the heterogeneous system as compared with the same catalyst in solution. Accordingly, further experiments were conducted in large part with an aim toward explaining this phenomenon.

Table 6. Dehydrogenation of *n*-pentane “[8.7 M]” under 2 atm and 6 atm propene at 200 °C and 240 °C catalyzed by **2-C₂H₄**

Entry	Conditions	Time / min	Total Olefins ^c / mM	1-Pentene / mM (% total monoenes)	% Propene conversion (by GC)	Dienes / mM
1	240 °C	10	630	140 (24%)	63	40
	2 atm	40	850	170 (22%)	77	70
	“1.2 M”	180	1050	230 (24%)	90	110
2	240 °C	10	1370	420 (37%)	56	210
	4 atm	40	1450	440 (36%)	66	230
	“2.5 M”	180	1590	430 (33%)	73	290
3	240 °C	10	700	300 (48%)	20	76
	6 atm	40	870	400 (51%)	20	87
	“3.7 M”	180	1060	440 (46%)	30	116
4	240 °C	10	695	380 (58%)	8	40
	6 atm	40	930	485 (56%)	10	65
	“7.4 M” ^d	80	1420	575 (46%)	16	170
5	200 °C	10	410	150 (41%)	36	34
	2 atm	40	690	190 (32%)	60	75
	“1.2M”	180	720	190 (30%)	67	74
6	200 °C	10	370	155 (46%)	15	30
	4 atm	40	510	210 (45%)	20	40
	“2.5M”	180	800	260 (37%)	39	94
7	200 °C	10	270	130 (50%)	ND	17
	6 atm	40	470	220 (50%)	14	30
	“3.7M”	180	950	320 (40%)	35%	110



^a Concentrations given represent concentrations obtained after the indicated time of heating, followed by cooling of the reaction vessel to 25 °C so that all species are condensed or dissolved into liquid solution phase.

^b Reaction vessels (glass ampoules) were oriented vertically.

^c Most runs were repeated; results given are the average of two or more runs. Reproducibility averaged $\pm 3\%$.

^d Volume of pentane in each vial was reduced from 100 μ L to 50 μ L; thus the propene/pentane ratio was doubled.

When propene pressure is varied from 2 atm to 4 atm at 240 °C (Table 6) the overall rate of dehydrogenation increases by ca. 2-fold. Further increase in propene pressure to 6

atm results in a decreased rate, which is comparable to the rate observed with 2 atm of propene. The yield of α -olefin, however, depends significantly upon propene pressure; for example, after 40 min at 240 °C, conversion was very similar at 2 atm and 6 atm propene (850 – 870 mM), but yields of α -olefin were quite different, 170 mM (22%) and 400 mM (51%), respectively. Reducing the amount of pentane to 50 μ L allowed us to have approximately “7.4 M” propene while working under 6 atm (entry 4, Table 6). This reaction system, when heated at 240 °C for 80 min, gave the highest yield of 1-pentene yet reported from transfer-dehydrogenation, ca. 575 mM, which is about 5.9 times greater than the α -olefin yields obtained in previous reports.³ At lower temperatures, a similar dependence of propene pressure on yields of 1-pentene was observed (entries 5, 6 and 7, Table 6) as illustrated in Figure 3.

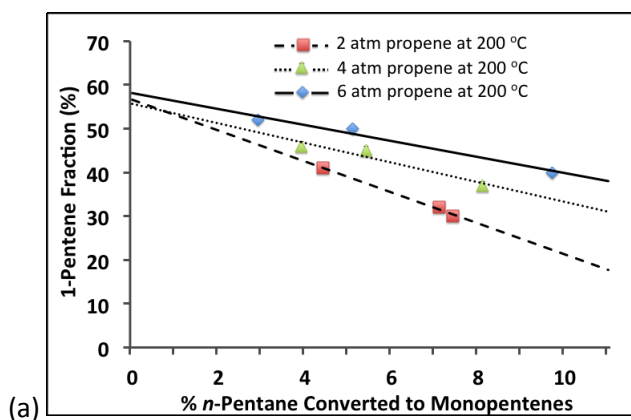
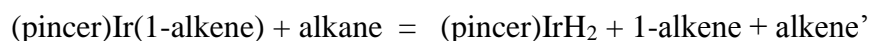


Figure 3. Plot of 1-pentene as fraction of pentenes formed in the dehydrogenation of *n*-pentane catalyzed by **2-C₂H₄** under 2 atm, 4 atm, and 6 atm propene at 200 °C

Origin of the high α -olefin yields. As discussed above, high yields of α -olefin are obtained when using ethylene as acceptor and under high pressures of propene in particular. Both olefins, but ethylene in particular, are expected to bind strongly to the

pincer-iridium complex. This strong binding explains the relatively low rate of dehydrogenation obtained in the presence of ethylene, given that (pincer)Ir(ethylene) is presumably not catalytically active. We have recently shown that the dehydrogenation catalyst ($t\text{Bu}^4\text{PCP}$)Ir (**1**) catalyzes olefin isomerization via an η^3 -allyl pathway which, in turn, proceeds via C-H addition prior to olefin coordination.⁵⁷ Thus olefins like ethylene that bind very strongly, or high pressures of propene which binds fairly strongly, would be expected to inhibit isomerization of the α -olefin primary product. However, such binding of the acceptor olefins would also be expected to inhibit (equally) the rate of dehydrogenation; if the rate of isomerization relative to dehydrogenation were unchanged, the maximum concentration of α -olefin would also be unchanged (although it would of course take more time to reach that maximum).

The conclusion, in our earlier study, of an η^3 -allyl isomerization pathway being operative for catalyst **1** was based on several lines of evidence.⁵⁷ In particular, we gave very strong consideration to the most commonly proposed pathway for olefin isomerization: insertion into an M-H bond (e.g. 2,1-addition of 1-alkene), followed by β -H migration at C3 to give the more stable double-bond isomer, 2-alkene); we will refer to this as a “hydride addition pathway”. Under the conditions of our studies the only observable resting state was always ($t\text{Bu}^4\text{PCP}$)Ir(1-alkene). Thus, a hydride addition pathway would proceed via a small, if unobservable, concentration of a catalytically active hydride, most likely ($t\text{Bu}^4\text{PCP}$)IrH₂, which should be present according to eq 1.



(1)

The concentration of the hydride species would be much greater in alkane than in arene solvent due to the steady state behavior of eq 1; therefore, isomerization rates would be commensurately much greater if such a species were largely responsible for isomerization. In fact we found that rates of 1-alkene isomerization by **1** were identical in *n*-octane and *p*-xylene solvent⁵⁷ (and this result was reproduced during the present study).

In the case of (ⁱPr⁴PCP)Ir (**2**), as with **1**, the major resting state in the presence of any appreciable concentration of 1-alkene is the 1-alkene complex (or the propene or ethylene complex in the presence of these olefins). However, the effect of alkane vs. arene solvent on the rate of isomerization proved to be very different in the case of **2**. Addition of 1-octene [100 mM] to **2**-C₂H₄ (1 mM) in either *n*-octane or *p*-xylene solvent resulted in complete conversion to (ⁱPr⁴PCP)Ir(1-octene), *without any hydride species observable in either solvent*. However, in contrast with the catalytic behavior of **1**, 1-octene isomerization is indeed significantly faster in *n*-octane than in *p*-xylene, by ca. two-fold (Figure 4). This indicates that dihydride **2**-H₂ is a much more active catalyst (on a per mol basis) than **2**-(1-octene). Nevertheless, given that the small concentration of dihydride would be many times greater in alkane than in arene (eq 1), the fact that there is *only* a ca. 2-fold difference indicates that isomerization by **2** does not proceed exclusively via the hydride pathway. Instead, it can be concluded that the observed isomerization in *p*-xylene solvent is not due to a hydride pathway, but is presumably due to an allyl pathway; the rate of this pathway might be considered a “baseline”, while the presence of any **2**-H₂ could add to this baseline rate.

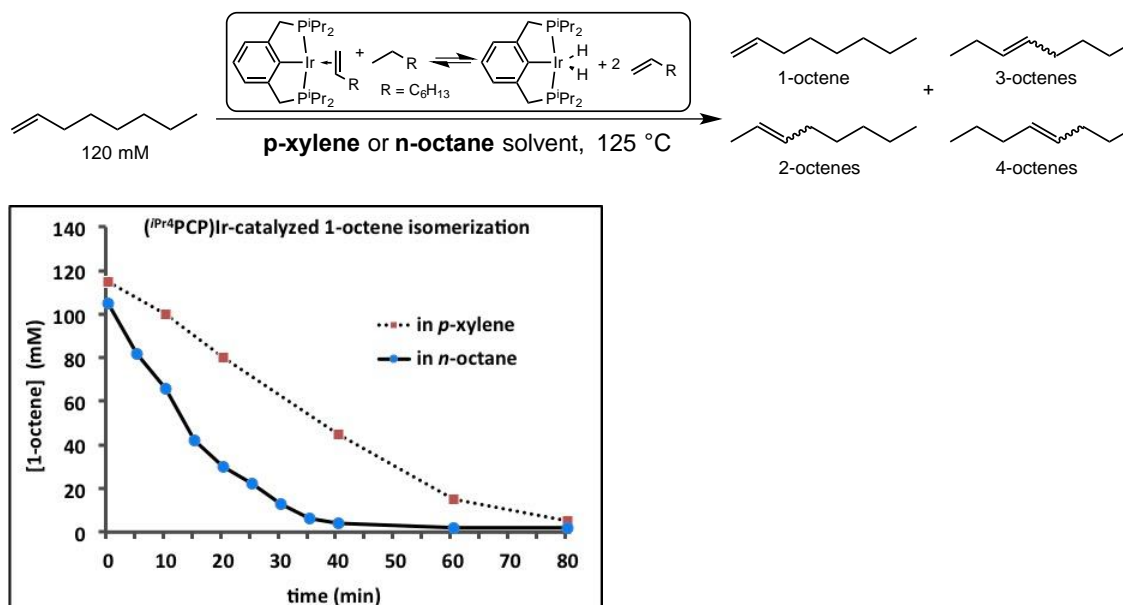


Figure 4. Isomerization of 1-octene in *n*-octane and *p*-xylene at 125 °C catalyzed by **2**

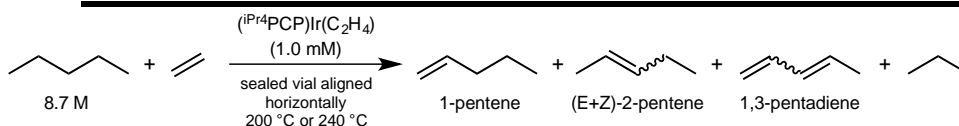
Ethylene is presumably a better hydrogen acceptor than propene, given that the thermodynamics of its insertion and hydrogenation are more favorable, and that it is sterically less demanding. Thus any contribution to isomerization from a hydride pathway would be expected to be minimized by the presence of ethylene, particularly at high pressure. Indeed, under 4 atm ethylene (and with the reaction ampoule oriented horizontally so as to maximize surface area and minimize diffusion limitations) the yield of 1-pentene was the highest we have obtained to date, 520 mM (after condensation) after 180 min (entry 1, Table 7).

With 2 atm instead of 4 atm ethylene (entry 2, Table 7), the reaction rate is expected to be somewhat (up to 2-fold) faster due to decreased inhibition. Surprisingly, however, under these conditions the reaction was found to be ca. 4-fold faster. We suspect this result is due to a diffusion limitation which lowers the local ethylene concentration and thus (somewhat counter-intuitively) produces a rate even faster than

would be predicted. With respect to mechanistic study, the value of this experiment is thus doubtful.

Table 7. Dehydrogenation of *n*-pentane [“8.7 M”] with ethylene at 240 °C catalyzed by **2**.^{a,b}

Entry	Conditions	Time / min	Total Olefins ^c / mM	1-Pentene / mM (% total monoenes)	% Ethylene conversion (by GC)	Dienes / mM
1	240 °C	10	562	346 (64%)	63	24
	2 atm “1.2 M”	40	1292	115 (10%)	100	82
2	240 °C	10	132	114 (88%)	8	0
	4 atm	40	306	238 (79%)	16	4
	“2.4 M”	180	1096	524 (52%)	60	90
3	200 °C	10	26	22 (85%)	85%	0
	2 atm	40	114	90 (80%)	80%	0
	“1.2M”	80	260	186 (72%)	24	3
		180	424	248 (61%)	61%	14
4	200 °C	10	3	3 (>97%)	ND	0
	4 atm	80	28	26 (93%)	1	0
	“2.4”	600	220	166 (78%)	8	3
		1200	456	278 (64%)	15	11



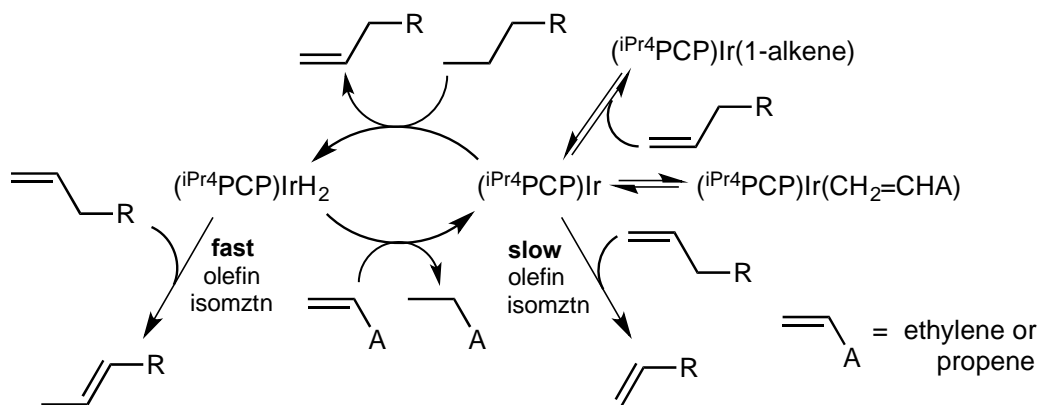
^a Concentrations given represent concentrations obtained after the indicated time of heating, followed by cooling of the reaction vessel to 25 °C so that all species are condensed or dissolved into liquid solution phase.

^b Reaction vessels (glass ampoules) were oriented horizontally.

^c Most runs were repeated; results given are the average of two or more runs. Reproducibility averaged $\pm 3\%$.

Overall, the picture that emerges from these studies is illustrated in Scheme 2.

Scheme 2



Implicit in the above explanation of selectivity is a model of reactivity that is at least qualitatively not different from the behavior of the catalyst in solution. We therefore further explored the liquid phase reactivity with the same acceptors and *n*-alkanes as an obvious test of this model. Moreover, the solution phase does not present the issue of irreproducible surface area and physical distribution of the catalyst, thus allowing a more rigorously quantitative study of the reaction kinetics.

2-catalyzed, solution-phase, transfer dehydrogenation of *n*-octane was conducted with ethylene and with propene as acceptor. As with the gas-solid phase reactions, a glass ampoule was charged with catalyst, alkane, and olefin acceptor, and then sealed. The ampoule was rotated in the oven to promote gas-liquid mixing. Transfer-dehydrogenation was run with 2 atm, 4 atm, and 6 atm propene pressure. Higher propene pressures resulted in somewhat lower rates, indicating that a significant fraction of the catalyst was present as the out-of-cycle species **2-propene**. The effect on the rate from a 3-fold increase in P_{propene} , however, was less than a factor of 3 (<2-fold), suggesting that **2-propene** is not the only major species present.

If we assume that **2-propene** is catalytically inactive with respect to both octane dehydrogenation and 1-alkene isomerization, then an increase in [**2-propene**] (effectuated by increasing the propene pressure) is expected to lower the rates of both processes equally. Assuming that fragment **2** can react with either *n*-alkane (leading to dehydrogenation) or with α -olefin (leading to isomerization), an increase in P_{propene} would not be expected to have any direct effect on the ratio of dehydrogenation to isomerization if these were the only paths leading to dehydrogenation and isomerization, respectively. In that case, at a given level of conversion (i.e. after dehydrogenation had proceeded to a given extent), the degree of isomerization would be proportional, and the fraction of unisomerized 1-alkene product formed would be independent of propene pressure. However, as seen in Table 8 and Figure 5a, at any given level of conversion the fraction of α -olefin is in fact higher under the higher propene pressure[s]. This is explained in terms of the left side of Scheme 2: if a small concentration of **2-H₂** is responsible for a significant fraction of the isomerization, then increasing propene concentration will decrease the steady-state concentration of **2-H₂**, thus resulting in decreased isomerization and higher α -olefin yields.

When ethylene is used as the hydrogen acceptor, the yields of 1-octene show a weak dependence on ethylene pressure. At high ethylene pressures, the yields of 1-octene are somewhat higher than with propene but the difference between the two acceptors is not large. We interpret these results as approaching a regime, where the concentration of **2-H₂** is too low to contribute significantly to isomerization; in such a regime, the ratio of dehydrogenation to isomerization should be independent of ethylene or propene concentration.

Table 8. Dehydrogenation of n-octane “[6.2 M]”^a catalyzed by **2** (1 mM) under varying propene or ethylene pressures at 180 °C (spinning reaction vials).^b

Acceptor, Pressure	Time / min	Total olefins ^c / mM	1-Octene / mM (Fraction %)	% Acceptor conversion (by GC)	Dienes /mM
propene	5	340	93 (29%)	18	17
2 atm	10	590	120 (22%)	32	49
“1.2 M”	20	990	120 (14%)	60	150
	30	1240	80 (8%)	82	280
	5	270	92 (35%)	10	10
propene	10	490	165 (30%)	15	25
4 atm	20	840	146 (20%)	30	90
“2.4 M”	50	1455	120 (11%)	60	345
	90	1980	< 5	100	750
	5	200	70 (37%)	4	10
propene	10	500	160 (33%)	9	25
6 atm	30	870	190 (24%)	18	88
“3.6 M”	60	1410	190 (16%)	30	250
	120	1860	170 (12%)	46	480
	10	23	9 (40%)	2	1
ethylene	40	87	35 (40%)	8	2
2 atm	110	210	76 (37%)	17	8
“1.2 M”	250	430	130 (32%)	38	25
	480	690	160 (26%)	55	64
	840	1040	160 (18%)	75	150
	10	12	8 (66%)	-	0
ethylene	40	24	15 (63%)	1	0
4 atm	80	92	62 (67%)	5	1
“2.4 M”	200	170	85 (52%)	7	3
	480	430	150 (37%)	17	18
	960	960	210 (24%)	40	100
	1440	1100	200 (21%)	44	140
	40	<4	3 (83%)	ND	0
(^t Bu ₄ PCP)Ir (1)	180	33	20 (67%)	3	0
ethylene	960	156	78 (56%)	15	2
2 atm	2160	455	127 (29%)	35	20
“1.2 M”	5400	1000	130 (15%)	75	135

^a Concentrations given represent concentrations obtained after the indicated time of heating, followed by cooling of the reaction vessel to 25 °C so that all species are condensed or dissolved into liquid solution phase.

^b Reaction vessels (glass ampoules) were oriented horizontally.

^c Most runs were repeated; results given are the average of two or more runs. Reproducibility averaged $\pm 1\%$.

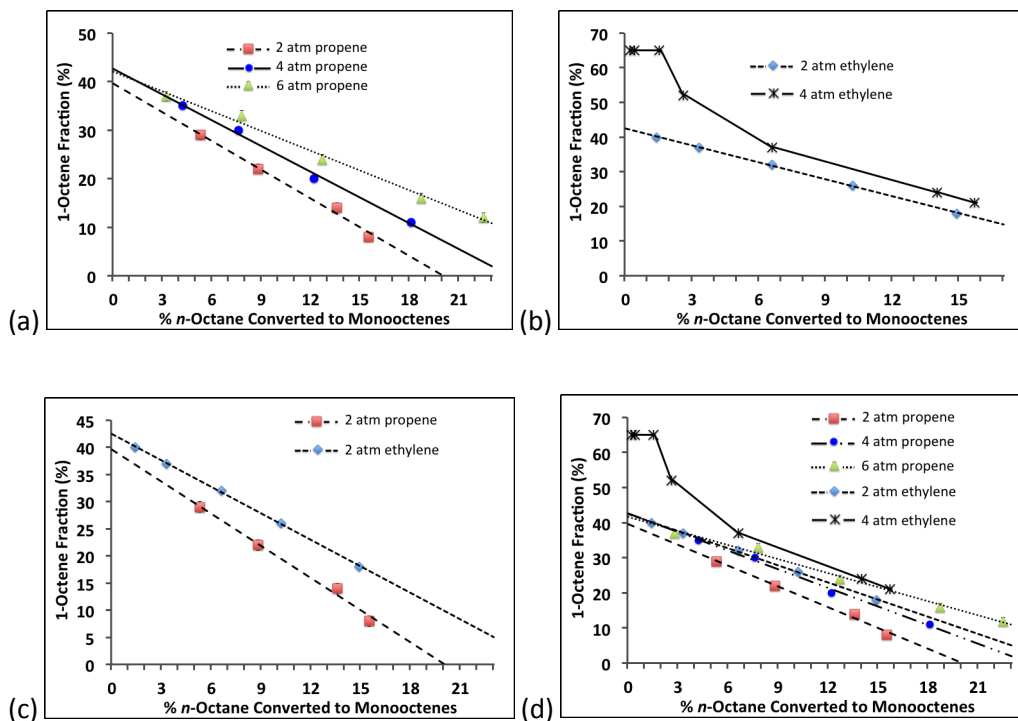


Figure 5. Plot of 1-octene as percentage fraction of octenes formed in the dehydrogenation of *n*-octane catalyzed by **2-C₂H₄** at 180 °C under (a) 2 atm, 4 atm, and 6 atm propene, (b) 2 atm and 4 atm ethylene, (c) 2 atm ethylene and propene, (d) data from all plots combined.

The reaction of *n*-octene with propene is probably too fast at 180 °C to obtain good kinetics data. For this reason, and also to investigate the effect of temperature further, we also conducted runs under propene at 160 °C. We also varied temperature with ethylene as acceptor, but in this case we raised the temperature to 200 °C, since the kinetics with ethylene were quite slow at 180 °C. Generally speaking, higher selectivity is of course associated with lower temperature – and this is particularly true in the case of formation of thermodynamically less favorable products. Inspection of Tables 8 and 9, however, reveals that at any given level of conversion, with any given pressure of either propene or ethylene, higher temperatures are found to give *greater* fractions of α -olefin.

Accordingly, at 200 °C and at the highest pressure of ethylene used (4 atm), an α -olefin yield as high as 250 mM (250 TO) is obtained, a factor of 2.5 greater than any previously reported value in solution.

Table 9. Dehydrogenation of *n*-octane (6.2 M) catalyzed by **2** (1.0 mM) under propene at 160 °C, and under ethylene at 200 °C

Acceptor	Condi tions	Time /min	Total Olefins / mM	1-Octene / mM (Selectivity %)	% Acceptor conversion (by GC)	Diene s / mM
propene	160 °C 2 atm "1.2 M"	10	96	55 (57%)	5	0
		20	190	76 (41%)	9	3
		40	450	100 (24%)	23	21
		90	720	105(16%)	40	66
		180	1310	52 (5%)	90	340
propene	160 °C 6 atm "3.6 M"	10	55	37 (67%)	1	0
		20	118	55 (47%)	2	2
		40	270	110 (40%)	4	7
		80	540	120 (25%)	11	40
		120	690	140 (22%)	12	50
		180	850	140 (19%)	20	110
ethylene	200 °C 2 atm "1.227 M"	10	170	90 (56%)	16%	2
		20	360	140 (40%)	23%	14±1
		40	580	200 (40%)	45%	28±1
		90	950	195 (24%)	75%	96±2
		120	1190	2(<1%)	100%	206±6
ethylene	200 °C 4 atm" "2.45 M"	10	40	28 (74%)	2%	1
		40	180	96 (56%)	7%	4±1
		80	390	170 (44%)	17%	13±1
		120	560	210 (40%)	25%	30±4
		180	770	250 (34%)	32%	55±1
		280	910	230 (27%)	38%	55±1

^a Concentrations given represent concentrations obtained after the indicated time of heating, followed by cooling of the reaction vessel to 25 °C so that all species are condensed or dissolved into liquid solution phase.

^b Reaction vessels (glass ampoules) were oriented horizontally.

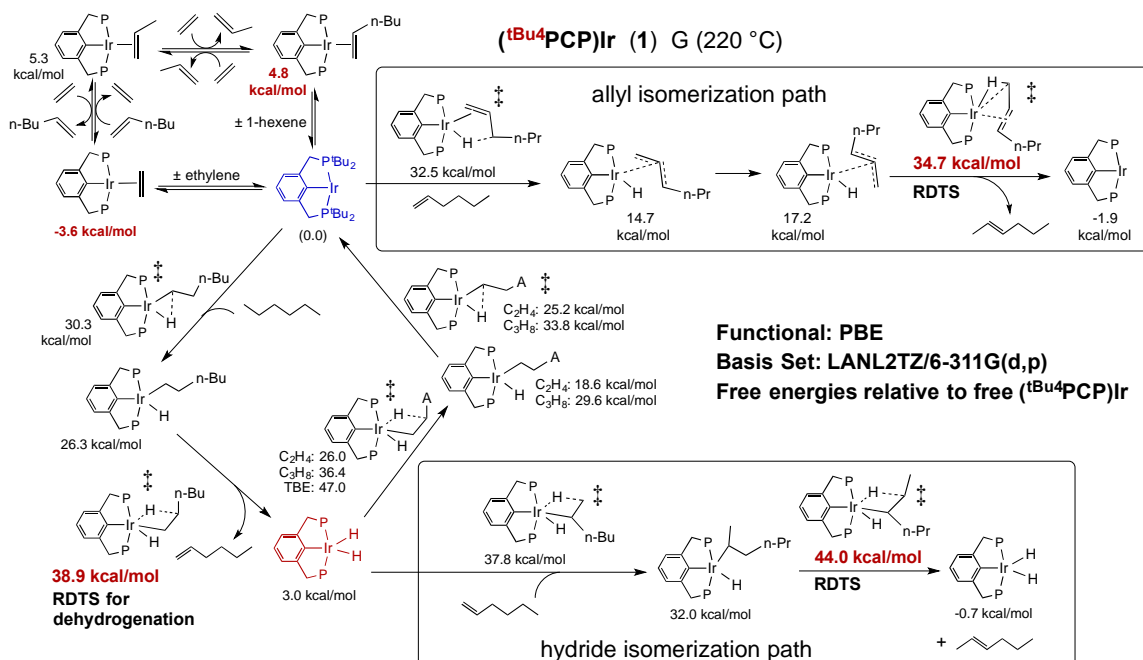
^c Most runs were repeated; results given are the average of two or more runs. Reproducibility averaged $\pm 1\%$.

Computational Results, Discussion, and Overview. Quantum mechanical calculations (DFT, see Computational Details) modeling (*in vacuo*) the $i\text{Pr}^4\text{PCP}$ (**2**) and $t\text{Bu}^4\text{PCP}$ (**1**) systems offer significant insight into the surprisingly high yields of α -olefin obtained in this work, both in solution and solid-gas phase experiments, and enable us to put the mechanistic hypotheses advanced above on a much firmer footing. Moreover, while we have previously reported that **2** is a more effective catalyst than **1** for several alkane dehydrogenation reactions,^{2,6,19} the difference was not as pronounced as in much of the present experimental work; the present set of DFT calculations help explain this observation as well.

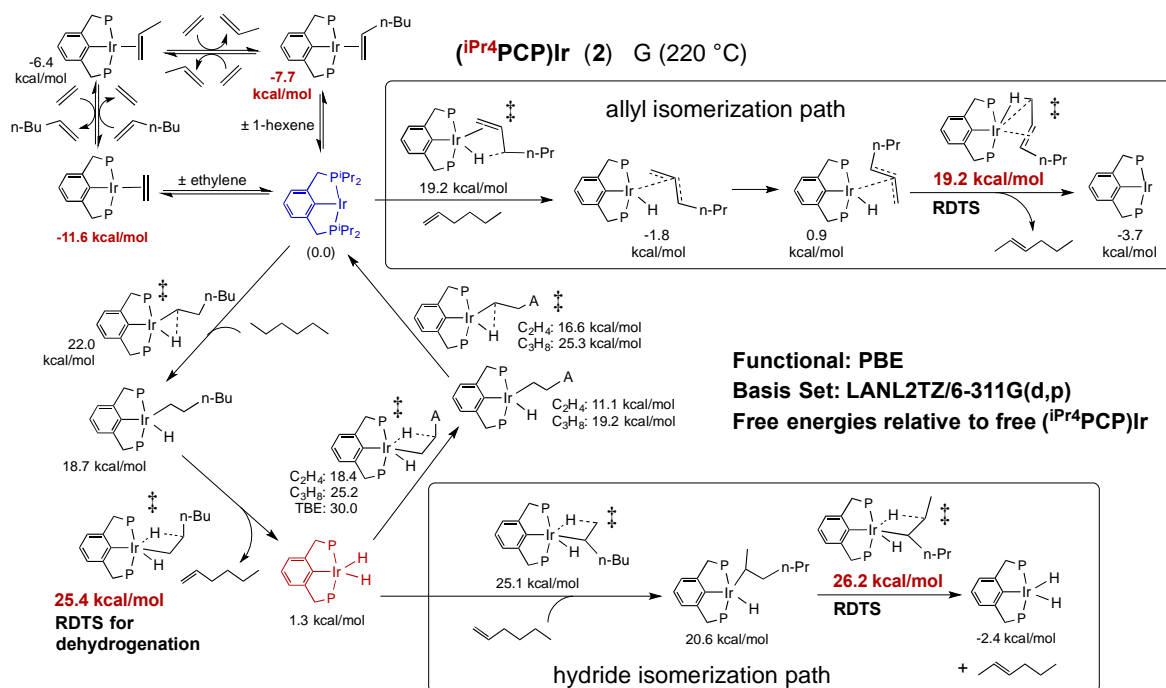
In the following, we use hexane/1-hexene as our representative *n*-alkane/1-alkene pair. If we consider the simple case of an *n*-alkane/1-alkene transfer-dehydrogenation cycle, the resting state of either catalyst **1** or **2** is the corresponding 1-alkene complex, while the rate-determining step is β -H elimination of the 1-alkyl iridium hydride C-H bond addition product (Schemes 3 and 4). For $(t\text{Bu}^4\text{PCP})\text{Ir}$, **1**, the difference in free energy between the 1-alkene complex resting state and the rate-determining TS (RDTS) is calculated to be 34.1 kcal/mol (38.9 kcal/mol - 4.8 kcal/mol) at 220 °C (ΔG_{220} ; most of the experiments in this work were conducted at 200 °C or 240 °C and for convenience, free energies are given at the intermediate temperature, 220 °C; Scheme 3). For catalyst **2** (Scheme 4), the difference in free energy between the RDTS for dehydrogenation and the 1-alkene complex resting state is $\Delta G_{220} = 33.1$ kcal/mol (25.4 kcal/mol - (-7.7) kcal/mol); the computed difference between the two catalysts, $\Delta G_{220} = 1.0$ kcal/mol, is consistent

with the experimentally observed significant but not extreme difference in catalytic activity of **2** vs. **1** for *n*-alkane/1-alkene transfer-dehydrogenation.⁶

Scheme 3. Calculated pathway with relative free energies (220 °C) for transfer-dehydrogenation and α -olefin isomerization catalyzed by **1**. Free energies of key resting states and rate-limiting (determining) transition states (RDTS) shown in red.



Scheme 4. Calculated pathway with relative free energies (220 °C) for transfer-dehydrogenation and α -olefin isomerization catalyzed by **2**. Free energies of key resting states and rate-limiting (determining) transition states (RDTS) shown in red.



However, catalyst **1** binds much more strongly to ethylene than to α -olefin ($\Delta G_{220} = 8.4$ kcal/mol, Scheme 3). The overall barrier for dehydrogenation in the ethylene reaction ($G_{\text{TS-beta-elim}} - G(\mathbf{1}\text{-ethylene})$) is therefore very high, $\Delta G_{220} = 42.5$ kcal/mol. In the case of the less crowded catalyst **2**, ethylene binds only 3.9 kcal/mol more strongly than does 1-hexene, and ΔG_{220} for the ethylene complex vs. the β -H elimination RDTS is 37.0 kcal/mol. Thus, in comparing catalysis by **2** vs. **1**, $\Delta G_{220} = 5.5$ kcal/mol in the case when ethylene is the acceptor; this corresponds to a very large difference in reaction rate between the two catalysts, in accord with observations (see Table 8, for example).

Both catalysts **1** and **2** are kinetically highly regioselective for the dehydrogenation of *n*-alkanes to give α -olefins;⁸ however, due to subsequent double-bond isomerization, with neither catalyst (nor with any other alkane dehydrogenation catalyst) have α -olefin yields previously been reported above 100 mM.⁸ The following computational results may explain why the conditions in the present work afford much higher α -olefin yields, in solution and especially in the solid-gas system.

As discussed above, we have previously determined that the major pathway for olefin isomerization by **1**⁵⁷ proceeds via formation of an iridium allyl complex (involving addition of the allylic sp^3 C-H bond to 14-electron fragment **1**). While allyl-based olefin isomerization pathways have long been known,⁵⁸⁻⁶⁴ the more commonly proposed “hydride isomerization pathway” involves insertion into a metal-H bond, followed by β -H elimination at the adjacent position (e.g. 2,1-addition of M-H to an α -olefin), and then 2,3-elimination.⁶³⁻⁷¹ This mechanism would seem to be a particularly likely path for a transfer-dehydrogenation system in which insertion of olefin (the acceptor) into M-H bonds is a necessary part of the catalytic cycle. The computational results shown in Scheme 3, however, explain why the “allyl isomerization pathway” predominates for isomerization catalyzed by **1**.

Dehydrogenation of *n*-alkane substrate yields (pincer)IrH₂. The predicted importance of the hydride isomerization pathway can be expressed in terms of the three possible reactions of the dihydride (Scheme 3). The RDTS for the hydride isomerization pathway by (*t*Bu⁴PCP)IrH₂ (**1-H₂**) (3,2- β -H-elimination) has a free energy of 44.0 kcal/mol (all energies are expressed relative to the free (pincer)Ir complex plus appropriate substrates unless noted otherwise). Alternatively, **1-H₂** can hydrogenate acceptor to complete one

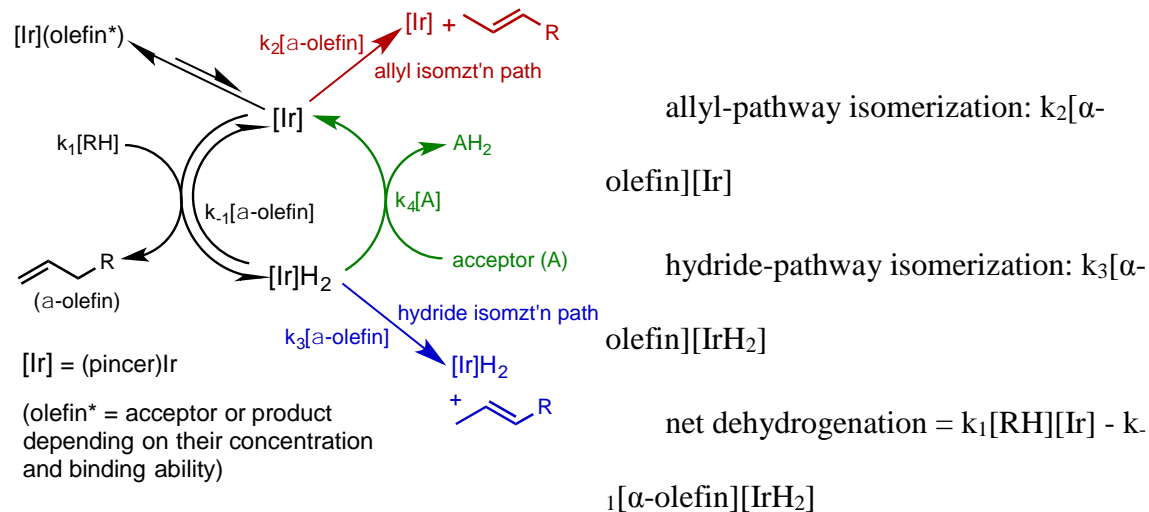
catalytic cycle. The respective RDTS free energies for hydrogenation are much lower: 26.0 kcal/mol and 36.4 kcal/mol for ethylene or propene, and 38.9 kcal/mol for higher α -olefin acceptors (the reverse of the β -H elimination step in dehydrogenation), respectively. Thus, the calculations predict that isomerization by **1-H₂** would be negligible in the presence of these acceptors. Even if the barrier to hydrogenation of the acceptor were much higher, as is calculated in the case of TBE at 47.0 kcal/mol, back reaction with the α -olefin product ($G_{\text{RDTS}} = 38.9$ kcal/mol) followed by isomerization via the allyl path ($G_{\text{RDTS}} = 34.7$ kcal/mol) would be much more rapid than isomerization by the hydride path.

In the case of catalyst **2** the free energy of the RDTS for the hydride isomerization path is much lower (26.2 kcal/mol, Scheme 4) than that of **1** and, importantly, in contrast with **1**, much lower relative to the competitive hydrogenations of acceptor or α -olefin. As with **1-H₂**, hydrogenation of ethylene still has a RDTS of much lower energy (18.4 kcal/mol); but for the much less crowded dihydride **2-H₂**, the RDTS for hydrogenation of propene (25.3 kcal/mol) and for the back reaction with α -olefin (25.4 kcal/mol) are quite comparable to the hydride isomerization RDTS. The calculations thus indicate that for catalyst **2** in the presence of ethylene, or in the limit of very high propene concentration or pressure, isomerization via the hydride path will not play a large role. In the case of low propene concentration or pressure, however, or in the case of an acceptor with a higher barrier to hydrogenation (e.g. TBE), the hydride isomerization path can be significant. Moreover, at lower concentrations of propene or in the case of a poor acceptor, the back reaction of α -olefin product will predominate over the forward

hydrogenation of acceptor. This back-reaction lowers the net rate of hydrogenation, while isomerization can still proceed via the allyl pathway.

The relative rates of isomerization and dehydrogenation (which determine the ultimate build-up of α -olefin) are expressed algebraically in eq 2, based on the rate constants indicated in Scheme 5.

Scheme 5. Simplified scheme illustrating relative rates of isomerization and dehydrogenation as well as corresponding rate constants. (Terms in the numerator of equation 2 are color-coded to indicate their origin in the corresponding isomerization pathways depicted in the scheme.)



$$[\text{IrH}_2] = \frac{k_1[\text{Ir}][\text{RH}]}{\{k_{-1}[\alpha\text{-olefin}] + k_4[\text{A}]\}}$$

$$\frac{\text{isomerization}}{\text{net dehydrogenation}} = \frac{k_2[\alpha\text{-olefin}] + \frac{k_3[\alpha\text{-olefin}]k_1[\text{RH}]}{\{k_{-1}[\alpha\text{-olefin}] + k_4[\text{A}]\}}}{k_1[\text{RH}] \left[1 - \frac{k_{-1}[\alpha\text{-olefin}]}{\{k_{-1}[\alpha\text{-olefin}] + k_4[\text{A}]\}} \right]} \quad (2)$$

From eq 2 it can be seen that in the limit of $k_4[\text{A}] \gg k_{-1}[\alpha\text{-olefin}]$ and $k_4[\text{A}] \gg k_3[\alpha\text{-olefin}]$ (i.e. conditions of fast hydrogenation of the sacrificial acceptor) the isomerization/dehydrogenation ratio reduces to $k_2[\alpha\text{-olefin}]/k_1[\text{RH}]$ (eq 3). Eq 3 reflects the competing reactions of (pincer)Ir (present in a very small steady-state concentration) with α -olefin (isomerization) vs. alkane (dehydrogenation).

If $k_4[\text{A}] \gg k_{-1}[\alpha\text{-olefin}]$ and $k_4[\text{A}] \gg k_3[\alpha\text{-olefin}]$:

$$\text{isomerization/dehydrogenation} = \frac{k_2[\alpha\text{-olefin}]}{k_1[\text{RH}]} \quad (3)$$

When ethylene is the acceptor, the difference in free energies of the respective RDTs's is very large for **1**, ca. 13 kcal/mol, and large even for **2** (ca. 7 kcal/mol); thus, either catalyst should be in the fast-acceptor hydrogenation limit and eq 3 is expected to be applicable, with no significant contribution to isomerization from a hydride pathway.

In the case of *propene* acceptor and (^tBu⁴PCP)Ir catalyst (**1**) the difference in free energies for the RDTs's of propene hydrogenation vs. isomerization via the hydride pathway is also very large (7.6 kcal/mol). The difference between propene hydrogenation vs. back-reaction with α -olefin is 2.5 kcal/mol. Hence, as long as propene concentration is comparable to α -olefin concentration the back-reaction rate will be small, and the system will still be in the fast-acceptor hydrogenation limit described by eq

3. Similarly, when α -olefin is used as acceptor, the relative rate of back reaction will be small as long as the acceptor is present in excess.

In the case of propene acceptor and the less bulky (iPr^4 PCP)Ir catalyst (**2**), however, the calculated difference in free energies for the RDTs's of propene hydrogenation vs. isomerization via the hydride pathway is small (1.0 kcal/mol), and the difference between propene hydrogenation vs. back-reaction with higher α -olefin is negligible (0.2 kcal/mol). In both cases this represents a competition between the reaction of **2-H₂** with propene vs. α -olefin. Thus, only in the limit of very high propene concentration or pressure (relative to concentration or pressure of α -olefin) will the isomerization/dehydrogenation ratio approach the lower limit of eq 3. As the reaction progresses and reaches the limit of complete consumption of propene the isomerization/dehydrogenation ratio will rapidly increase.

Regarding ethylene or propene acceptors, it should be noted that as the overall rate of dehydrogenation is inhibited by their binding to the iridium center, as the acceptor concentration or local pressure is *lowered*, its rate of consumption is *increased*. Thus, *slow* diffusion could result in a (counter-intuitive) *faster-than-expected* rate (either in the gas or solution phase) and a self-propagating cycle which in turn could further lower concentrations of acceptor; consecutively, this would result in a higher-than-expected rate of isomerization (eq 2) as well as a fast but diffusion-limited rate of hydrogenation.

The use of a higher α -olefin as sacrificial acceptor (one with chain length different from the n -alkane substrate so that the reaction is non-degenerate) allows simplification of eq 2, since we can then assume $k_4 = k_{-1}$. If we consider the point at which the acceptor

concentration is equal to the product (α -olefin) concentration, eq 2 can be simplified to eq 4:

$$\text{If } [\alpha\text{-olefin acceptor}] = [\alpha\text{-olefin product}]: \quad \frac{\text{isomerization}}{\text{net dehydrogenation}} = \frac{2k_2[\alpha\text{-olefin}]}{k_1[\text{RH}]} + \frac{k_3}{k_{-1}} \quad (4)$$

In the case of catalyst **1**, the term k_3/k_{-1} is predicted to be negligible due to the RDTs difference of 5.1 kcal/mol for the respective steps. For **2** the calculated difference (0.8 kcal/mol) is small, even within the range of error of the calculations, consistent with a significant contribution to isomerization from the hydride-isomerization pathway under this (fairly typical) set of conditions. This is also consistent with the results of the isomerization experiment in which only α -olefin is present (in that case α -olefin of only one chain length is present but that will not affect the rates of isomerization resulting from the different isomerization pathways.)

Note that in the case of catalyst **2** the use of highly reactive acceptors suppresses the dihydride path, which could otherwise play a significant role. But even independent of suppressing the hydride path, in the case of **1** or **2**, higher concentrations of more active acceptors (i.e. high values of $k_4[A]$) will favor a higher α -olefin fraction of total olefin produced by disfavoring the back-reaction of dihydride with α -olefin product. This is reflected in eq 2 in that, even in the limit of $k_3 = 0$, the ratio of isomerization to net dehydrogenation (eq 2) is still inversely dependent on $k_4[A]$.

(Pincer)Ir-catalyzed alkane dehydrogenation has been of particular interest in the context of alkane metathesis in which (pincer)Ir catalysts operate in tandem with olefin

metathesis catalysts.²⁶ As noted above, the hydride isomerization pathway is suppressed by the presence of effective hydrogen-acceptors in high concentration. In the course of an alkane metathesis reaction, however, the steady-state concentration of olefin is quite low, and the conditions favor the build-up of dihydride complex. Given that both catalyst **1** and **2** dehydrogenate alkanes with high regioselectivity for the terminal position, these results may well explain why catalyst **1** gives much better yields of C_{2n-2} product in alkane metathesis (e.g. *n*-decane from *n*-hexane) than does **2**.⁶ Indeed, although **2** and several other catalysts have shown high regioselectivity for dehydrogenation, catalyst **1** has proven nearly unique with respect to good selectivity in alkane metathesis;^{6,20,26} a possible explanation is that the dihydride isomerization path in particular is anomalously unfavorable for the highly crowded catalyst **1**.

The effect of the nature and concentration of acceptor on the α -olefin fraction as elucidated above may offer insight into the higher yields of α -olefin obtained in the gas phase vs. liquid. In a gas-phase experiment the ratio of total acceptor to α -olefin present in the reaction vessel equals the relative concentrations of these species to which the catalyst is exposed. In the solution phase experiments, however, while essentially all catalyst and α -olefin are in the solution phase, a large fraction of the ethylene or propene acceptor is in the gas phase, thus biasing the system toward isomerization vs. hydrogenation.

We note one additional effect which the DFT calculations suggest would contribute to the high yields of α -olefins reported in this work. High temperature is generally associated with a lack of selectivity. However, the RDTS (β -H elimination) for the dehydrogenation of *n*-alkane by **2** has an enthalpy barrier calculated to be 4.4 kcal/mol

greater than that of the RDTS for α -olefin isomerization catalyzed by **2**. Higher temperatures should thus favor dehydrogenation vs. isomerization, and ultimately the apparent “selectivity” for α -olefin production. The error in the calculated difference in enthalpy between these very different TSs (allyl-isomerization vs. β -H-elimination) is surely large relative to the small difference itself, but taking the calculated value of 4.4 kcal/mol as a “best guess”, we can consider the effect of conducting the reaction at 220 °C, for example, compared with a more typical reaction temperature of 150 °C. The predicted change in the ratio of dehydrogenation to isomerization via the allyl pathway is significant, viz. a factor of $\exp[(4.4 \text{ kcal}\cdot\text{mol}^{-1}/R)(1/T_1 - 1/T_2)] = 2.1$ ($T_1 = 423 \text{ K}$; $T_2 = 493 \text{ K}$). Note, however, that the RDTS for the *hydride* isomerization pathway has a slightly *higher* calculated enthalpy than the RDTSs for the competitive hydrogenation reactions; thus, the hydride pathway will be favored by higher temperature, highlighting further the importance of the use of highly effective hydrogen acceptors in obtaining high yields of α -olefin.

Conclusions

We report that pure solid phase (pincer)Ir catalysts are highly effective for the dehydrogenation of *n*-alkanes in the gas phase. ($i\text{Pr}^4\text{PCP}$)Ir (**2**) was found to be particularly effective for this purpose, while commonly used bulkier catalysts such as ($t\text{Bu}^4\text{PCP}$)Ir (**1**) or ($t\text{Bu}^4\text{POCOP}$)Ir are much less effective. High selectivity for α -olefin (the thermodynamically least stable double-bond isomer) is obtained, demonstrating that the solid catalyst is operating as the molecular species. Remarkably, the fractional yields of

α -olefin obtained from the heterogeneous systems are actually much greater than have been previously reported with homogeneous solution-phase systems.

In an effort to elucidate the origin of the unusually high α -olefin fraction, as well as the much greater reactivity of the less crowded catalysts, we conducted solution-phase studies and DFT calculations on complexes **1** and **2**. With ethylene as hydrogen acceptor the much greater reactivity of complex **2** is well explained by the DFT calculations. The difference in energy between the RDTS for dehydrogenation and the ethylene-bound resting state is calculated to be much greater for the bulky complex **1** than for **2**; in the case of higher olefins the difference is much smaller. This effect is applicable to propene also, but to a much lesser extent. However, decomposition of catalyst **1** seems to be promoted by propene via a mechanism that we do not yet understand.

While both **1** and **2** are known to be regioselective for dehydrogenation of *n*-alkanes to give α -olefins, yields of α -olefin are limited by double-bond isomerization; the highest yield of α -olefin previously reported in solution experiments was 97 mM (obtained with the use of **2**). We have reported that the mechanism of isomerization in the case of catalyst **1** proceeds entirely by reaction of the 14-electron fragment **1** with olefin via an allyl intermediate and not via the more typical hydride class of mechanism. DFT calculations show that the hydride pathway is much more competitive in the case of **2**; this is supported by experiments showing that 1-octene is isomerized ca. 2-fold more rapidly by **2** in *n*-octane vs. *p*-xylene solvent (whereas, in the case of complex **1**, the rate of isomerization in these two solvents is identical).

The contribution of the hydride pathway to isomerization is dependent upon a competition for the dihydride complex between hydrogenation of acceptor,

hydrogenation of α -olefin (i.e. back-reaction), and 2,1-insertion of the α -olefin leading to isomerization. DFT calculations indicate that the reaction of either **1-H₂** or **2-H₂** with ethylene is much more rapid than either back-reaction with α -olefin or isomerization of α -olefin. Hence the use of ethylene as hydrogen acceptor gives the highest yields of α -olefin in either solution-phase or solid-phase experiments; at high pressures, propene gives α -olefin yields that are only slightly lower. As the calculated activation enthalpy for dehydrogenation is higher than that for isomerization via the allyl pathway, higher temperatures favor the dehydrogenation/isomerization ratio and therefore higher α -olefin yields. Thus the high α -olefin yields obtained from the gas-solid systems with catalyst **2** are in large part simply a result of the conditions that lead to the gas/solid-phase state: use of highly volatile hydrogen acceptors and the high temperature, both of which mitigate the hydride isomerization pathway. A further advantage of the gas phase is that the catalyst is exposed to the same ratio of acceptor to α -olefin product that is present in the reaction vessel. In contrast, in the solution runs, the volatile acceptors propene and ethylene are partitioned largely into the gas phase while the α -olefin product remains in solution, thus favoring isomerization via the hydride path, as well as hydrogenation of α -olefin (back reaction); both effects contribute to an increase in the ratio of isomerization to dehydrogenation.

Thus we report a novel molecular gas-solid system which shows high kinetic selectivity for dehydrogenation of *n*-alkanes at the terminal position. The solid phase itself has little if any effect on the intrinsic selectivity and reactivity; indeed DFT calculation modeling the system *in vacuo* capture the key properties of the catalyst in the gas-solid system as well as in solution. Experiment and calculation have led to greater

insight into the factors that determine the yields of the desirable terminal dehydrogenation products. We find that it is possible to effectively eliminate one of two pathways for olefin isomerization with the appropriate conditions and hydrogen acceptor. A focus of further work will be on the design of catalysts for which the remaining η^3 -allyl isomerization pathway is less active relative to dehydrogenation.

References

- (1) Gupta, M.; Hagen, C.; Flesher, R. J.; Kaska, W. C.; Jensen, C. M. *Chem. Commun.* **1996**, 2083-2084.
- (2) Liu, F.; Goldman, A. S. *Chem. Commun.* **1999**, 655-656.
- (3) Liu, F.; Pak, E. B.; Singh, B.; Jensen, C. M.; Goldman, A. S. *J. Am. Chem. Soc.* **1999**, *121*, 4086-4087.
- (4) Xu, W.; Rosini, G. P.; Gupta, M.; Jensen, C. M.; Kaska, W. C.; Krogh-Jespersen, K.; Goldman, A. S. *Chem. Commun.* **1997**, 2273-2274.
- (5) Zhu, K.; Achord, P. D.; Zhang, X.; Krogh-Jespersen, K.; Goldman, A. S. *J. Am. Chem. Soc.* **2004**, *126*, 13044-13053.
- (6) Kundu, S.; Choliy, Y.; Zhuo, G.; Ahuja, R.; Emge, T. J.; Warmuth, R.; Brookhart, M.; Krogh-Jespersen, K.; Goldman, A. S. *Organometallics* **2009**, *28*, 5432-5444.
- (7) Punji, B.; Emge, T. J.; Goldman, A. S. *Organometallics* **2010**, *29*, 2702-2709.
- (8) Choi, J.; MacArthur, A. H. R.; Brookhart, M.; Goldman, A. S. *Chem. Rev.* **2011**, *111*, 1761-1779.
- (9) Findlater, M.; Choi, J.; Goldman, A. S.; Brookhart, M. In *Alkane C-H Activation by Single-Site Metal Catalysis*; Pérez, P. J., Ed.; Springer: New York, 2012; Vol. 38.
- (10) Haenel, M. W.; Oevers, S.; Angermund, K.; Kaska, W. C.; Fan, H.-J.; Hall, M. B. *Angew. Chem., Intl. Ed.* **2001**, *40*, 3596-3600.
- (11) Bezier, D.; Brookhart, M. *ACS Catal.* **2014**, *4*, 3411-3420.
- (12) Adams, J. J.; Arulsamy, N.; Roddick, D. M. *Organometallics* **2012**, *31*, 1439-1447.
- (13) Adams, J. J.; Lau, A.; Arulsamy, N.; Roddick, D. M. *Organometallics* **2011**, *30*, 689-696.
- (14) Shi, Y.; Suguri, T.; Dohi, C.; Yamada, H.; Kojima, S.; Yamamoto, Y. *Chem.-Eur. J.* **2013**, *19*, 10672-10689.
- (15) Göttker-Schnetmann, I.; Brookhart, M. *J. Am. Chem. Soc.* **2004**, *126*, 9330-9338.
- (16) Göttker-Schnetmann, I.; White, P.; Brookhart, M. *J. Am. Chem. Soc.* **2004**, *126*, 1804 - 1811.
- (17) Göttker-Schnetmann, I.; White, P. S.; Brookhart, M. *Organometallics* **2004**, *23*, 1766-1776.
- (18) Morales-Morales, D.; Redon, R.; Yung, C.; Jensen, C. M. *Inorg. Chim. Acta.* **2004**, *357*, 2953-2956.
- (19) Ahuja, R.; Punji, B.; Findlater, M.; Supplee, C.; Schinski, W.; Brookhart, M.; Goldman, A. S. *Nature Chem.* **2011**, *3*, 167-171.
- (20) Nawara-Hultsch, A. J.; Hackenberg, J. D.; Punji, B.; Supplee, C.; Emge, T. J.; Bailey, B. C.; Schrock, R. R.; Brookhart, M.; Goldman, A. S. *ACS Catalysis* **2013**, *3*, 2505-2514.
- (21) Brayton, D. F.; Beaumont, P. R.; Fukushima, E. Y.; Sartain, H. T.; Morales-Morales, D.; Jensen, C. M. *Organometallics* **2014**, Ahead of Print.
- (22) Yao, W.; Zhang, Y.; Jia, X.; Huang, Z. *Angew. Chem., Intl. Ed.* **2014**, *53*, 1390-1394.
- (23) Jia, X.; Zhang, L.; Qin, C.; Leng, X.; Huang, Z. *Chem. Commun. (Cambridge, U. K.)* **2014**, *50*, 11056-11059.
- (24) Goldman, A. S.; Roy, A. H.; Huang, Z.; Ahuja, R.; Schinski, W.; Brookhart, M. *Science* **2006**, *312*, 257-261.
- (25) Ahuja, R.; Kundu, S.; Goldman, A. S.; Brookhart, M.; Vicente, B. C.; Scott, S. L. *Chem. Commun.* **2008**, 253-255.
- (26) Haibach, M. C.; Kundu, S.; Brookhart, M.; Goldman, A. S. *Acc. Chem. Res.* **2012**, *45*, 947-958.

- (27) Dobereiner, G. E.; Yuan, J.; Schrock, R. R.; Goldman, A. S.; Hackenberg, J. D. *J Am Chem Soc* **2013**, *135*, 12572-5.
- (28) Goldman, A.; Ahuja, R.; Schinski, W. Rutgers, The State University of New Jersey, USA . 2013 US20130123552A1
- (29) Steffens, A. M.; Goldman, A. S. *Abstracts of Papers, 245th ACS National Meeting & Exposition, New Orleans, LA, United States, April 7-11, 2013* **2013**, INOR-1328.
- (30) Goldman, A. S.; Stibrany, R. T.; Schinski, W. L. Chevron U.S.A. Inc., USA; Rutgers, The State University of New Jersey . 2013 US20130090503A1
- (31) Leitch, D. C.; Labinger, J. A.; Bercaw, J. E. *Organometallics* **2014**, *33*, 3353-3365.
- (32) Leitch, D. C.; Lam, Y. C.; Labinger, J. A.; Bercaw, J. E. *J. Am. Chem. Soc.* **2013**, *135*, 10302-10305.
- (33) Gupta, M.; C. Kaska, W.; M. Jensen, C. *Chem. Commun.* **1997**, 461-462.
- (34) Zhang, X.; Fried, A.; Knapp, S.; Goldman, A. S. *Chem. Commun.* **2003**, 2060-2061.
- (35) Chianese, A. R.; Drance, M. J.; Jensen, K. H.; McCollom, S. P.; Yusufova, N.; Shaner, S. E.; Shopov, D. Y.; Tendler, J. A. *Organometallics* **2014**, *33*, 457-464.
- (36) Chianese, A. R.; Shaner, S. E.; Tendler, J. A.; Pudalov, D. M.; Shopov, D. Y.; Kim, D.; Rogers, S. L.; Mo, A. *Organometallics* **2012**, *31*, 7359-7367.
- (37) Chianese, A. R.; Mo, A.; Lampland, N. L.; Swartz, R. L.; Bremer, P. T. *Organometallics* **2010**, *29*, 3019-3026.
- (38) Knapp, S. M. M.; Shaner, S. E.; Kim, D.; Shopov, D. Y.; Tendler, J. A.; Pudalov, D. M.; Chianese, A. R. *Organometallics* **2014**, *33*, 473-484.
- (39) Gruver, B. C.; Adams, J. J.; Warner, S. J.; Arulsamy, N.; Roddick, D. M. *Organometallics* **2011**, *30*, 5133-5140.
- (40) Adams, J. J.; Gruver, B. C.; Donohoue, R.; Arulsamy, N.; Roddick, D. M. *Dalton Trans.* **2012**, *41*, 12601-12611.
- (41) Roddick, D. M. *Top. Organomet. Chem.* **2013**, *40*, 49-88.
- (42) Gruver, B. C.; Adams, J. J.; Arulsamy, N.; Roddick, D. M. *Organometallics* **2013**, *32*, 6468-6475.
- (43) Allen, K. E.; Heinekey, D. M.; Goldman, A. S.; Goldberg, K. I. *Organometallics* **2013**, *32*, 1579-1582.
- (44) Allen, K. E.; Heinekey, D. M.; Goldman, A. S.; Goldberg, K. I. *Organometallics* **2014**, *33*, 1337-1340.
- (45) (a) Crabtree, R. H.; Mihelcic, J. M.; Quirk, J. M. *J. Am. Chem. Soc.* **1979**, *101*, 7738-7740. (b) Crabtree, R. H.; Mellea, M. F.; Mihelcic, J. M.; Quirk, J. M. *J. Am. Chem. Soc.* **1982**, *104*, 107-113. (c) Burk, M. J.; Crabtree, R. H.; McGrath, D. V. *J. Chem. Soc., Chem. Commun.* **1985**, 1829-30. (d) Baudry, D.; Ephritikine, M.; Felkin, H. *J. Chem. Soc., Chem. Commun.* **1980**, 1243-1244. (d) Baudry, D.; Ephritikine, M.; Felkin, H.; Holmes-Smith, R. *J. Chem. Soc., Chem. Commun.* **1983**, 788-789. (e) Burk, M. J.; Crabtree, R. H.; Parnell, C. P.; Uriarte, R. J. *Organometallics* **1984**, *3*, 816-817.
- (46) (a) Galvita, V.; Siddiqi, G.; Sun, P.; Bell, A. T. *J. Catal.* **2010**, *271*, 209-219. (b) Siddiqi, G.; Sun, P.; Galvita, V.; Bell, A. T. *J. Catal.* **2010**, *274*, 200-206. (c) Sun, P.; Siddiqi, G.; Vining, W. C.; Chi, M.; Bell, A. T. *J. Catal.* **2011**, *282*, 165-174. (d) Lobera, M. P.; Escolastico, S.; Serra, J. M. *ChemCatChem* **2011**, *3*, 1503-1508. (e) Solsona, B.; Concepcion, P.; Hernandez, S.; Demicol, B.; Nieto, J. M. L. *Catal. Today* **2012**, *180*, 51-58. (f) Ausavasukhi, A.; Sooknoi, T. *Catal. Commun.* **2014**, *45*, 63-68. (g) Wu, J.; Peng, Z.; Bell, A. T. *J. Catal.* **2014**, *311*, 161-168. (h) Avila, A. M.; Yu, Z.; Fazli, S.; Sawada, J. A.; Kuznicki, S. M. *Microporous Mesoporous Mater.* **2014**, *190*, 301-308. (j) Sui, K.; Yang,

- M.; Zhou, T.; Guan, Z.; Sun, R.; Han, D. *Integr. Ferroelectr.* **2014**, *154*, 57-63. (j) Shin, H. H.; McIntosh, S. *ACS Catal.* **2015**, *5*, 95-103.
- (47) Kundu, S.; Lyons, T. W.; Brookhart, M. *ACS Catalysis* **2013**, *3*, 1768-1773.
- (48) Lyons, T. W.; Guironnet, D.; Findlater, M.; Brookhart, M. *J. Am. Chem. Soc.* **2012**, *134*, 15708-15711.
- (49) Kumar, A.; Goldman, A. S. Abstracts of Papers, 245th ACS National Meeting & Exposition, New Orleans, LA, United States, April 7-11, 2013, INOR-1202.
- (50) Kumar, A.; Mironov, O.; Saxton, R. J.; Goldman, A. S. Abstracts of Papers, 248th ACS National Meeting & Exposition, San Francisco, CA, United States, August 10-14, 2014, INOR-1041.
- (51) Ohe, S. *Computer Aided Data Book of Vapor Pressure*; Data Book Publishing Company, 1976.
- (52) Ohe, S. In *Vapor Pressure Calculation*; <http://e-data.jp/vpcal2/e/>; Vol. 2015.
- (53) Choi, J.; Choliy, Y.; Zhang, X.; Emge, T. J.; Krogh-Jespersen, K.; Goldman, A. S. *J. Am. Chem. Soc.* **2009**, *131*, 15627-15629.
- (54) Kundu, S.; Choi, J.; Wang, D. Y.; Choliy, Y.; Emge, T. J.; Krogh-Jespersen, K.; Goldman, A. S. *J. Am. Chem. Soc.* **2013**, *135*, 5127-5143.
- (55) Some lead references to organometallic C-H addition, with particular emphasis on selectivity: (a) Bennett, J. L.; Vaid, T. P.; Wolczanski, P. T. *Inorg. Chim. Acta.* **1998**, *270(1-2)*, 414-423 (b) Wick, D. D.; Jones, W. D. *Organometallics* **1999**, *18*, 495-505. (c) Asbury, J. B.; Hang, K.; Yeston, J. S.; Cordaro, J. G.; Bergman, R. G.; Lian, T. *J. Am. Chem. Soc.* **2000**, *122*, 12870-12871 and references 4-11 therein. (d) Vetter, A. J.; Flaschenriem, C.; Jones, W. D. *J. Am. Chem. Soc.* **2005**, *127*, 12315-12322. (e) Balcells, D.; Clot, E.; Eisenstein, O. *Chem. Rev.* **2010**, *110*, 749-823.
- (56) Liu, F.; Pak, E. B.; Singh, B.; Jensen, C. M.; Goldman, A. S. *J. Am. Chem. Soc.* **1999**, *121*, 4086-4087.
- (57) Biswas, S.; Huang, Z.; Choliy, Y.; Wang, D. Y.; Brookhart, M.; Krogh-Jespersen, K.; Goldman, A. S. *J. Am. Chem. Soc.* **2012**, *134*, 13276-13295.
- (58) Manuel, T. A. *J. Org. Chem.* **1962**, *27*, 3941-3945.
- (59) Alper, H.; LePort, P. C.; Wolfe, S. *J. Am. Chem. Soc.* **1969**, *91*, 7553-7554.
- (60) Cowherd, F. G.; Von Rosenberg, J. L. *J. Am. Chem. Soc.* **1969**, *91*, 2157-2158.
- (61) Misono, M.; Grabowski, W.; Yoneda, Y. *J. Catal.* **1977**, *49*, 363-8.
- (62) Casey, C. P.; Cyr, C. R. *J. Am. Chem. Soc.* **1973**, *95*, 2248-53.
- (63) Herrmann, W. A.; Prinz, M. In *Applied Homogeneous Catalysis with Organometallic Compounds (2nd Edition)*; Cornils, B., Herrmann, W. A., Eds.; Wiley-VCH Verlag GmbH: Weinheim, Germany, 2002; Vol. 3, p 1119-1130.
- (64) Crabtree, R. H. In *The Organometallic Chemistry of the Transition Metals*; 5th ed.; John Wiley & Sons: Hoboken, NJ, 2009, p 229-231.
- (65) Mol, J. C. *J. Mol. Catal. A Chem.* **2004**, *213*, 39-45.
- (66) van Leeuwen, P. W. N. M. In *Homogeneous Catalysis: Understanding the Art*; Kluwer Academic Publishers: Dordrecht, 2004, p 101-107.
- (67) Schmidt, B. *Eur. J. Org. Chem.* **2004**, 1865-1880.
- (68) Otsuka, S.; Tani, K. *Transition Metals for Organic Synthesis (2nd Edition)* **2004**, *1*, 199-209.
- (69) Seayad, A.; Ahmed, M.; Klein, H.; Jackstell, R.; Gross, T.; Beller, M. *Science* **2002**, *297*, 1676-1678.

- (70) Scarso, A.; Colladon, M.; Sgarbossa, P.; Santo, C.; Michelin, R. A.; Strukul, G. *Organometallics* **2010**, 29, 1487-1497.
- (71) Casey, C. P.; Cyr, C. R. *J. Am. Chem. Soc.* **1973**, 95, 2240-2248.
- (72) Krogh-Jespersen, K.; Czerw, M.; Zhu, K.; Singh, B.; Kanzelberger, M.; Darji, N.; Achord, P. D.; Renkema, K. B.; Goldman, A. S. *J. Am. Chem. Soc.* **2002**, 124, 10797-10809.
- (73) Romero, P. E.; Whited, M. T.; Grubbs, R. H. *Organometallics* **2008**, 27, 3422-3429.

Computational Details

All electronic structure calculations employed the DFT method¹ and the PBE² exchange-correlation functional. A relativistic, small-core ECP and corresponding basis set were used for the Ir atom (LANL2TZ model);^{3,4} all-electron 6-311G(d,p) basis sets were applied to all P, C, and H atoms.⁵ The (^{R4}PCP)Ir species was modeled with R = *t*-Bu and *i*-Pr, the phosphine substituents actually used in the experiments. Reactant, transition state and product geometries were fully optimized, and the stationary points were characterized further by normal mode analysis. Expanded integration grid sizes (pruned (99,590) atomic grids invoked using the integral=ultrafine keyword) were applied to increase numerical accuracy and stability in both geometry optimizations and normal mode analysis.⁶ The (unscaled) vibrational frequencies formed the basis for the calculation of vibrational zero-point energy (ZPE) corrections; standard thermodynamic corrections (based on the harmonic oscillator/rigid rotor approximations and ideal gas behavior) were made to convert from purely electronic (reaction or activation) energies (E) to (standard) enthalpies (H) and Gibbs free energies (G; P = 1 atm).⁷ H, entropy (S), and G were evaluated at two temperatures, T = 25 °C (= 298 K) and T = 220 °C (= 493 K). The latter T corresponds approximately to the temperature used in the experiments, and all energy values quoted in the principal text refer to T = 220 °C unless noted otherwise. We tabulate E, H, S, and G at T = 25 °C (298 K; P = 1 atm) as well as G at T =

220 °C ($P = 1$ atm). All calculations were executed using the GAUSSIAN 09 series of computer programs.⁸

Reaction mechanism and energy tables

Figure S1. Reaction mechanism with free energy values for alkane dehydrogenation by $t\text{Bu}^4\text{PCPIr}$ [PBE/LANL2TZ/6-311G(d,p)]

Alkane Dehydrogenation Using $t\text{Bu}^4\text{PCP}$; Functional: PBE; Basis Set: LANL2TZ/6-311G(d,p); G (220 °C)

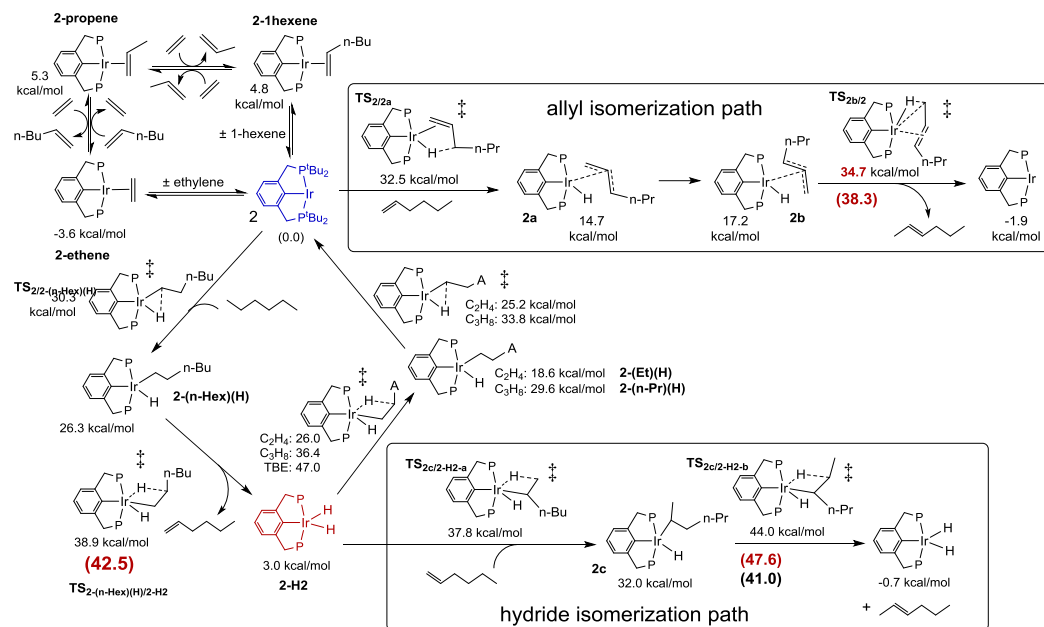


Table S1. Potential energies, enthalpies, entropies and free energies for alkane dehydrogenation by ($t\text{Bu}^4\text{PCP}$)Ir [PBE/LANL2TZ/6-311G(d,p)].^a

File name	Structure label	ΔE	ΔH	$\Delta G(298 \text{ K})$	ΔS	$\Delta G(493 \text{ K})$
tBu-PCPIr-ethene	2-ethene	-30.3	-27.9	-13.2	-49.4	-3.6
tBu-PCPIr-propene	2-propene	-22.6	-20.3	-4.8	-51.9	5.3
tBu-PCPIr-TBE	2-TBE	-11.9	-9.6	6.6	-54.2	17.1
tBu-PCPIr-1hexene	2-1hexene	-23.0	-20.6	-5.2	-51.6	4.8
tBu-PCPIr + 1-hexene		0.0	0.0	0.0	0.0	0.0
tBu-TS-Hmigration	TS _{2/2a}	7.1	5.6	21.9	-54.5	32.5
tBu-Interm-1allyl-anti	2a	-8.1	-8.5	5.5	-46.9	14.7
tBu-Interm-3cor-allyl-syn	2b	-12.6	-11.8	5.7	-58.7	17.2
tBu-TS-Hmigration-sec	TS _{2/2b}	8.4	7.1	23.8	-56.0	34.7
tBu-PCP+ 2-hexene		-3.4	-3.6	-3.6	-3.4	-1.9
tBu-PCPIr-2hexene	2-2hexene	-19.2	-16.7	-0.9	-47.7	6.8
tBu-TS-CH-C1-C2	TS _{2/2-(n-Hex)(H)}	7.6	6.6	20.9	-48.0	30.3
tBu-Interm-CH-C1-C2	2-(n-Hex)(H)	2.4	2.2	16.7	-48.9	26.3
tBu-TS-elim-C1-C2	TS _{2-(n-Hex)(H)/2-H2}	12.3	9.4	27.2	-59.9	38.9
tBu-PCPIrH2+1-hexene		6.8	2.5	2.8	-1.0	3.0
tBu-TS-elim-C2-C1	TS _{2c/2-H2-a}	11.8	9.2	26.5	-58.0	37.8
tBu-Interm-CH-C2-C1	2c	8.5	8.0	22.5	-48.8	32.0
tBu-TS-elim-C2-C3-E	TS _{2c/2-H2-b}	17.4	14.4	32.3	-60.1	44.0
tBu-PCPIrH2+2-hexene		3.4	-1.1	-0.9	-0.7	-0.7
tBu-TS-elim_ethane	TS _{2-H2/2-(Et)(H)}	2.2	-0.4	15.6	-53.4	26.0
tBu-Interm-CH_ethane	2-(Et)(H)	-3.1	-3.7	9.8	-45.2	18.6
tBu-TS-CH_ethane	TS _{2-(Et)(H)/2}	4.2	3.2	16.5	-44.7	25.2
tBu-PCPIr+ethane		-3.7	-3.7	-3.2	-1.5	-3.0
tBu-TS-elim-C2-C1_propane	TS _{2-H2/2-(n-Pr)(H)}	11.3	8.7	25.5	-56.2	36.4
tBu-Interm-C2-C1_propane	2-(n-Pr)(H)	6.5	6.0	20.3	-47.9	29.6
tBu-TS-CH-C2-C1_propane	TS _{2-(n-Pr)(H)/2}	11.5	10.3	24.5	-47.7	33.8

for concentrations is $P = 1$ atm for each species participating in the reaction; $T = 298.15$ K.

Figure S2. Reaction mechanism with free energy values for alkane dehydrogenation by $(i\text{Pr}^4\text{PCP})\text{Ir}$ [PBE/LANL2TZ/6-311G(d,p)]

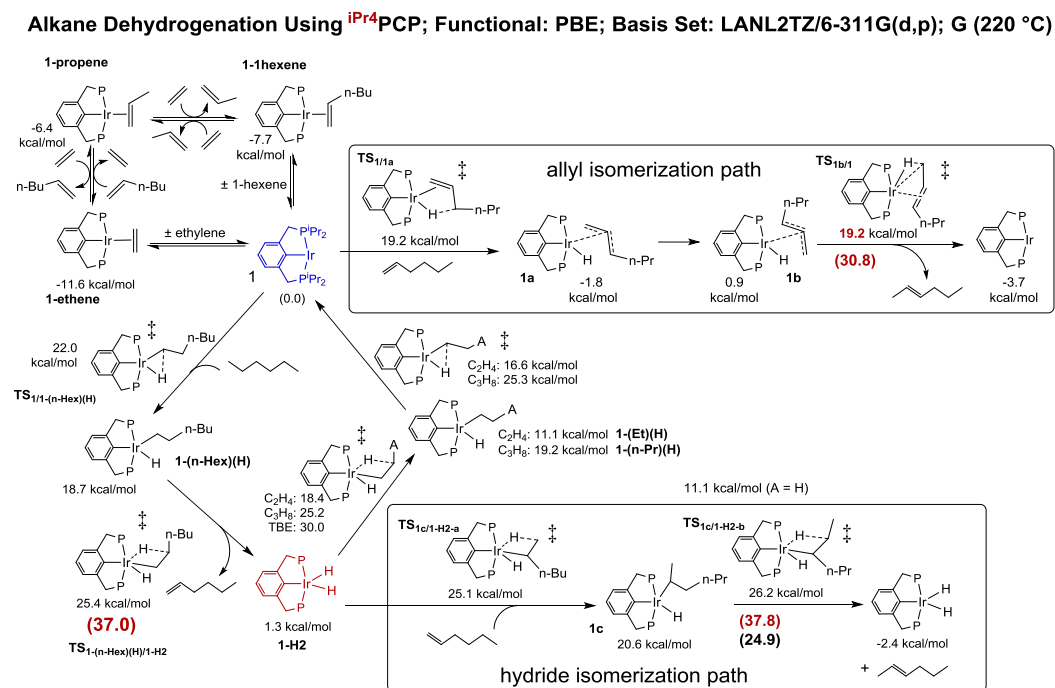


Table S2. Potential energies, enthalpies, entropies and free energies for alkane dehydrogenation by ($i\text{Pr}^4\text{PCP}$)Ir [PBE/LANL2TZ/6-311G(d,p)].^a

File name	Structure label	ΔE	ΔH	$\Delta G(298\text{ K})$	ΔS	$\Delta G(493\text{ K})$
iPr-PCPIr-ethene	1-ethene	-34.1	-32.8	-19.9	-43.0	-11.6
iPr-PCPIr-propene	1-propene	-31.4	-30.1	-15.8	-48.0	-6.4
iPr-PCPIr-TBE	1-TBE	-24.2	-22.8	-7.9	-49.7	1.8
iPr-PCPIr-1hexene	1-1hexene	-33.1	-31.9	-17.3	-49.0	-7.7
iPr-PCPIr+ 1-hexene		0.0	0.0	0.0	0.0	0.0
iPr-TS-Hmigration	TS _{1/1a}	-4.7	-7.1	8.8	-53.3	19.2
iPr-Interm-1allyl-anti	1a	-30.7	-31.0	-13.3	-59.3	-1.8
iPr-Interm-3cor-allyl-syn	1b	-27.4	-27.6	-10.4	-57.6	0.9
iPr-TS-Hmigration-sec	TS _{1/1b}	-4.7	-7.1	8.8	-53.3	19.2
iPr-PCP+ 2-hexene		-3.4	-3.6	-3.6	0.3	-3.7
iPr-PCP-2hexene	1-2hexene	-27.7	-26.5	-12.1	-48.2	-2.7
iPr-TS-CH-C1-C2	TS _{1/1-(n-Hex)(H)}	1.7	-0.2	13.2	-44.9	22.0
iPr-Interm-CH-C1-C2	1-(n-Hex)(H)	-2.3	-3.8	9.8	-45.6	18.7
iPr-TS-elim-C1-C2	TS _{1-(n-Hex)(H)/1-H2}	0.6	-2.7	14.3	-57.0	25.4
iPr-PCPIrH2+1-hexene		6.0	1.4	1.3	0.3	1.3
iPr-TS-elim-C2-C1	TS _{1c/1-H2-a}	0.8	-2.8	14.1	-56.7	25.1
iPr-Interm-CH-C2-C1	1c	-2.4	-3.8	11.0	-49.5	20.6
iPr-TS-elim-C2-C3-E	TS _{1c/1-H2-b}	1.6	-2.1	15.0	-57.5	26.2
iPr-PCPIrH2+2-hexene		2.6	-2.1	-2.3	0.5	-2.4
iPr-TS-elim_ethane	TS _{1-H2/1-(Et)(H)}	-2.8	-6.2	8.7	-49.9	18.4
iPr-Interm-CH_ethane	1-(Et)(H)	-8.3	-9.7	2.9	-42.1	11.1
iPr-TS-CH_ethane	TS _{1-(Et)(H)/1}	-2.4	-4.3	8.3	-42.3	16.6
iPr-PCPIr+ethane		-3.7	-3.7	-3.2	-1.5	-3.0
iPr-TS-elim-C2-C1_propane	TS _{1-H2/1-(n-Pr)(H)}	1.4	-2.1	14.4	-55.4	25.2
iPr-Interm-C2-C1_propane	1-(n-Pr)(H)	-3.4	-4.7	9.7	-48.5	19.2
iPr-TS-CH-C2-C1_propane	TS _{1-(n-Pr)(H)/1}	3.7	1.8	16.0	-47.7	25.3

iPr-PCPIr + propane		0.1	0.2	0.2	0.1	0.2
iPr-TS-elim-C1-C2_TBA	TS _{1-H2/1-} (TBA)(H)	4.3	0.9	18.5	-59.1	30.0
iPr-Interm-C1-C2_TBA	1- (TBA)(H))	-4.9	-6.4	7.1	-45.1	15.9
iPr-TS-CH-C1-C2_TBA	TS ₁₋ (TBA)(H)/1	0.2	-2.0	11.2	-44.1	19.8
iPr-PCPIr + TBA		0.5	0.4	0.3	0.3	0.3

^a Units are kcal/mol for ΔE , ΔH , and ΔG ; units are cal/(deg·mol) for ΔS . The standard state for concentrations is $P = 1$ atm for each species participating in the reaction; $T = 298.15$ K.

Computational Section References

- (1) Koch, W.; Holthausen, M. C. *A Chemist's Guide to Density Functional Theory*; Wiley: New York, 2001.
- (2) Perdew, J. P.; Burke, K.; Ernzerhof, M. *Phys Rev. Lett.* **1996**, 77, 3865-3868.
- (3) Hay, P. J.; Wadt, W. R. *J. Chem. Phys.* **1985**, 82, 299-310.
- (4) Roy, L. E.; Hay, P. J.; Martin, R. L. *J. Chem. Theory Comput.* **2008**, 4, 1029-1031.
- (5) (a) Ditchfield, R.; Hehre, W. J.; Pople, J. A. *J. Chem. Phys.* **1971**, 54, 724-728. (b) Hariharan, P. C.; Pople, J. A. *Molecular Physics* **1974**, 27, 209-214. (c) Raghavachari, K.; Binkley, J. S.; Seeger, R.; Pople, J. A. *J. Chem. Phys.* **1980**, 72, 650-654. (d) McLean, A. D.; Chandler, G. S. *J. Chem. Phys.* **1980**, 72, 5639-5648.
- (6) Frisch, A.; Frisch, M. J.; Clemente, F. R.; G. W. Trucks *Gaussian 09 User's Reference*, 147.
- (7) McQuarrie, D. A. *Statistical Thermodynamics*; Harper and Row: New York, 1973.
- (8) Frisch, M. J.; Trucks, G. W.; Schlegel, H. B.; Scuseria, G. E.; Robb, M. A.; Cheeseman, J. R.; Scalmani, G.; Barone, V. *et al.* Gaussian 09, Revision D.01, Gaussian, Inc., Wallingford, CT, 2009.

Chapter 5: Computational Study of N-H Activation by (PCP)IrH₂

Introduction

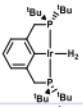
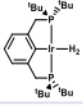
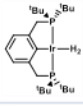
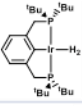
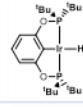
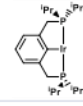
Heterogeneously catalyzed ammonia synthesis by iron based catalysts has long been known and is well studied, while the homogeneously catalyzed synthesis of NH₃ from N₂ and H₂ by a defined transition-metal homogeneous system remains unsolved in the field of chemistry. Iron heterogeneously catalyzed Haber-Bosch process is the only industrial process we humans have successfully developed for transforming nitrogen. This process now produces 500 million tons of nitrogen fertilizer per year.¹ But the Haber-Bosch process is conducted at high pressure (15-25 MPa) and high temperature (300-550 °C), which consumes 3-5% of world natural gas production (~1-2% of the world's annual energy supply).¹ Design of a new catalyst which can be an alternative to conduct nitrogen hydrogenation under low pressure and low temperature will be a tremendous contribution to the farming and energy industries.

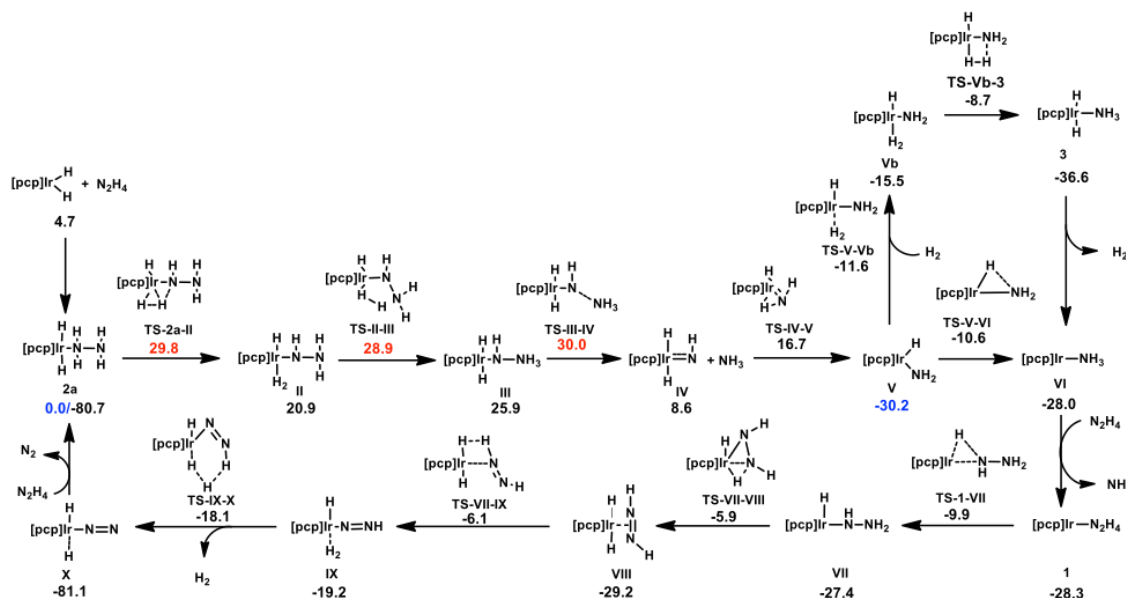
A former group member, Dr. Kathleen Field, found that a common pincer alkane dehydrogenation catalyst (^tbu⁴PCP)IrH(phenyl) has the ability to run the hydrazine N-H activation reaction, including both dehydrogenation and N-N bond cleavage to form ammonia.

A thorough DFT study about both processes were made using DFT calculation methods. Several possible mechanisms were proposed and studied. With the experimental results in hands, we were looking for a mechanism supporting those results which maintained self-correctness among the mechanisms proposed.

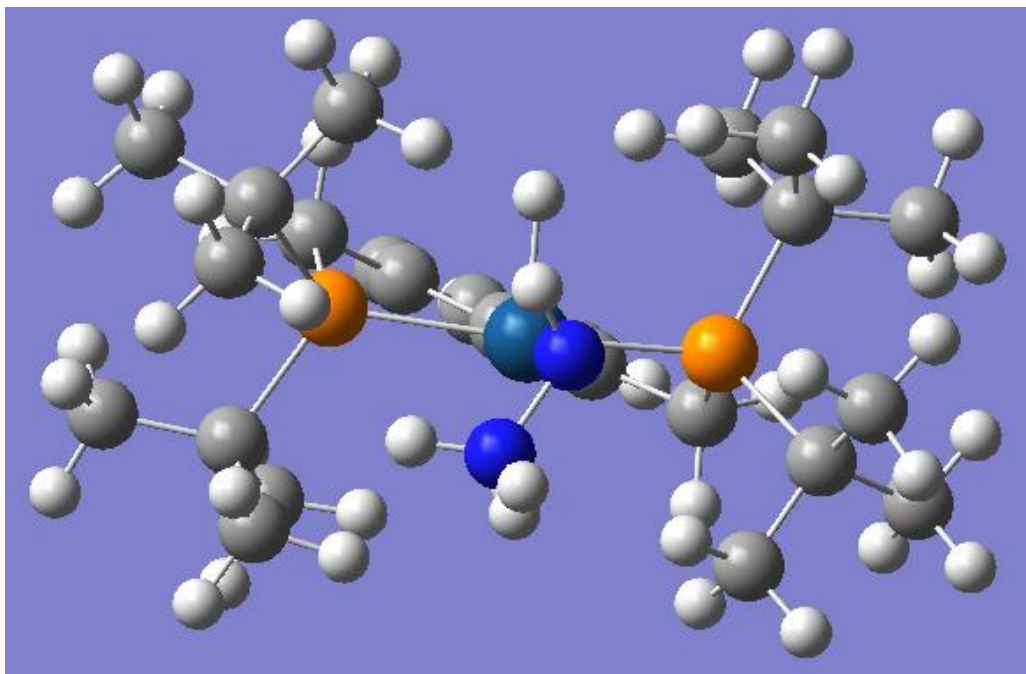
Result and Discussion

(PCP)IrH₂ mechanism: The mechanism involving single molecule (PCP)IrH₂ catalysing the whole process is not intuitive, since it is quite different from the C-H activation reaction that is catalyzed by the same molecule. In the C-H activation reaction, the active catalyst is a 14e (PCP)Ir molecule with an olefin acting as the hydrogen acceptor. In this hydrazine N-H activation reaction system, there is no strong hydrogen acceptor to react with the metal dihydride in order to form (PCP)Ir. So the active species in this N-H activation system should be 16 electron (PCP)IrH₂. Based on such assumptions, we proposed and calculated the following (PCP)IrH₂ mechanism pathways: we have two different reaction systems under different conditions. When the system was put under vacuum, only dehydrogenation reaction happened with N₂ and H₂ forming. When we put the system under 100 °C temperature, we had ammonia formed as well as N₂ and H₂. Both reactions are catalytic rather than stoichiometric with the experimental results obtained by Dr. Field in the following Table

Catalyst	[Catalyst] M	[Hydrazine] M	Time	[NH₃] M	% yield	TON
	0.02	0.10	30 min	0.1	99	5
	0.005	0.10	2 hours	0.1	99	20
	0.017	0.40	24 hours	0.35	87	24
 under 1 atm H ₂	0.025	0.14	65 hours	0.0949	58	4
	0.016	0.10	30 min	0.1	95	8
	0.016	0.10	3.5 hours	0.0346	36	2



Addition of hydrazine to (PCP)IrH₂, to yield **2a** is calculated to be downhill and **2a** has been experimentally isolated, crystallized and characterized by Dr. Field. This can be seen as our starting point. The first three steps are possible rate determining steps. First, N-H activation assisted by an Ir-H bond to form an iridium hydride gives complex II. The idea of small molecule assisted mechanisms will be explored in the later chapter. Subsequent transfer of that one hydrogen atom to the β -nitrogen gives III, a precursor with -NH₃ structure formed. Finally, release of one molecule of ammonia yields IV. The two hydrogen transfers steps and the N-N bond cleavage step each have an energy barrier of approximately 30 kcal/mol; the energy differences between them are within the error of DFT calculation. We need to also consider experimental result to determine which step is the RDS. If release of ammonia is rate determining, steric effects should play a big role to break the N-N bond and push the ammonia molecule out considering four large *t*bu groups around the active site. The calculated intermediate (^{*t*bu}PCP)Ir(H)₂(NHNH₃) structure is shown below:



Based on that less sterically hindered ($i\text{Pr}^4\text{PCP}$)Ir catalyst should be less likely to release NH_3 most likely due to a high energy barrier for the release or the high stability of the four coordinate complex, and therefore the reaction is much slower. Based on the kinetics experimental results of Dr. Field, the ($i\text{Pr}^4\text{PCP}$)Ir catalyst is indeed much less active showing the ammonia release step could be the RDS of the process. Reverse N-H activation hydrogenated the α N atom in IV to yield V, which had been reported and characterized at $-30\text{ }^\circ\text{C}$.² From V, there are several possible pathways leading to ammonia formation. Two possible ones are shown here as (a) from V to VI and (b) V to Vb; the difference here is whether H_2 is involved in the process. But since both transformations have a low kinetic barrier, it is possible that both reactions happened under the reaction conditions; indeed, both were observed and VI had also been reported and characterized at room temperature². The transformation between V and VI was thermodynamically

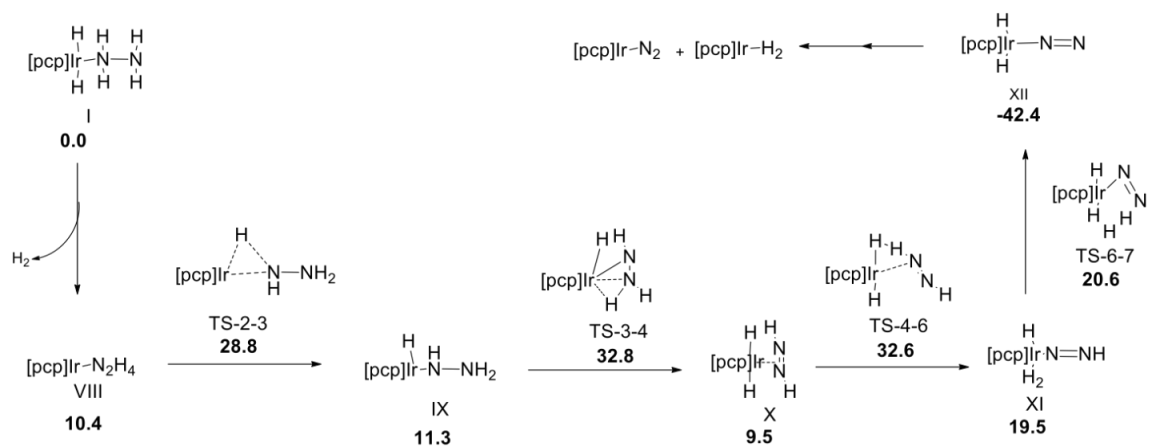
neutral and had a low kinetic barrier around 20 kcal/mol, which was 10 kcal/mol lower than the RDS. One thing worth mentioning is that neither V nor VI are observed during the reaction, most likely due to the stability of **3**, which is calculated as having the lowest free energy. This fact also explains its observance by NMR during the reaction. Extra amount of hydrazine to substitute ammonia from the metal center is a driving force from VI to **1**, which gives the second equivalent of ammonia.

Also, another molecule of hydrazine undergoes N-H activation with an even stronger activation fragment 14e (PCP)Ir other than 16e (PCP)IrH₂. N-H activation followed by a β N-H elimination leads to a side-on diazene intermediate, VIII. Though this diazene molecule doesn't play a crucial role in our proposed mechanism, it is reported by a lot of studies as a critical intermediate during the synthesis of ammonia from nitrogen and hydrogen.^{3,4,5} Subsequent dehydrogenation by hydrogen atom transfer to the metal center results in IX. Small molecule assisted effect shows again in the following step as β -N-H elimination with loss of one molecule of hydrogen, which ends up as dihydrogen dinitrogen metal complex X. Nitrogen release from X to give the dihydride complex or another molecule of hydrazine substitution is easily accessible and finishes our complete catalytic cycle.

Overall, the whole process is extremely downhill with -80.7 kcal/mol energy release thermodynamically. Most of this negative energy is due to the stability of products and entropic favorability, as hydrogen, nitrogen and ammonia are very stable species in comparison to hydrazine. The backwards reaction would encounter a kinetic barrier of 111 kcal/mol; the overall forward reaction barrier is 30 kcal/mol. Presumably, the second half of the reaction mechanism starting from **1** is the pathway for the

dehydrogenation of hydrazine to form nitrogen and hydrogen, and we will see a similar pathway under vacuum conditions, rather than heating.

The reaction under vacuum is quite different in comparison, since we have a "hydrogen acceptor" in this case: the vacuum. Under the low air pressure, I can convert to VIII with low kinetic barrier. And 16 electron species VIII could undergo N-H dehydrogenation extremely similar to its C-H dehydrogenation reaction catalysed by the same pincer (PCP)Ir complex.



Via N-H activation from VIII to IX, followed by β -N-H elimination from IX to X, we would get the iridium dihydride diazene complex. α -N-H activation to form a hydrogen coordinated XI was a possible route for the further dehydrogenation. Simple dissociation of the diazene complex would result in the same product under low kinetic barrier as well. Self disproportionation reaction would result into the same product as N_2 and H_2 .

Conclusions

Using experimental and DFT computational methods, we demonstrate that a $(\text{PCP})\text{Ir}(\text{H})(\text{N}_2\text{H}_4)$ complex follows a hydrogen transfer mechanism to undergo both dehydrogenation to form N_2 and H_2 , as well as hydrogen transfer followed by N-N bond

cleavage to form NH_3 , N_2 , and H_2 . Small molecule assistance plays a key role in the hydrogen transfer step during the process. Three key steps (α -N-H activation, β -N-H transfer, N-N bond cleavage) are our potential RDS for ammonia formation. The effect of a vacuum to remove dihydrogen from the metal center is supposed to lead to the pure dehydrogenation reaction.

References

- (1) Ullmann's Encyclopedia of Industrial Chemistry 2006 Wiley-VCH, Weinheim.
- (2) Kanzelberger, M.; Zhang, X.; Emge, T. J.; Goldman, A. S.; Zhao, J.; Incarvito, C.; Hartwig, J. F. *J. Am. Chem. Soc.* **2003**, *125*, 13644.
- (3) Rozenel, S. S.; Arnold, J. *Inorg. Chem.* **2012**, *91*, 9730.
- (4) Field, L. D.; Li, H. L.; Dalgarno, S. J.; McIntosh, R. D. *Inorg. Chem.* **2013**, *52*, 1570.
- (5) Lukoyanov, D.; Dikanov, S. A.; Yang, Z.-Y.; Barney, B. M.; Samoilova, R. I.; Narasimhulu, K. V.; Dean, D. R.; Seefeldt, L. C.; Hoffman, B. R. *J Am Chem Soc* **2011**, *133*, 11655.

Computational Details

All calculations used DFT methodologies implemented in the Gaussian 09 program.¹ All the data presented here results from calculations which employed the TPSS functional.² However, we did also examine results using other two different functionals M06³ and PBE⁴. Calculation results from these two functionals also support the mechanism we propose in this work. For Ir, we applied the Hay-Wadt relativistic effective (small) core potential⁵ and the LANL2TZ basis set^{6a} augmented by a diffuse d-type function (exponent=0.07645)^{6b}; all other atoms (P,N,C and H) were assigned 6-311G(d,p) basis sets.⁷

Geometries and potential energies were calculated for all the stationary points along the reaction paths by standard optimization procedures. Normal mode analysis was performed to further verify the nature of a particular stationary point (intermediate or transition state). The resulting set of vibrational frequencies was employed (without scaling) to determine zero-point energy corrections. Enthalpies (ΔH , ΔH^\ddagger) and Gibbs' free energies (ΔG , ΔG^\ddagger ; $T = 298.15$ K, $P = 1$ atm) were subsequently obtained from the potential energies (ΔE , ΔE^\ddagger) using standard thermodynamic corrections.⁸ In order to enhance computational stability and accuracy⁹ in geometry optimizations and normal mode calculations, we used increased atomic grid sizes (via the grid=ultrafine option).¹⁰

Energy Table

Table 1. Potential energies, enthalpies, entropies and free energies using the TPSS functional for the proposed N-H activation of hydrazine by (^tBu⁴PCP)IrH₂^a

Species	ΔE	ΔH	ΔG	ΔS
2a	0.00	0.00	0.00	0.00
TS-2a-II	33.2	29.4	29.8	-1.5
II	23.3	20.7	20.9	-0.4
TS-II-III	31.8	27.6	28.9	-4.3
III	26.2	25.1	25.9	-2.6
TS-III-IV	33.7	30.7	30.0	2.4
IV	24.0	20.2	8.6	38.9
TS-IV-V	32.5	27.7	16.7	36.8
V	-18.3	-18.9	-30.2	37.7
TS-V-VI	5.6	3.0	-10.6	45.3
VI	-15.4	-14.2	-28.0	46.0
TS-V-Vb	-8.0	-8.2	-11.6	11.6
Vb	-13.7	-12.3	-15.5	10.6
TS-Vb-3	-5.9	-6.1	-8.7	8.7
3	-37.5	-33.7	-36.6	9.7
1	-17.3	-16.4	-28.3	39.9
TS-1-VII	4.3	1.5	-9.9	38.2
VII	-17.4	-18.5	-27.4	37.2
TS-VII-VIII	8.6	3.7	-5.9	32.2
VIII	-15.6	-19.3	-29.2	33.2
TS-VIII-IX	6.6	2.2	-6.1	28.1
IX	-2.4	-8.3	-19.2	36.5
TS-IX-X	1.1	-8.4	-18.1	32.6
X	-53.0	-62.6	-81.1	61.9

^a Units are kcal/mol for ΔE, ΔH, and ΔG; units are cal/(deg.mol) for ΔS. The standard state

for concentrations is 1 M for each species participating in the reaction; T = 298.15 K.

Computational Section References

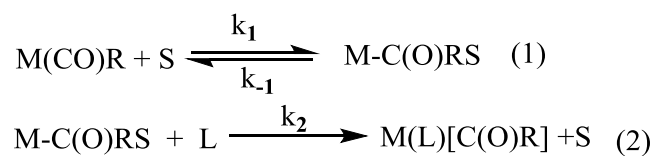
1. Frisch, M. J.; et al., Gaussian 09, revision C.01; Gaussian, Inc.: Wallingford, CT, 2009.
2. J. M. Tao, J. P. Perdew, V. N. Staroverov, and G. E. Scuseria, *Phys. Rev. Lett.*, **91**, 2003, 146401.
3. Zhao, C. Y.; Truhlar, D. G. *Theo. Chem. Acc.* **2008**, 120, 215–241.
4. Perdew, J. P.; Burke, K.; Ernzerhof, M. *Phys. Rev. Lett.* **1996**, 77, 3865.
5. Hay, P. J.; Wadt, W. R. *J. Chem. Phys.* **1985**, 82, 299–310.
6. (a) Roy, L. E., Hay, P. J. & Martin, R. L. *J. Chem. Theory Comput.* **2008**, 4, 1029-1031.
(b) Value obtained as one-half times the exponent of the outermost d-type function in the LANL2TZ basis set for Ir.
7. Raghavachari, K.; Binkley, J. S.; Seeger, R.; Pople, J. A. *J. Chem. Phys.* **1980**, 72, 650-654.
8. McQuarrie, D. A. *Statistical Thermodynamics*; Harper and Row: New York, 1973.
9. Wheeler, S. E.; Houk, K. N. *J. Chem. Theory Comput.* **2010**, 6, 395–404.
10. Frisch, Æ.; Frisch, M. J.; Clemente, F. R.; Trucks, G. W. Gaussian 09 User's Reference, 147.

Chapter 6: Computational Study of the Solvent Catalysed CO Insertion Reaction for $\text{RMn}(\text{CO})_5$ Complexes

Introduction

The origin of the strong solvent effect in CO insertion reactions is difficult to understand, because such reactions would not be expected to accumulate charge in the transition state. Bergman's work suggests that the nucleophilicity of the solvent influences the reaction rate,¹ and he proposed an associative mechanism for such solvent effects (Scheme 1).

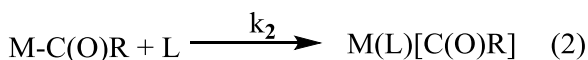
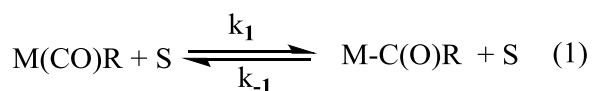
Scheme 1. Associative mechanism for solvent catalysed CO insertion reaction



S: Solvent molecule L: Trap molecule

Halpern and co-workers showed that various solvent molecules have catalytic ability for the formation of $M[C(O)R]$.² Among them, phosphine oxides and arsine oxides show outstanding accelerating performance, but their study clearly supports a dissociative mechanism (Scheme 2).

Scheme 2. Dissociative mechanism for solvent catalysed CO insertion reaction

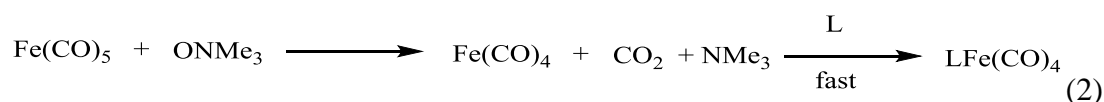
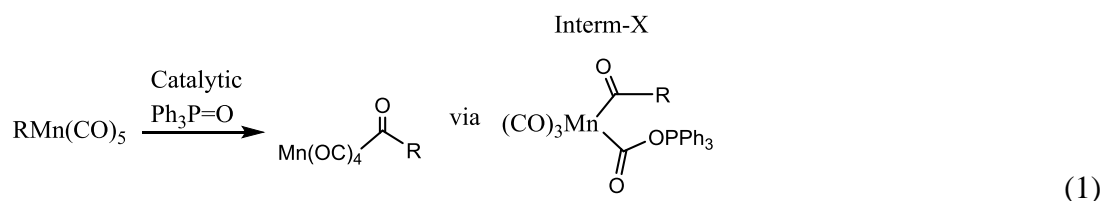


S: Solvent molecule L: Trap molecule

Results and Discussion

Although the catalytic effect is well documented, the nature of the interaction is still unknown. Halpern et al. inferred that the catalyst attacked at the carbonyl carbon other than coordination at the metal center, causing the solvent effect (Equation 1). This idea may have come from a well known amine oxide reaction (Equation 2), but our DFT calculations strongly argue against such a similar attack happening for phosphine oxide. The calculated barrier for $OPMe_3$ reacting with $Fe(CO)_5$ is 55.2 kcal/mol, which is 42 kcal/mol higher than $ONMe_3$'s calculated barrier. This high barrier would prevent such an attack from happening. Darensbourg's experimental study also suggests phosphine oxide would not attack CO as amine oxide does.³ This result is not surprising, since the strength of the P-O bond is much higher than that of the N-O bond. Also, the proposed intermediate IntermX does not exist from a calculation perspective. The reaction is a complete oxygen transfer reaction, which yields CO_2 and PPh_3 . Ford's elegant

spectroscopic studies suggests some solvents could attack the metal center other than the CO ligand for the dissociative solvent involved CO insertion step, though he was not able to pinpoint the nature of the interactions or explain the outstanding catalytic effect of phosphine oxide.⁴ In order to fully understand this unusual solvent effect, an extensive DFT study was conducted, which revealed the role of phosphine oxide in this CO insertion reaction as well as other catalytic molecules and show a completely different mechanism compared to the one proposed by Halpern.



Geometry optimizations and frequency computations were performed using Gaussian09 and the PBE exchange-correlation functional; the SDD ECP and valence basis set were used for metal atoms, and all-electron 6-311G(d,p) basis sets were applied to all P, C, O, H, N, and As atoms. Single-point energies of all the structures were also calculated using PBE-D3(BJ), B3LYP-D3(BJ) and M06-L-D3 functionals with the same basis sets. M06-L-D3//PBE results are presents in the main text, but all tested density functional methods yield identical trends and free energies of similar magnitudes for all the catalytic TSs. Thus, the same conclusions about the origins of catalytic effect are reached irrespective of the functional used.

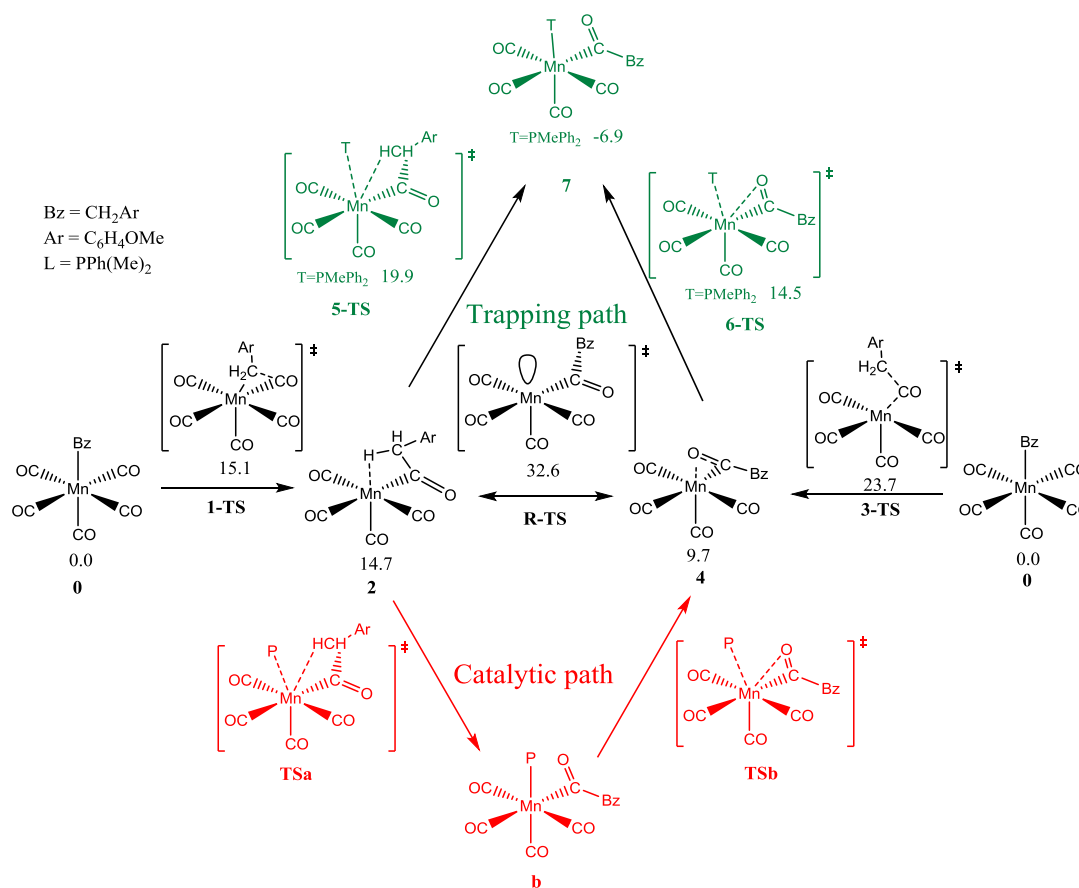


Figure 1. Free energy profile for the catalytic CO insertion reaction of $\text{Mn}(\text{CO})_5(\text{Bz})$ trapped by $\text{Mn}(\text{CO})_4(\text{PMe}_2\text{Ph})\text{H}$ or PMePh_2

The first step in the reaction is CO insertion (or alkyl migration) for reactant $\text{MnR}(\text{CO})_5$. As shown in Figure 1, the alkyl migration TS is an extremely late transition state. The free energy difference between **1-TS** and **2** is only 0.4 kcal/mol; intermediate **2** has an agostic bond with $\text{H} \cdots \text{Mn}$ distance of 2.01 Å. It is worth mentioning that the barrier for the alkyl migration/CO insertion step is only 15.1 kcal/mol. The late transition state and low barrier imply that a catalytic process accelerating this step does not exist, contrary to the fundamental idea behind the previous explanation for the solvent effect in this reaction. There is agostic NMR experimental evidence suggesting the presence of agostic structures of molybdenum acetyl complexes under static and dynamic

conditions,^{5,6} but a CO insertion step can go through a 8.6 kcal/mol higher route (**3-TS**) to reach an η^2 -acyl intermediates. Meanwhile, there is convincing evidence for η^2 -acyl intermediates for several CO insertion reaction systems.^{7,8} Several theoretical calculations on the $\text{Mn}(\text{CO})_4(\text{C}(\text{O})\text{CH}_3)$ system also suggest that an agostic intermediate and an η^2 -acyl intermediate are two key intermediate for non-solvent involved CO insertion reaction, and an η^2 -acyl mode is more stable than an agostic one.^{9,10} We got the similar result like the previous calculation work as η^2 -acyl intermediate **4** is 5.0 kcal/mol more stable than agostic intermediate **2**. But we think the key is they can be transformed between each other with the help of a solvent molecule. Experimental evidence supports there is an equilibrium between these two species in molybdenum systems.^{5,6} From our calculations, **2** can be transformed to complex **4** through a high energy RDTS (32.6 kcal/mol) without catalyst. The obvious reason behind this high barrier is that **3-TS** has an unsaturated 16e metal center with one empty site. Both **2** and **4** can be trapped by phosphine or metal hydride to form the product, but the path goes from **2** with a 5.4 kcal/mol higher barrier compared to path from **4** using PMePh_2 as trap reagent, or 8.1 kcal/mol using $\text{HMn}(\text{CO})_4(\text{PMePh}_2)$. This is not a surprising result, since the easy route is the route through the stable η^2 -acyl intermediate to the product, while the harder route is the route going through the higher energy agostic intermediate to the same product. After trapping, other than forming the final product when using phosphine, the metal hydride trap reagent will go through a hydrogen transfer to yield the more stable dimanganese carbonyl complex.

The catalytic effect for all catalysts comes from their ability to achieve the transformation between agostic intermediate **2** and η^2 -acyl complex **4** with a lower

barrier, as shown in Table 1. After this transformation, they can go through an easy channel in the following trapping step to accelerate the whole reaction. Phosphine oxide and arsine oxide are particular good catalysts for such transformation with barriers ranging from 12.3 kcal/mol to 15.5 kcal/mol, much lower than all the other catalytic reagents. The interesting part is that the transformation step is extremely similar to the trapping step, which react with phosphine or metal hydride. The difference is intermediate **b** formed between the transformation step is quite unstable compared to the final product which yields by trapping step, while the barrier for catalytic pathway is considerable lower than trapping pathway. The nature of this catalytic mechanism lies between these differences as compared in Scheme 3.

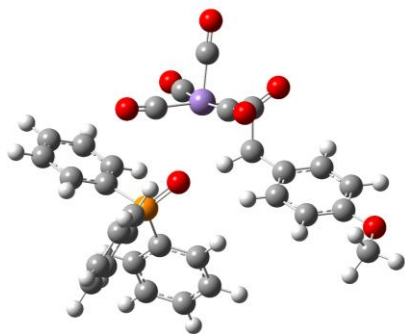
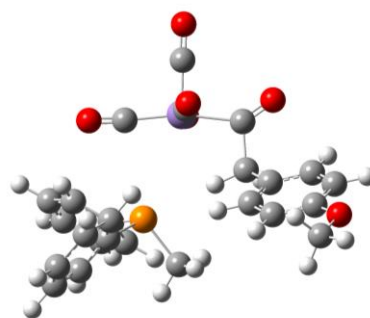
Table 1. Catalytic effects for $\text{Mn}(\text{CO})_5(\text{Bz})$ -CO insertion reaction by various catalysts. Free energy profiles (kcal/mol).

Entry	Catalysts	TSa	b	TSb
1	CH_3CN	21.5	5.6	16.7
2	DMF	20.5	6.2	16.4
3	HMPA	15.2	3.3	12.2
4	OAsBu_3	12.3	0.6	8.1
5	OPBu_3	14.4	2.8	10.3
6	OPPh_3	15.5	3.2	11.7
7	Pyridine	21.6	3.1	16.8
8	THF	21.0	8.2	15.7

From Scheme 3 we can see phosphine trapping molecule has an early TS (**5-TS**). While the catalyst molecule OPPh_3 has a relatively late TS (**TSa**), the O-Mn distance is 2.95 Å while the P-Mn distance is 3.67 Å. Most importantly, in **TSa_OPPh₃** the O...H distance between the agostic H and the oxide atom in triphenylphosphine oxide is only 2.08 Å, which means it forms a strong C-H...O hydrogen bond, since the shortest C-H...O hydrogen bonds known today have H...O distances around 2.0 Å.¹¹ It is worth mentioning that phosphine oxide is among the most strong acceptors for such hydrogen bonds. In **5-TS_PPh₂Me**, the P...H distance is 2.72 Å which is too long to have any hydrogen bond interaction. Such hydrogen interactions happen only in the TS for most catalysts, which explains the kinetic and thermodynamic result of the catalytic step. Not only hydrogen bond exists for outstanding catalysts like phosphine oxide and arsine oxide, we think such an interaction exists for all the catalyst reagents used in Halpern's work as shown in Table 2.

Scheme 3. Calculated bond lengths and angles for atoms in the coordination sphere of **TSa_OPPh₃** and **5-TS_PPh₂Me**, and graphic illustrations of both.



**TSa_OPPPh3****5-TS_PPh2Me****Table 2.** Hydrogen bond properties for different catalysts

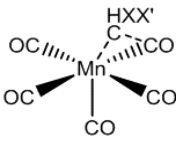
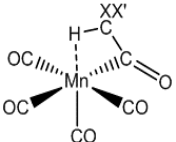
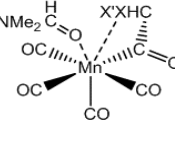
Species	CH...X type	H...X distance (Å)	ΔG (kcal/mol)	k_1^a
TSa_CH3CN	CH...N \equiv C	2.33048	21.5	1.5
TSa_DMF	CH...O=C	2.13390	20.5	7.8
TSa_HMPA	CH...O=P	2.10819	15.2	95
TSa_OAsBu3	CH...O=As	2.02387	12.3	1620
TSa_OPBu3	CH...O=P	2.06843	14.4	148
TSa_OPPPh3	CH...O=P	2.08339	15.5	38
TSa_pyridine	CH...N	2.30700	21.6	3.34
TSa_THF	CH...O	2.21162	21.0	0.9

^aRelative rate constant

The basicity of the catalyst molecule determines the strength of the hydrogen bond interaction during the catalytic path and determines its catalytic power. Phosphine oxides and arsine oxides have the shortest hydrogen bonds, lowest calculated barriers and largest rate constants. In order to further prove that the barrier for the transformation between the agostic intermediate and η^2 -acyl complex is determined by the strength of the hydrogen bond forming during the transformation, we do model calculations of $\text{Mn}(\text{CO})_5\text{CH}_3$, $\text{Mn}(\text{CO})_5\text{CH}_2\text{Cl}$, and $\text{Mn}(\text{CO})_5\text{CHCl}_2$ (Table 3). One of the strongest types of evidence for the hydrogen bond nature of the C-H...O interaction is that the H...O distance decreases systematically with increasing acidity of the C-H bond. The acidity of the C-H bond is increased by the number of Cl atom connected to the C. The calculations show the H...O distance indeed decreased systematically and ranges from 2.12 Å to 1.98

Å and the $\Delta\Delta G^\ddagger$ for such transformation process decreased from 4.8 kcal/mol to -0.1 kcal/mol. However, ΔG^\ddagger for **TS-Association** increased from 19.2 kcal/mol to 23.5 kcal/mol, because the alkyl migration step barrier increased from 15.1 kcal/mol to 24.4 kcal/mol following the increasing number of Cl substituents on the C atom.

Table 3. Effects of donor acidity (hydrogen bond strength)

Entry	Substance	TS-migration 	Agostic-Interm 	TS-Association 	$\Delta\Delta G$ (kcal/mol)	H...O (Å)
1	X=H,X'=H	15.1	14.4	19.2	4.8	2.12
2	X=H,X'=Cl	19.4	19.1	21.2	2.1	2.06
3	X=Cl,X'=Cl	24.4	23.6	23.5	-0.1	1.98

Conclusions

The basicity of the catalyst molecules determines the strength of the hydrogen bond interaction during the catalytic path and determines their catalytic power. The key for the catalytic effect of solvent molecule in CO insertion reaction for $\text{RMn}(\text{CO})_5$ is hydrogen bond assisted interaction. Based on whether such interaction exists, we can predict the solvent catalytic effect for similar metal complex CO insertion reactions as well. The mechanism proposed in this work applies to various catalytic molecules as well as different metal CO insertion systems. Performing calculations for $\text{Mo}(\text{Cp})(\text{CO})_3\text{Me}$ system based on this mechanism, we also got perfect agreement with the catalytic CO insertion experiment result.

References

1. Wax, M.J; Bergman, R.G. *J. Am. Chem. Soc.* **1981**, *103*, 7028.
2. Webb, S. L.; Giandomenico, C. M.; Halpern, J. *J. Am. Chem. Soc.* **1986**, *108*, 345.
3. Darensbourg, D.J *J. Am.Chem.Soc.* **1980**,*102*,1213
4. Ford, P.C.; Massick, S. *Coord. Chem. Rev.* **2002**, *226*, 39–49
5. Carmona, E.; Sa´nchez, L.; Poveda, M. L. *J. Am. Chem. Soc.* **1984**, *106*, 3214-3222.
6. Carmona, E.; Poveda, M. L.; Sa´nchez, L. *J. Am. Chem. Soc.* **1991**, *113*, 4322-4324.
7. Boese, W. T.; Ford, P. C. *J. Am. Chem. Soc.* **1995**, *117*, 8381- 8391.
8. Sweany, R. L. *Organometallics* **1989**, *8*, 175-179.
9. Ziegler, T.; Verluis, L.; Tscinke, V. *J. Am. Chem. Soc.* **1986**, *108*, 612- 617.
10. Derecskei-Kovacs, A.; Marynick, D. S. *J. Am. Chem. Soc.* **2000**, *122*, 2078- 2086
11. Gautam R. D. *The Weak Hydrogen Bond: In Structural Chemistry and Biology*,Oxford 1999

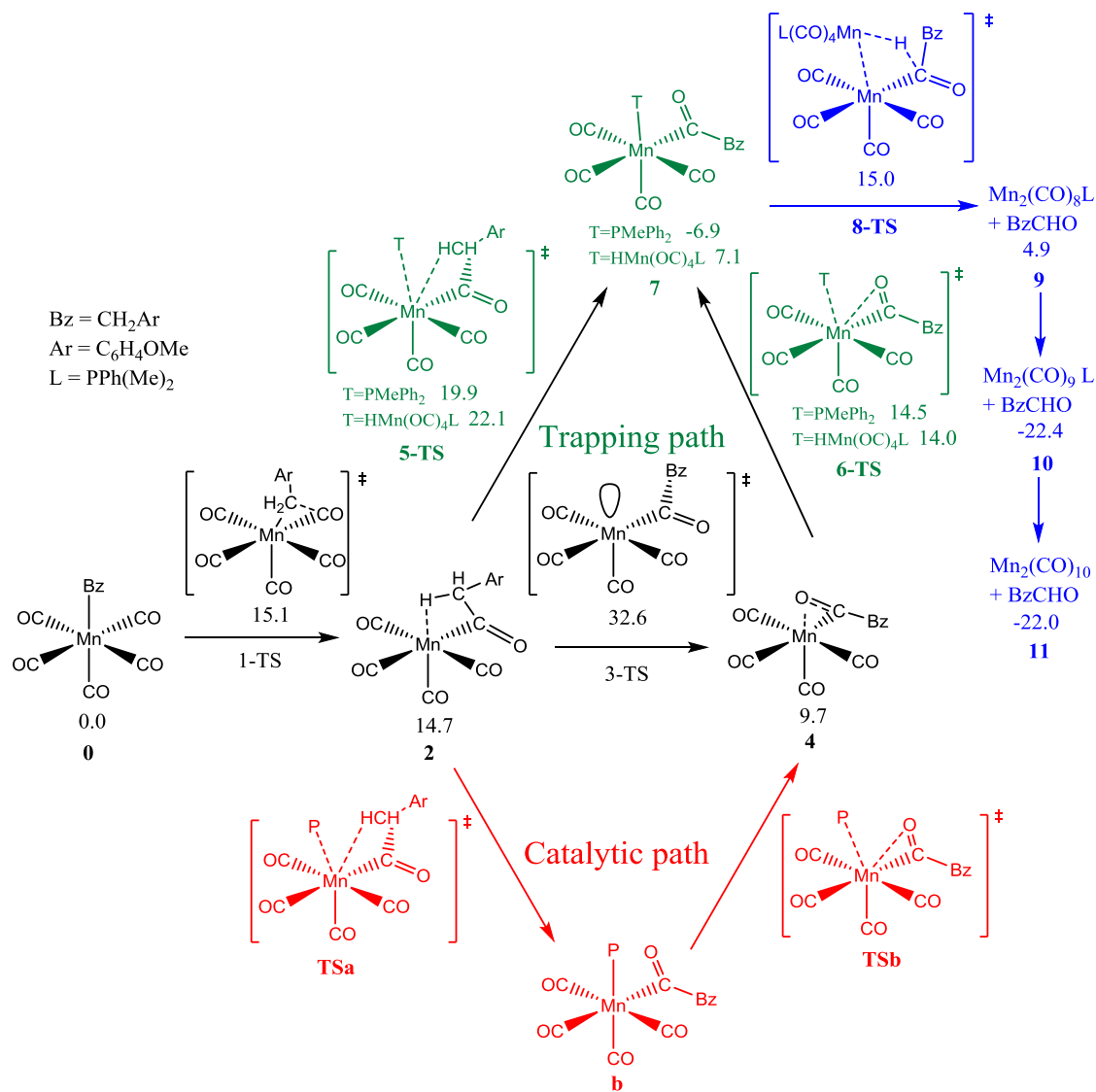
Computational details

All calculations used DFT methodologies implemented in the Gaussian 09 program.¹ Geometries were optimized using the PBE functional.² For metal atoms (Fe,Mn,Mo), we applied the SDD relativistic effective(small) core potentials and the associated (6s5p3d) valence basis sets;³ all other atoms (P, C, N, As, O, H) were assigned 6-311G(d,p) basis sets.⁴ Optimized geometries were verified by frequency computations as intermediate or transition state structures. Expanded integration grid sizes (pruned (99,590) atomic grids invoked using the integral=ultrafine keyword) were applied to increase numerical accuracy and stability in both geometry optimizations and normal

mode analysis.⁵ The (unscaled) vibrational frequencies formed the basis for the calculation of vibrational zero-point energy (ZPE) corrections; standard thermodynamic corrections (based on the harmonic oscillator/rigid rotor approximations and ideal gas behavior) were made to convert from purely electronic (reaction or activation) energies to (standard) enthalpies (H) and Gibbs free energies (G; P = 1 atm).⁶ H, entropy (S), and G were evaluated at room temperature: T = 25 °C (= 298 K), the reaction temperature reported in the experiments. Single-point energy on the optimized geometries were evaluated using the dispersion-corrected density functional methods M06-L-D3⁷(with the original D3 damping function⁸), and the same ecp/basis set level. The data presented here is using results from this M06-L-D3/PBE method. Additionally, single-point energies were calculated using PBE-D3^{7b,c}(with a Becke-Johnson damping function) and B3LYP-D3^{7b,c}(with a Becke-Johnson damping function) as well to check for robustness of our conclusions regarding the origin of catalytic effect across different functional methods.

Reaction mechanisms and energy tables

Figure S1. Reaction mechanism with free energies (kcal/mol) calculated as single point energies using M06-L-D3 functional for CO insertion reaction in $\text{Mn}(\text{CO})_5\text{CH}_2\text{C}_6\text{H}_4\text{OMe}$ system catalyzed by various molecules.



	TSa	b	TSb
CH ₃ CN	21.5	5.6	16.7
DMF	20.5	6.2	16.4
HMPA	15.2	3.3	12.2
OPBu ₃	14.4	2.8	10.3
OAsBu ₃	12.3	0.6	8.1
OPPh ₃	15.5	3.2	11.7
Pyridine	21.6	3.1	16.8

Table S1. Potential energies, enthalpies, entropies and free energies using PBE functionals for CO insertion reaction in $\text{Mn}(\text{CO})_5\text{CH}_2\text{C}_6\text{H}_4\text{OMe}$ system catalyzed by various molecules.^a

Description	Label_TZ	E	H	G	S
$\text{Mn}(\text{CO})_5\text{Bz}$	0	0.0	0.0	0.0	0.0
Bz group migration TS	1-TS	11.6	10.8	12.3	-5.1
R group migration	2	11.3	11.1	12.1	-3.1
sigma CH bond breaking TS	3-TS	30.0	29.2	30.4	-4.0
Carbonyl coordinated Interm	4	6.9	7.2	6.8	1.5
sigma CH bond dissociation TS	TSa_CH3CN	12.7	13.5	21.8	-27.8
	TSa_DMF	8.7	9.7	20.5	-36.3
	TSa_HMPA	7.6	8.6	21.8	-44.1
	TSa_OAsBu3	2.8	3.7	16.9	-44.3
	TSa_OPBu3	5.9	6.8	19.4	-42.2
	TSa_OPPh3	7.9	8.6	21.2	-42.1
	TSa_pyridine	11.2	11.9	22.5	-35.4
Carbonyl coordinated association TS	TSb_CH3CN	8.0	8.7	16.7	-26.6
	TSb_DMF	4.3	5.3	15.0	-32.7
	TSb_HMPA	4.6	5.5	16.4	-36.5
	TSb_OAsBu3	1.3	2.3	14.8	-42.1
	TSb_OPBu3	3.6	4.5	17.8	-44.4
	TSb_OPPh3	4.3	5.2	17.0	-39.8
	TSb_pyridine	5.1	6.1	15.8	-32.5
catalysts coordinate Interm	b_CH3CN	-6.5	-4.8	4.7	-31.9
	b_DMF	-5.2	-3.3	7.9	-37.5
	b_HMPA	-4.3	-2.4	10.2	-42.3
	b_OAsBu3	-6.8	-4.7	8.3	-45.4
	b_OPBu3	-4.0	-2.3	9.7	-40.3
	b_OPPh3	-3.6	-2.0	10.6	-42.2
	b_pyridine	-9.7	-7.8	4.5	-41.1
HMn trapping TS A	5-TS_HMn	14.6	14.9	28.2	-44.7
PMePh2 trapping TS A	5-TS_PPh2Me	12.7	13.4	24.3	-36.5
HMn trapping TS B	6-TS_HMn	7.8	8.1	19.3	-37.3
PMePh2 trapping TS B	6-TS_PPh2Me	5.9	6.8	17.1	-34.5
PMePh2 trapping Intermediate	7_HMn	2.0	3.2	16.3	-43.9

HMn trapping Intermediate	7_PPh2Me	-16.9	-14.6	0.8	-51.7
H transfer TS	8-TS	7.9	8.6	23.8	-51.2
Mn2CO8L	9	8.7	10.7	12.0	-4.3
Mn2CO9L	10	-30.3	-26.3	-12.9	-45.0
Mn2CO10	11	-34.8	-31.0	-21.6	-31.6

^a Units are kcal/mol for ΔE , ΔH , and ΔG ; units are cal/(deg.mol) for ΔS . The standard state for concentrations is 1 M for each species participating in the reaction; T = 298.15 K.

Table S2. Free energies (kcal/mol) for CO insertion reaction in $\text{Mn}(\text{CO})_5\text{CH}_2\text{C}_6\text{H}_4\text{OMe}$ system catalyzed by various molecules using different functional methods

Description	Label_TZ	PBED3BJ	B3LYPD3BJ	M06LD3
Mn(CO) ₅ Bz	0	0.0	0.0	0.0
Bz group migration TS	1-TS	11.7	14.0	15.1
R group migration	2	12.8	16.4	14.7
sigma CH bond breaking TS	3-TS	31.4	31.7	32.6
Carbonyl coordinated Interm	4	8.2	8.7	9.7
sigma CH bond dissociation TS	TSa_CH3CN	18.8	18.1	21.5
	TSa_DMF	16.9	16.0	20.5
	TSa_HMPA	13.5	11.4	15.2
	TSa_OAsBu3	9.1	7.6	12.3
	TSa_OPBu3	11.5	9.8	14.4
	TSa_OPPh3	12.7	10.3	15.5
	TSa_pyridine	17.7	17.3	21.6
Carbonyl coordinated association TS	TSb_CH3CN	14.5	13.0	16.7
	TSb_DMF	13.2	12.1	16.4
	TSb_HMPA	10.5	8.4	12.2
	TSb_OAsBu3	7.0	4.6	8.1
	TSb_OPBu3	9.4	7.0	10.3
	TSb_OPPh3	9.6	7.0	11.7
	TSb_pyridine	13.0	12.4	16.8
catalysts coordinate Interm	b_CH3CN	3.3	5.5	5.6
	b_DMF	5.8	5.3	6.2
	b_HMPA	4.0	2.9	3.3
	b_OAsBu3	0.8	-0.3	0.6
	b_OPBu3	4.0	2.5	2.8
	b_OPPh3	4.0	2.4	3.2

	b_pyridine	0.6	2.6	3.1
HMn trapping TS A	5-TS_HMn	19.5	17.0	22.1
PMePh2 trapping TS A	5-TS_PPh2Me	16.9	16.7	19.9
HMn trapping TS B	6-TS_HMn	11.8	9.9	14.0
PMePh2 trapping TS B	6-TS_PPh2Me	11.7	11.2	14.5
PMePh2 trapping Intermediate	7_HMn	7.6	5.5	7.1
HMn trapping Intermediate	7_PPh2Me	-10.3	-8.4	-6.9
H transfer TS	8-TS	10.9	13.5	15.0
Mn2CO8L	9	6.8	5.9	4.9
Mn2CO9L	10	-24.0	-23.9	-22.4
Mn2CO10	11	-24.0	-20.1	-22.0

Table S3. Potential energies, enthalpies, entropies and free energies using the PBE functional for species in $\text{Mn}(\text{CO})_5\text{CH}_3$, $\text{Mn}(\text{CO})_5\text{CH}_2\text{Cl}$ and $\text{Mn}(\text{CO})_5\text{CHCl}_2$ CO insertion reaction catalyzed by DMF.^a

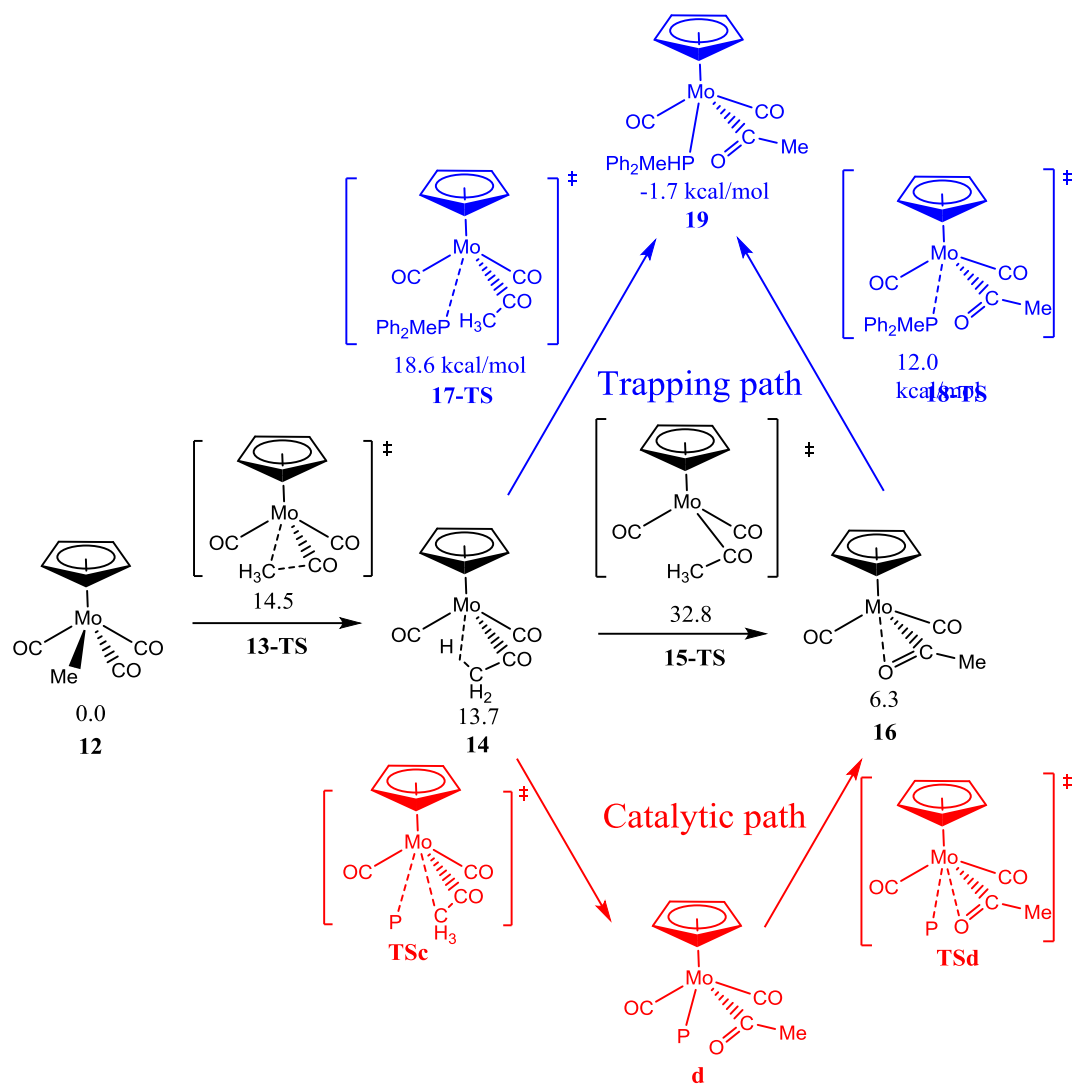
Description	Label_TZ	E	H	G	S
R group migration transition state	TS-migration-CH3	11.6	10.9	13.3	-8.0
	TS-migration-CH2Cl	16.4	15.4	16.6	-4.2
	TS-migration-CHCl2	20.6	19.6	20.8	-4.0
Agostic Intermediate	Agostic-Interm-CH3	11.0	10.9	12.9	-6.9
	Agostic-Interm-CH2Cl	16.3	15.9	16.5	-1.9
	Agostic-Interm-CHCl2	20.6	20.2	20.0	0.4
sigma CH bond dissociation TS	TS-Association-CH3	8.1	9.0	19.5	-34.9
	TS-Association-CH2Cl	10.1	10.9	21.0	-33.8
	TS-Association-CHCl2	11.1	11.9	21.8	-33.2

^aPotential energies, enthalpies, and free energies in units of kcal/mol; entropies in unit of cal/mol deg.

Table S4. Free energies (kcal/mol) for species in $\text{Mn}(\text{CO})_5\text{CH}_3$, $\text{Mn}(\text{CO})_5\text{CH}_2\text{Cl}$ and $\text{Mn}(\text{CO})_5\text{CHCl}_2$ CO insertion reaction catalyzed by DMF using different functionals.

Description	Label_TZ	PBED3BJ	B3LYPD3BJ	M06LD3
R group migration transition state	TS-migration-CH3	13.4	17.4	15.1
	TS-migration-CH ₂ Cl	17.0	21.6	19.4
	TS-migration-CHCl ₂	21.2	26.0	24.4
Agostic Intermediate	Agostic-Interm-CH ₃	13.2	17.6	14.4
	Agostic-Interm-CH ₂ Cl	16.8	21.5	19.1
	Agostic-Interm-CHCl ₂	20.5	25.3	23.6
sigma CH bond dissociation TS	TS-Association-CH ₃	15.9	16.0	19.2
	TS-Association-CH ₂ Cl	17.2	17.7	21.2
	TS-Association-CHCl ₂	18.1	19.3	23.5

Figure S2. Reaction mechanism with free energies (kcal/mol) calculated as single point energies using M06-L-D3 functional for CO insertion reaction in $\text{CpMo(CO)}_3\text{CH}_3$ system catalyzed by various molecules.



	TSc	d	TSd
CH_3CN	21.4	10.4	15.8
DMF	21.0	13.3	14.1
DMSO	18.5	6.4	10.8
OAsBu_3	14.3	-1.2	7.4
OAsPh_3	15.0	0.7	7.9
OPBu_3	15.9	3.8	9.8
OP(OMe)_3	19.4	9.5	13.1
OPPh_3	16.2	5.6	11.4
Pyridine	20.5	10.5	15.0

Table S5. Potential energies, enthalpies, entropies and free energies using PBE functionals for CO insertion reaction in $\text{CpMn}(\text{CO})_3\text{CH}_3$ system catalyzed by various molecules.^a

Description	Label_TZ	E	H	G	S
$\text{Mo}(\text{Cp})(\text{CO})_3\text{Me}$	12	0.0	0.0	0.0	0.0
Me group migration TS	13-TS	12.3	11.6	12.8	-4.1
R group migration	14	12.2	12.2	12.3	-0.2
sigma CH bond breaking TS	15-TS	32.9	32.5	33.1	-2.0
Carbonyl coordinated Interm	16	6.2	6.7	6.0	2.3
sigma CH bond dissociation TS	TSc_CH3CN	14.5	15.3	23.9	-28.8
	TSc_DMF	12.6	13.7	24.0	-34.7
	TSc_DMSO	9.1	10.0	21.8	-39.4
	TSc_OAsBu3	7.2	8.2	20.9	-42.6
	TSc_OAsPh3	8.6	9.5	21.6	-40.7
	TSc_OPBu3	10.0	10.9	23.1	-40.9
	TSc_OPOMe3	12.6	13.5	25.3	-39.5
	TSc_OPPh3	10.7	11.6	24.4	-43.0
	TSc_pyridine	12.2	13.2	24.5	-37.8
Carbonyl coordinated association TS	TSd_CH3CN	9.1	10.1	18.5	-28.3
	TSd_DMF	4.7	5.9	16.8	-36.6
	TSd_DMSO	2.0	3.1	14.6	-38.6
	TSd_OAsBu3	1.3	2.5	15.3	-42.9
	TSd_OAsPh3	2.9	3.9	16.0	-40.6
	TSd_OPBu3	4.2	5.4	17.9	-42.0
	TSd_OPOMe3	6.6	7.6	19.9	-41.1
	TSd_OPPh3	5.9	6.9	19.0	-40.7
	TSd_pyridine	6.7	7.8	18.9	-37.4
catalysts coordinate Interm	d_CH3CN	0.4	2.1	11.8	-32.3
	d_DMF	4.8	6.8	17.6	-36.3
	d_DMSO	-3.7	-1.9	10.7	-42.1
	d_OAsBu3	-5.6	-3.7	9.5	-44.4
	d_OAsPh3	-5.2	-3.6	9.8	-45.2
	d_OPBu3	-0.2	1.5	14.0	-42.0
	d_OPOMe3	2.8	4.6	17.7	-44.1
	d_OPPh3	1.9	3.4	16.0	-42.3
	d_pyridine	-0.4	1.6	13.8	-41.0
PMePh2 trapping TS A	17-TS	12.9	13.8	26.3	-41.9
PMePh2 trapping TS B	18-TS	6.4	7.5	19.1	-39.0
$\text{Mo}(\text{Cp})(\text{CO})_2(\text{PMePh}_2)\text{COMe}$	19	-9.9	-7.8	6.5	-47.9

^aPotential energies, enthalpies, and free energies in units of kcal/mol; entropies in units of cal/mol deg.

Table S6. Free energies (kcal/mol) for CO insertion reaction in $\text{CpMo}(\text{CO})_3\text{CH}_3$ system catalyzed by various molecules using different functionals

Description	Label_TZ	PBED3BJ	B3LYPD3BJ	M06LD3
$\text{Mo}(\text{Cp})(\text{CO})_3\text{Me}$	12	0.0	0.0	0.0
Me group migration TS	13-TS	13.2	16.0	14.5
R group migration	14	12.7	15.4	13.7
sigma CH bond breaking TS	15-TS	34.0	34.5	32.8
Carbonyl coordinated Interm	16	7.3	8.8	6.3
sigma CH bond dissociation TS	TSc_CH3CN	21.4	23.4	21.4
	TSc_DMF	21.0	22.2	21.0
	TSc_DMSO	17.6	18.4	18.5
	TSc_OAsBu3	14.4	14.8	14.3
	TSc_OAsPh3	14.8	14.9	15.0
	TSc_OPBu3	16.6	17.0	15.9
	TSc_OPOMe3	20.0	20.0	19.4
	TSc_OPPh3	16.7	16.6	16.2
	TSc_pyridine	20.0	21.6	20.5
Carbonyl coordinated association TS	TSd_CH3CN	16.2	18.1	15.8
	TSd_DMF	14.1	15.1	14.1
	TSd_DMSO	11.3	11.5	10.8
	TSd_OAsBu3	8.9	8.9	7.4
	TSd_OAsPh3	9.2	8.8	7.9
	TSd_OPBu3	11.5	11.6	9.8
	TSd_OPOMe3	14.4	14.5	13.1
	TSd_OPPh3	12.3	12.1	11.4
	TSd_pyridine	14.9	16.2	15.0
catalysts coordinate Interm	d_CH3CN	8.7	11.3	10.4
	d_DMF	13.9	13.5	13.3
	d_DMSO	5.9	5.1	6.4
	d_OAsBu3	0.8	-1.0	-1.2
	d_OAsPh3	0.8	-0.9	0.7
	d_OPBu3	5.7	4.1	3.8

	d_OPOMe3	11.1	9.0	9.5
	d_OPh3	7.0	4.9	5.6
	d_pyridine	8.0	9.5	10.5
PMePh2 trapping TS A	17-TS	18.5	20.0	18.6
PMePh2 trapping TS B	18-TS	12.3	13.8	12.0
Mo(Cp)(CO) ₂ (PMePh2) COMe	19	-5.5	-4.6	-1.7

Computational Section References

1. Frisch, M. J.; et al., Gaussian 09, revision D.01; Gaussian, Inc.: Wallingford, CT, 2009.
2. Perdew, J. P.; Burke, K.; Ernzerhof, M. *Phys. Rev. Lett.* **1996**, 77, 3865.
3. D. Andrae, U. Haeussermann, M. Dolg, H. Stoll and H. Preuss, *Theor. Chim. Acta*, **1990**, 77, 123–141
4. (a) R. Ditchfield, W. J. Hehre and J. A. Pople, *J. Chem. Phys.*, **1971**, 54, 724–728; (b) P. C. Hariharan and J. A. Pople, *Mol. Phys.*, **1974**, 27, 209–214; (c) K. Raghavachari, J. S. Binkley, R. Seeger and J. A. Pople, *J. Chem. Phys.*, **1980**, 72, 650–654; (d) A. D. McLean and G. S. Chandler, *J. Chem. Phys.*, **1980**, 72, 5639–5648.
5. Frisch, Æ; Frisch, M. J.; Clemente, F. R.; Trucks, G. W. *Gaussian 09 User's Reference*, Gaussian, Inc., Wallingford CT, 2009, pp 167.
6. McQuarrie, D. A. *Statistical Thermodynamics*; Harper and Row: New York, 1973.
7. (a) Y. Zhao and D. G. Truhlar, *Theor. Chem. Acc.*, **2008**, 120, 215–241; (b) T. Schwabe and S. Grimme, *Phys. Chem. Chem. Phys.*, **2007**, 9, 3397–3406; (c) S. Grimme, J. Antony, S. Ehrlich and H. Krieg, *J. Chem. Phys.*, **2010**, 132, 154104.
8. (a) Grimme, S.; Ehrlich, S.; Goerigk, L. *J. Comput. Chem.* **2011**, 32, 1456. (b) Johnson, E. R.; Becke, A. D. *J. Chem. Phys.* **2006**, 124, 174104. (c) Johnson, E. R.; Becke, A. D. *J. Chem. Phys.* **2005**, 123, 024101.

**Chapter 7: Computational Study of Catalytic Dehydrogenative C-C Coupling by a
Pincer-Ligated Iridium Complex**

Majority of this chapter is reproduced from

Catalytic Dehydrogenative C-C Coupling by a Pincer-Ligated Iridium Complex

Miles Wilklow-Marnell[†], Bo Li[‡], Tian Zhou[‡], Karsten Krogh-Jespersen[‡], William
W. Brennessel[†], Alan S. Goldman^{‡*}, and William D. Jones^{†*}

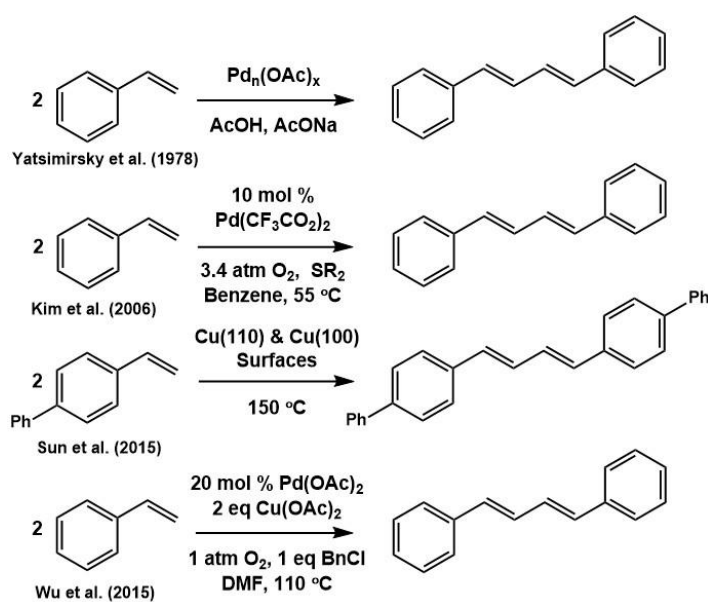
Manuscript submitted (December 2016) for publication

Introduction

Carbon-carbon bond forming reactions are clearly among the most useful and important reactions in organic synthesis. Over the past several decades, transition metal complexes have revolutionized the ability to effect C-C bond formation. The majority of transition metal catalyzed systems for C-C bond formations, however, require pre-activated substrates, including organometallic and/or organohalide species. (Of course, this applies even more so to non-transition-metal catalyzed C-C bond formations.) Significant progress has been made with respect to C-C bond formation between non-functionalized alkanes, alkenes, and alkynes, with the dehydrogenative Heck (or Fujiwara-Moritani) reaction, involving aryl and alkene C(sp²)-C(sp²) coupling, being perhaps the most well developed class of such reactions. However, these methodologies often require high to stoichiometric amounts of palladium species and/or oxidants, and the presence of directing groups, and often display poor selectivity and/or yields.¹⁻³ The few published examples of C_{vinyl}-C_{vinyl} bond formation by double C_{vinyl}-H activation suffer from the same issues.⁴

Examples of the direct formation of C_{vinyl}-C_{vinyl} bonds by transition metal mediated dehydrogenative coupling of vinyl arenes to form specifically aryl substituted 1,3-butadienes are particularly quite limited. Scheme 1 depicts notable examples to date. In

an early example, Yatsimirsky *et al.* studied the kinetics of stoichiometric dehydrogenative coupling of styrene by various palladium(II) acetate species in glacial acetic acid.⁵ Much later, in 2006 the formation of 1,4-diphenyl-1,3-butadiene was identified by Kim *et al.* as a component (up to 53%) in the product mixture resulting from Fujiwara-Moritani coupling between benzene and styrene using $\text{Pd}(\text{CF}_3\text{CO}_2)_2$ as catalyst in the presence of thioether type ligands and 3.4 atm O_2 .⁶ Recently, 4-vinylbiphenyl was shown to undergo dehydrogenative coupling when deposited as a monolayer on copper surfaces;⁷ however, the coupled product was only observed *in situ*. Also in 2015, the dehydrogenative coupling of various vinyl arenes was reported in up to 66% yield using $\text{Pd}(\text{OAc})_2$ as catalyst (20 mol %) and $\text{Cu}(\text{OAc})_2$ as oxidant under 1 atm O_2 .⁸ In addition, one equivalent benzyl chloride was found to be required.



Scheme 1. Reported examples of dehydrogenative coupling of vinyl arenes.

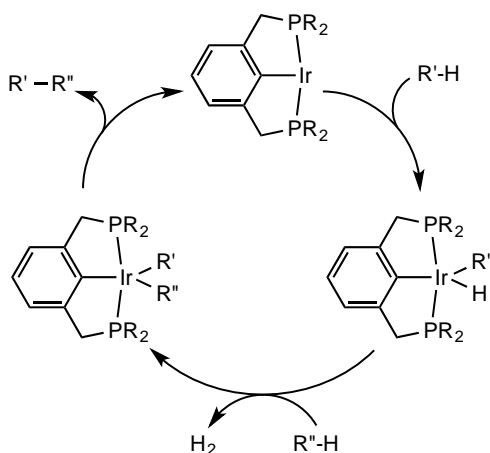
Although iridium has played a leading role in the development of stoichiometric C-H bond activation, as well as catalytic C-H bond functionalization, particularly alkane

dehydrogenation, there are surprisingly few examples of iridium-catalyzed dehydrogenative couplings of C-H bonds. Intramolecular ligand-based C(sp³)-H couplings forming new C=C double bonds,^{9,10} and several inter/intramolecular couplings to form heterocycles^{11,12} and fluorenols¹³ have been reported. In the present work, we report the efficient dehydrogenative coupling of vinyl arenes to form (*E,E*)-1,4-diaryl-1,3-butadienes catalyzed by the reactive (ⁱPrPCP)Ir fragment. In addition, we demonstrate efficient catalytic intramolecular C(sp³)-C(sp²) dehydrogenative coupling. These results indicate that the established ability of pincer-ligated iridium complexes to effect both C-H addition and C-C bond coupling¹⁴ can be integrated into productive catalytic dehydrogenative coupling reactions.

Result and Discussion

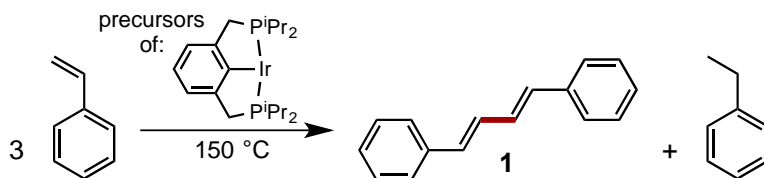
Catalytic intermolecular coupling by (ⁱPrPCP)Ir. Pincer-ligated iridium fragments (^RPCP)Ir have been reported to undergo facile and rapid addition of aryl and vinyl C-H bonds at room temperature, as well as catalyzing alkane dehydrogenation. More recently, we have also reported the *double* C-H activation of biphenyl and phenanthrene to form iridacycles at (^RPCP)Ir with concomitant release of H₂.^{15,16} In addition, we have demonstrated that (^RPCP)IrRR' complexes can undergo relatively facile C-C bond reductive elimination¹⁴ and, conversely, (^RPCP)Ir fragments can oxidatively add strained C-C bonds.¹⁷ With this in mind, we have attempted to determine whether these stoichiometric reactions could be employed in catalytic dehydrogenative C-C bond coupling reactions as indicated in Scheme 2.

Scheme 2. Simplified catalytic cycle for dehydrogenative coupling by (^RPCP)Ir proceeding via C-H addition to yield an Ir(III) hydrocarbyl hydride followed by a second C-H addition to the Ir(III) species.



A solution of styrene (0.654 M) in toluene containing 5 mol % (ⁱPrPCP)IrHCl and 2 equivalents KO^tBu (based on Ir) was heated at 150 °C in a sealed ampoule, with stirring, for 24 h, presumably generating the reactive fragment (ⁱPrPCP)Ir. In accord with the hypothesis indicated above, (*E,E*)-1,4-diphenyl-1,3-butadiene (**1**) was observed as one of two major organic product as indicated by GC-MS and ¹H NMR spectroscopy, in comparison with an authentic sample (Entry 1, Table 1). The other major product is ethylbenzene, resulting from the hydrogenation of styrene. Thus the reaction is a disproportionation, wherein one equivalent of styrene is hydrogenated to form ethylbenzene for each equivalent of **1** produced (Scheme 3). In the absence of (ⁱPrPCP)IrHCl, under otherwise identical conditions, the formation of **1** was not observed (Entry 2, Table 1).

Scheme 3. Dehydrogenative coupling of styrene by disproportionation



(ⁱPrPCP)Ir(C₂H₄) was also found to be an effective precatalyst for dehydrogenative coupling, presumably yielding the active (ⁱPrPCP)Ir fragment by dissociation of ethylene without the need for base or other activating agents. Our typical protocol with this precatalyst used 1 mole % (ⁱPrPCP)Ir(C₂H₄) with respect to substrate, in *p*-xylene-*d*₁₀ heated at 150 °C.

The (ⁱPrPCP)Ir catalyst was found to tolerate various substituents at the para-position of the aryl ring, including methyl, *t*-butyl, trifluoromethyl, methoxy, and fluorine, although conversions were lowered in some cases, perhaps due to C-H activation at the position ortho to the substituent.¹⁸ 2-vinylnaphthalene (Entry 6, Table 1) was also converted to the corresponding dimer. Functional groups at the para position that are known to react with (PCP)Ir derivatives, such as C-Cl bonds or ester groups, prevented catalysis as did a diphenylphosphino substituent. Vinylferrocene and 2-vinylpyridine proved incompatible, affording low conversions and complicated product mixtures.

Substitution with methyl groups at the styrene meta positions had little effect on the reaction. Likewise, substitution with a methyl group at *one* of the ortho positions did not significantly inhibit the reaction (Entry 7, Table 1). Substitution at the vinylic positions, however, severely limited dimerization. α -Methylstyrene was not efficiently coupled, affording only 9% conversion (Entry 8, Table 1). Allylbenzene did not produce observable coupling products (Entry 9, Table 1), instead only isomerization to form 1-phenylpropene was observed.

Entry	Substrate (styrene/derivative)	Catalyst Precursor (conc.)	Acceptor	Conversion (%)	Hydrogenated styrene derivative (mM)	Yield dimer (%) ^c
1 ^a	Styrene	(ⁱ PrPCP)IrHCl (33 mM)	none	92	241	70 (77 ^f)
2 ^a	Styrene	None	none	0	0	n/a
3 ^a	Styrene	(ⁱ PrPCP)IrHCl (6.5 mM)	none	43	n/d	n/d
10 ^{b1}	Styrene	(ⁱ PrPCP)Ir(C ₂ H ₄) (5 mM)	none	83	?	? ^l
12 ^{b3}	4-methylstyrene	(ⁱ PrPCP)Ir(C ₂ H ₄) (5 mM)	none	69	n/a	? ^l
13 ^{b4}	4- <i>tert</i> -butylstyrene	(ⁱ PrPCP)Ir(C ₂ H ₄) (5 mM)	none	84	n/a	? ^l
2	4-(trifluoromethyl)styrene	(ⁱ PrPCP)IrHCl (33 mM)	none	80	yes	Yes
14 ^{b5}	4-trifluoromethylstyrene	(ⁱ PrPCP)Ir(C ₂ H ₄) (5 mM)	none	66	n/a	n/a
3	4-methoxystyrene	(ⁱ PrPCP)IrHCl (33 mM)	none	76	yes	Yes
16 ^{b7}	4-methoxystyrene	(ⁱ PrPCP)Ir(C ₂ H ₄) (5 mM)	none	42	n/a	n/a
19 ^{m1}	4-fluorostyrene	(ⁱ PrPCP)Ir(C ₂ H ₄) (10 mM)	none	57		35
1	4-chlorostyrene	(ⁱ PrPCP)IrHCl (33 mM)	none	17 ^h	yes	Yes
4	4-acetoxystyrene	(ⁱ PrPCP)IrHCl (33 mM)	none	98	yes	yes ⁱ
6 ^a	2-vinylnaphthalene	(ⁱ PrPCP)IrHCl (33 mM)	none	98	n/a	55
6	2-vinylpyridine	(ⁱ PrPCP)IrHCl (33 mM)	none	99 ^k	no	No
5	vinylferrocene	(ⁱ PrPCP)IrHCl (33 mM)	none	21	yes	no ^j
7	4-vinylphenol	(ⁱ PrPCP)IrHCl (33 mM)	none	5	yes	No
18 ^{b9}	3,5-dimethylstyrene	(ⁱ PrPCP)Ir(C ₂ H ₄) (5 mM)	none	66	n/a	n/a
17 ^{b8}	3,5-dimethylstyrene	(ⁱ PrPCP)Ir(C ₂ H ₄) (5 mM)	none	6	n/a	n/a
7 ^a	2-methylstyrene	(ⁱ PrPCP)IrHCl (33 mM)	none	98	n/a	48
15 ^{b6}	2-methylstyrene	(ⁱ PrPCP)Ir(C ₂ H ₄) (5 mM)	none	81	n/a	n/a
11 ^{b2}	2,4,6-trimethylstyrene	(ⁱ PrPCP)Ir(C ₂ H ₄) (5 mM)	none	0	n/a	n/a
20 ^{m2}	2,3,4,5,6-pentamethylstyrene	(ⁱ PrPCP)Ir(C ₂ H ₄) (10 mM)	none	0	0	0
21 ^{m3}	2,6-difluorostyrene	(ⁱ PrPCP)Ir(C ₂ H ₄) (10 mM)	none	0	0	0
8 ^a	α -methylstyrene	(ⁱ PrPCP)IrHCl (33 mM)	none	9	n/a	n/d
9 ^a	Allylbenzene	(ⁱ PrPCP)IrHCl (33 mM)	none	82 ^g	n/a	n/d

Table 1. Iridium catalyzed dehydrogenative coupling of non-functionalized vinyl arenes. Conditions: a) 5 mole% (ⁱPrPCP)IrHCl, 654 mM substrate in toluene, 2 equivalents KO^tBu, 150 °C, 24 hours. b) 5 mM (ⁱPrPCP)Ir(C₂H₄), 500 mM substrate in *p*-xylene-d₁₀, J-Young NMR tube, 150 °C; 1) 42 hours, 2) 47 hours, 3) 54 hours, 4) 93 hours, 5) 152 hours, 6) 92 hours. c) Isolated yield of diarylbutadiene unless noted, based on a disproportionation mechanism. f) GCMS yield, dodecane standard. g) olefin isomerization. h) Product mixture complicated by extensive H/Cl scrambling. i) Trace. j) Decomposes upon melting, fragments observed. k) Numerous unidentified products formed. Common m/z values detected: 170, 224, and 288. l) ¹H-NMR. n/d = not determined, n/a = not applicable. m) 10 mM (ⁱPrPCP)Ir(C₂H₄), 500 mM substrate in mesitylene, sealed tubes, 150 °C, 1) 32h, 2) 32h, 3) 32h.

Increased coupling yields were also obtained using (ⁱPrPCP)Ir(C₂H₄) as precatalyst in the presence of 1 atm of either ethylene or propylene as acceptor (Entries 14 and 15,

Table 1). In each case, yields were improved and ethylbenzene production was significantly limited. The reactions proceeded cleanly but prolonged reaction times were found to be necessary, which is presumably attributable to inhibition due to the acceptor binding relatively strongly to (ⁱPrPCP)Ir.¹⁹

The formation of almost exclusively the (*E,E*)-stereoisomer of 1,4-diphenyl-1,3-butadiene is noteworthy. GC-MS revealed that an additional species with the same mass and very similar GC retention time as the major (*E,E*) product, likely the (*E,Z*) isomer, was present in all reaction samples in low concentration (ca. 7% of the (*E,E*) isomer).

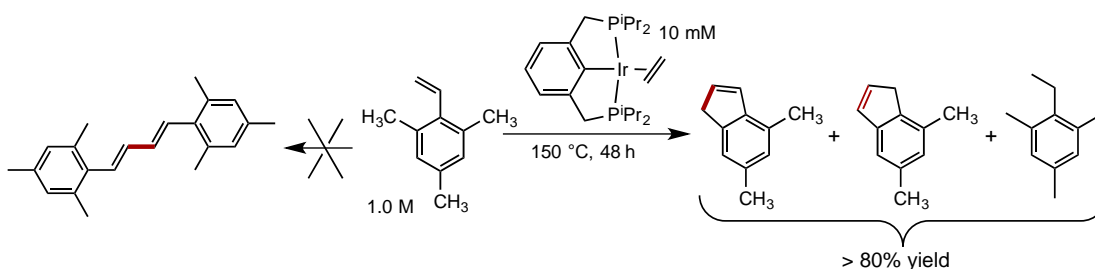
We considered the possibility that the (*E,Z*) isomer was actually a major kinetic product but underwent isomerization to the more thermodynamically stable (*E,E*) isomer. To assess this possibility, a mixture of (*E,E*) and (*E,Z*)-diphenylbutadiene was independently generated by visible light irradiation of a dilute hexane solution of **1**.²⁰ This solution was concentrated *in vacuo* to provide an oily semi-solid residue, which was then used to prepare a toluene solution 0.2 M in total 1,4-diphenyl-1,3-butadienes. When samples of this solution were heated at 150 °C for 24 hours under normal laboratory lighting in the presence of KO^tBu/(ⁱPrPCP)IrHCl, almost all (*E,Z*) isomer was converted to the (*E,E*) isomer, along with some formation of diphenylbutene and diphenylbutane. In the absence of (ⁱPrPCP)IrHCl, under otherwise identical conditions, no isomerization was observed. Thus the observation of predominantly (*E,E*) product in the coupling reaction does not indicate that this isomer is the major kinetic product.

During the course of the coupling reactions we observe signals in the ¹H NMR spectrum that appear to be attributable to the unsubstituted metalloindene analog of **2**. While we have been unable to isolate this species, the reaction of (ⁱPrPCP)Ir(C₂H₄) with

3,5-bis-trifluoromethylstyrene does afford the corresponding analog (**3**). Crystals were obtained by recrystallization in hexane at $-40\text{ }^{\circ}\text{C}$, and the structure (of what appears to be the *n*-hexane solvate) was obtained by X-ray diffraction. It has previously been reported that the presence of an ortho-trifluoromethyl group greatly stabilizes (PCP)Ir(aryl)H;^{18,21} the apparently greater stability of **3** as compared with its unsubstituted analogue presumably derives from the same or closely related factors.

Catalytic intramolecular coupling by (*i*PrPCP)Ir. Surprisingly, in contrast with the fairly efficient coupling observed with *p*-substituted substrates or mono-ortho substituted substrates, 2,4,6-trimethylstyrene failed to yield any observable butadiene coupling product. Instead, however, intramolecular C(sp³)-C(sp²) coupling was achieved with >80% yield (93% total conversion) giving two major dehydrogenative coupling products, 4,6-dimethylindene and 5,7-dimethylindene, as well as 2-ethylmesitylene (Scheme 4).

Scheme 4. Intramolecular C(sp³)-C(sp²) dehydrogenative coupling catalyzed by (*i*PrPCP)Ir



Stoichiometric reactions of (*t*BuPCP)Ir with styrenes. In contrast to the *i*PrPCP analogs, no catalysis was obtained with the more crowded pincer-iridium species (*t*BuPCP)Ir. The reaction of (*t*BuPCP)IrH₄ with styrene at 150 °C for 6 h instead resulted in a species, **3**, in 80% yield (by ¹H NMR) which may be described as the product of

dehydrogenative coupling between a phosphino-*t*-butyl methyl group and a molecule of styrene, plus C-H addition of the β -vinyl and ortho-aryl C-H bonds of the coupled product (eq 1). Crystals were obtained by recrystallization in hexane at $-40\text{ }^{\circ}\text{C}$, and X-ray diffraction revealed the structure shown in Figure 1.

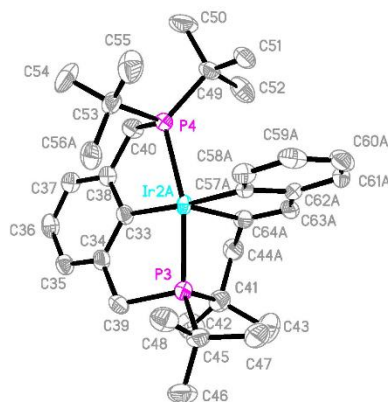
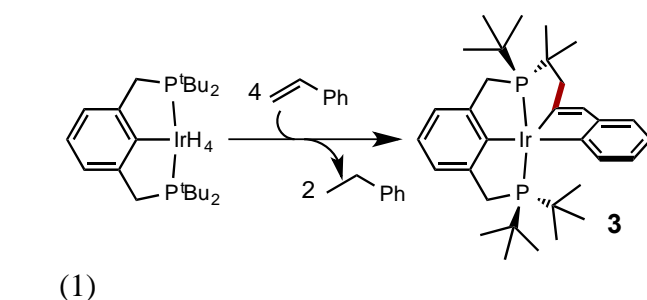


Figure 1. ORTEP representation of complex **3** (50% probability ellipsoids)

With either α -methyl styrene or β -methyl styrene, the reaction of $(^t\text{BuPCP})\text{IrH}_4$ at $150\text{ }^{\circ}\text{C}$ gave the simple metalloindene complex (complex **4** and **5**, respectively) resulting from C-H addition of the β -vinyl and ortho-aryl C-H bonds of the respective uncoupled styrene (and presumably hydrogenation of another molecule of styrene; eq 2). The iridium-containing products were identified by ^1H and ^{31}P NMR spectroscopy of the reaction solutions, as well as single-crystal X-ray diffraction (Figure 2).

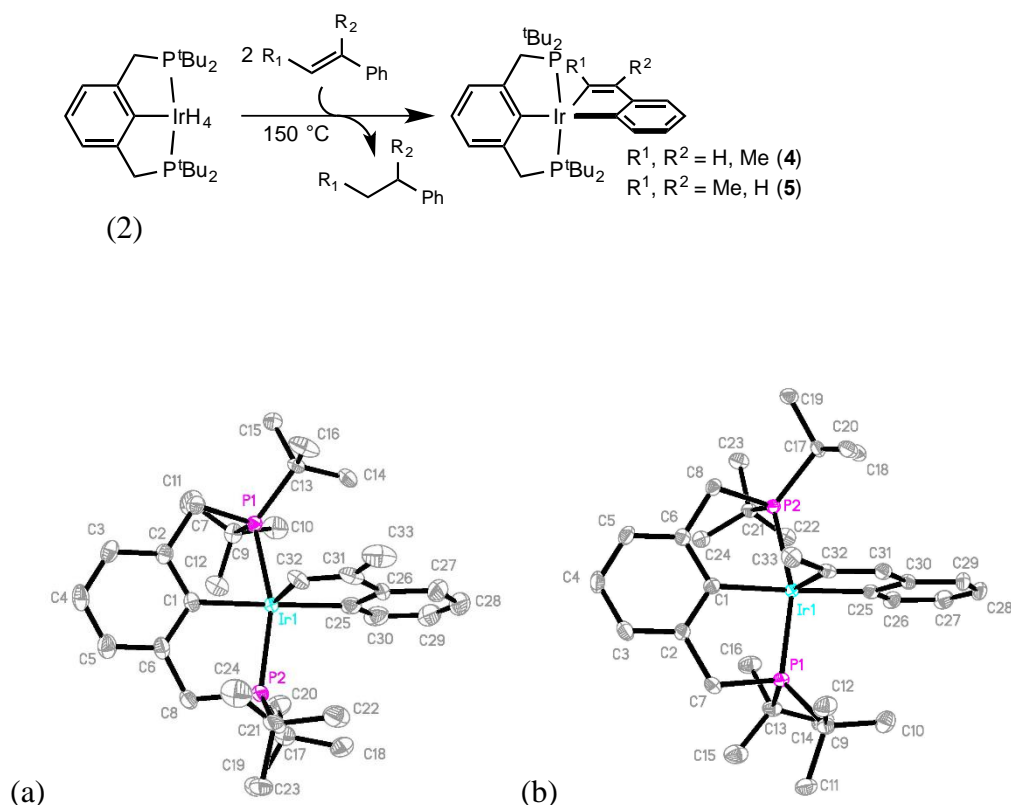


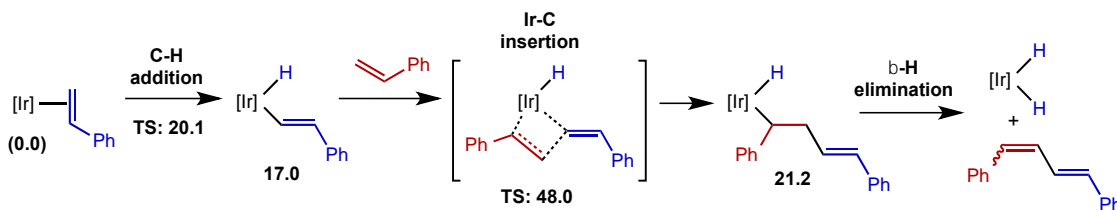
Figure 2. ORTEP representation of products of reaction with α -methyl and β -methyl styrene, **4** and **5** (50% probability ellipsoids).

Thus, it is seen, that both ($i^{\text{Pr}}\text{PCP}$)Ir and ($t^{\text{Bu}}\text{PCP}$)Ir fragments have a strong tendency to react with styrenes to form metallocene complexes. It appears likely that the greater steric bulk of the *t*-Bu groups mitigates the reactivity of the ($t^{\text{Bu}}\text{PCP}$) complexes, facilitating their isolation.

Double bond insertion mechanisms. A priori, several possible mechanisms for the tail-to-tail coupling reaction can be envisaged. In general, olefin dimerization probably proceeds most commonly via insertion of an olefin into a metal-carbon bond. The 14e fragments (R^{PCP})Ir have been well established to oxidatively add C-H bonds, including the addition of a *trans*- β -C-H bond of an α -olefin²² to give an observable 16e

product. Addition of the styrene *trans*- β -C-H bond, followed by 1,2-insertion of a second styrene molecule into the resulting Ir-C bond, and then β -H elimination (which is known to be facile for $(i\text{PrPCP})\text{Ir}(\text{alkyl})\text{H}$) would give the observed diphenylbutadiene (Scheme 5). Insertion of double bonds into Ir-C bonds, and metal-vinyl bonds more generally, however, is relatively rare.

Scheme 5. Dehydrogenative styrene coupling via C-H addition and insertion into the resulting Ir-C bond; calculated pathway with free energies shown (kcal/mol).

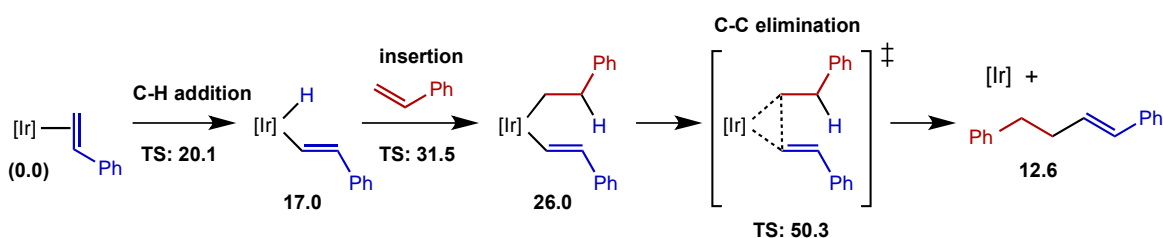


DFT calculations (see Computational Details) indicate that the kinetics of styrene β -vinyl C-H addition to $(i\text{PrPCP})\text{Ir}$ are facile (in accord with experimental results with C-H addition of TBE to $(t\text{BuPCP})\text{Ir}$),²² giving an oxidative addition product calculated to be 17.0 kcal/mol higher in free energy than the isomeric styrene π -adduct. (Free energies were calculated at 423 K (150 °C) and 34.7 atm styrene, which corresponds to a styrene concentration of 1.0 mol/L at 423 K.) Following C-H addition, however, addition of a second molecule of styrene is endoergic by 0.8 kcal/mol and insertion of its double bond into the Ir-vinyl bond is calculated to have a very high barrier, $\Delta G^\ddagger = 30.2$ kcal/mol. The TS for insertion is thus 48.0 kcal/mol above the resting state free energy, arguing against the likelihood of such a mechanism.

Insertion of olefins into Ir-H bonds is much more facile than insertion into Ir-C bonds. Styrene insertion into the Ir-H bond of the C-H addition product $(i\text{PrPCP})\text{Ir}(\text{H})(\text{CH}=\text{CHPh})$ yields $(i\text{PrPCP})\text{Ir}(\text{CH}_2\text{CH}_2\text{Ph})(\text{CH}=\text{CHPh})$ (Scheme 6); the styrene insertion TS and product are calculated to be 31.5 kcal/mol and 26.0 kcal/mol

above the π -styrene complex, respectively, presenting a substantial but not prohibitively high barrier. However, C-C elimination from this complex has a barrier of $\Delta G^\ddagger = 24.3$ kcal/mol and a prohibitively high-energy TS, 50.3 kcal/mol above the resting state. (Moreover, the monoene resulting from such a reaction would need to undergo subsequent dehydrogenation to give the observed diphenylbutadiene.) Our electronic structure calculations therefore argue strongly against this pathway.

Scheme 6. Styrene dimerization via C-H addition and insertion into Ir-H bond; calculated pathway with free energies shown (kcal/mol)



A “direct” coupling mechanism. We have previously demonstrated that 16e Ir(III) complexes such as $(^R\text{PCP})\text{IrH}_2$ ²³ and $(^R\text{PCP})\text{Ir}(\text{CCPh})(\text{H})$ ²⁴ will undergo addition of C-H bonds. Further, we have shown that C-C bond reductive elimination from complexes $(\text{PCP})\text{IrRR}'$ can be relatively favorable for C(sp²)-bound R groups.^{14,24} Thus, there is good precedent for what is perhaps the simplest and most direct pathway that might be envisioned for reaction 1, namely, a mechanism involving initial oxidative addition of a styrene *trans*- β vinylic C-H bond to $(^i\text{PrPCP})\text{Ir}$, followed by addition of the same bond of a second styrene molecule; subsequent loss of H₂ and then C-C elimination would afford the coupled product. The calculated free energy profile pertaining to this “direct” mechanism is shown in Figure 3.

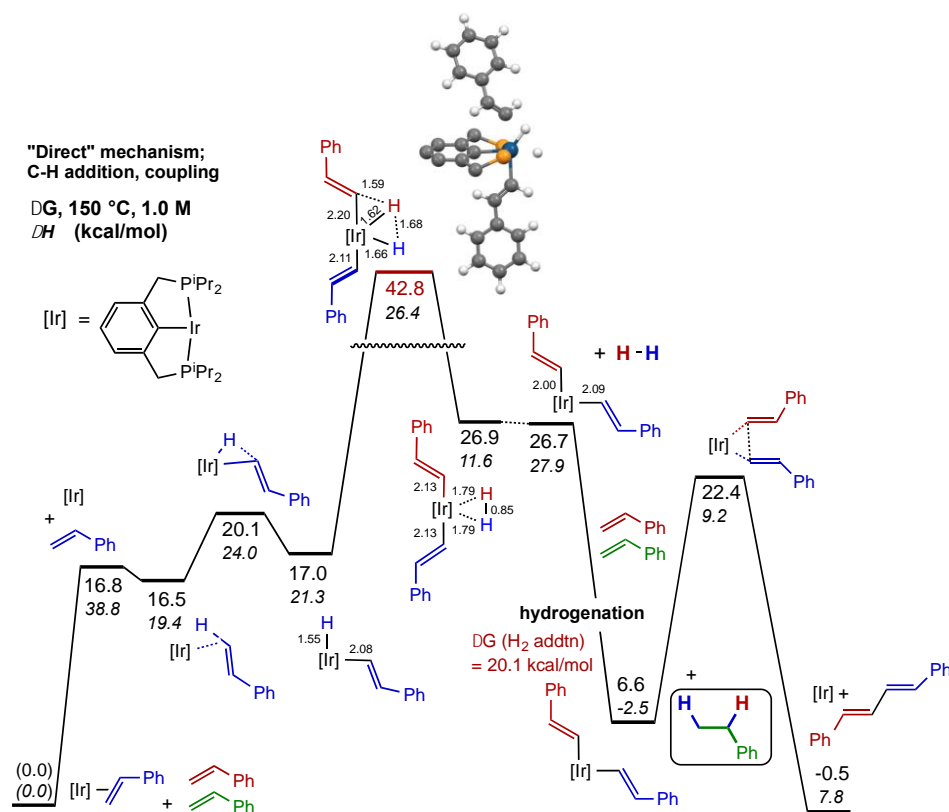


Figure 3. Calculated free energies and enthalpies (below, italic) for the tail-to-tail coupling of styrene at 150 °C (423 K) and 1.0 mol/L styrene, via a “direct” mechanism (addition of C-H bonds, followed by loss of H₂ and C-C reductive elimination). Ball-and-stick model of calculated highest-energy TS shown (ⁱPr groups and pincer-backbone H atoms omitted for clarity). Energy units are kcal/mol; bond lengths in Å.

The calculated TS for C-H oxidative addition connects a C-H bond σ-complex with the oxidative addition product, and has a favorable enthalpy 14.8 kcal/mol *below* that of the free 14e fragment plus styrene. (The calculated entropy of the oxidative addition TS, however, is 43 eu less than that of the free 14e fragment plus styrene; thus, the (unfavorable for addition) -TΔS term results in a free energy at 150 °C slightly higher than that of the free species). As noted above, the resulting vinyl hydride is 17.0 kcal/mol higher in free energy than the styrene β-adduct.

Subsequent C-H addition of a second molecule of styrene proceeds via a TS that is clearly Ir(V) in character (cf. Figure 3); the Ir-H distances (1.62 Å and 1.66 Å) are typical

of stable Ir hydrides, the C-H bond is essentially fully cleaved ($d_{\text{C-H}} = 1.59 \text{ \AA}$), and the H-H distance (1.68 \AA) is greater than that of even an “elongated” dihydrogen complex.²⁵ This second C-H addition step is calculated to have a free energy barrier of $\Delta G^\ddagger = 25.8 \text{ kcal/mol}$, arising from a very small activation enthalpy, $\Delta H^\ddagger = 5.1 \text{ kcal/mol}$, and a very unfavorable activation entropy, $\Delta S^\ddagger = -49 \text{ eu}$ ($-T\Delta S^\ddagger = 20.7 \text{ kcal/mol}$). Although the crowded TS has largely Ir(V) character, it does not lead to an Ir(V) intermediate, but rather to an Ir(III) dihydrogen complex ($d_{\text{H-H}} = 0.85 \text{ \AA}$). Periana has termed processes proceeding through such TSs without a net change in oxidation state as ‘Oxidative Hydrogen Migrations’.^{26,27}

The next step in this pathway would be loss of H_2 . The reverse of this step, the corresponding addition of H_2 , appears to have no barrier on the potential energy (E) surface, and we are therefore unable to locate a conventional TS for the process. We may estimate the enthalpic barrier to H_2 loss as equal to the (thermodynamic) enthalpy of the elimination process ($\Delta H = 16.3 \text{ kcal/mol}$). The entropy of the H_2 -loss “TS” will not have reached the full entropy of the resulting fragment and a free molecule of H_2 , but we can assume that the entropy of the H_2 -loss “TS” will be at least equal to the entropy of the reactant H_2 complex. If 20 eu is regarded as a reasonable upper limit to a gain in entropy in this TS, its free energy at 150°C is between 7.8 kcal/mol and 16.3 kcal/mol above the H_2 complex, or between 34.7 kcal/mol and 43.2 kcal/mol above the π -styrene complex (thus just barely allowing for the possibility that this loss of H_2 is rate-determining).

The free energy of the H_2 -loss products, $(i\text{PrPCP})\text{Ir}(\text{CH}=\text{CHPh})_2$ and H_2 , is 26.7 kcal/mol above the π -styrene complex. Addition of H_2 to an unsaturated species such as $(i\text{PrPCP})\text{Ir}(\text{styrene})$ and hydrogenation of another molecule of styrene (indicated in green

in Figure 3) is presumed to be very rapid on the overall time-scale of this reaction, and certainly more rapid than the back reaction with $(^{i\text{Pr}}\text{PCP})\text{Ir}(\text{CH}=\text{CHPh})_2$ which would be present in an extremely small concentration. The free energy of the resulting products, $(^{i\text{Pr}}\text{PCP})\text{Ir}(\text{CH}=\text{CHPh})_2$ plus PhEt, is 6.6 kcal/mol above that of $(^{i\text{Pr}}\text{PCP})\text{Ir}(\pi\text{-styrene})$ plus two molecules of free styrene. C-C reductive elimination from $(^{i\text{Pr}}\text{PCP})\text{Ir}(\text{CH}=\text{CHPh})_2$, with a calculated barrier $\Delta G^\ddagger = 15.8$ kcal/mol, affords the observed coupling product, *E,E*-1,4-diphenylbutadiene, plus the $(^{i\text{Pr}}\text{PCP})\text{Ir}$ fragment; this would rapidly bind styrene to give $(^{i\text{Pr}}\text{PCP})\text{Ir}(\pi\text{-styrene})$, with the free energy of addition, $\Delta G = -16.8$ kcal/mol, as indicated in the first step in the energy profile of Figure 3.

Thus, the calculated overall barrier to the pathway of Scheme 3 is 42.8 kcal/mol, assuming that C-H addition of the second styrene molecule is rate-determining; the TS for H₂ loss from $(^{i\text{Pr}}\text{PCP})\text{Ir}(\text{CHCH}_2\text{Ph})_2(\text{H}_2)$ could possess an even higher free energy, if the activation entropy for H₂ loss is in fact negligible. Although a predicted barrier of 40-45 kcal/mol is notably lower than the barriers of the insertion mechanisms discussed above, it remains significantly greater than the barrier that would be inferred from the very approximately determined rate of styrene coupling ($\sim 3 \times 10^{-4} \text{ s}^{-1}$), $\Delta G^\ddagger \sim 32$ kcal/mol. Nevertheless, we might not consider this calculated difference (ca. 10 kcal/mol) to be great enough to reject the “direct” mechanism solely on this basis, particularly since entropy plays such a large role in determining the barrier heights. As a rule, the entropy computed from electronic structure calculations is derived from the statistical mechanical expressions pertaining to an ideal gas and make use of the rigid rotor/harmonic oscillator approximations. A consequence of this treatment is that entropy changes computed for bimolecular reactions tend to be much larger than indicated by (solution phase)

experimental values. Note, however, that any major errors in the entropy calculations would largely apply as well to the insertion mechanisms proposed above and would thus not affect the calculated difference in the overall barriers to these reactions, all of which have a TS comprised of the (ⁱPrPCP)Ir unit and two molecules of styrene.

Arguing even more strongly against the mechanism of Figure 3 is a combination of experimental results and DFT calculations with 2,4,6-trimethylstyrene as the substrate. As discussed in the experimental section above, the presence of *o*-methyl groups completely inhibited the tail-to-tail dimerization reaction. Based only on cursory consideration of the structures shown in Figure 3, such a result would probably not be expected. Indeed, the DFT calculations predict that the overall barrier to tail-to-tail dimerization via the mechanism of Figure 3 is *lower* for 2,6-dimethylstyrene by 4.0 kcal/mol than for styrene. This result is attributable to the lower binding energy of the sterically hindered olefin in the π -olefin complex, not to any advantage conferred by the methyl groups to the TS

Metalloindene mechanism. Figure 4 shows our proposed pathway for the tail-to-tail coupling of styrene. Like the “direct” coupling mechanism of Figure 3, the initial in-cycle step is addition of a styrene β -vinyl C-H bond but, in this case, it is addition of the β -C-H bond that is *cis* to the phenyl group. This is kinetically and thermodynamically less favorable than addition *trans* to phenyl ($\Delta\Delta G^\ddagger = 4.4$ kcal/mol and $\Delta\Delta G = 0.5$ kcal/mol) but the overall predicted barrier ($\Delta G^\ddagger = 24.5$ kcal/mol) is certainly not prohibitive. The product is related to the product of addition of an *ortho*-C-H bond of biphenyl or phenanthrene. We have recently demonstrated (based on experimental and computational evidence), that such Ir(III) C-H addition products undergo a surprisingly facile secondary

addition of the ortho-C-H bond of the other phenyl group in the case of biphenyl (or the analogous C-H bond in the case of phenanthrene).^{15,16} In the present case also, the barrier to the analogous addition by the Ir(III) complex is calculated to be low: $\Delta G^\ddagger = 8.9$ kcal/mol and $\Delta H^\ddagger = 7.8$ kcal/mol. As in the case of the vinylic C-H bond addition to (*i*PrPCP)IrCH=CHPh(H) (Figure 3), the C-H addition to this Ir(III) hydride proceeds via a TS that is essentially Ir(V) in character, to give an Ir(III) dihydrogen complex (Figure 4).

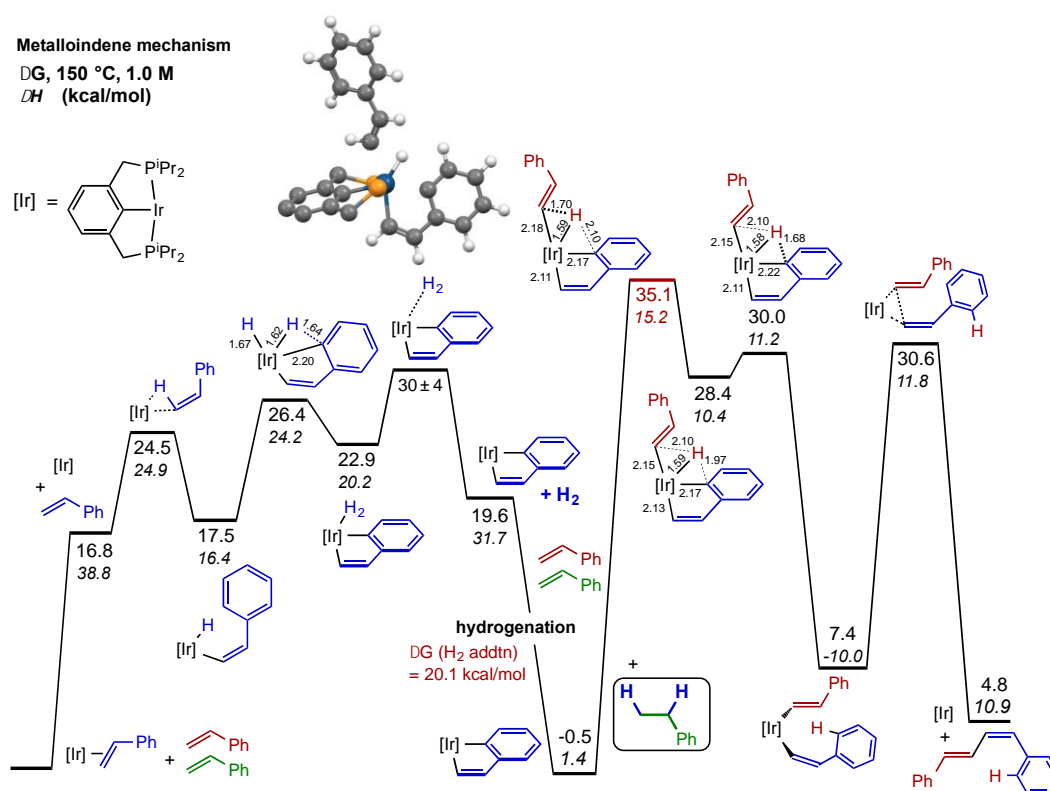


Figure 4. Calculated free energies and enthalpies (below, italic) for the tail-to-tail coupling of styrene at 150 °C via a cyclometalation (metalloindene) mechanism. Internuclear distances (Å) indicated for some key species. Ball-and-stick model of calculated highest-energy TS shown (*i*Pr groups and pincer-backbone H atoms omitted for clarity). Energy units are kcal/mol; bond lengths in Å.

The facile cyclometalation to give a metalloindene dihydrogen complex is followed by loss of H₂. As with loss of H₂ from (ⁱPrPCP)Ir(*trans*-CH=CHPh)₂(H₂), this reaction appears to have no barrier on the potential energy surface in the reverse direction, and we were unable to locate a true TS (first-order saddle point on the potential energy surface). Again, we assume that the enthalpic barrier to H₂ loss is at least equal to the (thermodynamic) enthalpy of H₂ loss, which is 11.5 kcal/mol in the present case, while the entropy of activation is larger than zero but no more than ca. 20 eu. This implies that the highest point on the free energy surface for H₂ loss from the metalloindene dihydride is ca. 26 - 34 kcal/mol above the π -styrene complex.

The H₂ evolved from dissociation from the metalloindene dihydrogen complex is presumably quickly consumed in the hydrogenation of styrene. The resulting products, metalloindene plus ethylbenzene, are calculated to have a free energy that is 0.5 kcal below that of the π -styrene complex plus an additional styrene molecule (indicated as green in Figure 4). This calculated free energy is consistent with the observation during catalysis of the π -styrene complex, the metalloindene complex of butadiene addition, and a third species, not isolated, believed to be the parent metalloindene

The Ir(III) metalloindene then undergoes addition of the *trans*- β C-H bond of another molecule of styrene. This reaction is calculated to proceed via a TS with a free energy that is 35.1 kcal/mol above the π -styrene complex, leading to the Ir(V) metalloindene complex (ⁱPrPCP)Ir(Ind)(CHCHPh)(H). Aryl-H reductive elimination from this species is closely related to the aforementioned cyclometalation of (ⁱPrPCP)Ir biphenyl or phenanthrenyl hydride complexes, and likewise has an extremely low kinetic barrier (ΔG^\ddagger

= 1.6 kcal/mol and $\Delta H^\ddagger = 0.8$ kcal/mol), leading to $(^{\text{iPr}}\text{PCP})\text{Ir}(\text{cis-CH=CHPh})(\text{trans-CH=CHPh})$.

The bis(vinyl) complex $(^{\text{iPr}}\text{PCP})\text{Ir}(\text{cis-CH=CHPh})(\text{trans-CH=CHPh})$ (shown in Figure 4) is very slightly higher in free energy than the *trans,trans* isomer (Figure 4). More significantly, the calculated barrier to C-C elimination from the *cis,trans* isomer is $\Delta G^\ddagger = 23.2$ kcal/mol, as compared with $\Delta G^\ddagger = 15.8$ kcal/mol for the *trans,trans* isomer, and the TS for C-C bond elimination is 8.2 kcal/mol higher for formation of the *cis,trans* isomer. This greater barrier to elimination can be explained in terms of steric factors, which we have previously demonstrated to play a key role in the kinetics of C-C elimination reactions.¹⁴ Elimination requires that the vinyl groups face each other, i.e. the vinyl groups must occupy approximately parallel planes which also approximately contain the P-Ir-P axis. For the *cis*-vinyl species, in particular, this orientation is sterically very unfavorable in the TS compared to the orientation held in the reactant, where the vinyl groups lie in the plane perpendicular to the P-Ir-P axis. Nevertheless, this TS is calculated to be 4.5 kcal/mol lower in free energy than the TS for C-H addition to the metallocene, which necessarily gives rise to a *cis*-vinyl unit and ultimately the *E,Z* isomeric product. As noted above, control experiments show that *cis-trans* isomerization of this species to give the observed *E,E* isomer is rapid relative to the overall reaction rate.

The overall barrier calculated for the metallocene mechanism of Figure 4 (35.1 kcal/mol) is thus significantly lower than that for the “direct” addition mechanism of Figure 3 (42.8 kcal/mol) and in very good agreement with the approximate experimentally determined barrier, $\Delta G^\ddagger \sim 32$ kcal/mol.

The energy profile of the proposed mechanism of Figure 4 suggests that addition of the phenyl *ortho*-C-H bond leads reversibly to the metalloindene dihydrogen complex. Assuming that the dihydrogen ligand can undergo rotation, this process would lead to H/D exchange. When the reaction is conducted with C₆H₅C₂D₅, we see extensive H/D scrambling at all sites on styrene, including the styrene *o*-C-H bond; exchange at the meta and para positions is presumably the result of intermolecular H-D scrambling. However, we have previously found that any substituent on an arene ring, even a methyl group, strongly inhibits C-H addition^{22,28,29}; the failure of the vinyl group to prevent H/D exchange at the *o*-C-H position is consistent with the reversible cyclometalation implied by Figure 4.

Intramolecular coupling. Consistent with the proposed mechanism of Figure 4, the tail-to-tail coupling is not observed for 2,4,6-trimethylstyrene, which cannot form a metalloindene intermediate (no *ortho* C-H bond). Instead, the *c4n*version of 2,4,6-trimethylstyrene to 4,6-dimethylindene occurs, representing an unusual example of dehydrogenative C(sp³)-C(sp²) coupling with an unfunctionalized hydrocarbon. For this reaction, a “direct” C-C coupling pathway is calculated (Figure 5). As in the case of the metalloindene mechanism shown in Figure 5, the coupling pathway begins with C-H addition to give the *cis*-2-arylvinyl iridium hydride (Figure 5). The bulkiness of the trimethylphenyl group slightly raises the barrier to vinylic C-H addition to the 14e (iPr⁴PCP)Ir fragment, but it raises the relative energy of the π -olefin complex (relative to free fragment plus olefin) even more. *Cis*- β -vinyl C-H addition of 2,4,6-trimethylstyrene is thus kinetically, as well as thermodynamically, slightly more favorable, relative to the

respective π -complex, than for the parent styrene (cf. Figure 4; $\Delta\Delta G^\ddagger = -2.1$ kcal/mol and $\Delta\Delta G = -1.5$ kcal/mol).

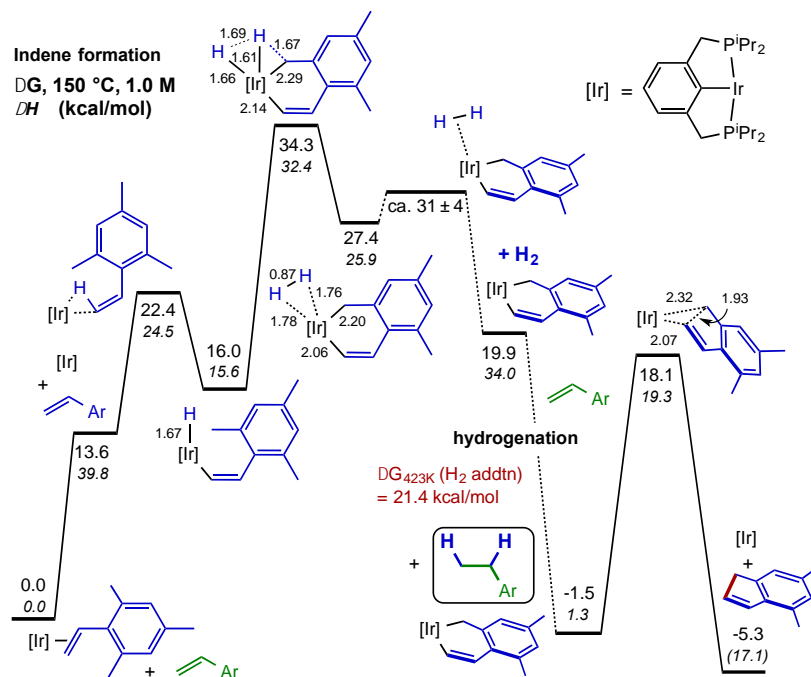


Figure 5. Calculated free energies and enthalpies (below, italic) for the ($i\text{Pr}_4\text{PCP}$)Ir-catalyzed conversion of 2,4,6-trimethylstyrene to 4,6-dimethylindene at 150 °C. Energy units are kcal/mol; bond lengths in Å.

Intramolecular addition of an ortho-methyl C-H bond then proceeds through an intermediate with significant Ir(V) character (cf. Figure 4). The length of the newly formed Ir-H bond in the TS (1.61 Å) is actually slightly less than that of the Ir-H bond in the preceding intermediate or that same bond in the TS (1.67 Å and 1.66 Å, respectively). The incipient Ir-C bond is nearly, but not quite fully, formed ($d_{\text{C-Ir}} = 2.29$ Å) and the C-H bond is fully or nearly fully cleaved ($d_{\text{C-H}} = 1.67$ Å). This addition of the methyl C-H bond (Figure 5; $\Delta G^\ddagger = 18.3$ kcal/mol and $\Delta G = 11.4$ kcal/mol) is much less favorable than addition of the aryl C-H bond to give a metalloindene (Figure 4; $\Delta G^\ddagger = 8.9$ kcal/mol and $\Delta G = 5.4$ kcal/mol); the TS has a free energy 34.3 kcal/mol above the π -complex

resting state. The product of this benzylic C-H activation is an Ir(III) dihydrogen complex ($d_{\text{H-H}} = 0.87 \text{ \AA}$).

The TS for loss of H_2 from the metallacycle dihydrogen complex could not be located but, again, in the reverse direction, addition of H_2 appears to be barrierless on the potential energy surface. This implies a TS enthalpy equal to that of the product and, again assuming that $\Delta S^\ddagger = 0$ to 20 eu, a free energy of the TS approximately 27-35 kcal/mol above the resting state. Following hydrogenation of an additional molecule of styrene ($\Delta G = -21.4 \text{ kcal/mol}$), C-C reductive elimination from this metallacyclic species is relatively facile ($\Delta G^\ddagger = 19.6 \text{ kcal/mol}$), releases indene and regenerates the 14e ($i\text{Pr}^4\text{PCP}$)Ir intermediate.

Hence, the overall barrier to the intramolecular dehydrogenative $\text{C}(\text{sp}^3)\text{-C}(\text{sp}^2)$ coupling is calculated to be 34.3 kcal/mol with formation of the metallacycle dihydrogen complex as the rate-determining step. Loss of dihydrogen from that complex appears to have a lower calculated barrier, although we cannot rule out that step as rate-determining, particularly in view of the error limits of the calculations. In either case, the calculations seem to be in very good agreement with the experimental rate of the cyclization which implies a barrier of ca. 32 kcal/mol.

Hetero-coupling with pentafluorophenylethylene. Like 2,4,6-trimethylstyrene, pentafluorophenylethylene ($\text{F}_5\text{-styrene}$) cannot form a metalloindene intermediate. Thus, it cannot undergo coupling via the proposed metalloindene mechanism and, accordingly, $\text{F}_5\text{-styrene}$ is found to undergo no detectable homocoupling. However, addition of the $\text{F}_5\text{-styrene}$ $\beta\text{-vinyl C-H}$ bond to the (unsubstituted) metalloindene complex is calculated to be *more* favorable (by 1.4 kcal/mol) than addition of the corresponding styrene bond,

which is the rate-determining step proposed in the mechanism of Fig. 4. Accordingly, a *p*-xylene- d_{10} solution with (i PrPCP)Ir(C₂H₄) catalyst (5 mM) and roughly equal concentrations of F₅-styrene (270 mM) and styrene (230 mM) reveals high selectivity for dehydrogenative heterocoupled product **1-F5**. Over the course of the first five hours at 150 °C, with 46% of total styrenes consumed, the ratio of **1-F5**:**1** remains constant at ca. 11:1 (Figure 6), implying that ΔG^\ddagger is 1.9 kcal/mol lower for addition of F₅-styrene than for styrene, in excellent agreement with the calculated value of 1.4 kcal/mol. It should also be noted that F₅-styrene is preferentially hydrogenated vs. styrene (ca. 4.5:1). Hence, the ratio of F₅-styrene:styrene decreases during the course of the reaction and styrene is present in greater concentration after 4 hours, although the rate of formation of heterocoupled product continues to greatly exceed that of homocoupled product. After 40 hours, quantitative conversion to dimer and hydrogenated products is observed; the observed (¹H NMR) concentrations of heterodimer and styrene homodimer are 161 mM and 19 mM, respectively, while concentrations of C₆F₅CH₂CH₃ and ethylbenzene are 124 mM and 28 mM, respectively.

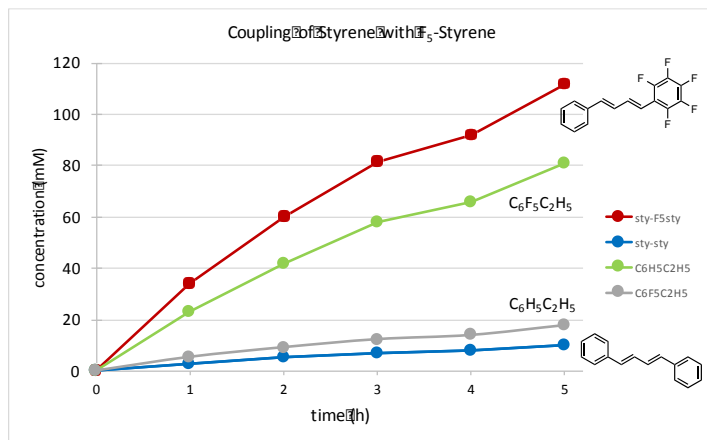


Figure 6. Products of (i PrPCP)Ir-catalyzed dehydrogenative coupling of styrene and F₅-styrene (150 °C).

The failure of F₅-styrene to undergo homodimerization, even under conditions where styrene homodimerization and cross-coupling occurs, argues strongly against the “direct” addition mechanism. With a common resting state (as is necessarily the case in a single-solution competition experiment of the type described above) the rate-determining step for homocoupling of F₅-styrene via the “direct addition” mechanism is calculated to be 2.8 kcal/mol lower in free energy than that for styrene. (It is 40.0 kcal/mol above the styrene σ -complex and two molecules of free F₅-styrene, but the nature of the actual resting state affects only this absolute value and not the relevant differences). This would imply that the rate of F₅-styrene homocoupling would be ca. 30-fold greater than that of styrene homocoupling, in direct contradiction with the failure to observe *any* F₅-styrene homocoupling product. The TS for F₅-styrene homocoupling in the “direct” mechanism is also calculated to be slightly lower in free energy than those for heterocoupling (40.6 kcal/mol above the styrene σ -complex for styrene C-H addition to the C-H adduct of F₅-styrene, and 41.4 kcal/mol for the converse heterocoupling TS; Figure 7), again in contradiction with experimental results. Since the expected error in computed free energies for such isodesmic comparisons are quite small, the implication that the “direct” addition” mechanism would strongly favor formation of the F₅-styrene homocoupling product (which is experimentally not observed) argues strongly against this being the operative mechanism.

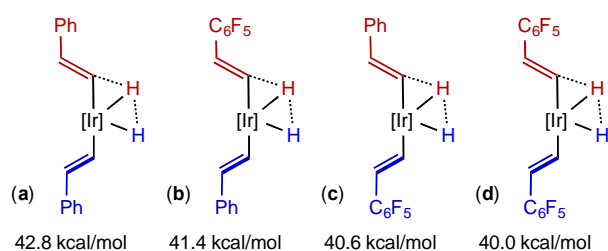


Figure 7. Schematic diagrams of the TSs for the calculated rate-determining step for dehydrogenative coupling, via the “direct” mechanism, for homocoupling of styrene (**a**); heterocoupling of F₅-styrene with styrene (**b**) and (**c**); homocoupling of F₅-styrene (**d**). Absolute energies are given relative to the (ⁱPrPCP)Ir(π -styrene) complex plus the corresponding two molecules of styrene. Note that relative energies are not affected by the choice of reference state.

Additionally, the greater rate of hydrogenation of F₅-styrene relative to that of styrene, noted above, suggests that F₅-styrene inserts more favorably into an Ir-H bond. This observation offers an additional argument against the insertion-based mechanisms of Scheme 3 (proceeding through insertion into an Ir-C bond) and particularly Scheme 4 (insertion into an Ir-H bond). In agreement with this inference, DFT calculations indicate that the TS for the rate-determining step for the mechanism of Scheme 4 (C-C elimination) is 7.8 kcal/mol lower in free energy for the homocoupling of F₅-styrene than for styrene, and 2.8 kcal/mol lower than for heterocoupling of F₅-styrene and styrene. Likewise, for the mechanism of Scheme 3, the TS of the rate-determining step (insertion into the Ir-C bond) is 5.7 kcal/mol lower in free energy for homocoupling of F₅-styrene than for styrene, and 3.8 kcal/mol lower than for heterocoupling.

Conclusions

Dehydrogenative coupling of unactivated C-H bonds (intermolecular vinyl-vinyl, intramolecular vinyl-benzyl) is found to be catalyzed by precursors of the (ⁱPrPCP)Ir fragment. The reactions proceed via C-H activation to (ⁱPrPCP)Ir(I), followed by a second C-H activation by the resulting (ⁱPrPCP)Ir(III) product. The C-H additions to Ir(III) occur via TSs that are strongly Ir(V) in character although the reactions generally do not lead to an Ir(V) product, but rather to the formation of a new Ir(III) complex.

For the intermolecular dehydrogenative vinyl-vinyl coupling reaction, addition of a vinylic C-H bond to Ir(I), followed by addition of a second vinylic C-H bond to the resulting Ir(III) vinyl hydride, loss of H₂, and then C-C elimination would comprise what we refer to as a “direct” pathway. Instead, however, the Ir(III) vinyl hydride complex undergoes addition of a styrenyl ortho C-H bond to give an Ir(III) metallocene plus H₂. The activation enthalpy of this reaction (7.8 kcal/mol) is slightly greater than the intermolecular addition (5.1 kcal/mol), but the entropic penalty is much less. Subsequent, intermolecular, vinyl C-H addition to the Ir(III) metallocene has a much *greater* calculated barrier ($\Delta G^\ddagger = 35.6$ kcal/mol) than addition to the Ir(III) vinyl hydride (25.8 kcal/mol) in the “direct” mechanism. However, the metallocene pathway is driven by addition of the dihydrogen produced to another molecule of olefin, prior to the second vinylic C-H addition; this significantly lowers the free energy of the system (by 20 kcal/mol), which would lead to a commensurately much greater concentration of Ir(III) metallocene, thus favoring occurrence of the subsequent intermolecular reaction. In contrast, in the case of the “direct” mechanism, loss of H₂ and hydrogenation of styrene does not occur until after the entropically unfavorable second addition of a vinyl C-H bond, and thus cannot provide any driving force.

As we have shown previously, elimination from (pincer)IrRR' complexes can be relatively facile when R and R' are sp²-C-bound fragments.¹⁴ Accordingly in all mechanisms investigated, C-C elimination is not calculated to be rate-determining.

Although in most of this work the H₂ by-product of the reaction is consumed by an additional molecule of styrene, it is found that other olefins can play the same role as

hydrogen-acceptor; this allows, in principle, complete conversion of the styrene to dehydrogenatively coupled dimer.

In accord with the proposed metalloindene mechanism, styrenes that lack a C-H bond ortho to the vinyl group are found not to undergo tail-to-tail coupling. In contrast, the DFT calculations predict that the ortho-substituents would not adversely favor coupling via the “direct” mechanism. In the case of 2,4,6-trimethylstyrene, the product of vinylic C-H addition to (ⁱPrPCP)Ir(I) undergoes cyclometalation by subsequent C-H addition of an ortho-methyl C-H bond. This reaction is enthalpically much less favorable than any of the C(sp²) C-H bond additions considered above, but due to the low entropy penalty the calculated barrier is high although not prohibitive. Subsequent loss of H₂ and then C-C elimination to give indene are calculated to proceed relatively rapidly. The calculated overall barrier, corresponding to the cyclometalation TS, is 34.3 kcal/mol above the π -complex resting state, in good agreement with the observed rates.

The absence of an ortho-C-H bond prevents homocoupling of C₆F₅CH=CH₂ via the metalloindene mechanism; this is fully confirmed experimentally. However, although C₆F₅CH=CH₂ cannot form a metalloindene complex, the fluorination of the aryl ring is calculated to favor β -vinylic C-H bond addition to a metalloindene complex. Accordingly, although it undergoes no homocoupling, the dehydrogenative heterocoupling of C₆F₅CH=CH₂ and styrene is much more favorable than styrene homocoupling. This is well explained by the metalloindene mechanism, and the calculations even capture fairly well the ratio of hetero- to homocoupling. The calculations predict that if any of the other mechanisms investigated were operative, the homocoupling of F₅-styrene would be more favorable than either heterocoupling or

styrene homocoupling. We believe that the principles elucidated in this work will be applicable to the development of more general dehydrogenative coupling reactions. Most obviously, the metalloidene mechanism should be viable for the coupling of styrenes and their derivatives with other C-H bonds (including both alkenes and non-alkenes). While a “direct” mechanism was found to not be operative in the intermolecular case studied in this work, it was found to operate for intramolecular coupling involving sp^3 C-H bonds. Even for the intermolecular case, the barrier to the direct mechanism was not calculated to be extremely high. Thus such a mechanism, or more generally sequential C-H activations and C-C coupling, may well be viable with closely related catalysts. In that context, efforts in our lab are underway to determine the factors favoring such pathways.

References

- (1) Le Bras, J.; Muzart, J. *Chem. Rev.* **2011**, *111*, 1170-1214.
- (2) Wu, Y.; Wang, J.; Mao, F.; Kwong, F. Y. *Chemistry – An Asian Journal* **2014**, *9*, 26-47.
- (3) Kitamura, T.; Fujiwara, Y. In *From C-H to C-C Bonds: Cross-Dehydrogenative-Coupling*; Li, C.-J., Ed.; The Royal Society of Chemistry: 2015, p 33-54.
- (4) Shang, X.; Liu, Z.-Q. *Chem. Soc. Rev.* **2013**, *42*, 3253-3260.
- (5) Yatsimirsky, A. K.; Ryabov, A. D.; Berezin, I. V. *J. Mol. Cat.* **1978**, *4*, 151-162.
- (6) Hwang, Y.-A.; Kim, D.-H.; Baek, D.-J. *J. Korean Chem. Soc.* **2006**, *50*, 369-373.
- (7) Sun, Q.; Cai, L.; Ding, Y.; Xie, L.; Zhang, C.; Tan, Q.; Xu, W. *Angew. Chem., Intl. Ed.* **2015**, *54*, 4549-4552.
- (8) Wen, Y.; Xie, J.; Deng, C.; Wu, Y. *Synlett* **2015**, *26*, 1755-1758.
- (9) Baratta, W.; Ballico, M.; Del Zotto, A.; Zangrando, E.; Rigo, P. *Chem.-Eur. J.* **2007**, *13*, 6701-6709.
- (10) Polukeev, A. V.; Marcos, R.; Ahlquist, M. S. G.; Wendt, O. F. *Chem. Sci.* **2015**, *6*, 2060-2067.
- (11) Nie, S.-z.; Sun, X.; Wei, W.-t.; Zhang, X.-j.; Yan, M.; Xiao, J.-l. *Organic Letters* **2013**, *15*, 2394-2397.
- (12) Zhou, T.; Li, L.; Li, B.; Song, H.; Wang, B. *Organic Letters* **2015**, *17*, 4204-4207.
- (13) Itoh, M.; Hirano, K.; Satoh, T.; Shibata, Y.; Tanaka, K.; Miura, M. *J. Org. Chem.* **2013**, *78*, 1365-1370.
- (14) Ghosh, R.; Emge, T. J.; Krogh-Jespersen, K.; Goldman, A. S. *J. Am. Chem. Soc.* **2008**, *130*, 11317-11327.
- (15) Wilklow-Marnell, M.; Brennessel, W. W.; Jones, W. D. *Polyhedron* **2016**, *116*, 38-46.
- (16) Laviska, D. A.; Zhou, T.; Kumar, A.; Emge, T. J.; Krogh-Jespersen, K.; Goldman, A. S. *Organometallics* **2016**, *35*, 1613-1623.
- (17) Laviska, D. A.; Guan, C.; Emge, T. J.; Wilklow-Marnell, M.; Brennessel, W. W.; Jones, W. D.; Krogh-Jespersen, K.; Goldman, A. S. *Dalton Trans.* **2014**, *43*, 16354-16365.
- (18) Laviska, D. A. Ph.D. thesis, Rutgers University, 2013.
- (19) Kumar, A.; Zhou, T.; Emge, T. J.; Mironov, O.; Saxton, R. J.; Krogh-Jespersen, K.; Goldman, A. S. *J. Am. Chem. Soc.* **2015**, *137*, 9894-9911.
- (20) Sandoval, A.; Zechmeister, L. *J. Am. Chem. Soc.* **1947**, *69*, 553-557.
- (21) Laviska, D. A.; Wang, D. Y.; Krogh-Jespersen, K.; Goldman, A. S. *Abstracts of Papers, 244th ACS National Meeting & Exposition, Philadelphia, PA, United States, August 19-23, 2012* 2012 INOR-1223
- (22) Kanzelberger, M.; Singh, B.; Czerw, M.; Krogh-Jespersen, K.; Goldman, A. S. *J. Am. Chem. Soc.* **2000**, *122*, 11017-11018.
- (23) Krogh-Jespersen, K.; Czerw, M.; Summa, N.; Renkema, K. B.; Achord, P. D.; Goldman, A. S. *J. Am. Chem. Soc.* **2002**, *124*, 11404-11416.
- (24) Ghosh, R.; Zhang, X.; Achord, P.; Emge, T. J.; Krogh-Jespersen, K.; Goldman, A. S. *J. Am. Chem. Soc.* **2007**, *129*, 853-866.
- (25) Heinekey, D. M.; Lledos, A.; Lluch, J. M. *Chem. Soc. Rev.* **2004**, *33*, 175-182.
- (26) Oxgaard, J.; Muller, R. P.; Goddard, W. A.; Periana, R. A. *J. Am. Chem. Soc.* **2004**, *126*, 352-363.
- (27) Oxgaard, J.; Periana, R. A.; Goddard, W. A., III *J. Am. Chem. Soc.* **2004**, *126*, 11658-11665.
- (28) Krogh-Jespersen, K.; Czerw, M.; Zhu, K.; Singh, B.; Kanzelberger, M.; Darji, N.; Achord, P. D.; Renkema, K. B.; Goldman, A. S. *J. Am. Chem. Soc.* **2002**, *124*, 10797-10809.
- (29) Zhang, X.; Kanzelberger, M.; Emge, T. J.; Goldman, A. S. *J. Am. Chem. Soc.* **2004**, *126*, 13192-13193.

Computational details

All electronic structure calculations employed the DFT method.¹ Data presented in the text result from calculations which employed the M06-L exchange-correlation functional.² We did also examine two additional functionals, M06³ and PBE⁴, in selected calculations; the results obtained with these functionals fully support the mechanisms we propose based on calculations with the M06-L functional. For Ir, we applied the Hay-Wadt relativistic effective (small) core potential⁵ and the LANL2TZ basis set^{6a} augmented by a set of diffuse d-type functions (exponent=0.07645)^{6b}; all other atoms (P, F, C, and H) were assigned 6-311G(d,p) basis sets.⁷

Geometries were calculated for stationary points along the reaction paths by standard optimization procedures.⁸ Normal mode analysis was performed to further verify the nature of a particular stationary point (minimum or transition state). The resulting set of vibrational frequencies was employed (without scaling) to determine zero-point energy corrections. Enthalpies (ΔH , ΔH^\ddagger) and Gibbs' free energies (ΔG , ΔG^\ddagger ; $T = 298.15$ K, $P = 1$ atm) were subsequently obtained from the potential energies using standard statistical mechanical expressions.⁹ For better comparisons with measured energetics, we further corrected the Gibbs's free energies so they corresponded to a standard state of 1 M for all species and $T = 423$ K (the temperature applied in the experiments reported here).⁹ In order to enhance computational stability and accuracy¹⁰ in geometry optimizations and normal mode calculations, we used increased atomic grid sizes (grid=ultrafine option).¹¹ All calculations made use of the Gaussian 09 electronic structure program.¹²

Reaction mechanisms and energy tables.

Figure S1. Ir(V) reaction mechanism with free energies (kcal/mol) for styrene coupling catalyzed by ($i\text{Pr}^4\text{PCP}$)Ir.

functional:M06L

basis set:6-311G(d,p)+Lanl2TZ

Free energy diagram:G

standard condition: 1M

reaction temperature: 423K

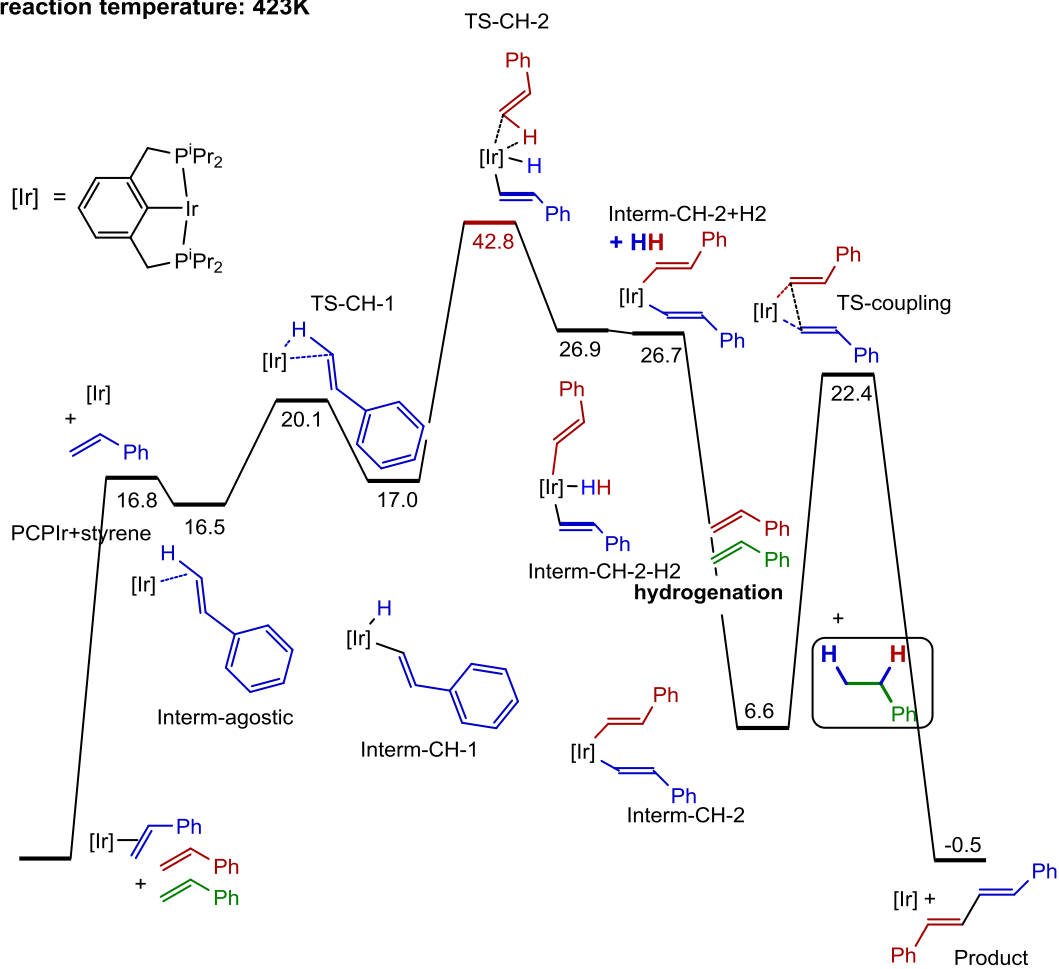


Table S1. Ir(V) reaction mechanism for styrene coupling by (ⁱPr⁴PCP)Ir: Energetics.^a

Species	E	H	G	S	ΔG(corrected)
Resting_state	0.0	0.0	0.0	0.0	0.0
PCPIr+styrene	40.0	38.8	24.6	47.5	16.8
Interm-agostic	19.9	19.4	18.7	2.3	16.5
TS-CH-1	26.9	24.0	22.6	4.7	20.1
Interm-CH-1	23.4	21.3	19.6	5.6	17.0
TS-CH-2	29.5	26.4	40.6	-47.8	42.8
TS-CH-2_H5_F5	23.8	38.3	38.3	-49	40.6
TS-CH-2_F5_H5	28.2	25.0	39.3	-48	41.4
TS-CH-2_F5_F5	25.9	22.8	37.6	-49	40.0
Interm-CH-2-H2	13.3	11.6	25.0	-45.1	26.9
Interm-CH-2+H2	33.4	27.9	29.7	-6.1	26.7
Interm-CH-2	-3.9	-2.5	7.9	-34.9	6.6
TS-coupling	7.6	9.2	22.5	-44.7	22.4
Product	6.0	7.8	5.9	6.2	-0.5

^a Units are kcal/mol for ΔE, ΔH, and ΔG; units are cal/(deg.mol) for ΔS. The standard state

for concentrations is 1 M for each species participating in the reaction; T = 298.15 K.

Figure S2. Vinylidene reaction mechanism with free energies (kcal/mol) for styrene coupling catalyzed by ($i\text{Pr}^4\text{PCP}$)Ir.

functional: M06L

basis set: 6-311G(d,p)+LanI2TZ

Free energy diagram: G

standard condition: 1M

reaction temperature: 423K

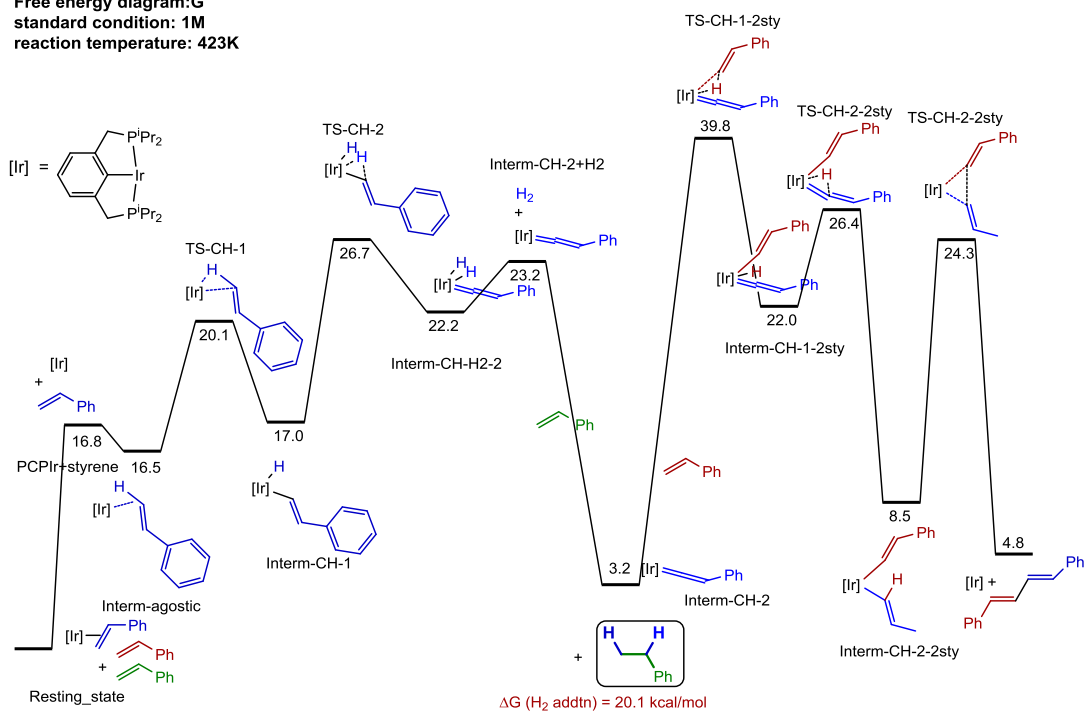


Table S2. Vinylidene reaction mechanism for styrene coupling catalyzed by (ⁱPr⁴PCP)Ir: Energetics.^a

Species	E	H	G	S	ΔG(corrected)
Resting_state	0.0	0.0	0.0	0.0	0.0
PCPIr+styrene	40.0	38.8	24.6	47.5	16.8
Interm-agostic	19.9	19.4	18.7	2.3	16.5
TS-CH-1	26.9	24.0	22.6	4.7	20.1
Interm-CH-1	23.4	21.3	19.6	5.6	17.0
TS-CH-2	33.7	28.6	28.6	-0.2	26.7
Interm-CH-H2-2	29.0	24.8	24.3	1.6	22.2
Interm-CH-2+H2	44.8	38.3	29.0	31.1	23.2
Interm-CH-2	7.5	8.0	7.2	2.4	3.2
TS-C-C-coupling	7.6	9.2	22.5	-44.7	24.3
TS-CH-1-2sty	25.3	24.0	37.8	-46.2	39.8
TS-CH-2-2sty	11.7	10.6	24.4	-46.3	26.4
Interm-CH-1-2sty	8.1	8.0	20.6	-42.1	22.0
Interm-CH-2-2sty	-3.9	-2.5	7.9	-34.9	8.5

^a Units are kcal/mol for ΔE, ΔH, and ΔG; units are cal/(deg.mol) for ΔS. The standard state

for concentrations is 1 M for each species participating in the reaction; T = 298.15 K.

Figure S3. Ir-C bond insertion reaction mechanism with free energies (kcal/mol) for styrene coupling catalyzed by $i\text{Pr}^4\text{PCPIr}$.

functional:M06L

basis set:6-311G(d,p)+LanI2TZ

Free energy diagram:G

standard condition: 1M

reaction temperature: 423K

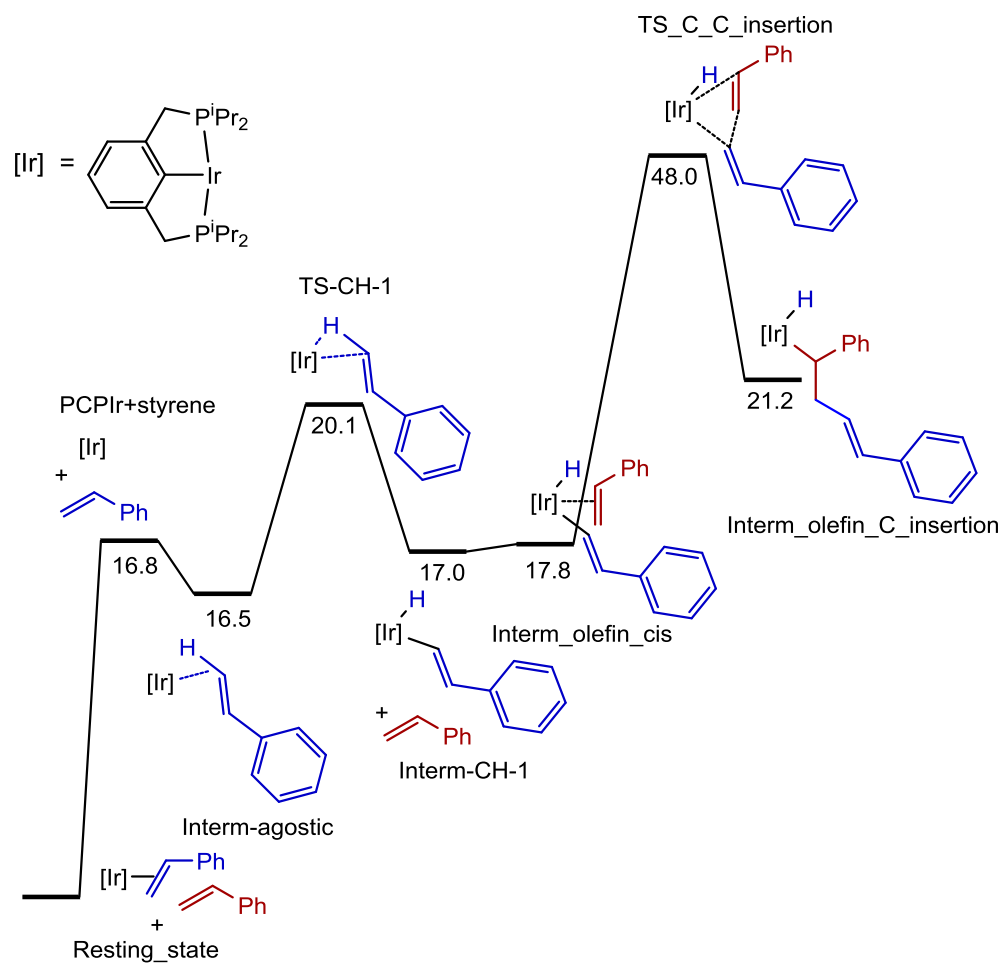


Table S3. Ir-C bond insertion reaction mechanism for styrene coupling catalyzed by (*i*Pr⁴PCP)Ir: Energetics.^a

Species	E	H	G	S	$\Delta G(\text{corrected})$
Resting_state	0.0	0.0	0.0	0.0	0.0
PCPIr+styrene	40.0	38.8	24.6	47.5	16.8
Interm-agostic	19.9	19.4	18.7	2.3	16.5
TS-CH-1	26.9	24.0	22.6	4.7	20.1
Interm-CH-1	23.4	21.3	19.6	5.6	17.0
Interm_olefin_cis	-2.3	-2.1	14.6	-55.9	17.8
TS_C_C_insertion	30.1	29.4	45.2	-52.9	48.0
Interm_olefin_C_insertion	1.8	2.3	18.3	-53.6	21.2

^a Units are kcal/mol for ΔE , ΔH , and ΔG ; units are cal/(deg.mol) for ΔS . The standard state

for concentrations is 1 M for each species participating in the reaction; T = 298.15 K.

Figure S4. Ir-H bond insertion reaction mechanism with free energies (kcal/mol) for styrene coupling catalyzed by ($i^{\text{Pr}}_4\text{PCP}$)Ir..

functional:M06L

basis set:6-311G(d,p)+Lanl2TZ

Free energy diagram:G

standard condition: 1M

reaction temperature: 423K

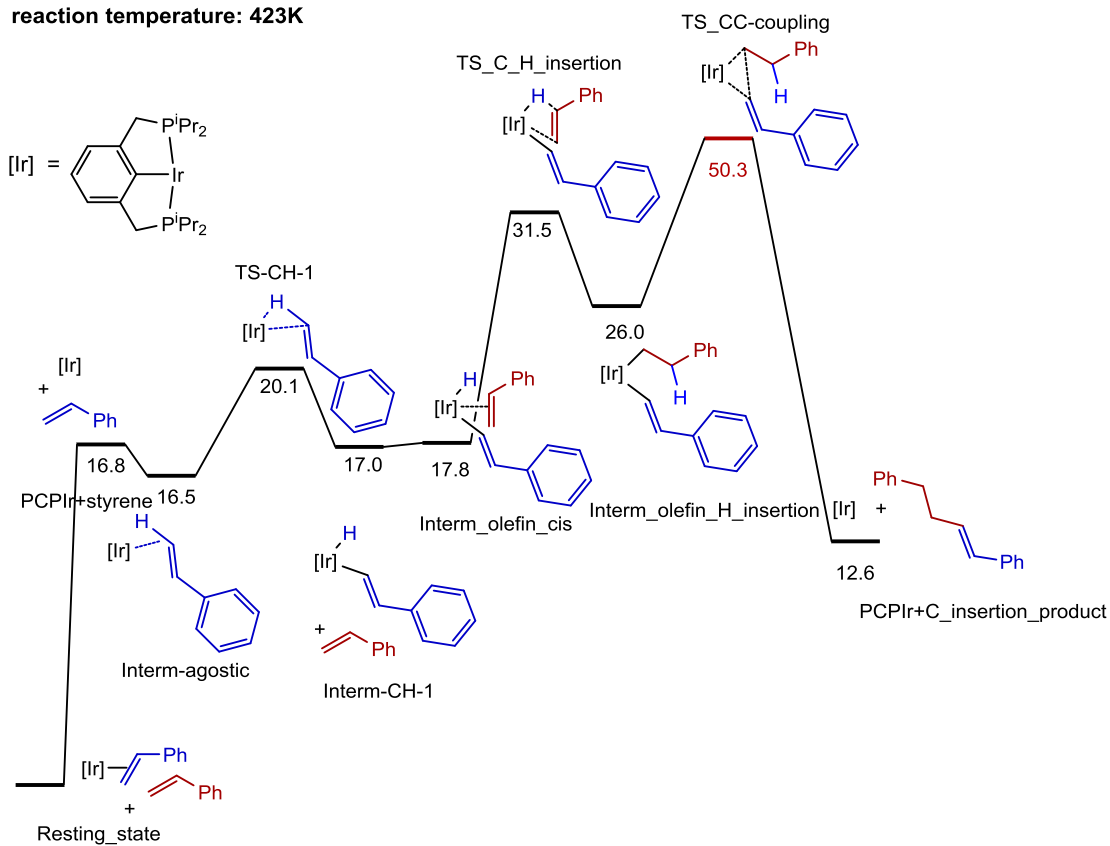


Table S4. Ir-H bond insertion reaction mechanism for styrene coupling catalyzed by (ⁱPr₄PCP)Ir: Energetics.^a

Species	E	H	G	S	ΔG(corrected)
Resting_state	0.0	0.0	0.0	0.0	0.0
PCPIr+styrene	40.0	38.8	24.6	47.5	16.8
Interm-agostic	19.9	19.4	18.7	2.3	16.5
TS-CH-1	26.9	24.0	22.6	4.7	20.1
Interm-CH-1	23.4	21.3	19.6	5.6	17.0
Interm_olefin_cis	-2.3	-2.1	14.6	-55.9	17.8
TS_C_H_insertion	13.4	12.3	28.5	-54.5	31.5
Interm_olefin_H_insertion	9.7	11.2	24.3	-43.9	26.0
TS_CC-coupling	31.4	33.1	47.9	-49.8	50.3
PCPIr+C_insertion_product	18.0	19.7	17.4	7.9	12.6

^a Units are kcal/mol for ΔE, ΔH, and ΔG; units are cal/(deg.mol) for ΔS. The standard state

for concentrations is 1 M for each species participating in the reaction; T = 298.15 K.

Figure S5. MetalloIndene reaction mechanism with free energies (kcal/mol) for styrene coupling catalyzed by (ⁱPr⁴PCP)Ir.

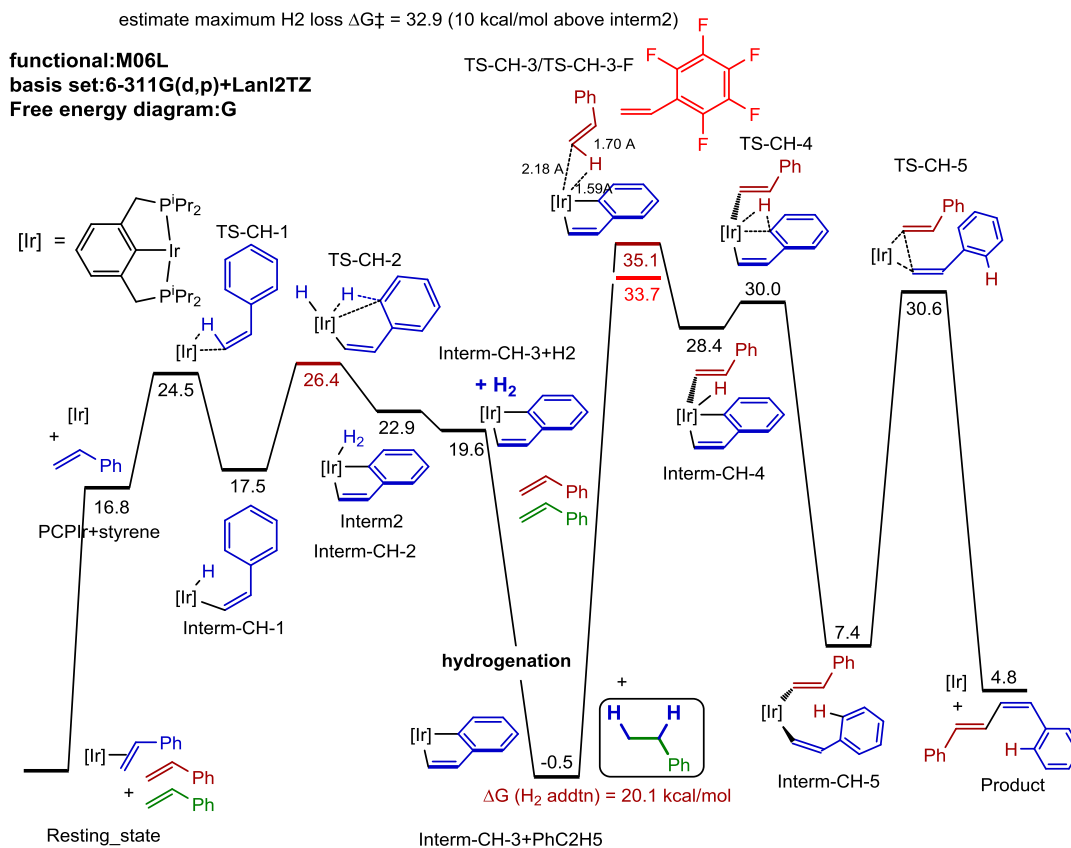


Table S5. Metalloindene reaction mechanism for styrene coupling catalyzed by (*i*Pr⁴PCP)Ir: Energetics.^a

Species	E	H	G	S	$\Delta G(\text{corrected})$
Resting_state	0.0	0.0	0.0	0.0	0.0
PCPIr+styrene	40.0	38.8	24.6	47.5	16.8
Interm-agostic	19.9	19.4	18.7	2.3	16.5
TS-CH-1	27.9	24.9	26.0	-3.6	24.5
Interm-CH-1	18.7	16.4	18.6	-7.1	17.5
TS-CH-2	29.3	24.2	27.1	-9.6	26.4
Interm-CH-2	23.4	20.2	23.5	-11.0	22.9
Interm-CH-3+H ₂	38.7	31.7	24.5	24.2	19.6
Interm-CH-3+PhC ₂ H ₅ -styrene	1.5	1.4	2.7	-4.5	-0.5
TS-CH-3	15.6	15.2	31.9	-56.1	35.1
TS-CH-3-F	12.9	12.5	30.1	-59.0	33.7
TS-CH-4	12.0	11.2	27.1	-53.3	30.0
TS-CH-5	10.3	11.8	27.7	-53.6	30.6
Interm-CH-4	10.0	10.4	25.7	-51.3	28.4
Interm-CH-5	-11.5	-10.0	5.0	-50.0	7.4
Product	8.9	10.9	9.3	5.6	4.8

^a Units are kcal/mol for ΔE , ΔH , and ΔG ; units are cal/(deg.mol) for ΔS . The standard state for concentrations is 1 M for each species participating in the reaction; T = 298.15 K.

Figure S6. Metalloindene reaction mechanism with free energies (kcal/mol) 2,4,6-trimethyl-styrene coupling vs cyclization catalyzed by (ⁱPr₄PCP)Ir.

functional:M06L

basis set:6-311G(d,p)+Lanl2TZ

Free energy diagram:G

standard condition: 1M

reaction temperature: 423K

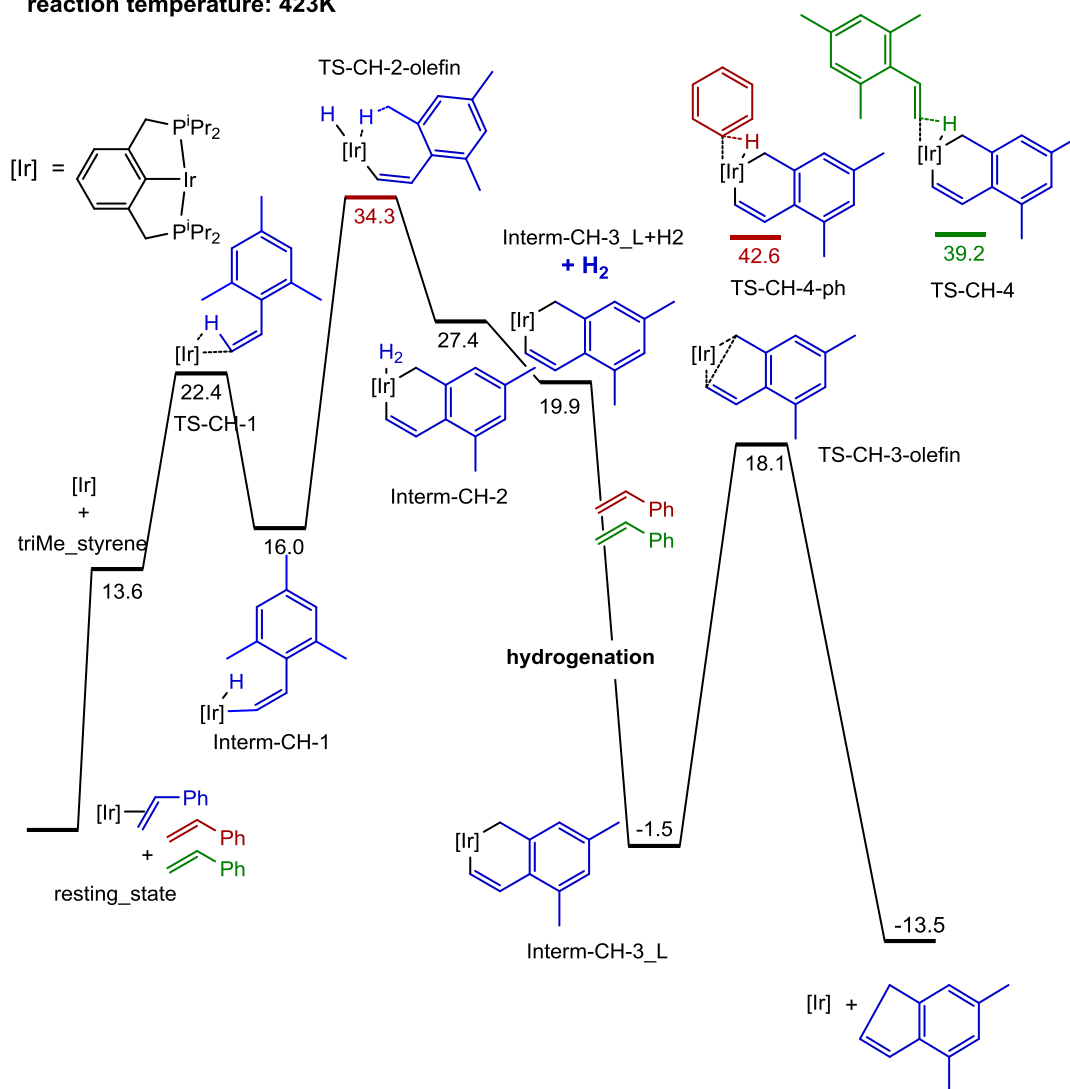


Table S6. Metalloindene reaction mechanism for 2,4,6-trimethyl-styrene coupling vs cyclization catalyzed by (ⁱPr⁴PCP)Ir: Energetics.^a

Species	E	H	G	S	ΔG(corrected)
resting_state	0.0	0.0	0.0	0.0	0.0
Ir+styrene	41.3	39.8	22.7	57.5	13.6
TS-CH-1	28.0	24.5	24.4	0.5	22.4
Interm-CH-1	18.7	15.6	17.2	-5.5	16.0
TS-CH-2-olefin	37.3	32.4	35.1	-8.9	34.3
Interm-CH-2	29.3	25.9	28.2	-8.0	27.4
Interm-CH-3_L+H2	41.4	34.0	25.4	28.9	19.9
Interm-CH-3_L	1.7	1.3	2.0	-2.3	-1.5
TS-CH-3-olefin	20.4	19.3	21.1	-6.0	18.1
TS-CH-4	18.8	18.4	35.7	-58.1	39.2
TS-CH-5	9.7	10.9	27.8	-56.6	31.1
Interm-CH-3	-4.0	-2.1	13.7	-53.2	16.6
Interm-CH-4	-7.0	-5.2	9.8	-50.3	12.3
TS-CH-4-ph	25.0	24.0	39.8	-52.8	42.6
TS-CH-5-ph	14.4	15.4	30.8	-52.0	33.6
Interm-CH-3-ph	24.5	25.0	42.6	-58.8	46.1
Interm-CH-4-Ph	-1.5	0.6	16.5	-53.3	19.4

^a Units are kcal/mol for ΔE, ΔH, and ΔG; units are cal/(deg.mol) for ΔS. The standard state

for concentrations is 1 M for each species participating in the reaction; T = 298.15 K

Computational Section References

1. Koch, W.; Holthausen, M. C. *A Chemist's Guide to Density Functional Theory*; Wiley: New York, 2001.
2. Zhao, Y.; Truhlar, D. G. *J. Chem. Phys.* **2006**, *125*, 194101:1-18.
3. Zhao, Y.; Truhlar, D. G. *Theo. Chem. Acc.* **2008**, *120*, 215–241.
4. Perdew, J. P.; Burke, K.; Ernzerhof, M. *Phys. Rev. Lett.* **1996**, *77*, 3865.
5. Hay, P. J.; Wadt, W. R. *J. Chem. Phys.* **1985**, *82*, 299–310.
6. (a) Roy, L. E., Hay, P. J.; Martin, R. L. *J. Chem. Theory Comput.* **2008**, *4*, 1029-1031.
(b) Value obtained as one-half times the exponent of the outermost d-type function in the LANL2TZ basis set for Ir.
7. (a) Ditchfield, R.; Hehre, W. J.; Pople, J. A. *J. Chem. Phys.* **1971**, *54*, 724-728. (b) Hariharan, P. C.; Pople, J. A. *Molecular Physics* **1974**, *27*, 209-214. (c) Raghavachari, K.; Binkley, J. S.; Seeger, R.; Pople, J. A. *J. Chem. Phys.* **1980**, *72*, 650-654. (d) McLean, A. D.; Chandler, G. S. *J. Chem. Phys.* **1980**, *72*, 5639-5648.
8. Hratchian, H. P.; Schlegel, H. B. in *Theory and Applications of Computational Chemistry: The First 40 Years*, Dykstra, C. E.; Frenking, G.; Kim, K. S.; Scuseria, G., Ed; Elsevier: Amsterdam, 2005, pp. 195-249.
9. McQuarrie, D. A. *Statistical Thermodynamics*; Harper and Row: New York, 1973.
10. Wheeler, S. E.; Houk, K. N. *J. Chem. Theory Comput.* **2010**, *6*, 395–404.
11. Frisch, A.; Frisch, M. J.; Clemente, F. R.; Trucks, G. W. *Gaussian 09 User's Reference*, 147.
12. Frisch, M. J.; et al., Gaussian 09, Revision D.01; Gaussian, Inc.: Wallingford, CT, 2009.